



**Iola Melissa  
Fernandes Duarte**

**Application of Nuclear Magnetic Resonance  
Spectroscopy and Vibrational Spectroscopy for the  
Characterisation of Fruit Products and Beverages**

**Aplicação de Espectroscopia de Ressonância  
Magnética Nuclear e Espectroscopia Vibracional  
para a Caracterização de Frutos e Bebidas**



**Iola Melissa  
Fernandes Duarte**

**Application of Nuclear Magnetic Resonance  
Spectroscopy and Vibrational Spectroscopy for the  
Characterisation of Fruit Products and Beverages**

**Aplicação de Espectroscopia de Ressonância  
Magnética Nuclear e Espectroscopia Vibracional  
para a Caracterização de Frutos e Bebidas**

Dissertação apresentada à Universidade de Aveiro para cumprimento dos requisitos necessários à obtenção do grau de Doutor em Química, realizada sob a orientação científica da Doutora Ana Maria Pissarra Coelho Gil e da Doutora Ivonne Delgadillo, Professoras Associadas do Departamento de Química da Universidade de Aveiro

Trabalho realizado com o apoio financeiro da Fundação para a Ciência e a Tecnologia através da Bolsa Praxis XXI/BD/15666/98



## O Júri

Presidente

**Doutor Joaquim José Borges Gouveia**  
Professor Catedrático do Departamento de Economia, Gestão e Engenharia Industrial da  
Universidade de Aveiro

**Doutor John Christopher Lindon**  
Senior Research Investigator and Visiting Professor, Biological Chemistry, Biomedical Sciences  
Division, Faculty of Medicine, Imperial College of Science, Technology and Medicine, U.K.

**Doutora Maria Helena Santos**  
Professora Associada da Faculdade de Ciências e Tecnologia da Universidade Nova de Lisboa

**Doutora Cristina Luísa Miranda Silva**  
Professora Auxiliar da Escola Superior de Biotecnologia da Universidade Católica Portuguesa do  
Porto

**Doutora Ana Maria Pissarra Coelho Gil (orientadora)**  
Professora Associada do Departamento de Química da Universidade de Aveiro

**Doutora Ivonne Delgadillo (co-orientadora)**  
Professora Associada do Departamento de Química da Universidade de Aveiro

## Acknowledgements

I would like to express my sincere gratitude to my supervisors Dr. Ana Gil and Dr. Ivonne Delgadillo, who early stimulated my interest for scientific research and, in particular, for the field of NMR spectroscopy. I thank them for the many useful and refreshing discussions about my work, for their continuous guidance and help and for the critical reading and correction of this thesis.

I would also like to especially acknowledge Dr. Manfred Spraul, Dr. Eberhard Humpfer, Dr. Markus Godejohann and Dr. Ulrich Braumann, who kindly received me in the Bruker site of Silberstreifen (Germany) and allowed me to use the NMR and HPLC-NMR/MS instruments and to take advantage of the latest technical developments. I deeply thank their indispensable technical support and help.

My work has also benefited from the collaboration and helpful advice of Dr. Ian Colquhoun, who assisted me during my stay at the Institute of Food Research (IFR) in Norwich (U.K.), and of Dr. Peter Belton from the University of East Anglia, Norwich (U.K.).

I would like to acknowledge the fundamental contribution to this thesis of Dr. António Barros from the Chemistry Department of the University of Aveiro for assisting me in the multivariate analysis of my data. I am also indebted to Dr. Brian Goodfellow for his assistance with the NMR equipment and to Cláudia Almeida for her help in the laboratory. My thanks go also to Dr. Pablo Pereira from the National Institute of Engineering and Industrial Technology (INETI), in Lisbon, for providing one of the moulds used in this work, and to Dr. Marcelo Maraschin from the University of Santa Catarina, Florianopolis (Brazil), for providing the grape juice and the wine phenolic extract samples.

I wish to acknowledge the Portuguese Foundation for Science and Technology (FCT) for their financial support through the grant Praxis XXI/BD/15666/98. I also thank the Chemistry Department of the University of Aveiro for providing the physical conditions for this work.

Finally, I deeply thank my mother and father for their love and continuous encouragement, and my husband Paulo for his constant patience, understanding and support. Also, I express my sincere gratitude to my parents in law and to all my family and friends for being with me always, in good and difficult moments!

## Resumo

O trabalho apresentado nesta tese pretendeu desenvolver e aplicar métodos espectroscópicos, em especial espectroscopia de ressonância magnética nuclear e técnicas acopladas, e também espectroscopia de infravermelho, para estudar a composição e a bioquímica de frutos e bebidas. No Capítulo I, apresenta-se o estado do conhecimento sobre a composição e bioquímica dos alimentos em análise neste trabalho, evidenciando-se os aspectos que justificam o seu estudo mais aprofundado e completo, para o qual a presente tese pretende contribuir. O Capítulo II descreve, de forma resumida, os fundamentos das técnicas analíticas utilizadas, focando nomeadamente a espectroscopia de RMN de estado líquido e de estado sólido, o acoplamento da RMN com cromatografia líquida e espectrometria de massa (HPLC-RMN/MS) e a espectroscopia de infravermelho. Os métodos de análise multivariada usados encontram-se também sumariamente descritos neste Capítulo.

No Capítulo III, descreve-se a aplicação de técnicas de RMN de alta resolução para caracterizar a composição de sumo e polpa de manga. O espectro de RMN-<sup>1</sup>H do sumo (600 MHz) apresenta elevada complexidade e contém informação sobre uma vasta gama de compostos. Recorrendo a espectros bidimensionais, conseguem identificar-se cerca de 50 compostos, incluindo vários açúcares, ácidos orgânicos e aminoácidos. O fruto intacto (polpa) é estudado directamente e de forma não-invasiva por RMN de estado sólido (400 e 500 MHz), utilizando a técnica de rotação segundo o ângulo mágico (MAS) e uma sonda de alta resolução (HR-MAS). A técnica de HR-MAS permite obter espectros com uma resolução seis vezes maior do que a obtida com MAS, sendo possível registar espectros 2D e caracterizar detalhadamente a composição da polpa. Comparando os espectros da polpa e do sumo respectivo, encontram-se algumas diferenças na composição em lípidos e pectinas, que se encontram em maior abundância no fruto intacto, demonstrando que a usual extrapolação da composição do sumo como composição global do fruto pode não ser totalmente aplicável.

No Capítulo IV apresenta-se um estudo sistemático do processo de amadurecimento da manga (cv. Tommy Atkins), levado a cabo através de medições físico-químicas e de espectroscopia de RMN-<sup>1</sup>H de alta resolução aplicada a sumos e polpas. A quantificação de alguns componentes do sumo é efectuada por integração dos sinais de RMN, usando uma referência interna (TSP). As principais alterações de composição com o amadurecimento consistem no aumento dos teores de sacarose, alguns aminoácidos (ex. valina, alanina, ácido  $\gamma$ -aminobutírico), constituintes pécnicos e polifenóis e na diminuição dos teores de glucose, ácido cítrico, ácido xiquímico, arginina, tirosina e fenilalanina. Uma segunda variedade estudada (cv. Haden) apresenta diferenças no processo de amadurecimento sobretudo ao nível da variação de alguns aminoácidos e compostos aromáticos. Ainda neste capítulo, um estudo preliminar sobre o efeito da refrigeração mostra que a maior parte das alterações indicadas acima são retardadas ou não ocorrem a baixa temperatura, daí resultando frutos com baixa qualidade organoléptica.

O Capítulo V descreve a quantificação dos três principais açúcares do sumo de manga em função do amadurecimento, usando regressão parcial dos mínimos quadrados (PLS) aplicada a espectros de infravermelho (FTIR-ATR) e de RMN-<sup>1</sup>H. A calibração é efectuada com base em soluções padrão de glucose, frutose e sacarose, seguindo um desenho experimental triangular, com seis níveis de concentração para cada açúcar. O método de PLS-FTIR permite prever a concentração dos três açúcares com elevada exactidão, excepto no caso da glucose quando, nos últimos estágios de amadurecimento,

esta atinge teores abaixo da gama de concentrações usada na calibração. Por outro lado, a aplicação de PLS aos espectros de RMN das soluções padrão e dos sumos de manga apresenta erros elevados, cuja magnitude parece depender do alinhamento dos espectros, necessitando este método de optimização.

No Capítulo VI, a espectroscopia de RMN-<sup>1</sup>H de alta resolução é usada para monitorizar e identificar alterações de composição em sumos de manga sujeitos a degradação natural, aquecimento e contaminação microbiológica. Permitindo identificar muitos dos compostos que se alteram em função destes efeitos, de forma rápida e simultânea, e seguir a sua variação ao longo do tempo, a técnica de RMN revela-se promissora para a detecção de indicadores de degradação/contaminação do sumo, sendo potencialmente útil para fins de controlo de qualidade.

No Capítulo VII, alguns componentes minoritários de sumo de manga, sumo de uva e vinho são investigados através do acoplamento das técnicas de RMN, cromatografia líquida e espectrometria de massa (HPLC-RMN/MS). Em particular, o sumo de manga é analisado com vista ao estudo dos hidratos de carbono menos abundantes, tendo-se alcançado uma melhor caracterização da fracção pécica. A análise de sumo de uva e vinho (extracto fenólico) destina-se a caracterizar os constituintes aromáticos destas amostras, tendo-se conseguido identificar vários compostos fenólicos de difícil atribuição só com base na análise directa por RMN. Os compostos identificados na uva incluem o ácido gálico e vários ácidos cinâmicos (ex. *p*-cumárico, *trans*-cutárico e *trans*-caftárico), enquanto que no vinho se detectam catequina e epicatequina, *trans*-resveratrol, tirosol e ácido cafeico.

O Capítulo VIII centra-se na caracterização da composição química da cerveja através das técnicas de RMN e de HPLC-RMN/MS. A análise directa por RMN uni- e bidimensional (500 MHz) permite a identificação de cerca de 30 compostos, entre os quais vários ácidos orgânicos, aminoácidos e álcoois. Os oligossacarídeos de maltose (dextrinas) dão origem aos sinais mais largos e intensos do espectro, mas o elevado grau de sobreposição impede a sua caracterização estrutural. A identificação de dextrinas de diferentes tamanhos é conseguida através da análise da cerveja por HPLC-RMN/MS, que requer apenas a desgaseificação da amostra. A análise por HPLC-RMN/MS permite também confirmar a presença de vários compostos aromáticos e revelar outros não identificados só com base na análise por RMN, tais como os álcoois aromáticos 2-feniletanol, tirosol e triptofol.

Finalmente, no Capítulo IX, descreve-se a análise de componentes principais (PCA) dos espectros de RMN-<sup>1</sup>H e de FTIR-ATR de um conjunto de 50 cervejas de diferentes marcas, tipos e países de origem. Por PCA dos espectros de RMN as cervejas são separadas de acordo com a sua composição em hidratos de carbono, embora alguns componentes minoritários (em particular compostos aromáticos) também contribuam para a distinção das amostras, nomeadamente em termos dos dois tipos principais 'ale' e 'lager'. A aplicação de PCA aos espectros de FTIR origina a distinção das cervejas com base no seu teor alcoólico e na sua composição em hidratos de carbono. A análise canónica de correlação (CCA) entre os espectros de RMN e de FTIR mostra uma correlação elevada entre os dois domínios, permitindo identificar os sinais que variam no mesmo sentido.

## Abstract

The work reported in this thesis aimed at developing and applying spectroscopic methods, principally nuclear magnetic resonance (NMR) spectroscopy and hyphenated techniques (HPLC-NMR and HPLC-NMR/MS), along with infrared spectroscopy, for studying the complex composition and biochemistry of different fruit products and beverages. Chapter I summarises some of the present knowledge about the food systems studied, giving particular emphasis to the aspects that frame the problems investigated in this thesis. The fundamentals of the analytical methods employed are shortly presented in Chapter II, focusing on the principles underlying the experiments that have been carried out in this work, namely solution and solid state high resolution  $^1\text{H}$  NMR spectroscopy, HPLC-NMR/(MS) and Fourier-transform infrared spectroscopy. The multivariate analysis methods that have been applied to the spectroscopic data are also briefly presented.

In Chapter III, the application of high resolution NMR to characterise the composition of mango juice and intact pulp is described. The high field (600 MHz)  $^1\text{H}$  spectra of juices show a high degree of complexity, revealing the potential of the technique for the simultaneous detection of a wide range of components. Spectral assignment is carried out with basis on 1D and 2D spectra, resulting in the identification of about 50 components, including several sugars, organic acids and amino acids. Mango pulps are studied directly and non-invasively by techniques derived from solid state NMR, namely  $^1\text{H}$  HR-MAS NMR (400 and 500 MHz), which results in a six-fold resolution improvement compared to standard  $^1\text{H}$  MAS. HR-MAS enables 2D experiments to be carried out, thus allowing for the pulp composition to be thoroughly characterised. The pulp is found to have a richer composition in lipids and pectins than the corresponding juice, showing that the composition of the liquid phase is not fully representative of the composition of the whole fruit as usually assumed.

Chapter IV presents a systematic study of the ripening process of mango (cv. Tommy Atkins), monitored by physicochemical parameters and by high resolution  $^1\text{H}$  NMR of both juices and pulps. Some juice components are quantified by integration of NMR signals, using an internal reference (TSP). Mango ripening is found to be characterised by increases in the contents of sucrose, some amino acids (e.g. valine, alanine, GABA), pectic constituents and polyphenols, and by decreases in the contents of glucose, citric acid, shikimic acid, arginine, tyrosine and phenylalanine, reflecting the complex biochemistry of ripening. The other cultivar studied (cv. Haden) is found to differ mainly in the variation patterns of some amino acids and aromatic compounds. Furthermore, a preliminary study of the effect of refrigeration on ripening shows that most changes indicated above do not occur under low temperature, resulting in fruits with poor edible quality.

In Chapter V, partial least squares (PLS1) regression is applied to FTIR-ATR and to  $^1\text{H}$  NMR data in order to quantify the three main sugars in mango juices as a function of ripening. Calibration is based on standard solutions of glucose, fructose and sucrose, following a triangular experimental design with six concentration levels for each sugar. The PLS-FTIR method shows good predictive ability, although the accuracy of glucose determination decreases at later ripening stages, when concentrations fall below the lower limit of the concentration range used for calibration. The PLS-NMR method shows much higher prediction errors, which seem to depend on spectral alignment, and needs further optimisation.

In Chapter VI, the application of high resolution NMR to monitor the complex compositional changes of mango juices subject to natural degradation, heat treatment and microbial contamination is described. Enabling the identification of many compounds undergoing changes upon these effects, in a rapid and simultaneous manner, and their variations to be followed throughout time, the NMR technique may be regarded as a sensitive and powerful tool for detecting indicators of spoilage/contamination, being potentially useful for quality control purposes.

Chapter VII describes the application of hyphenated NMR methods (HPLC-NMR and HPLC-NMR/MS) to investigate minor components in mango juice, grape juice and wine. In particular, the carbohydrate composition of mango juice is investigated and further advances in the characterisation of the pectic fraction achieved. The analysis of grape juice and wine (phenolic extract) aims at characterising their complex aromatic composition and results in the identification of several phenolic compounds, overcoming the difficulties found when using standard NMR. Gallic acid and several cinnamic acids (e.g. *p*-coumaric, *trans*-coutaric and *trans*-caftaric) are identified in grape juice, whereas catechin, epicatechin, *trans*-resveratrol, tyrosol and caffeic acid are found in the wine phenolic extract.

Chapter VIII is focused on the characterisation of beer chemical composition by high resolution NMR and HPLC-NMR/MS. Direct analysis of beer by 1D and 2D NMR (500 MHz) is shown to enable the identification of about 30 components, such as several organic acids, amino acids and alcohols. Malto-oligosaccharides (dextrins) give rise to the broadest and most intense signals in the spectrum, but the strong spectral overlap hinders their structural characterisation. The identification of dextrins of different sizes is achieved by HPLC-NMR/MS of beer, preceded only by degassing of the sample. In addition, HPLC-NMR/MS is shown to be useful for confirming the identity of some aromatic compounds previously assigned by NMR alone, and for revealing new ones, such as the aromatic alcohols 2-phenylethanol, tyrosol and tryptophol.

Finally, in Chapter IX, principal component analysis (PCA) is applied to the  $^1\text{H}$  NMR spectra and to the FTIR-ATR spectra of a set of 50 beers differing in label, type and country of origin. PCA of NMR data results in the separation of beers mainly according to their carbohydrate composition, although minor components (aromatic compounds in particular) are also found to contribute for the distinction of beers, namely in terms of the two main types ale and lager. PCA of FTIR data separates beers with basis on differences in their alcoholic content and carbohydrate composition. Canonical correlation analysis of NMR and FTIR spectra shows a high correlation between the two domains, enabling the identification of the spectral features varying in the same direction.

Accounts of some of the work reported here are given in:

1. Gil, A.M.; Duarte, I.F.; Delgadillo, I.; Colquhoun, I.J.; Casuscelli, J.; Humpfer, E.; Spraul, M. Study of the compositional changes of mango during ripening by use of nuclear magnetic resonance spectroscopy. *Journal of Agricultural and Food Chemistry* **2000**, *48*, 1524-1536.
2. Duarte, I.F.; Delgadillo, I.; Spraul, M.; Humpfer, E.; Gil, A.M. An NMR study of the biochemistry of mango: the effects of ripening, processing and microbial growth. In *Magnetic Resonance in Food Science - a View to the Future*; Webb, G.A, Belton, P.S., Gil, A.M., Delgadillo, I., Eds.; The Royal Society of Chemistry: Cambridge, 2001; 259-266.
3. Duarte, I.F.; Barros, A.; Belton, P.S.; Righelato, R.; Spraul, M.; Humpfer, E.; Gil, A.M. High resolution NMR spectroscopy and multivariate analysis for the characterisation of beer. *Journal of Agricultural and Food Chemistry* **2002**, *50*, 2475-2481.
4. Duarte, I.F.; Barros, A.; Delgadillo, I.; Almeida, C.; Gil, A.M. Application of FTIR spectroscopy for the quantification of sugars in mango juice as a function of ripening. *Journal of Agricultural and Food Chemistry* **2002**, *50*, 3104-3111.
5. Duarte, I.F.; Spraul, M.; Godejohann, M.; Gil, A.M. Application of NMR and hyphenated NMR spectroscopy for the study of beer components. *Magnetic Resonance in Food Science - Latest Developments*; Webb, G.A., Belton, P.S., Gil, A.M., Rutledge, D.N., Eds. (*in press*).
6. Duarte, I.F.; Godejohann, M.; Braumann, U.; Spraul, M.; Gil, A.M. Application of NMR spectroscopy and LC-NMR/MS to the identification of carbohydrates in beer (*submitted*).
7. Gil, A.M.; Duarte, I.F.; Godejohann, M.; Braumann, U.; Spraul, M. Characterisation of the aromatic composition of some liquid foods by NMR spectroscopy and LC-NMR/MS (*submitted*).

In preparation:

Duarte, I.; Barros, A.; Almeida, C.; Spraul, M.; Gil, A.M. Multivariate analysis of NMR and FTIR data of beer as a potential tool for its quality control.



## Contents

### Chapter I. Compositional and Biochemical Aspects of the Food Systems Studied

I.1. Mango Fruit.....	2
I.1.1. General Chemical Composition.....	2
I.1.2. The Ripening Process of Mango Fruit.....	4
I.1.2.1. Changes in Composition and Organoleptic Properties.....	4
I.1.2.2. Respiration Pattern.....	8
I.1.2.3. Fruit Maturity at Harvest and Postharvest Problems.....	9
I.2. Grape and Wine.....	11
I.2.1. General Chemical Composition.....	11
I.2.2. Phenolic Constituents and Their Functionality.....	13
I.3. Beer: Brewing Process and Chemical Composition.....	18
References.....	25

### Chapter II. Fundamentals of the Analytical Methods Employed

II.1. High Resolution Nuclear Magnetic Resonance (NMR) Spectroscopy of Liquids....	34
II.1.1 Principles of NMR Spectroscopy.....	34
II.1.2. NMR Spectral Parameters: Chemical Shift, Spin-Spin Coupling and Signal Area.....	39
II.1.3. Two-Dimensional (2D) NMR Spectroscopy.....	42
II.2. NMR Spectroscopy of Solids.....	50
II.2.1. Nuclear Spin Interactions in Solids.....	50
II.2.2. High Resolution Solid-State NMR Techniques.....	51
II.3. Hyphenated NMR Methods (HPLC-NMR and HPLC-NMR/MS).....	53
II.4. Fourier Transform Infrared (FTIR) Spectroscopy.....	56
II.5. Some Multivariate Analysis Methods.....	59
II.5.1. Principal Components Analysis (PCA).....	60
II.5.2. Partial Least Squares (PLS) Regression .....	61
II.5.3. Canonical Correlation Analysis (CCA).....	62
References.....	62

### Chapter III. Study of the Composition of Mango by NMR

III.1. Introduction.....	66
III.2. Materials and Methods.....	67
III.2.1. Sample Preparation.....	67
III.2.2 NMR Measurements.....	68
III.3. High Resolution NMR Study of Mango Juice.....	70
III.3.1. Spectral Assignment.....	70
III.3.2. Compositional Differences Within and Between Cultivars.....	80
III.4. NMR Study of Mango Pulp.....	83
III.4.1. Standard Magic Angle Spinning (MAS) NMR.....	83
III.4.2. High Resolution Magic Angle Spinning (HR-MAS) NMR.....	85
III.4.3. Compositional Differences Between Pulp and Juice.....	90
III.5. Conclusions.....	93
References.....	94

## **Chapter IV. Study of the Ripening Process of Mango: Physical and Biochemical Changes**

IV.1. Introduction.....	98
IV.2. Materials and Methods.....	100
IV.2.1. Sample Preparation.....	100
IV.2.2. Texture, pH, Soluble Solids and Enzymatic Determinations.....	101
IV.2.3. NMR Measurements.....	102
IV.3. Compositional Changes of Mango During Ripening.....	102
IV.3.1. Changes in Texture, pH and Soluble Solids.....	102
IV.3.2. Changes Assessed by NMR.....	104
IV.3.2.1. Qualitative Changes in the Composition of Juices.....	104
IV.3.2.2. Quantitative Analysis of Juices and Pulps.....	108
IV.4. Preliminary Study of the Effect of Refrigeration on Mango Ripening.....	115
IV.4.1. Changes in Texture, pH and Soluble Solids.....	115
IV.4.2. Changes Assessed by NMR.....	117
IV.5. Conclusions.....	119
References.....	120

## **Chapter V. Sugar Quantification in Mango Juice by Multivariate Analysis of FTIR and NMR Data**

V.1. Introduction.....	126
V.2. Materials and Methods.....	128
V.2.1. Sample Preparation.....	128
V.2.2. FTIR Measurements.....	130
V.2.3. NMR Measurements.....	130
V.2.4. Enzymatic Determinations.....	130
V.2.5. Multivariate Analysis.....	131
V.3. Sugar Quantification by Partial Least Squares (PLS)-FTIR.....	131
V.3.1. Application to Sugar Standard Solutions.....	131
V.3.2. Application to Mango Juices as a Function of Ripening.....	135
V.4. Sugar Quantification by Partial Least Squares (PLS)-NMR.....	138
V.4.1. Application to Sugar Standard Solutions.....	138
V.4.2. Application to Mango Juices as a Function of Ripening.....	142
V.5. Conclusions.....	144
References.....	144

## **Chapter VI. Study of Spoilage, Heat Treatment and Microbial Contamination in Mango Juices by NMR Spectroscopy**

VI.1 Introduction.....	148
VI.2. Materials and Methods.....	150
VI.2.1. Sample Preparation.....	150
VI.2.1.1. Culture of Microorganisms.....	150
VI.2.1.2. Preparation of Spores Suspensions.....	150
VI.2.1.3. Preparation and Inoculation of Juices.....	151
VI.2.2. Soluble Solids, pH and Enzymatic Determinations.....	152
VI.2.3. NMR Measurements.....	152

VI.3. Natural Mango Juice: Changes Upon Spoilage, Heat Treatment and Microbial Contamination.....	153
VI.3.1. Changes Assessed by Soluble Solids and pH.....	153
VI.3.2. Changes Assessed by NMR Spectroscopy.....	154
VI.3.2.1. Effect of Natural Spoilage.....	154
VI.3.2.2. Effect of Heat Treatment.....	163
VI.3.2.3. Effect of Inoculation with <i>Penicillium expansum</i> .....	164
VI.4. Commercial Mango Juice: Changes Upon Microbial Contamination.....	170
VI.4.1. Changes Assessed by Soluble Solids and pH.....	171
VI.4.2. Changes Assessed by NMR Spectroscopy.....	172
VI.4.2.1. Effect of Inoculation with <i>Penicillium expansum</i> .....	172
VI.4.2.2. Effect of Inoculation with <i>Neosartorya fischeri</i> .....	177
VI.5 Conclusions.....	181
References.....	183

**Chapter VII.** Application of Hyphenated NMR (HPLC-NMR and HPLC-NMR/MS) for the Detection of Minor Components in Fruit Juices and Wine

VII.1. Introduction.....	186
VII.2. Materials and Methods.....	187
VII.2.1. Sample Preparation.....	187
VII.2.2. Instrumentation and Measurements.....	187
VII.3. Characterisation of Carbohydrates in Mango Juice.....	190
VII.3.1. Application to Fresh Mango Juices.....	190
VII.3.2. Application to Spoiled and Contaminated Mango Juices.....	196
VII.4. Characterisation of Aromatic Compounds in Grape Juice.....	200
VII.5. Characterisation of Aromatic Compounds in a Wine Phenolic Extract.....	212
VII.6. Conclusions.....	216
References.....	217

**Chapter VIII.** Characterisation of Beer Composition by NMR and Hyphenated NMR (HPLC-NMR/MS)

VIII.1. Introduction.....	222
VIII.2. Materials and Methods.....	223
VIII.2.1. Sample Preparation.....	223
VIII.2.2. NMR and HPLC-NMR/MS Measurements.....	223
VIII.3. Characterisation of Beer Composition by High Resolution NMR .....	226
VIII.4. Characterisation of Beer Composition by HPLC-NMR/MS.....	233
VIII.4.1. Application to Carbohydrates.....	233
VIII.4.2. Application to Aromatic Compounds.....	240
VIII.5. Conclusions.....	244
References.....	244

**Chapter IX. Multivariate Analysis of NMR and FTIR of Beer as a Potential Tool for Beer Quality Control**

IX.1. Introduction.....	24
IX.2. Materials and Methods.....	8
IX.2.1. Sample Preparation.....	24
IX.2.2. Spectroscopic Measurements.....	9
IX.2.3. Multivariate Analysis.....	24
IX.3. Principal Components Analysis (PCA) of NMR Data.....	9
IX.4. Principal Components Analysis (PCA) of FTIR Data.....	24
IX.5. Canonical Correlation Analysis (CCA) of NMR and FTIR Data.....	9
IX.6. Conclusions.....	25
References.....	1
.	25
	1
	26
	1
	26
	3
	26
	5
	26
	6

**Chapter X. Final Conclusions and Future Work..... 270**

**Appendix**

NMR Pulse Programs Used in This Work.....	278
---	-----

## Abbreviations & Symbols

?	chemical shift (in ppm)
$\delta_{1/2}$	line width at half height
ATR	attenuated total reflectance
CCA	canonical correlation analysis
CV	canonical variate
COSY	correlation spectroscopy
DAD	diode array detector
FID	free induction decay
FT	Fourier transform
FTIR	Fourier transform infrared (spectroscopy)
HMQC	heteronuclear multiple quantum correlation
HPLC	high-performance liquid chromatography
HR-MAS	high resolution-magic angle spinning
HSQC	heteronuclear single quantum correlation
$J$	coupling constant
LB	line broadening
$m/z$	mass over charge
MAS	magic angle spinning
MLEV-17	Malcom Levitt's composite-pulse decoupling sequence
$M_w$	molecular weight
MS	mass spectrometry
NMR	nuclear magnetic resonance
PC	principal component
PCA	principal component analysis
PDA	potato dextrose agar
PLS	partial least squares (regression)
ppm	parts per million
r.f.	radiofrequency
RMSECV	root mean square error of cross validation
RMSEP	root mean square error of prediction
RT	retention time
S/N	signal-to-noise
SR	spinning rate
SS	soluble solids
SSB	spinning side band
$T_1$	longitudinal (spin-lattice) relaxation time
$T_2$	transverse (spin-spin) relaxation time
TA	titratable acidity
TIC	total ion current
TOCSY	total correlation spectroscopy
TSP	sodium 3-(trimethylsilyl)-propionate
UV	ultraviolet



# **I. COMPOSITIONAL AND BIOCHEMICAL ASPECTS OF THE FOOD SYSTEMS STUDIED**

I.1. Mango Fruit.....	2
I.1.1. General Chemical Composition.....	2
I.1.2. The Ripening Process of Mango Fruit.....	4
I.1.2.1. Changes in Composition and Organoleptic Properties.....	4
I.1.2.2. Respiration Pattern.....	8
I.1.2.3. Fruit Maturity at Harvest and Postharvest Problems.....	9
I.2. Grape and Wine.....	11
I.2.1. General Chemical Composition.....	11
I.2.2. Phenolic Constituents and Their Functionality.....	13
I.3. Beer: Brewing Process and Chemical Composition.....	18
References.....	25

## I.1. Mango Fruit

Mango fruit, or the fruit of *Mangifera indica* L. of the family Anacardiaceae, is one of the world's most important fruit crops in terms of production, acreage and popularity. The world production of mangoes in 1996 was 19.2 million tons, 75% of which were produced in Asian countries (Belitz and Grosch, 1999). European countries do not produce mango and import it from countries like India (the major producer), Thailand, Brazil and Venezuela. Among the hundreds of cultivars grown all over the world, only a few are grown commercially, some of the most often found in the European market being the Alphonso, Haden, Kent, Keitt and Tommy Atkins cultivars.

### I.1.1. General Chemical Composition

Table I.1 shows general compositional data reported for different cultivars of mango in the ripe, edible stage. The content in soluble solids, for which sugars account the most, normally varies between 12 and 21%. Titratable acidity is about 0.1-0.2% (expressed as citric acid) and the pH values of ripe mango fall in the 4-5 range. Besides sugars and organic acids, which are the major components and may account for more than 20% of the fruit fresh weight, mango usually contains less than 3.5% polysaccharides, 0.3-1.5% protein, 0.05-0.6% lipid, 0.014-0.16% phenolic compounds, 0.004-0.20% carotenoids and small amounts of vitamin B complex, as well as aroma compounds (Wu *et al.*, 1993).

Table I.1. Approximate chemical composition of ripe mangoes. Adapted from Salunkhe and Desai (1984) and Medicott *et al.* (1986).

Cultivar	% SS (Soluble Solids)	% TA (Titratable Acidity)	pH	Total Sugars  (% fresh weight)	Reducing Sugars	Vitamin C  (mg/100 g fresh weight)	Carotenoids  (mg/100 g fresh weight)
Alphonso	17.6	0.15	4.7	16.2	3.2	60.7	8.3
Haden	18.9	0.22	4.9	16.2	3.5	32.1	n.d.
Kent	21.0	0.12	n.d.	20.9	5.5	23.5	0.93
Keitt	18.4	0.11	4.8	13.6	4.5	13.9	5.9
Tommy Atkins	12.7	n.d.	4.2	10.7	3.7	n.d.	n.d.

n.d.: not determined

The principal sugars present in mango are glucose, fructose and sucrose, reported to occur in the ripe fruits of different cultivars at 1.0-3.2%, 4.0-5.6%, and 6.3-9.6% of fresh weight, respectively (Wu *et al.*, 1993). Small amounts of xylose, arabinose and heptulose have also been detected. In what concerns polysaccharides, mango usually contains 1.0 to 3.5% of alcohol-insoluble solids (AIS), which include residual starch, pectin, cellulose and hemicellulose (Wu *et al.*, 1993).

Citric acid is usually the predominant organic acid in mango, malic and succinic acids being also found in significant quantities (Lizada, 1993). The minor organic acids which have been identified in ripe mango pulp include oxalic, malonic, tartaric, pyruvic, glucuronic, galacturonic,  $\alpha$ -ketoglutaric and ascorbic acids (Hulme, 1971; Wu *et al.*, 1993). Mango is a good source of ascorbic acid (vitamin C), the reported values per 100 g of ripe mango pulp varying between 1.5 and 175 mg (Wu *et al.*, 1993). Differences in cultivar and postharvest storage conditions may account for this large variation. Besides the acids indicated above, quinic and shikimic acids are also found in mango, as shown in this work (Chapter III) for the first time to our knowledge.

Like the majority of fruits, mango is a poor source of protein, the total content for most cultivars falling within the range of 0.5 to 1.5% of fresh weight. The free amino acid profile differs significantly among cultivars and stages of maturity. Nevertheless, alanine, glutamic acid, serine and aspartic acid are usually among the major free amino acids (Wu *et al.*, 1993; Kalra *et al.*, 1995).

Lipids are found in low contents in mango (0.05-0.6% of fresh weight). The oil extracted from ripe "Alphonso" fruit has been seen to contain mostly triglycerides, while monoglycerides, diglycerides and phospholipids were present in small amounts. Myristic, palmitic, palmitoleic, stearic, oleic, linoleic and linolenic acids (some of which are shown in Figure I.1a) are commonly among the fatty acids found in ripe mangoes of several cultivars, although with different quantitative distributions (Wu *et al.*, 1993). The amount and proportion of these compounds are thought to influence the flavour of mango pulp. In particular, it has been reported that the cultivars with stronger aroma had lower palmitic/palmitoleic ratios (Wu *et al.*, 1993).

Phenolic compounds also make an important contribution to the flavour of mango fruit, namely with respect to the astringency of green pulp, even though they are present in very small quantities (0.014-0.16% of fresh weight). There is not much data on the identity

of the phenolics present in mango, as the analysis of these compounds is hindered by their low concentrations and by their physical/chemical interactions with other components (e.g. polysaccharides). Gallic acid, *m*-digallic acid, *m*-trigallic acid, mangiferin and ellagic acid are the main phenolic compounds identified (Wu *et al.*, 1993), some of which are shown in Figure I.1b.

Mango contains some vitamins of the B complex, namely thiamine (B<sub>1</sub>), riboflavin (B<sub>2</sub>) and niacin (Figure I.1c). The ranges found for the amounts of these vitamins in ripe mangoes are, respectively, 0.06-0.08, 0.07-0.09 and 0.06-0.9 mg/100 g of pulp, niacin being the most abundant (Wu *et al.*, 1993).

Mango is a rich source of carotenoid pigments capable of being converted by the human body into vitamin A. In most cultivars, more than half of the total carotenoid content consists of  $\beta$ -carotene (Wu *et al.*, 1993; Lizada, 1993). Other carotenoids in fresh mango pulp, recently identified by HPLC and mass spectrometry, include  $\beta$ -cryptoxanthin, zeaxanthin, luteoxanthin, neoxanthin and violaxanthin (Mercadante *et al.*, 1997). The structures of some of these pigments are shown in Figure I.1d. The carotenoid composition of mango may, however, change significantly during processing. For instance, Cano and Ancos (1994) verified that the pigment pattern of fresh mango fruit changed slightly upon freezing and drastically upon canning of mango slices into syrup, which showed a dark orange colour, different from that of the fresh fruit.

The aroma of mango varies markedly between cultivars and is related to the complex volatile composition of the fruit. More than a hundred volatile components have been identified in ripe mango, the major ones being terpenes, although several other hydrocarbon esters and alcohols were also found to be present (MacLeod and Pieris, 1984; Idstein and Schreir, 1985; Wilson *et al.*, 1986; Wu *et al.*, 1993). *Cis*-ocimene, myrcene, car-3-ene, limonene and  $\beta$ -terpinolene are among the most important aroma compounds (some structures are shown in Figure I.1e). More recently, mango glycosidically bound volatile compounds have also been characterised (Sakho *et al.*, 1997).

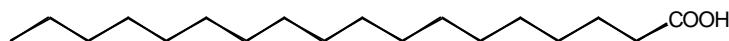
## **I.1.2. The Ripening Process of Mango Fruit**

### **I.1.2.1. Changes in Composition and Organoleptic Properties**

Ripening may be defined as the process through which the fruit attains edible quality, involving drastic changes in flavour, colour and texture properties. The flavour of

a) Fatty acids

Stearic acid 18:0



Oleic acid 18:1 (9)

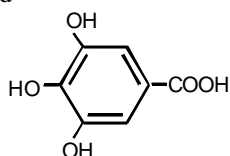


Linoleic acid 18:2 (9, 12)

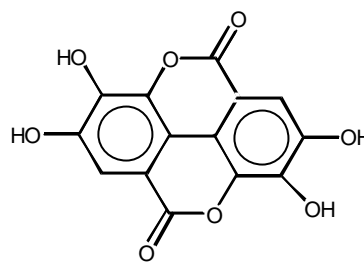


b) Phenolic compounds

Gallic acid

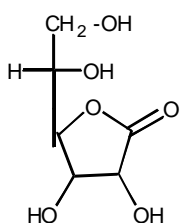


Ellagic acid

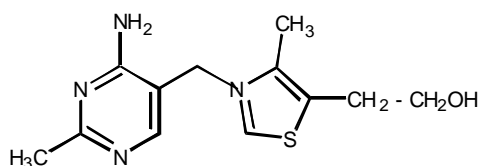


c) Vitamins

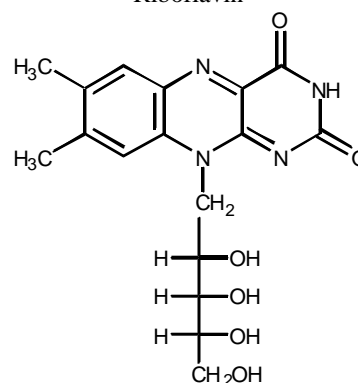
L-Ascorbic acid



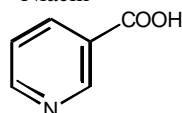
Thiamine



Riboflavin

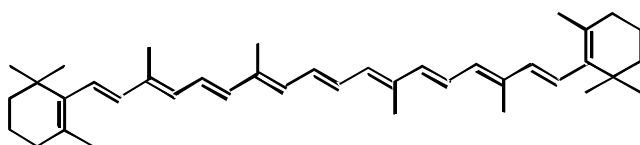


Niacin

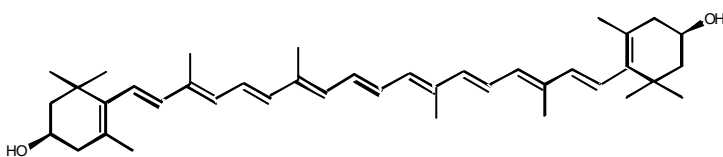


d) Pigments

?-Carotene

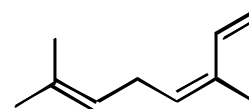


Zeaxanthin

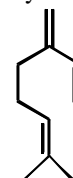


e) Aroma Compounds (terpenes)

*cis*-Ocimene



Myrcene



Limonene

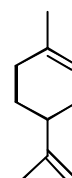


Figure I.1. Examples of some compounds found in low abundance in mango fruit.

the fruit depends on the complex interaction of sugars, organic acids, phenolic compounds and more specialised flavour compounds, including a wide range of volatiles. The colour changes are determined by the degradation and synthesis of different pigments, while the variations in texture reflect changes in cell wall composition and structure. The variations of those compounds during mango fruit ripening are briefly described in the next few paragraphs.

Most starch that has accumulated in the mature green fruit (which can be as high as 13%) is hydrolysed during ripening and the ripe fruit usually contains negligible levels of this polysaccharide (Salunkhe and Desai, 1984; Selvaraj *et al.*, 1989). As a consequence of starch hydrolysis, associated with the activity of the enzyme amylase, total sugars increase during ripening, although a net loss may occur at late stages, probably due to the intensification of respiration and lack of starch reserves to replenish the sugars being metabolised (Lizada, 1993; Medlicott and Thompson, 1985). In addition, it is possible that some gluconeogenesis, that is the biosynthesis of glucose from noncarbohydrate precursors such as organic acids, can also occur during ripening, although this is expected to account for only a small percentage of the sugar accumulating in the fruit (Tucker, 1993). Sucrose usually registers the largest increase, remaining the predominant sugar throughout ripening. Fructose has also been reported to increase, while glucose has shown a decreasing trend in some cultivars (Medlicott and Thompson, 1985; Medlicott *et al.*, 1986).

Similarly to other fruits, the total acidity has been consistently observed to decrease during mango ripening (and the pH values to increase from about 3.0 to 5.0), probably due to the utilization of organic acids as respiratory substrates. Citric acid declines in all mango cultivars examined (from 125-500 mg/100g in unripe fruit to 54-123 mg/100g in ripe fruit, according to Selvaraj *et al.*, 1989), but malic acid exhibits different patterns of changes in different cultivars (Medlicott *et al.*, 1986; Selvaraj *et al.*, 1989). Little information is available on the variations of minor organic acids and amino acids. Selvaraj *et al.* (1989) registered no significant changes in the concentration of total soluble amino acids during ripening, although the total amount present at different ripening stages varied significantly between different cultivars. In addition, the levels of arginine, phenylalanine, aspartate, glutamate, lysine, threonine and serine have been found to decline in some mango cultivars, while the levels of alanine, valine, leucine, isoleucine,  $\gamma$ -aminobutyric acid and proline were seen to increase upon ripening (Kalra *et al.*, 1995).

The progressive loss of astringency of some mango cultivars has been associated with the total phenolic content decrease (particularly in the levels of tannins). However, there are non-astringent cultivars for which the phenolics were not seen to decrease in the course of ripening (Lizada, 1993), which indicates that astringency is determined not only by the total phenolic content, but also by the specific phenolic compounds present and their interaction with other components, as observed for other fruits (Spanos and Wrolstad, 1992).

The content and composition of lipids vary throughout ripening and are related to mango aroma (Lizada, 1993). Total lipids, unsaponifiables and total fatty acids have been seen to increase during mango ripening, whereas free fatty acids and phospholipids were seen to decrease (Selvaraj *et al.*, 1989). The decreasing pattern of free fatty acids is related to their role as a potential source for the synthesis of other metabolites, including aroma compounds, such as alcohols, esters, and terpenes.

The most common variation in the peel colour of mango during ripening is from green to yellow/orange due to chlorophyll degradation and carotenoids synthesis. There are also cultivars that develop a reddish blush, which has been attributed to anthocyanins, while others retain most of the green colour, even at the full ripe stage. The pulp usually develops a more intense yellow colour, due to the continuous increase in the levels of carotenoids (Lizada, 1993). The rate and magnitude of carotenoids accumulation increase with the ripening temperature, in the range 12-37°C, as shown by Medlicott *et al.* (1986).

The fruit texture is an important quality attribute since it is directly related to shelf life, susceptibility to bruising and consumer appeal. Mango ripening is accompanied by pronounced softening, which strongly limits its marketable life. Therefore, there has been a lot of interest in studying the changes in cell-wall components and the enzymes that are thought to be associated with tissue softening (Tucker and Seymour, 1991; Aina and Oladunjoye, 1993; El-Zoghbi, 1994; Muda *et al.*, 1995; Labib *et al.*, 1995). These changes are often more apparent in the pectic components of the cell wall and usually involve an increase in pectin solubility, a decrease in pectin molecular weight and a loss of pectic neutral sugars (such as arabinose and galactose) from the cell wall into the liquid phase. The exact biochemical mechanisms which are responsible for these events are not clear, but it is likely that some of these wall modifications are brought about by pectolytic enzymes such as polygalacturonase, pectinesterase or galactosidase.

### **I.1.2.2. Respiration Pattern**

The ripening process requires the synthesis of novel proteins and nucleic acids, as well as new pigments and flavour compounds. These anabolic processes require both energy and a supply of carbon skeleton building blocks which in fruit, just as in other tissues, are supplied by respiration.

The two major respiratory substrates in fruits are sugars and organic acids. They are both found largely sequestered within the vacuole, and form a major contribution to the overall flavour of the fruit. However, they are presumably also released in a controlled manner from the vacuole, or alternatively a separate pool is maintained, and hence are available for respiration (Tucker, 1993). The respiratory pathways utilised by the fruit for the oxidation of sugars are those common to all plant tissues namely glycolysis, oxidative pentose phosphate pathway (OPP) and the tricarboxylic acid (TCA) pathway (Voet and Voet, 1990). In what regards organic acids, citrate and succinate can feed directly into the TCA cycle, while malate is first decarboxylated to pyruvate, which can then be fed into the TCA cycle. However, the control and utilization of these metabolic pathways during fruit ripening is still poorly understood.

Fruits in general can be classified as either climateric or nonclimateric on the basis of their respiration pattern during ripening. Mango fruit is of the climateric type (similarly to apple, banana, peach, etc.) meaning that it displays a characteristic peak of respiratory activity during ripening. Moreover, there is an increase in the production of ethylene, a plant growth regulator that promotes ripening. In contrast, non-climateric fruit (e.g. citrus, grape, pineapple) simply exhibit a gradual decline in their respiration during ripening and the endogenous levels of ethylene remain low (Tucker, 1993). The role of the climateric peak in ripening is still unclear. Increased levels of ATP may be required to drive ripening events such as starch breakdown, or nucleic acid, protein and pigment synthesis. However, the calculated energy demand in most fruit during ripening is much less than that produced during the climateric period, and non-climateric fruit ripen without any increase in respiration. Thus, it is thought that respiration is neither dependent on, nor integrated with, the other ripening events. It is possible that respiratory increases result simply as a general response to the ethylene produced by climateric fruit (Tucker, 1993).

### I.1.2.3. Fruit Maturity at Harvest and Postharvest Problems

The stage of maturity at harvest is an important factor determining mango fruit quality, especially when the fruit is being exported to distant market places. Mangoes harvested immature fail to ripen properly and, conversely, ripe mangoes are highly susceptible to bruising and mechanical damage during handling and transport, and will decay rapidly during storage. Therefore, mangoes to be exported should be harvested in the physiologically mature, hard, green condition.

The common indices utilised to assess mango fruit maturity comprise several physical parameters such as size, shape, weight, peel and pulp colour, specific gravity, and other measurements such as firmness, total soluble solids, acidity, total carotenoids and phenolics (Kalra *et al.*, 1995). Moreover, in recent years, methods to estimate the maturity of mango in a non-destructive way have been investigated. Guthrie and Walsh (1997) measured the NIR spectra of intact mango fruit and showed that the spectral features correlated well with mango pulp dry matter; Barcelon *et al.* (1999) used an X-ray scanner and found high correlations between this non-invasive measurement and some physicochemical properties, namely density, moisture content, soluble solids, titratable acidity and pH; and Mizrach *et al.* (1999) established relationships between ultrasonic measurements and storage time, firmness, sugar content and acidity.

The recommended conditions for ripening mangoes are 80-90% relative humidity and temperatures in the 20-30°C range. Higher temperatures may result in ripe fruit with low, undesirable sugar/acid ratios, off-flavours and pitting of the peel. Initiation, synchronisation and acceleration of ripening may be achieved by exposure to ethylene gas. Ripening may also be promoted by other chemicals, such as abscisic acid (Figure I.2), ethrel (2-chloroethylphosphoric acid) and acetylene gas liberated from calcium carbide in water (Wu *et al.*, 1993).

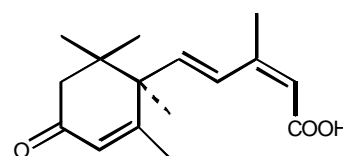


Figure I.2. Structure of abscisic acid.

The major causes of postharvest losses in mango fruit are mechanical damage (which may be avoided by careful handling), microbial infection and fast ripening. Anthracnose, caused by fungal infection with *Glomerella cingulata*, and stem-end-rot, caused by *Gloeosporium magiferae*, are some of the most important diseases affecting

mango trees and fruit. Their incidence can be reduced by good orchard management, preharvest cultural practices, appropriate handling of the fruit and postharvest treatment procedures, such as hot-water treatments (Jacobi and Giles, 1997; Nyanjage *et al.*, 1998). Microbial infection may also take place during storage and processing of mango fruit, and detection of contamination is critical for efficient quality control and safety assurance.

Mango ripening may be delayed by storage at temperatures lower than 20°C, which reduces the respiration rate and possibly lowers the production of ethylene (Kalra *et al.*, 1995). However, the lowest safe temperature is 10-13°C, since storage below this temperature range results in chilling injury, leading to a drastic reduction in fruit quality and increased spoilage. The symptoms of chilling injury include pitting, greyish scald-like discolouration of the skin, increased water loss, poor development of pulp colour and flavour, higher acidity with lower sugar content, and reduced resistance to pathogens (Salunkhe and Desai, 1984; Wu *et al.*, 1993).

There are other postharvest technologies which may be employed to delay ripening, although none is well established in the case of mango. Some success has been achieved with experiments on controlled atmosphere storage (relatively low O<sub>2</sub> and high CO<sub>2</sub> concentration), currently used for the major temperate fruit crops. However, flavour problems due to anaerobic respiration and increased ethanol production have been reported to limit the application of this technology to mango fruit (Wu *et al.*, 1993). More recently, precooling treatments, namely water cooling (Puttaraju and Reddy, 1997) and modified atmosphere storage techniques, such as plastic bagging (Pesis *et al.*, 2000) and skin coating (Baldwin *et al.*, 1999), have shown promising results in the extension of mango fruit shelf life.

Solutions to the postharvest problems of mango fruit, which are particularly relevant for importing markets like European countries, may come from a better understanding of the chemical and biochemical changes occurring during the processes affecting fruit quality, namely ripening and microbial decay. Mango fruit has thus been chosen for the investigation presented in this thesis (Chapters III to VI), concerning composition, ripening and microbial contamination studies, conducted by means of the modern and powerful spectroscopic techniques that nuclear magnetic resonance spectroscopy and infrared spectroscopy are.

## I.2. Grape and Wine

### I.2.1. General Chemical Composition

Grapevine belongs to the genus *Vitis* (family Ampelidaceae), which includes several species, the species of European origin *Vitis vinifera* being, by far, the one with higher economical importance. The major components of grapes are carbohydrates, organic acids and amino acids, whereas a wide range of phenolics and volatiles are present at much lower levels (Table I.2).

Table I.2. Major components of grape juice and their corresponding quality attributes (McLellan and Race, 1995).

Chemical class	Concentration (g/100 ml)	Quality attribute
Carbohydrates	20	Sweetness
Acids	1	Sourness
Phenolics	0.1	Colour and astringency
Volatiles	0.0001	Aroma

Glucose and fructose account for 99% or more of the carbohydrates in grape juice and for 12 to 27% of the fresh weight of the mature berry, constituting a large proportion of the total soluble solids. In unripe grapes, glucose accounts for 85% of the sugar content, while in ripe grapes there is generally a slight excess of fructose (Peynaud and Ribéreau-Gayon, 1971). Minor sugars identified in grapes include arabinose, xylose, sucrose (less than 0.1% in ripe berries), raffinose, stachyose, melibiose, maltose and galactose (Kanellis and Roubelakis-Angelakis, 1993).

The acid fraction of grape consists mainly of tartaric and malic acids, which account for about 90% of the total acidity. Other acids found in minor amounts are citric (5-10% of total acidity), isocitric, succinic, fumaric, acetic, pyruvic, glycolic, lactic, aconitic, quinic, shikimic and mandelic acids. The resulting pH of grape juice typically ranges from 3 to 4. Proline, threonine and glutamic acid are usually the most abundant amino acids, with concentrations typically ranging from 170 to 330 mg/L but many other amino acids are present, the total amount ranging from 2 to 8 g/L (Kanellis and Roubelakis-Angelakis, 1993).

Grapes, especially black grapes, contain a wide range of phenolic compounds, including benzoic acids, cinnamic acids, flavonols, anthocyanins, as well as various

flavans which constitute the tannin precursors. The presence and importance of these compounds in grapes is further discussed in the next section, since their detection and identification in grape juice is one of the subjects investigated in this thesis.

Aroma is a significant and complex character of grape quality, distinctive of the different fruit varieties. It consists of a natural blend of several hundred chemically different compounds, which are synthesised during ripening and localised mainly in the skin of the berries. In general, the most abundant aroma compounds in grapes are the monoterpenes linalool and geraniol. Certain alcohols such as benzyl and 2-phenylethyl alcohols, as well as several esters and aldehydes are also among the compounds responsible for grape aroma (Kanellis and Roubelakis-Angelakis, 1993).

The largest percentage of the world's grape production is used for wine making. Resulting from the fermentation of the juice of grapes, wine is a complex mixture of compounds, which are derived from grapes, produced or metabolised by yeast during fermentation, extracted from oak, and formed from chemical reactions that occur during processing and ageing. The typical gross composition of table wines is given in Table I.3.

Table I.3. Typical gross composition (% by weight) of white and red wines. Adapted from Ebeler (1997).

Component	White wine	Red Wine
Water	87	87
Ethanol	10	10
Other volatiles	0.04	0.04
Glycerol and related	1.10	1.10
Sugar	0.05	0.05
Pectin and related	0.30	0.30
Acids	0.70	0.60
Amino acids and related	0.25	0.25
Phenolic compounds	0.01	0.02
Vitamins and other micronutrients	0.01	0.01
Lipids	0.01	0.02
Ash	0.20	0.20

Among the alcohols present in wine, ethanol is, naturally, the most abundant, with amounts varying between 55 and 110 g/L (Belitz and Grosch, 1999). Methanol (38-200

mg/L) and higher alcohols such as propyl, butyl and amyl alcohols are also present. There are hundreds of other volatile compounds, namely terpenes and esters, which are present in small quantities, and originate both from the grapes and from fermentation. Polyols form another class of compounds with relevant contribution to the flavour of wine, glycerol (6-10 g/L) often being the third major wine component after water and ethanol. Other polyols include 2,3-butanediol, derived from diacetyl by yeast fermentation and usually present at 0.4-0.7 g/L, sorbitol, found in very low amounts, and mannitol, which is not present in healthy wines but may reach levels up to 35 g/L in spoiled, bacteria-infected wines (Belitz and Grosch, 1999).

Sugars are present in highly variable concentrations, glucose and fructose being the most abundant. The average ratio of glucose to fructose is 0.6:1.0 but it varies to a great extent. Other sugars present in wine include rhamnose and the nonfermentable pentoses arabinose, xylose and ribose (Belitz and Grosch, 1999).

Wine acids originally present in grapes are tartaric (which is the most abundant), malic and citric acids, whereas the major acids resulting from fermentation are succinic, lactic, acetic and carbonic (carbon dioxide) acids (Belitz and Grosch, 1999). Amino acids are present in concentrations of about hundreds of milligrams per litre, with the exception of proline, which can reach very high amounts (3.5 g/L).

Phenolic compounds play a decisive role in the make-up of a wine's character, especially of red wines. Some originate from the grapes and others are formed in the maturation process. The phenolic composition of wine will be addressed with more detail in the following section.

### **I.2.2. Phenolic Constituents and Their Functionality**

Phenolic compounds constitute one of the most numerous and ubiquitous groups of plant metabolites, ranging from simple molecules to highly polymerised compounds with molecular weights greater than 30000 Da (Bravo, 1998). They are generally important with respect to various sensory qualities of plant foods and beverages, such as colour, bitterness and astringency. Moreover, interest in food phenolics has increased greatly in recent years, owing to their antioxidant capacity (free radical scavenging and metal chelating activities) and their possible beneficial implications in human health, such as in the treatment and prevention of cancer, cardiovascular disease and other pathologies. In this regard, the

'French paradox' is often cited, referring to the lower prevalence of heart attacks in France than in other countries where the consumption of saturated fat is similar, and ascribing the difference to red wine in French diet. The nutritional effects of the main groups of phenolic compounds, including their metabolism, effects on nutrient bioavailability, and antioxidant activity have been recently reviewed by Bravo (1998). The purpose of this section is simply to acquaint the reader with the main phenolic compounds found in grape and wine, and the methods commonly employed for their analytical determination.

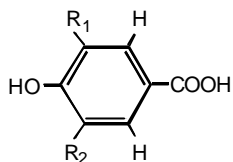
Figure I.3 illustrates the structures of phenolic compounds commonly occurring in grape and wine. Table I.4 presents quantitative data reported for some of these substances in white and red wines.

Benzoic ( $C_7$ ) and cinnamic acids ( $C_6-C_3$ ) belong to the group of phenolic acids (Figures I.3a and I.3b) and usually occur in combination with other compounds, namely in the form of esters. Compared to other free benzoic acids, such as gentisic and vanillic acids, gallic acid has been consistently observed to predominate in several white and red wines (Soleas *et al.*, 1997). Among the free cinnamic acids (e.g. caffeic, coumaric, ferulic), caffeic has been found to be the most abundant (Soleas *et al.*, 1997). These acids may also be esterified with several compounds, such as glucose, tartaric, quinic, shikimic and malic acids. The most common combination in grapes is with tartaric acid, *trans*-caffeoyltartaric acid (caftaric acid) and *p*-coumaroyltartaric acid (coutaric acid) being the most abundant (Spanos and Wrolstad, 1992).

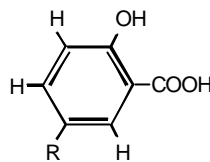
The other main group of phenolic compounds is the group of flavonoids, which are built upon a diphenylpropane skeleton ( $C_6-C_3-C_6$ ) in which the three-carbon bridge between the phenyl groups is usually cyclized with oxygen. The different classes within the group differ in the number of substituent hydroxyl groups, degree of unsaturation, and degree of oxidation of the three-carbon segment. Flavonols (Figure I.3c) occur mostly as glycosides. The flavonols identified in grapes and wines include 3-glucosides of quercetin, myricetin and kaempferol, quercetin-3-rhamnoside, kaempferol-3-galactoside and quercetin-3-glucuronide (Kanellis and Roubelakis-Angelakis, 1993). Anthocyanins are the major pigments of grapes and impart the characteristic colour of red wine. They are present as the anthocyanidins (Figure I.3d) modified by attachment of a glucose molecule at the 3-OH position, or by attachment of glucose at both the 3 and 5 positions. Further complication can result from the esterification of the glucose OH groups with cinnamic

## Phenolic Acids

### a) Benzoic acids

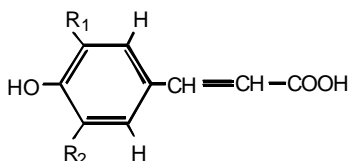


R<sub>1</sub>=R<sub>2</sub>=H: *p*-hydroxybenzoic  
 R<sub>1</sub>=R<sub>2</sub>=OH: gallic  
 R<sub>1</sub>=OH, R<sub>2</sub>=H: protocatechuic  
 R<sub>1</sub>=OCH<sub>3</sub>, R<sub>2</sub>=H: vanillic



R=OH: gentisic acid  
 R=H: salicylic acid

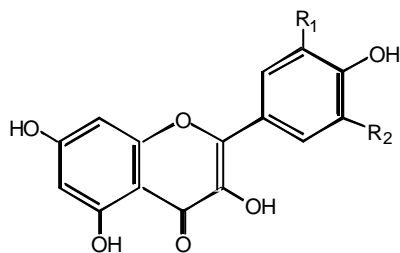
### b) Cinnamic acids



R<sub>1</sub>=R<sub>2</sub>=H: *p*-coumaric acid  
 R<sub>1</sub>=OH, R<sub>2</sub>=H: caffeic acid  
 R<sub>1</sub>=OCH<sub>3</sub>, R<sub>2</sub>=H: ferulic acid

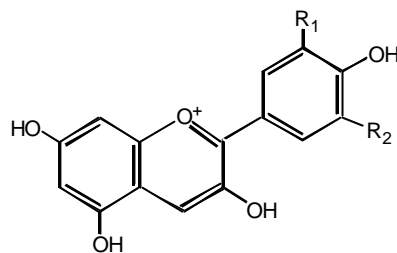
## Flavonoids

### c) Flavonols



R<sub>1</sub>=R<sub>2</sub>=H: kaempferol  
 R<sub>1</sub>=OH, R<sub>2</sub>=H: quercetin  
 R<sub>1</sub>=R<sub>2</sub>=OH: myricetin

### d) Anthocyanidins

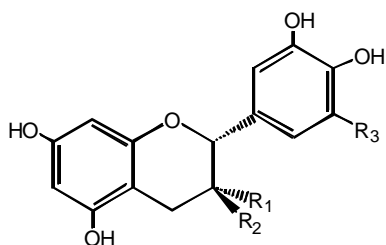


R<sub>1</sub>=OH, R<sub>2</sub>=H: cyanidin  
 R<sub>1</sub>=OCH<sub>3</sub>, R<sub>2</sub>=H: poenidin  
 R<sub>1</sub>=R<sub>2</sub>=OH: delphinidin  
 R<sub>1</sub>=OCH<sub>3</sub>, R<sub>2</sub>=OH: petunidin  
 R<sub>1</sub>=R<sub>2</sub>=OCH<sub>3</sub>: malvidin

### e) Proanthocyanidins (flavan-3-ol oligomers)

Procyanidin monomers:

R<sub>1</sub>=OH, R<sub>2</sub>=R<sub>3</sub>=H: epicatechin  
 R<sub>1</sub>=H, R<sub>2</sub>=OH, R<sub>3</sub>=H: catechin  
 R<sub>1</sub>=gallic acid ester, R<sub>2</sub>=R<sub>3</sub>=H: epicatechin gallate  
 R<sub>1</sub>=H, R<sub>2</sub>=gallic acid ester, R<sub>3</sub>=H: catechin gallate



Prodelphinidin monomers:

R<sub>1</sub>=OH, R<sub>2</sub>=H, R<sub>3</sub>=OH: epigallocatechin  
 R<sub>1</sub>=H, R<sub>2</sub>=OH, R<sub>3</sub>=OH: galocatechin  
 R<sub>1</sub>=gallic acid ester, R<sub>2</sub>=H, R<sub>3</sub>=OH: epigallocatechin gallate  
 R<sub>1</sub>=H, R<sub>2</sub>=gallic acid ester, R<sub>3</sub>=OH: galocatechin gallate

Figure I.3. Structures of some phenolic compounds commonly present in grape and wine. Adapted from Peynaud and Ribéreau-Gayon (1971).

acids (e.g. caffeic, *p*-coumaric) and acetic acid. The 3-glucosides of malvidin, delphinidin, cyanidin, petunidin and peonidin have been identified in grape and wine extracts, as well as some *p*-coumaroyl and caffeoyl derivatives, and some diglucosidic derivatives (Baldi *et al.*, 1995; Wang and Sporns, 1999). Proanthocyanidins (also called condensed tannins) are oligomers of flavan-3-ol monomer units (Figure I.3e). The most common classes are the procyanidins, which are chains of catechins, epicatechins and their gallic acid esters, and the prodelphinidins, which consist of gallocatechin, epigallocatechin and their galloylated derivatives as the monomeric units. In grapes, the bulk of the polymeric flavan-3-ols is found in the seeds, although they are also distributed through the skin and pulp of the fruit. In wines, the normal flavan-3-ol concentration is about 10-50 mg/L in white wine, and 800 mg/L in red wine, although these values significantly depend on many factors such as grape variety, environmental conditions and fermentation practises (Thorngate, 1993). The identification of monomers, dimers, trimers and higher oligomers in grape and wine has been recently carried out by several workers, by coupling liquid chromatography with mass spectrometry (Lazarus *et al.*, 1999; Pascual-Teresa *et al.*, 2000).

Table I.4. Concentration ranges (mg/L) of some phenolics found in white and red wines. Adapted from Goldberg *et al.* (1996), Soleas *et al.* (1997) and Viñas *et al.* (2000).

Phenolic compound	White wine	Red Wine
Gallic acid	<1-2.80	13.08-30.67
Gentisic acid	0.05-0.38	0.44-0.46
Vanillic acid	0.09-0.21	2.3-3.7
Caffeic acid	1.51-5.20	3.15-12.95
<i>p</i> -Coumaric acid	1.57-3.21	2.61-4.5
Ferulic acid	<1-4.42	<1-2.86
Catechin	3.80-4.20	50-213
Epicatechin	1.70-3.80	25-82
Quercetin	n.d.	0.50-5.26
<i>cis</i> -Resveratrol	<0.10	0.27-0.88
<i>trans</i> -Resveratrol	<0.26	0.71-2.50

There is a wide range of methods reported in the literature for the determination of the different phenolic classes described above. The most widely used is high performance liquid chromatography (HPLC), typically performed after some extraction procedure to concentrate the phenolic compounds of interest and free them from others that could

adversely affect the chromatographic resolution (Goldberg and Soleas, 1999). However, besides being laborious and time-consuming, extraction procedures can modify the phenolic composition of samples, due to oxidation, hydrolysis of esters, ethers and glycosidic bonds, and even isomerisation. Therefore, there has been some effort to develop methods that allow direct injection of filtered samples into an HPLC system, usually equipped with a diode array detector (DAD) in the UV/VIS region. Several workers have reported the application of HPLC-DAD to the identification and quantification of low molecular weight wine phenols (Goldberg *et al.*, 1996; Revilla and Ryan, 2000; Viñas *et al.*, 2000; López *et al.*, 2001). Although the method has recognised success, it has, however, some important limitations. A major one is that UV-Vis detection is not very structure specific and the identification of sample compounds relies on the comparison with standard compounds, resulting in ambiguous identification. Moreover, standards are often not available commercially or are very expensive. These problems are especially visible in the case of polymeric compounds with a large structural diversity.

The use of powerful structure elucidation techniques, such as mass spectrometry (MS) and NMR spectroscopy, for characterising the polyphenolic fraction of grape products has also been widely reported. Most studies involve some kind of extraction/purification procedure of the compounds of interest prior to MS and/or NMR analysis. There are several examples regarding the identification of wine pigments, namely anthocyanins and derivatives (Bakker *et al.*, 1997; Wang and Sporns, 1999; Giusti *et al.*, 1999; Mateus *et al.*, 2002). NMR data are also reported for several phenolic acids and flavonoids isolated from grape pomace (Lu and Foo, 1999), whereas Stobiecki (2000) recently reviewed the application of MS techniques to the structural characterisation of flavonoid glycosides. In recent years, the coupling of HPLC to MS and/or NMR has opened new perspectives by combining the advantages of avoiding lengthy sample preparation procedures and providing detailed structural information. HPLC-MS has become a routine technique and has shown to be of great value in the determination of phenolic compounds in grape and wine. Some examples regard the determination of low molecular mass phenols (Pérez-Magariño *et al.*, 1999), anthocyanins (Baldi *et al.*, 1995) and proanthocyanidins (Lazarus *et al.*, 1999; Fulcrand *et al.*, 1999; Pascual-Teresa *et al.*, 2000). The coupling of HPLC to NMR is not as widely used as HPLC-MS, and so far its major applications are in the field of biofluids analysis and drug metabolism. Nevertheless,

there are already a few studies showing the great possibilities of HPLC-NMR and HPLC-NMR/MS in the structure elucidation of plant constituents such as flavonoids (Hansen *et al.*, 1999; Lommen *et al.*, 2000).

In this work, the application of HPLC-NMR/MS to investigate the aromatic composition of grape juice and wine is explored and presented in Chapter VII. These samples have been chosen for analysis since, as briefly described above, they are expected to be rich natural sources of phenolic compounds with important sensorial and health-related properties.

### I.3. Beer: Brewing Process and Chemical Composition

Beer is a fermented beverage made from malted grains (usually barley), hops, yeast and water (Hughes and Baxter, 2001). In addition to malt from barley, other starch- and/or sugar-containing raw materials may be used, such as wheat malt, unmalted cereals called adjuncts, starch flour and fermentable sugars. Fruits, herbs and spices may also be added to give beer a particular character. The beer making process involves several steps that are schematically represented in Figure I.4 and briefly described in the following paragraphs (Belitz and Grosch, 1999; Hughes and Baxter, 2001).

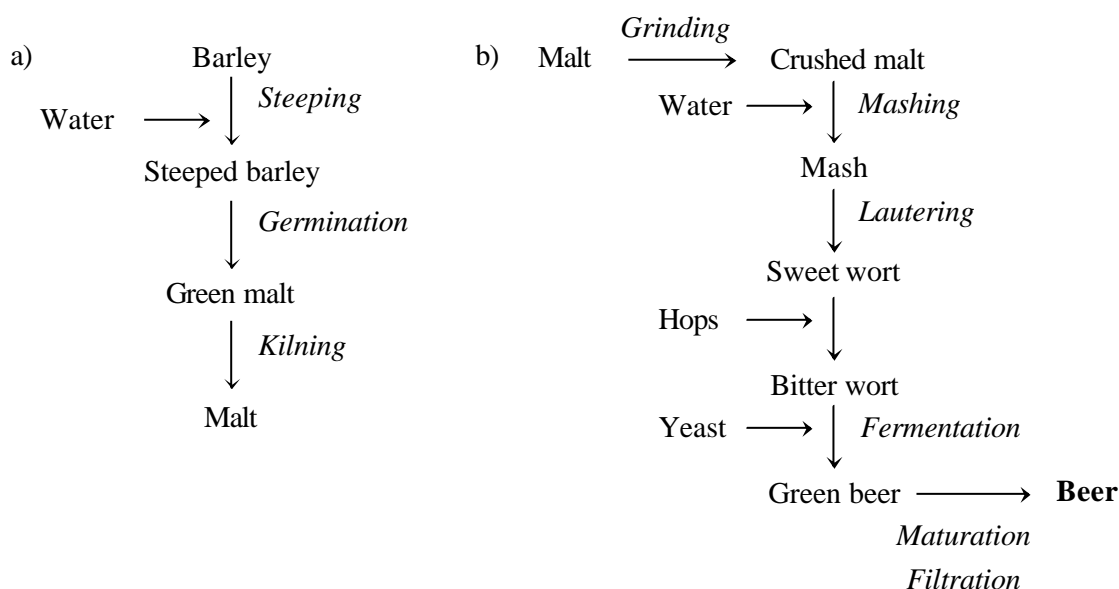


Figure I.4. Simplified flow diagram of the a) malting and b) brewing processes. Adapted from Hughes and Baxter (2001).

In the first step, the malt preparation, the barley is steeped to raise the water content from about 12% to 42-45%, and allowed to germinate for a few days (15-20°C). During this process, the cell walls are digested, part of the high molecular weight, insoluble protein is broken down into smaller fragments, and amylolytic enzymes are synthesised. Most of the starch remains intact. The 'green' malt is then dried in a kiln to prevent further enzyme activity and to produce a stable material (2-3% moisture), which can be safely stored until needed for brewing. The kilning process also forms the colour and roasted aroma of the malt by Maillard reactions.

The wort preparation step involves grinding the malt in a mill, mashing and lautering. During mashing, the malt meal is made into a paste with brewing water and partially degraded and solubilised by malt enzymes (amylases), which break down the starch into fermentable sugars. Cereal starch consists of approximately 75% amylopectin and 25% amylose. Amylopectin is a very large, branched molecule made of glucose units linked by  $\alpha$  (1-4) bonds (which give linear chains) and  $\alpha$  (1-6) bonds (which give branch points). Amylose, on the other hand, is a linear molecule made up of glucose units linked by  $\alpha$  (1-4) bonds only. The enzymes  $\alpha$ - and  $\beta$ -amylase reduce amylose to maltotriose, maltose and glucose, and amylopectin to many small branched dextrans which cannot be further broken down during mashing. The result of the mashing stage is a sweet syrupy liquid known as wort, which is then separated from insoluble remains of the malt in a lauter tun. The wort contains mainly maltose and glucose, which are fermentable, together with significant quantities of small branched dextrans and also some larger straight-chain dextrans.

In the next step, hops or hop extracts are added and the wort is boiled vigorously, so that much of the soluble protein is coagulated and can be separated, and the hops  $\alpha$ -acids are extracted into the wort and isomerised into iso- $\alpha$ -acids, which provide the characteristic bitter taste of beer. After boiling, the coagulated protein and the spent hops are removed (clarification), and the bitter wort is cooled to fermentation temperature.

The fermentation step consists of mixing the cooled wort with yeast (strains of *Saccharomyces*), which takes up amino acids, used for cell growth, and sugars, which are metabolised to ethanol and carbon dioxide. Yeast also produces a number of flavour-active volatile compounds, namely higher alcohols and esters, which vary from strain to strain and give each beer a unique character. There are two main types of fermenting yeasts: top-fermenting and bottom-fermenting. The former are used in the production of ale beers, for

which fermentation is carried out at 16-25°C, and the latter are used for producing lager beers, which are fermented at 6-13°C.

Once the yeast has fermented the available sugars, metabolism slows down and yeast cells flocculate and are removed from the fresh beer. This freshly produced or 'green' beer still contains undesirable flavour compounds, which are eliminated by conditioning. During this time, the small proportion of yeast that remains in contact with the beer produces more carbon dioxide, purging the beer of unwanted volatile compounds. Moreover, the yeast chemically removes certain other flavour-active components. In particular, it catalyses the reduction of vicinal diketones, such as diacetyl, to diols, which are not flavour-active.

After conditioning, the beer may be centrifuged to remove the remaining yeast, then chilled, filtered and packaged in bottles or cans.

The different combinations of ingredients and production processes give rise to an enormous variety of beers, ales and lagers being defined as the two main types according to their fermentation processes (Hughes and Baxter, 2001). As already mentioned, ales are brewed with top-fermenting yeasts at close to room temperatures over some days, and encompass the broadest range of styles, including bitters, porters, stouts, trappist and lambic. Lagers undergo longer and cooler fermentation and tend to be less alcoholic than ales. Bocks and pilsners belong to this type. The alcohol-free and diet beers constitute special types of beer, the production of which involves the application of suitable technology. Alcohol-free beers may be produced in different ways, such as throttling of fermentation and use of special yeasts, reduction of the stemwort content, and elimination of the alcohol formed (distillation, ultracentrifugation). Diet beers are produced by special fermentation processes, in order to contain almost no carbohydrates.

The main constituents of beer are listed in Table I.5 and their typical levels compared to those commonly found in wine and in carbonated soft drinks. It is apparent that beer contains more of some main nutrients (proteins, vitamins, fibre) than other beverages, and thus, can make an important contribution to the diet.

Table I.5. Typical beer composition compared to wine and carbonated soft drinks (Hughes and Baxter, 2001).

	Typical level (g/100 ml)		
	Beer	Wine	Carbonated soft drinks
Water	92-95	85-91	89
Alcohol	2.5-3.5	9-14	0
Total carbohydrates of which free sugars	1.5-3 <0.2	0.1-6.0 0.02	10 10
Fibre	0.3-1.0	negligible	negligible
Total proteins, peptides and amino acids	0.2-0.6	0.02	negligible
Lipids	negligible	negligible	0
Vitamins and other micronutrients	0.002	0.0003	0
Polyphenols and hop compounds	0.002-0.06	0.03-0.074	0

The ethanol content of most beers is between 3.1 and 4.3 (% by volume), but it may range from less than 0.05% in alcohol-free beers to 12.5% in very strong beers. Ethanol contributes directly to the flavour of beer and also plays a role in the flavour perception of other beer components. Thus, the production of low- or non-alcoholic beers is not simply a matter of removal or prevention of the formation of ethanol, but rather requires some form of modification to adjust for the lack of ethanol. Glycerol is the second major alcohol, with concentrations ranging from 1.2 to 2.0 g/L. Other alcohols, such as 1-propanol, 2-methylbutanol, 3-methylbutanol, 2-phenylethanol and tyrosol may be present in small quantities. These alcohols are produced by yeast, mainly as secondary metabolites of amino acid metabolism, and are the immediate precursors of the more flavour-active esters (Hughes and Baxter, 2001).

Besides water and ethanol, carbohydrates are the major components of beer with amounts typically ranging from 1.5 to 3 g/100 ml. These carbohydrates comprise mainly fermentable sugars (e.g. glucose, maltose, maltotriose, fructose, sucrose) and dextrans which are glucose oligosaccharides with varying degrees of polymerisation (DP) and branching patterns. Sugars directly contribute to the sweetness of beer, whereas carbohydrates with more than four glycosyl units possess little sweetness. However, these oligosaccharides can be beneficial to the perception of beer in that they contribute to body or mouthfeel by increasing the viscosity. The amounts of sugars and dextrans vary with the type of beer, as shown in Table I.6. Lagers are usually more fully fermented than ales and

contain less residual carbohydrates. Some beers also contain additional sugars (primings) which are added after fermentation to give a sweeter product or sometimes to balance excessive bitterness from high levels of hops. On the other hand, low carbohydrate beers ('lite beers') contain less carbohydrate due to the digestion and fermentation of dextrans by a combination of techniques, e.g. by using lightly kilned malts, which contain higher levels of debranching enzyme, and special yeasts, which can digest a wider range of dextrans. Several workers have reported the presence of different sugars and dextrans with up to 10 glucose units in the finished beer, by means of chromatographic analysis of degassed, diluted beer (Uchida *et al.*, 1991; Corradini *et al.*, 1997; Déséveaux *et al.*, 1997). Vinogradov and Bock (1998) identified dextrans up to DP 19 and studied their branching and substitution patterns, by using chromatographic separation techniques to obtain beer fractions containing different carbohydrates, followed by the application of sophisticated structure elucidation tools for analysing those fractions, namely NMR spectroscopy and MALDI-TOF mass spectrometry.

Table I.6. Carbohydrates found in different types of beer (Hughes and Baxter, 2001).

Beer type	Carbohydrate (g/100 ml)		
	Sugars (including maltotriose)	Higher dextrans	Total
Ales	0.5-3.0	1-4	1.5-6
Lagers	0.1-0.7	1-2	1-3
Primed beers	1.3-3.6	1-4	2-7
'Lite' beers	0.1-0.6	0.1-0.3	0.2-0.9

The non-starch polysaccharide fraction (dietary fibre) of malt and beer has also been recently investigated using GC and GC-MS methods (Han, 2000). On average, beer contains 0.3-1 g/100 ml of fibre, which is related to beer viscosity and is beneficial for human health because it contributes to the healthy functioning of the large intestine and can lower the levels of cholesterol in the blood serum (Hughes and Baxter, 2001).

Beer typically contains between 0.2 and 0.6 g/100 ml of protein-derived material, mainly originating from the malted barley. Most of this material is in the form of peptides and polypeptides, since the larger proteins are precipitated and removed during the wort boiling stage, and most of the free amino acids in wort are taken up by the yeast during fermentation. Nevertheless, most beers contain all the essential amino acids, at levels

generally between 5 and 10 mg/100 g (Hughes and Baxter, 2001). Proline is the most abundant amino acid present since it cannot be assimilated by yeast, and the amounts of other amino acids vary significantly with the beer type (Klampfl, 1999).

Lipids are present in beer in trace levels, mainly in the form of medium chain fatty acids (e.g. butyric, isovaleric, hexanoic, octanoic and decanoic) (Hawthorne *et al.*, 1986). These acids normally contribute to the characteristic beer flavour, but if present in excessive concentrations have deleterious effects on both flavour and foam.

Beer is a good source of a number of vitamins, niacin, riboflavin, pyridoxine and pantothenic acid being generally the most abundant, as shown in Table I.7. The presence of riboflavin is particularly important with respect to the detrimental effect of light on the aroma of beer, since it acts as a photosensitizer, thereby initiating degradation of beer components and causing the formation of the so-called sunstruck flavour (Andrés-Lacueva *et al.*, 1998; Duyvis *et al.*, 2002).

Table I.7. Vitamin contents in beer (Hughes and Baxter, 2001).

Vitamins	Range (mg/L)
Niacin	3-20
Riboflavin	0.07-1.3
Pyridoxine (B <sub>6</sub> )	0.13-1.7
Folates	0.03-0.10
Biotin	0.007-0.018
B <sub>12</sub>	0.09-0.14
Pantothenic acid	0.5-2.7
Thiamine	0.002-0.14

In what regards the phenolic composition, beer contains a wide range of phenolic compounds, derived both from the hops and the malt. Table I.8 shows the typical levels of some phenolics found in beer. These compounds have an important role in the physical stability and flavour of beer, as they are involved in the formation of haze on storage, and influence the flavour properties of mouthfeel, astringency and bitterness. Moreover, phenolic compounds are known to possess antioxidant activity, potentially beneficial to human health. Therefore, there has been a lot of interest in determining the phenolic composition of foods and beverages containing these substances, including beer (Pascual-Teresa *et al.*, 1998; Whittle *et al.*, 1999; Stevens *et al.*, 1999; Gorinstein *et al.*, 2000).

Table I.8. Phenolic composition of beer (Hughes and Baxter , 2001).

Phenolic compounds	Example in beer	Typical concentration (mg/L)
<u>Monophenols</u>		10-30
phenolic alcohols	tyrosol	
phenolic acids	ferulic acid	
phenolic amines and amino acids	hordenine, tyrosine	
<u>Monomeric Polyphenols</u>		1-23
flavan-3-ols	catechin, epicatechin	
flavan-3,4-diols	leucocyanidin	
flavonols	quercetin	
<u>Condensed Polyphenols</u>		20-140
dimeric and polymeric catechin		
proanthocyanidins	procyanidin B3	
prodelphinidins	delphinidin B3	

The characteristic bitterness of beer is largely attributable to a group of compounds called the iso- $\alpha$ -acids, which result from the isomerisation of hop  $\alpha$ -acids during wort boiling. The general structures of these compounds are shown in Figure I.5. Typical levels of native iso- $\alpha$ -acids in beers are 10-60 mg/L, although extremes do exist outside this range (Hughes and Baxter, 2001). Their determination is a major issue in the brewing industry, but the instability and the similarity in structure of the bitter acids create problems in their analysis. Recently, Pusecker *et al.* (1999) have demonstrated the applicability of the HPLC-NMR coupling for identifying these compounds in various hop products.

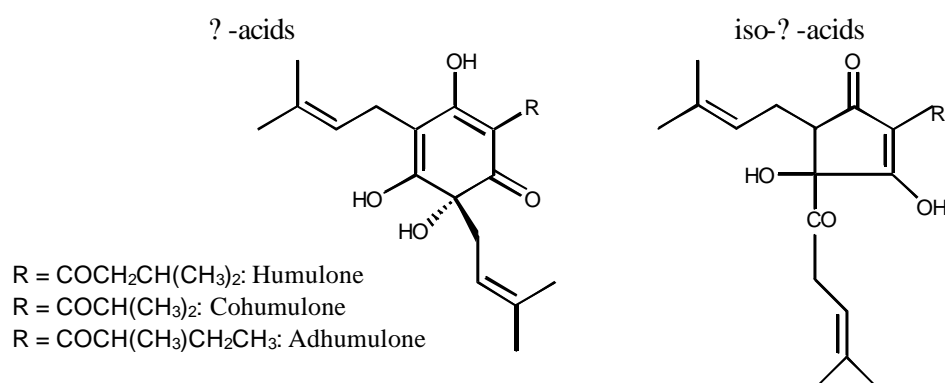


Figure I.5. Structure of hop bitter acids.

Other components play very important roles in the taste and aroma of beer. For instance, organic acids are responsible for the sour taste of beer. The major acids found in beer include acetic, lactic, pyruvic and succinic, with amounts varying between 15 and 200 mg/L (Hughes and Baxter, 2001). Citric and pyroglutamic acids have also been found in significant amounts in some beers (Klampfl, 1999). In respect to aroma, besides the alcohols already mentioned, a wide range of esters, vicinal diketones and sulfur compounds make important contributions. The most abundant ester is usually ethyl acetate (typical levels 10-60 mg/L), but many others are present (e.g. isoamyl acetate, ethyl hexanoate, 2-phenylethyl acetate, etc.). Unlike alcohols and esters, vicinal diketones, of which 2,3-butanedione (diacetyl) is the most abundant, have a negative impact on beer flavour and their elimination is desirable.

The sum and interaction of all the components described above makes beer a very complex mixture, the composition and sensory properties of which vary widely according to the different combinations of ingredients and production processes. In this thesis, the complex composition of beer is tackled by high-resolution NMR and HPLC-NMR/MS, as described in Chapter VIII. Moreover, in Chapter IX, the variability among beers of different labels is investigated by multivariate analysis of NMR and FTIR data.

## References

- Aina, J.O.; Oladunjoye, O.O. Respiration, pectolytic activity and textural changes in ripening african mango (*Irvingia gabonensis*) fruits. *Journal of the Science of Food and Agriculture* **1993**, *63*, 451-454.
- Andrés-Lacueva C.; Mattivi, F.; Tonon, D. Determination of riboflavin, flavin mononucleotide and flavin-adenin dinucleotide in wine and other beverages by high-performance liquid chromatography with fluorescence detection. *Journal of Chromatography A* **1998**, *823*, 355-363.
- Bakker, J.; Bridle, P.; Honda, T.; Kuwano, H.; Saito, N.; Terahara, N.; Timberlake, C.F. Identification of anthocyanin occurring in some red wines. *Phytochemistry* **1997**, *44*, 1375-1382.
- Baldi, A.; Romani, A.; Mulinacci, N.; Vincieri, F.F.; Casetta, B. HPLC/MS application to anthocyanins of *Vitis vinifera* L. *Journal of Agricultural and Food Chemistry* **1995**, *43*, 2104-2109.

Baldwin, E.A.; Burns, J.K.; Kazokas, W.; Brecht, J.K.; Hagenmaier, R.D.; Bender, R.J.; Pesis, E. Effect of two edible coatings with different permeability characteristics on mango (*Mangifera indica* L.) ripening during storage. *Postharvest Biology and Technology* **1999**, *17*, 215-226.

Barcelon, E.G.; Tojo, S.; Watanabe, K. Relating X-ray absorption and some quality characteristics of mango fruit (*Mangifera indica* L.). *Journal of Agricultural and Food Chemistry* **1999**, *47*, 3822-3825.

Belitz, H.-D.; Grosch, W. *Food Chemistry*; 2<sup>nd</sup> Ed.; Springer-Verlag: Berlin, 1999.

Bravo, L. Polyphenols: chemistry, dietary sources, metabolism and nutritional significance. *Nutrition Reviews* **1998**, *56*, 317-333.

Cano, M. P.; Ancos, B. Carotenoid and carotenoid ester composition in mango fruit as influenced by processing method. *Journal of Agricultural and Food Chemistry* **1994**, *42*, 2737-2742.

Corradini, C; Canali, G. Nicoletti, I. Application of HPAEC-PAD to carbohydrate analysis in food products and fruit juices. *Seminars in Food Analysis* **1997**, *2*, 99-111.

Désévaux, S; Daems, V.; Delvaux, F.; Derdelinckx, G. Analysis of fermentable sugars and dextrans in beer by anion exchange chromatography with electrochemical detection. *Seminars in Food Analysis* **1997**, *2*, 113-117.

Duyvis, M.G.; Hilhorst, R.; Laane, C.; Evans, D.J.; Schmedding, D.J.M. Role of riboflavin in beer flavor instability: determination of levels of riboflavin and its origin in beer by fluorimetric apoprotein titration. *Journal of Agricultural and Food Chemistry* **2002**, *50*, 1548-1552.

Ebeler, S.E. Phytochemicals and wine flavor. In *Functionality of Food Phytochemicals*; Johns, T., Romeo, J.T., Eds.; Plenum Press: New York, 1997; 155-178.

El-Zoghbi, M. Biochemical changes in some tropical fruits during ripening. *Food Chemistry* **1994**, *49*, 33-37.

Fulcrand, H.; Remy, S.; Souquet, J.-M.; Cheynier, V.; Moutounet, M. Study of wine tannin oligomers by on-line liquid chromatography electrospray ionization mass spectrometry. *Journal of Agricultural and Food Chemistry* **1999**, *47*, 1023-1028.

Giusti, M.M.; Rodríguez-Saona, L.E.; Griffin, D.; Wrolstad, R.E. Electrospray and tandem mass spectroscopy as tools for anthocyanin characterization. *Journal of Agricultural and Food Chemistry* **1999**, *47*, 4657-4664.

Goldberg, D.M.; Tsang, E.; Karumanchiri, A.; Diamandis, E.P.; Soleas, G.; Ng, E. Method to assay the concentrations of phenolic constituents of biological interest in wines. *Analytical Chemistry* **1996**, *68*, 1688-1694.

- Goldberg, D.M.; Soleas, G.J. Analysis of antioxidant wine polyphenols by high-performance liquid chromatography. *Methods in Enzymology* **1999**, *299*, 122-137.
- Gorinstein, S.; Caspi, A.; Zemser, M.; Trakhtenberg, S. Comparative contents of some phenolics in beer, red wine and white whines. *Nutrition Research* **2000**, *20*, 131-139.
- Guthrie, J.; Walsh, K. Non-invasive assessment of pineapple and mango fruit quality using near infra-red spectroscopy. *Australian Journal of Experimental Agriculture* **1997**, *37*, 253-263.
- Han, J.-Y. Structural characteristics of arabinoxylan in barley, malt and beer. *Food Chemistry* **2000**, *70*, 131-138.
- Hansen, S.H.; Jensen, A.G.; Cornett, C.; Bjornsdottir, I.; Taylor, S.; Wright, B.; Wilson, I.D. High-performance liquid chromatography on-line coupled to high-field NMR and mass spectrometry for structure elucidation of constituents of *Hypericum perforatum* L. *Analytical Chemistry* **1999**, *71*, 5235-5241.
- Hawthorne, D.B.; Jones, R.D.; Barrett, P.A.; Kavanagh, T.E.; Clarke, B.J. Methods for the analysis of C4 to C10 fatty acids in beer, wort and carbohydrate syrups. *Journal of the Institute of Brewing* **1986**, *92*, 181-184.
- Hughes, P. S.; Baxter, E. D. *Beer Quality, Safety and Nutritional Aspects*; The Royal Society of Chemistry: Cambridge, 2001.
- Hulme, A.C. The mango. In *The Biochemistry of Fruits and Their Products*; Hulme, A.C., Ed.; Academic Press: London, 1971; 233-254.
- Idstein, H.; Shreier, P. Volatile constituents of Alphonso mango (*Mangifera indica*). *Phytochemistry* **1985**, *24*, 2313-2316.
- Jacobi, K.K.; Giles, J.E. Quality of Kesington mango (*Mangifera indica* Linn.) fruit following combined vapour heat desinfestation and hot water disease control treatments. *Postharvest Biology and Technology* **1997**, *12*, 285-292.
- Kalra, S.K.; Tandon, D.K.; Singh, B.P. Mango. In *Handbook of Fruit Science and Technology. Production, Composition, Storage and Processing*; Salunkhe, D.K., Kadam, S.S. Eds.; Marcel Dekker Inc.: New York, 1995; 123-169.
- Kanellis, A.K.; Roubelakis-Angelakis, K.A. Grape. In *Biochemistry of Fruit Ripening*; Seymour, G.B., Taylor, J.E., Tucker, G.A., Eds.; Chapman & Hall: London, 1993; 189-234.
- Klampfl, C. Analysis of organic acids and inorganic anions in different types of beer using capillary zone electrophoresis. *Journal of Agricultural and Food Chemistry* **1999**, *47*, 987-990.

Labib, A.A.S.; El-Ashwah, F.A.; Omran, H.T.; Askar, A. Heat-inactivation of mango pectinesterase and polygalacturonase. *Food Chemistry* **1995**, *53*, 137-142.

Lazarus, S.A.; Adamson, G.E.; Hammerstone, J.F.; Schmitz, H.H. High-performance liquid chromatography/mass spectrometry analysis of proanthocyanidins in foods and beverages. *Journal of Agricultural and Food Chemistry* **1999**, *47*, 3693-3701.

Lizada, C. Mango. In *Biochemistry of Fruit Ripening*; Seymour, G.B., Taylor, J.E., Tucker, G.A., Eds.; Chapman & Hall: London, 1993; 255-271.

Lommen, A.; Godejohann, M.; Venema, D.P.; Hollman, P.C.H.; Spraul, M. Application of directly coupled HPLC-NMR-MS to the identification and confirmation of quercetin glycosides and phloretin glycosides in apple peel. *Analytical Chemistry* **2000**, *72*, 1793-1797.

López, M.; Martínez, F.; Valle, C.; Orte, C.; Miró, M. Analysis of phenolic constituents of biological interest in red wines by high-performance liquid chromatography. *Journal of Chromatography A* **2001**, *922*, 359-363.

Lu, Y.; Foo, L.Y. The polyphenol constituents of grape pomace. *Food Chemistry* **1999**, *65*, 1-8.

MacLeod, A.J.; Pieris, N.M. Comparison of the volatile components of some mango cultivars. *Phytochemistry* **1984**, *23*, 361-366.

Mateus, N.; Silva, A.M.S.; Santos-Buelga, C.; Rivas-Gonzalo, J.C.; Freitas, V. Identification of anthocyanin-flavonol pigments in red wines by NMR and mass spectrometry. *Journal of Agricultural and Food Chemistry* **2002**, *50*, 2110-2116.

McLellan, M.R.; Race, E.J. Grape juice processing. In *Production and Packaging of Non-carbonated Fruit Juices and Fruit Beverages*; Ashurst, P.R., Ed.; Blackie Academic & Professional: Glasgow, 1995; 89-105.

Medlicott, A.P.; Thompson, A.K. Analysis of sugars and organic acids in ripening mango fruits (*Mangifera indica* L. var Keitt) by high performance liquid chromatography. *Journal of the Science of Food and Agriculture* **1985**, *36*, 561-566.

Medlicott, A.P.; Reynolds, S.B.; Thompson, A.K. Effects of temperature on the ripening of mango fruit (*Mangifera indica* L. var Tommy Atkins). *Journal of the Science of Food and Agriculture* **1986**, *37*, 469-474.

Mercadante, A.Z.; Rodriguez-Amaya, D.B.; Britton, G. HPLC and mass spectrometric analysis of carotenoids from mango. *Journal of Agricultural and Food Chemistry* **1997**, *45*, 120-123.

Mizrach, A.; Flitsanov, U.; Schmilovitch, Z.; Fuchs, Y. Determination of mango physiological indices by mechanical wave analysis. *Postharvest Biology and Technology* **1999**, *16*, 179-186.

Muda, P.; Seymour, G.B.; Errington, N.; Tucker, G.A. Compositional changes in cell wall polymers during mango fruit ripening. *Carbohydrate Polymers* **1995**, *26*, 255-260.

Nyanjage, M.O.; Wainwright, H.; Bishop, C.F.H. The effects of hot-water treatments in combination with cooling and/or storage on the physiology and disease of mango fruits (*Mangifera indica* Linn.). *Journal of Horticultural Science & Biotechnology* **1998**, *73*, 589-597.

Pascual-Teresa, S. ; Rivas-Gonzalo, J.C.; Santos-Buelga, C. Prodelphinidins and related flavonols in wine. *International Journal of Food Science and Technology* **2000**, *35*, 33-40.

Pascual-Teresa, S.; Treutter, D.; Rivas-Gonzalo, J.C.; Santos-Buelga, C. Analysis of flavonols in beverages by high-performance liquid chromatography with chemical reaction detection. *Journal of Agricultural and Food Chemistry* **1999**, *46*, 4209-4213.

Pérez-Magariño, S.; Revilla, I.; González-SanJosé, M.L.; Beltrán, S. Various applications of liquid chromatography-mass spectrometry to the analysis of phenolic compounds. *Journal of Chromatography A* **1999**, *847*, 75-81.

Pesis, E.; Aharoni, D.; Aharon, Z.; Ben-Arie, R.; Aharoni, N.; Fuchs, Y. Modified atmosphere and modified humidity packaging alleviates chilling injury symptoms in mango fruit. *Postharvest Biology and Technology* **2000**, *19*, 93-101.

Peynaud, E.; Ribéreau-Gayon, P. The Grape. In *The Biochemistry of Fruits and Their Products*; Hulme, A.C., Ed.; Academic Press: London, 1971; 171-205.

Pusecker, K.; Albert, K.; Bayer, E. Investigation of hop and beer bitter acids by coupling of high-performance liquid chromatography to nuclear magnetic resonance spectroscopy. *Journal of Chromatography A* **1999**, *836*, 245-252.

Puttaraju, T.B.; Reddy, T.V. Effect of precooling on the quality of mango (cv. Mallika). *Journal of Food Science and Technology* **1997**, *34*, 24-27.

Revilla, E.; Ryan, J.-M. Analysis of several phenolic compounds with potential antioxidant properties in grape extracts and wines by high-performance liquid chromatography-diode array detection without sample preparation. *Journal of Chromatography A* **2000**, *881*, 461-469.

Sakho, M.; Chassagne, D.; Crouzet, J. African mango glycosidically bound volatile compounds. *Journal of Agricultural and Food Chemistry* **1997**, *45*, 883-888.

Salunkhe, D.K.; Desai, B.B. *Postharvest Biotechnology of Fruits*; CRC Press. Inc: 1984.

Selvaraj, Y.; Kumar, R.; Pal, D.K. Changes in sugars, organic acids, amino acids, lipid constituents and aroma characteristics of ripening mango (*Mangifera indica* L.) fruit. *Journal of Food Science and Technology* **1989**, *26*, 308-313.

Soleas, G.J.; Dam, J.; Carey, M.; Goldberg, D.M. Toward the fingerprint of wines: cultivar-related patterns of polyphenolic constituents in Ontario wines. *Journal of Agricultural and Food Chemistry* **1997**, *45*, 3871-3880.

Spanos, G.A.; Wrolstad, R.E. Phenolics of apple, pear and white grape juices and their changes with processing and storage – a review. *Journal of Agricultural and Food Chemistry* **1992**, *40*, 1478-1487.

Stevens, J.F.; Taylor, A.W.; Deinzer, M.L. Quantitative analysis of xanthohumol and related prenylflavonoids in hops and beer by liquid chromatography-tandem mass spectrometry. *Journal of Chromatography A* **1999**, *832*, 97-107.

Stobiecki, M. Application of mass spectrometry for identification and structural studies of flavonoid glycosides. *Phytochemistry* **2000**, *54*, 237-256.

Thorngate, J.H. Flavan-3-ols and their polymers. In *Beer and Wine Production*; Gump, B.H., Pruett, D.J., Eds.; American Chemical Society: San Francisco, 1993; 51-63.

Tucker, G.A. Introduction. In *Biochemistry of Fruit Ripening*; Seymour, G.B., Taylor, J.E., Tucker, G.A., Eds.; Chapman & Hall: London, 1993; 1-51.

Tucker, G.A.; Seymour, G.B. Cell wall degradation during mango fruit ripening. *Acta Horticulturae* **1991**, *291*, 454-460.

Uchida, M.; Nakatani, K.; Ono, M.; Nagami, K. Carbohydrates in brewing. I. Determination of fermentable sugars and oligosaccharides in wort and beer by partition high-performance liquid chromatography. *Journal of the American Society of Brewing Chemists* **1991**, *49*, 665-673.

Viñas, P.; López-Erroz, C.; Marín-Hernández, J.J.; Hernández-Córdoba, M. Determination of phenols in wines by liquid chromatography with photodiode array and fluorescence detection. *Journal of Chromatography A* **2000**, *871*, 85-93.

Vinogradov, E.; Bock, K. Structural determination of some new oligosaccharides and analysis of the branching patterns of isomaltooligosaccharides from beer. *Carbohydrate Research* **1998**, *309*, 57-64.

Voet, D.; Voet, J.G. *Biochemistry*; John Wiley & Sons, Inc.: New York, 1990.

Wang, J.; Sporns, P. Analysis of anthocyanins in red wine and fruit juice using MALDI-MS. *Journal of Agricultural and Food Chemistry* **1999**, *47*, 2009-2015.

Whittle, N.; Eldridge, H.; Bartley, J. Identification of the polyphenols in barley and beer by HPLC/MS and HPLC/electrochemical detection. *Journal of the Institute of Brewing* **1999**, *105*, 89-99.

Wilson, C.W.; Shaw, P.E.; Knight, R.J. Importance of selected volatile compounds to mango (*Mangifera indica* L.) flavor. In *Proceedings of the 10<sup>th</sup> International Congress of Essential Oils, Fragrances and Flavors*; Lawrence, B.M., Mookherjee, B.D., Willis, B.J. Eds.; Washington, 1986; 283-294.

Wu, J.S.; Chen, H.; Fang, T. Mango juice. In *Fruit Juice Processing Technology*; Nagy, S., Chen, C.S., Shaw, P.E. Eds.; Agscience: Auburnadale, 1993; 620-655.



## II. FUNDAMENTALS OF THE ANALYTICAL METHODS EMPLOYED

II.1. High Resolution Nuclear Magnetic Resonance (NMR) Spectroscopy of Liquids....	34
II.1.1 Principles of NMR Spectroscopy.....	34
II.1.2. NMR Spectral Parameters: Chemical Shift, Spin-Spin Coupling and Signal Area.....	39
II.1.3. Two-Dimensional (2D) NMR Spectroscopy.....	42
II.2. NMR Spectroscopy of Solids.....	50
II.2.1. Nuclear Spin Interactions in Solids.....	50
II.2.2. High Resolution Solid-State NMR Techniques.....	51
II.3. Hyphenated NMR Methods (HPLC-NMR and HPLC-NMR/MS).....	53
II.4. Fourier Transform Infrared (FTIR) Spectroscopy.....	56
II.5. Some Multivariate Analysis Methods.....	59
II.5.1. Principal Components Analysis (PCA).....	60
II.5.2. Partial Least Squares (PLS) Regression .....	61
II.5.3. Canonical Correlation Analysis (CCA).....	62
References.....	62

## II.1. High Resolution Nuclear Magnetic Resonance (NMR) Spectroscopy of Liquids

From its initial development in the 1950s, NMR spectroscopy has seen unprecedented growth and is now one of the most powerful and versatile analytical tools with increasing applications in chemistry, biology, medicine and materials science. The fundamentals and methods of NMR form a vast, complex and evolving discipline. In the present subchapter, a short overview is given, with the purpose of acquainting the reader with a few NMR basics that may aid interpreting the results presented in this thesis. For more details, the books by Harris (1987), Gunther (1995) and Claridge (1999), among many other textbooks, offer a comprehensive description of the NMR principles.

### II.1.1 Principles of NMR Spectroscopy

Nuclear Magnetic Resonance (NMR) spectroscopy detects nuclear-spin reorientation in an applied external magnetic field. For each kind of observed nuclei, the information provided by NMR depends on the electronic environment in which the nuclei are immersed and on the positions of nuclei within molecules. Thus, NMR is a powerful tool for probing molecular structure and dynamics.

The nuclei observable by NMR are those with a spin quantum number  $I$  showing positive half-integer or integer values. When such nuclei are placed under the influence of an external magnetic field of strength  $\mathbf{B}_0$ , applied in a direction defined as  $z$ , an interaction occurs between the magnetic moment of the nucleus,  $\boldsymbol{\mu}$ , and the applied magnetic field (Zeeman interaction). In classical terms, the energy of the nucleus in this situation is described by the vector product:

$$E = -\boldsymbol{\mu} \cdot \mathbf{B}_0 = -\mu_z B_0 = -(\gamma \hbar m_I / 2\pi) B_0 \quad \text{II.1.1}$$

where  $\mu_z$  is the component of  $\boldsymbol{\mu}$  along the direction  $z$ ,  $\gamma$  is the magnetogyric ratio of the nucleus,  $m_I$  is the magnetic quantum number representing the different orientations of  $\boldsymbol{\mu}$  relative to the applied magnetic field  $\mathbf{B}_0$ , and  $h$  is the Planck's constant. In the absence of a magnetic field, the energy of the nucleus is independent of the quantum number  $m_I$ . In the presence of  $\mathbf{B}_0$ , however, there are  $(2I + 1)$  non-degenerate energy levels, corresponding to  $2I + 1$  values of  $m_I$ . For instance, for magnetic nuclei with spin  $I = 1/2$  (e.g.  $^1\text{H}$ ,  $^{13}\text{C}$ ,  $^{15}\text{N}$ ,

$^{19}\text{F}$ ), there will be two possible orientations of the nuclear spin with respect to the static field ( $m_I = \pm 1/2$ ), either parallel (the  $\alpha$ -state) or anti-parallel (the  $\beta$ -state), the former being of lower energy (Figure II.1).

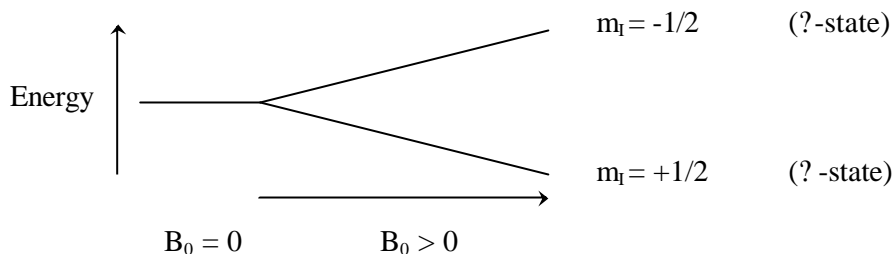


Figure II.1. Energy levels for a nucleus of spin quantum number  $I=1/2$ .

The energy difference  $\Delta E$  between quantised states is:

$$\Delta E = \gamma m_I \hbar / 2 B_0 = \hbar \gamma B_0 \quad \text{II.2}$$

Nuclear magnetic resonance occurs when the nucleus changes its spin state, driven by the absorption of a quantum of energy, applied as electromagnetic radiation. As the selection rule governing these transitions is  $\Delta m_I = \pm 1$ , the resonance condition for NMR is given by:

$$\nu = \gamma / 2\pi B_0 \quad \text{II.3}$$

Another approach to the fundamentals of the magnetic resonance phenomenon consists of describing the effect of the static field on the magnetic moment in terms of classical mechanics, with the field imposing a torque on the moment  $\mu$  and causing the rotation (precession) of its direction in a cone with its axis along  $\mathbf{B}_0$  (Figure II.2a). This motion is referred to as Larmor precession and occurs at a rate  $\omega_0 = -\gamma B_0$  ( $\text{rad s}^{-1}$ ) or  $\nu_0 = -\gamma / 2\pi B_0$  (Hz), the direction being determined by the sign of  $\gamma$ . For the resonance condition to be satisfied, the frequency of the electromagnetic radiation applied must match that of the Larmor precession. In other words, the resonant frequency of a nucleus is simply its Larmor frequency. At the magnetic fields currently applied (up to 21.1 T), the resonant frequencies for protons fall within the radiofrequency region of the electromagnetic spectrum (up to 900 MHz).

Now consider a collection of similar spin-half nuclei (e.g. protons) in the applied static magnetic field. As stated, the orientation parallel to the applied field ( $\alpha$ ) has slightly lower energy than the anti-parallel orientation ( $\beta$ ), so that, at equilibrium, there will be an excess of nuclei in the  $\alpha$  state, as defined by the Boltzmann distribution:

$$N_{\alpha} / N_{\beta} = \exp (-\Delta E/kT) = \exp (-\hbar\gamma B_0/2kT) \quad \text{II.4}$$

where  $N_{\alpha}$  and  $N_{\beta}$  represent the spin populations in the  $\alpha$  and  $\beta$  energy levels,  $k$  is the Boltzmann constant and  $T$  is the temperature of the system. Due to the small value of  $\Delta E$  and hence, the small population difference between the two levels, NMR has an intrinsic low sensitivity, that is further worsened by the low natural abundance of certain nuclei such as  $^{13}\text{C}$  (nat. abund.  $\sim 1\%$ ). The higher the magnetic field, the larger is the separation of the energy levels and their population difference, and thus, the better is the signal-to-noise ratio of the spectrum. The population excess of nuclear spins can be represented as a collection of spins distributed randomly about the precessional cone and parallel to the  $z$ -axis (Figure II.2b). These give rise to a resultant bulk magnetisation vector  $\mathbf{M}_0$  along this axis (Figure II.2c).

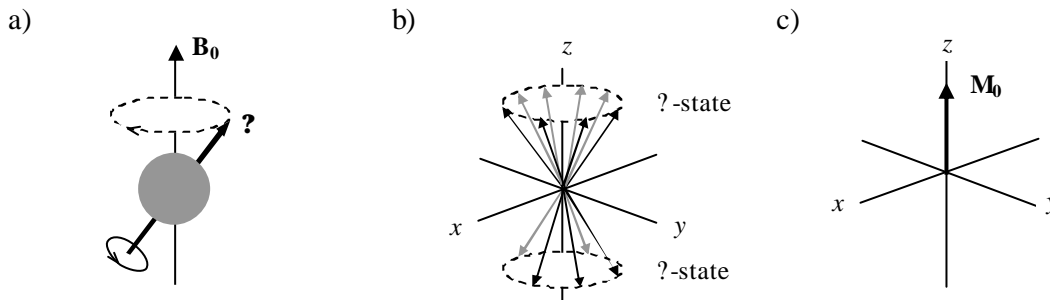


Figure II.2. a) Precession of a magnetic nucleus caused by the applied static magnetic field  $\mathbf{B}_0$ , b) the two precessional cones for a collection of spin-half nuclei in the  $\alpha$ - and  $\beta$ -states and c) the net spin magnetisation  $\mathbf{M}_0$  at equilibrium.

When the sample is subject to a short pulse of radiofrequency (rf) irradiation (typically a few  $\mu\text{s}$ ), with a magnetic component  $\mathbf{B}_1$ , to excite all frequencies of a given nucleus at a time, the net magnetisation  $\mathbf{M}_0$  is shifted away from  $\mathbf{B}_0$  toward the  $x$ - $y$  plane, where it can be detected. This rf is transmitted via a coil surrounding the sample, the geometry of which is such that the  $\mathbf{B}_1$  field exists in the transverse plane, perpendicular to

the static field (Claridge, 1999). Figure II.3 illustrates the effect of the oscillating field  $\mathbf{B}_1$  on the bulk magnetisation vector. This representation is simplified by using a reference frame  $(x', y', z')$  rotating at the frequency  $\omega_0$  around the  $z$ -axis (rotating frame), so that the  $\mathbf{B}_1$  vector appears static. The angle  $\theta$  through which the magnetisation vector  $\mathbf{M}$  turns will be dependent on the amplitude and duration of the pulse. For instance, if the rf is turned off just as  $\mathbf{M}$  reaches the  $y$ -axis, this represents a  $90^\circ$  pulse and the maximum signal intensity is observed. If  $\mathbf{M}$  becomes oriented along the  $-z$ -axis, the pulse is denoted to be a  $180^\circ$  pulse and no signal is observed, since only magnetisation in the  $x$ - $y$  plane is able to induce a signal in the detection coil.

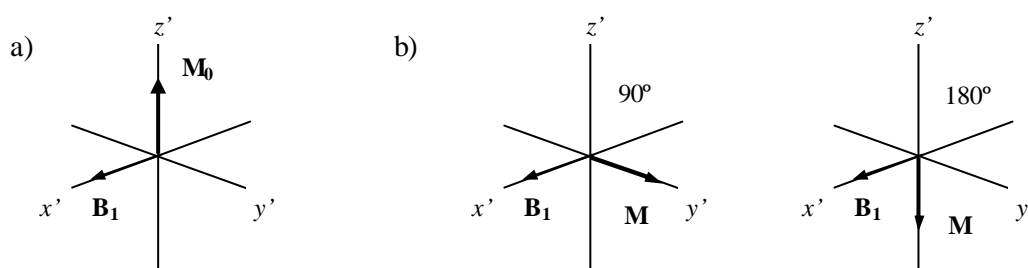


Figure II.3. a) The net spin magnetisation  $\mathbf{M}_0$  under equilibrium conditions and b) the effect of a  $90^\circ$  and a  $180^\circ$  rf pulse on  $\mathbf{M}_0$ .

As soon as the r.f. irradiation is switched off, the system will adjust to re-establish the Boltzmann equilibrium, and so the transverse magnetisation vector will gradually disappear and simultaneously grow along the  $z$ -axis toward its initial value and direction ( $\mathbf{M}_0$ ). This return to equilibrium is referred to as relaxation and it causes the NMR signal to decay with time, producing the observed Free Induction Decay (FID). Fourier transformation (FT) of the accumulated time-domain signal provides the frequency-domain NMR spectrum (Figure II.4).

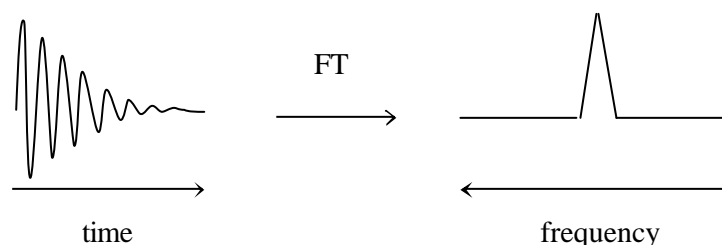


Figure II.4. Fourier transformation of the Free Induction Decay (FID) to the corresponding frequency domain spectrum.

Two relaxation processes may be distinguished: the recovery of magnetisation along the  $z$ -axis, termed longitudinal or spin-lattice relaxation, which involves energy transfer between the spins and the surroundings (lattice) in order to re-establish the equilibrium populations, and the decay of magnetisation in the  $x$ - $y$  plane, termed transverse or spin-spin relaxation, which involves energy transfer within the magnetised spins. Both processes are assumed to follow exponential behaviour, occurring simultaneously but at different rates denoted by  $T_1^{-1}$  and  $T_2^{-1}$ , respectively. The relaxation times  $T_1$  and  $T_2$  are closely related to molecular mobility, characterised by the correlation time  $\tau_c$ , which is the average time required for a molecule to rotate through 1 radian. For nonviscous liquids, containing rapidly tumbling molecules (short  $\tau_c$ ),  $T_1$  and  $T_2$  are identical (Harris, 1987). Values for protons in medium sized organic molecules tend to fall in the range 0.5-5 s (Claridge, 1999). As mobility decreases ( $\tau_c$  increases),  $T_1$  goes through a minimum (at  $\tau_c^2 = \tau_0^{-1}$ , where  $\tau_0$  is the resonance frequency), but  $T_2$  continues to decrease (Figure II.5).  $T_2$  eventually reaches a limiting value when the sample is in the solid state: typical  $T_2$  values are  $\sim 1$  s for a liquid and  $10^{-5}$  s for a solid (Colquhoun and Goodfellow, 1994). As the widths of the NMR resonances are inversely proportional to  $T_2$ , according to  $\Delta\nu_{1/2} = 1/(\pi T_2)$ , the signals of slowly tumbling molecules become rather broad as a result of short  $T_2$  values.

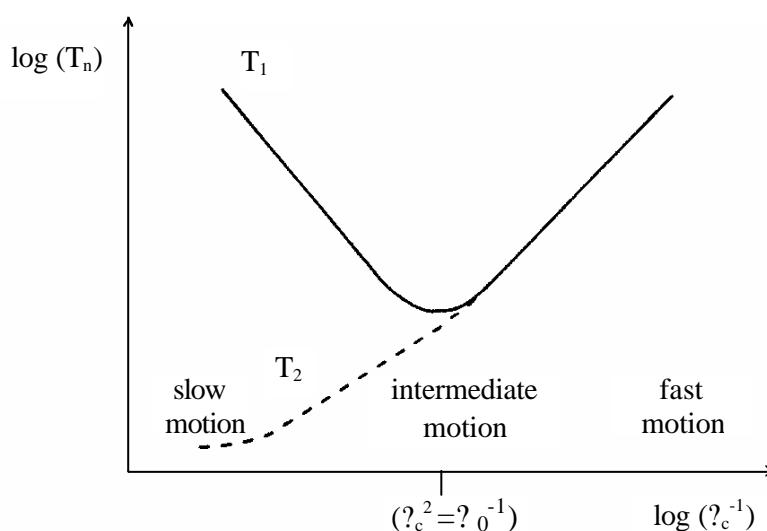


Figure II.5. Schematic representation of the dependence of the relaxation times  $T_1$  and  $T_2$  on the molecular tumbling rates expressed by the correlation time  $\tau_c$ .

## II.1.2. NMR Spectral Parameters: Chemical Shift, Spin-Spin Coupling and Signal Area

There are several parameters that can be readily obtained from the NMR spectra, providing valuable pieces of information for structure determination. These include the chemical shift ( $\delta$  in ppm), spin-spin coupling pattern (multiplicity), coupling constant ( $J$ ) and signal intensity. Nuclei are surrounded by electrons, which shield them from the applied magnetic field  $\mathbf{B}_0$ . The  $\mathbf{B}_0$  field induces currents in these electron clouds and, thus, the effective magnetic field experienced by the nucleus ( $\mathbf{B}_{\text{eff}}$ ) results from the addition of  $\mathbf{B}_0$  and the local magnetic fields produced by the surrounding electrons:

$$\mathbf{B}_{\text{eff}} = \mathbf{B}_0(1 - \sigma) \quad \text{II.5}$$

where  $\sigma$  is a shielding constant that depends on the nature of the electron cloud around the nucleus. Thus, in the case of proton observation for instance, protons at the various sites in the molecule are magnetically shielded to different extents, depending on their chemical environment (neighbouring atoms and type of chemical bonding), so that each site experiences a slightly different magnetic field and has a different position in the NMR spectrum. The position of an NMR signal is measured by its resonance frequency,  $\nu_{\text{sample}}$ , expressed in Hertz (Hz). This value is proportional to the magnetic field strength, depending directly on the operating frequency of the spectrometer. Therefore, the resonance frequency values of a given compound differ between spectra recorded at different field strengths. To overcome this inconvenience, the frequency scale is normalised by using a signal from a reference compound, which for proton is usually tetramethylsilane (TMS) or 3-(trimethylsilyl)propionate (TSP). The dimensionless quantity obtained is the chemical shift, given in parts per million (ppm) and defined as:

$$\delta = \frac{(\nu_{\text{sample}} - \nu_{\text{ref}}) (\text{Hz}) \times 10^6}{\nu_{\text{ref}} (\text{Hz})} \quad \text{ppm} \quad \text{II.6}$$

where  $\nu_{\text{sample}}$  and  $\nu_{\text{ref}}$  are, respectively, the positions, in Hz, observed for the signal of interest and for the reference compound. The chemical shift (in ppm) is thus independent of the measuring magnetic field strength. Some typical ranges of chemical shift values for

$^1\text{H}$  and  $^{13}\text{C}$  nuclei in chemical groups commonly occurring in natural and biological compounds are listed in the Table II.1.

Table II.1. Chemical shift (?) ranges for  $^1\text{H}$  and  $^{13}\text{C}$  in some common chemical groups (adapted from Fan, 1996).

$^1\text{H}$ chemical shifts		$^{13}\text{C}$ chemical shifts	
Chemical group	? (ppm)	Chemical group	? (ppm)
C-CH <sub>3</sub>	0.7-1.1	-CH <sub>3</sub> (methyl)	8-30
=C-CH <sub>3</sub>	1.5-1.8	-CH <sub>2</sub> (methylene)	14-55
COCH <sub>3</sub> (acetyl)	2.0-2.5	-CH- (methine)	22-60
N-CH <sub>3</sub>	2.5-3.3	-C- (quaternary)	30-40
O-CH <sub>3</sub>	3.3-4.3	CH <sub>2</sub> =C-R	100-150
C-CH <sub>2</sub> -C	1.3-2.5	C=C-C=C-R	110-150
O-CH <sub>2</sub> -C	4.0-5.0	Heteroaromatic ring	100-165
C-CH-OH	3.3-4.0	C-OH (alcohol)	44-85
C-CH-O-ester	4.2-5.3	C-O-C (ether)	55-85
=CH-C (olefinic)	5.5-8.5	R-COOH (saturated)	165-188
Aromatic ring	6.0-9.0	R-C=C-COOH	158-174
-CHO (aldehyde)	9.0-10.2	R-COOR' (saturated)	158-178
-COOH	10.5-13.5	R-C=C-COOR'	152-172
C-OH (alcohol)	1.5-6.0	R-CHO (saturated)	196-220
C-OH (phenol)	6.5-18.5	R-C=C-CHO	176-195
Primary amines	1.1-1.8	Saturated ketones	195-220
Secondary amines	1.2-2.1	C-N-R <sub>2</sub>	20-70
CO-NH	5.0-6.5	R-CO-NH <sub>2</sub>	150-178

The interaction between neighbouring magnetic nuclei within a molecule is referred to as spin-spin or scalar coupling and causes the splitting of NMR signals into multiplets. This interaction is transmitted indirectly via the electrons in chemical bonds and arises because the effective magnetic field of each nucleus is sensitive to the spin state of its neighbours. The multiplicity of a signal, i.e. the number of peaks in the split signal, is given by  $2nI + 1$ , where  $n$  is the number of neighbouring equivalent nuclei and  $I$  the spin quantum number. The line separations in Hz correspond to the coupling constants ( $J$ ) between the nuclei under consideration, and are independent of the magnetic field strength. For spin-half nuclei in first-order coupling patterns, i.e. when the chemical shift differences are much larger than the scalar coupling constants ( $\Delta\delta/J \gg 10$ ), the intensity of the peaks is determined according to the probability of the spin magnetisations of the neighbours to occur, following the binomial distribution of the Pascal triangle. For example, doublets,

triplets and quartets with intensity ratios 1:1, 1:2:1 and 1:3:3:1 represent first-order coupling from one, two and three chemically equivalent nuclei, respectively. As  $\nu/J$  becomes smaller, splitting patterns become more complex and difficult to analyse.

The coupling constant ( $J$ ) associated with each multiplet is dependent on a number of factors, including the number of intervening bonds, bond order, bond angle, bond length, types of coupled nuclei, electronegativity of attached substituents, extent of  $\pi$ -conjugation and aromatic substituents. Therefore, this parameter is very valuable to aid structure elucidation.  ${}^nJ$  denotes the coupling constant between nuclei separated by  $n$  bonds and, generally,  ${}^nJ$  decreases as the number of bonds between the coupled nuclei increases. For proton-proton coupling the  $J_{\text{H-H}}$  values lie between about  $-20$  and  $+20$  Hz (Hesse *et al.*, 1997). As for the heteronuclear coupling between  ${}^1\text{H}$  and  ${}^{13}\text{C}$ ,  ${}^1J_{\text{C-H}}$  ranges from 100 to 320 Hz, while  ${}^2J_{\text{C-H}}$  ranges from  $-20$  to 70 Hz (Hesse *et al.*, 1997). The  ${}^1\text{H}$ - ${}^{13}\text{C}$  coupling originates the so-called carbon satellites in the  ${}^1\text{H}$  spectrum, however, due to the low relative abundance of  ${}^{13}\text{C}$ , these peaks are often not noticeable.

For  ${}^1\text{H}$  spectra of isotropic liquids, the area under a signal, measured by integration, is proportional to the number of nuclei giving rise to that signal, provided that adequate experimental conditions are employed. A critical factor to obtain quantitative spectra is to allow for the spins to fully relax between pulses so that the observed signal intensities are not diminished by incomplete recovery of the magnetisation between acquisitions. This condition demands recycle times of at least  $5T_1$  between pulses, where  $T_1$  is the longest relaxation time found in the sample. The second fundamental requirement is for the data be sufficiently well digitised for the lineshape to be defined properly, and so, adequate spectral widths should be used. Processing of the spectra is also important to enhance the quantification results (Martin, 1995). The use of a matched exponential window will help to ensure sufficient digitisation and zero-filling will further assist the definition of the lineshape. Moreover, careful phasing of the spectrum is essential, in order to minimise deviations from pure absorption-mode lineshapes. Another potential source of error arises from distortions of the spectrum baseline. The integral of a signal, especially of signals with low S/N ratio, is very sensitive to small changes in the baseline of the spectrum. Therefore, it is very important to correct for baseline offset and distortions in a consistent way for the series of spectra to be compared. A final consideration regards the integration

limits. For a Lorentzian line, the tails extend a considerable distance from the centre and the integral should, ideally, cover 20 times the line width each side of the peak if it is to include 99% of it. For proton observation, this is likely to be 10-20 Hz each side (Claridge, 1999). However, in practice, this is sometimes not possible due to the proximity or even partial overlapping of other signals.

Having taken the precautions mentioned above, integration of the  $^1\text{H}$  NMR signals in the 1D spectrum of the sample can provide quantitative information on the sample components. If an internal reference compound is used, then absolute quantification should also be possible. If the area  $F_A$  corresponds to  $n_A$  protons of the internal reference A (as determined by the structural formula) and the area  $F_B$  similarly corresponds to  $n_B$  protons of substance B, then the molar concentrations  $C$  in the solution being measured are given by:

$$C_A / C_B = F_A n_B / F_B n_A \quad \text{II.7?}$$

The choice of the internal reference compound is of critical importance for the success of NMR quantitative analysis. There are some essential prerequisites that must be fulfilled: the reference compound must be stable at the temperature range used, soluble and inert, showing no physical interaction or chemical reaction with the sample; moreover, signals of the reference should not overlap with those of the sample components.

The quantitative analysis of complex mixtures, such as the food samples analysed in this work, involves additional problems, namely the possibility of physical or chemical interactions within the sample components and between these and the reference compound, leading to molecular hindrance and consequent loss in the signals areas. Moreover, overlapping of the peaks arising from the many sample components may severely hinder integration measurements.

### II.1.3. Two-Dimensional (2D) NMR Spectroscopy

The first tool generally used to assign the NMR signals of a complex mixture consists of comparing chemical shifts, spin-spin coupling patterns (multiplicity) and coupling constants ( $J$ ) data, measured in the 1D spectrum, with data compiled in the literature for common metabolites (Pretsch *et al.*, 1989; Nicholson *et al.*, 1995; Fan, 1996) and with spectra of reference compounds that are expected to be present in the sample.

However, the  $^1\text{H}$  spectra of such mixtures (e.g. food and biological samples) are often rather complex and signal assignment is hindered by the high degree of spectral overlap. In most cases, it is not possible to observe all the signals arising from one molecule and the determination of multiplicities and coupling constants is very difficult. In addition, care must be taken in utilizing literature values since they depend on several factors such as the pH, the solvent and the chemical shift reference used, and these conditions are often not reported.

Two-dimensional (2D) NMR methods provide a more valuable approach to carry out spectral assignment, as the information is spread in two dimensions and spectral overlap is significantly reduced. 2D methods and other multidimensional NMR methods are continuously being developed and form a vast area of NMR spectroscopy. It is not the purpose of this subchapter to give an exhaustive review on this subject, which can be found in several standard textbooks (Gunther, 1995; Braun *et al.*, 1998; Claridge, 1999), but rather to introduce the general scheme of a 2D experiment and describe briefly the 2D methods used in this work.

All 2D sequences have the same basic format and can be subdivided into four well defined units termed the *preparation*, *evolution*, *mixing* and *detection* periods (Figure II.6). The preparation and mixing periods typically comprise a pulse or a cluster of pulses and/or fixed time periods, the details of which vary depending on the nature of the experiment. The detection period is entirely analogous to the detection period of any 1D experiment, during which the spectrometer collects the FID of the excited spins. It is the evolution period that provides the key to the generation of the second dimension. The state of the spin system after a certain time  $t_1$  is generally altered by at least one further rf pulse. The resonance signal is then recorded during the subsequent detection time,  $t_2$ . The entire experiment is repeated with an increment evolution time  $t_1$ , whereby the initial state of the nuclear spin system during the detection period at  $t_2 = 0$  changes accordingly. After data collection, the FIDs are transformed with respect to  $t_2$  to obtain a set of spectra in which the peak intensities or phases are modulated as a function of the  $t_1$  delay. Fourier transformation with respect to  $t_1$  converts the frequency modulation into peaks in the 2D spectrum, generally represented as a contour plot.

There are essentially two classes of 2D NMR experiments: 1) *correlated* experiments, in which the resonance frequency of one peak is related to those of its

neighbours and thus molecular connectivities or distances between atoms can be determined, and 2) *resolved* experiments, in which the frequency axes show two different interactions; for example, in 2D  $J$ -resolved spectra one axis contains coupling constant information while the other has the chemical shift data. Both types of experiments have been used in this thesis to aid spectral assignment of the complex food mixtures analysed. The basic principles of each 2D method used are briefly presented in the next paragraphs, starting by the simplest homonuclear correlation method employed.

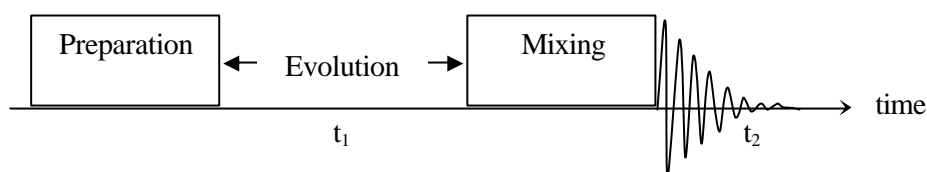


Figure II.6. General scheme for a 2D experiment, showing the different steps as a function of time.

The COSY (COrrelation SpectroscopY) experiment (Aue et al., 1976a) correlates the chemical shifts of nuclei (typically protons) that share a mutual  $J$ -coupling by utilising the sequence shown in Figure II.7a. The basis of this experiment is the process of coherence transfer in which magnetisation is transferred between  $J$ -coupled spins during the mixing part of the sequence. The outcome of this process in the final COSY spectrum may be explained as follows: consider the case of two  $J$ -coupled spins, A and X, with a coupling constant  $J_{AX}$  and chemical shifts offsets  $\nu_A$  and  $\nu_X$ . After the initial  $90^\circ$  pulse, the magnetisation associated with spin A will precess during  $t_1$  according to its chemical shift offset  $\nu_A$ . The second  $90^\circ$  pulse then transfers some part of this magnetisation to the coupled X spin, whilst some remains associated with the original spin A. That which remains with A will then precess in the detection period  $t_2$  at a frequency  $\nu_A$ , just as it did during  $t_1$ , so in the final spectrum it will produce a peak at  $\nu_A$  in both dimensions, denoted  $(\nu_A, \nu_A)$ , which sits on the diagonal of the 2D spectrum. In contrast, the transferred magnetisation will precess in  $t_2$  at the frequency of spin X, and will thus produce a peak corresponding to two different chemical shifts in the two dimensions  $(\nu_A, \nu_X)$ . This peak sits away from the diagonal, being referred to as an off-diagonal peak (or crosspeak), and provides direct evidence of coupling between spins A and X. The same arguments apply for the magnetisation originally associated with the X spin, giving rise to a diagonal peak

at  $(\nu_X, \nu_X)$  and a crosspeak at  $(\nu_X, \nu_A)$ . The COSY spectrum is thus symmetrical about the diagonal, with cross peaks on either side of it, as schematically illustrated in Figure II.7b. Most proton-proton couplings operate over two or three bonds, so the proton COSY spectrum typically identifies vicinal and geminal relationships.

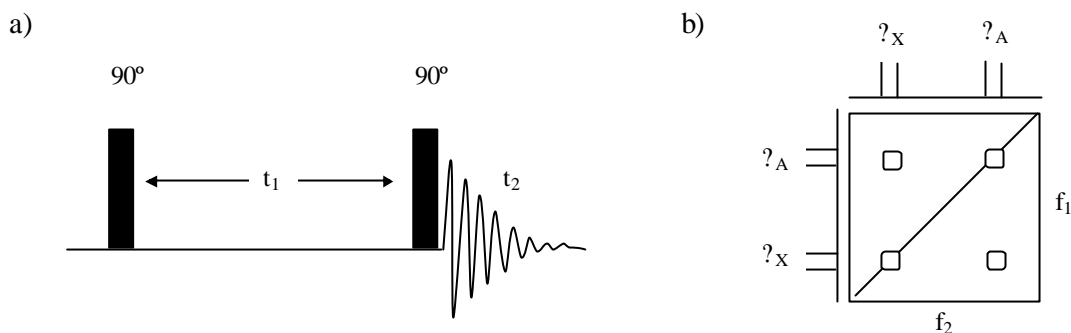


Figure II.7. a) Basic COSY pulse sequence and b) COSY spectrum of a coupled AX spin system.

The TOCSY (TOtal Correlation SpectroscopY) experiment (Braunschweiler *et al.*, 1983) also correlates homonuclear scalar-coupled spins, but is also able to establish correlations between protons that, although not sharing mutual coupling, reside in the same spin-system and form a continuous chain of spin-spin coupled protons. The TOCSY sequence (Figure II.8a) allows the magnetisation to propagate along this chain by relaying coherence from one proton to the next. Compared to the COSY sequence already shown (Figure II.7a), the only difference is the use of a mixing pulse sequence, referred to as the spin-lock sequence, instead of a single mixing pulse. The purpose of this is to execute the relayed magnetisation transfer mentioned above.

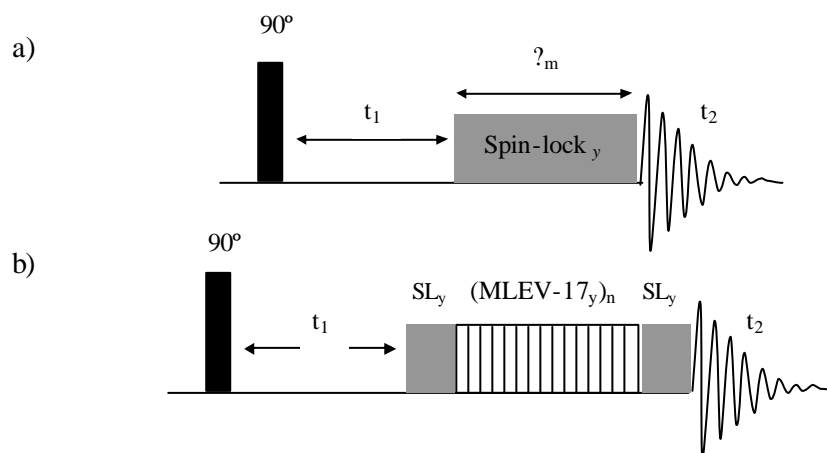


Figure II.8. a) Basic TOCSY pulse sequence using a continuous low-power pulse as spin-lock and b) TOCSY sequence with the MLEV-17 mixing scheme.

To understand the action of the spin-lock period in the TOCSY experiment, consider the sequence of events during the first transient ( $t_1 = 0$ ). The spins are first excited with a  $90^\circ$  pulse along the  $x$ -axis so that they all lie along the  $y$ -axis in the rotating frame. At this point, the spin-lock field is applied parallel to the nuclear vectors, spin-locking them along the  $y$ -axis. During this mixing period, all protons experience the same effective field, so that all chemical shift differences in the rotating frame are removed, although spin-spin couplings remain active. This corresponds to a strong coupling condition ( $\Delta \nu \ll J$ ), under which there exists oscillatory exchange of coherence between protons, leading to a propagation of magnetisation along the chain of coupled spins. This requirement for nuclei to experience identical local fields for magnetisation transfer to occur between them is also referred to as the Hartmann-Hann match. Since magnetisation may travel in either dimension along a spin-chain, 2D TOCSY spectra are again symmetrical about the diagonal. For short mixing times of about 20 ms, only single-step transfers have significant intensity and the correlations seen are equivalent to those seen in COSY. Longer mixing periods enable magnetisation to travel further along the coupled chain and peaks arising from multi-steps transfers appear. However, the use of very long mixing times also leads to sensitivity losses due to relaxation (in the rotating frame) of the spin-locked magnetisation.

Although in its simplest form the spin-lock is a continuous low-power pulse of constant phase, in practice, this is replaced with an extended sequence of composite  $180^\circ$  pulses which extend the effective bandwidth without excessive power requirements. One of these sequences, which was used for recording the TOCSY spectra shown in this thesis, is the so called MLEV-17 sequence (Malcom Levitt's composite-pulse decoupling sequence), in which an even number of cycles through the MLEV-17 sequence are used to produce the desired total mixing period (Figure II.8b) (Bax and Davis, 1985). This implementation also comprises the use of spin-lock trim-pulses (SL) applied for 2-3 ms along one chosen axis, so that magnetisation not parallel to this axis is eliminated before and after the transfer sequence. The purpose of this is to ensure the collection of absorption-mode data, eliminating dispersive contributions to the spectrum.

Heteronuclear shift correlation methods have also been employed to establish correlations between  $^1\text{H}$  and  $^{13}\text{C}$  chemical shifts. In particular, the HMQC (Heteronuclear Multiple-Quantum Correlation) and HSQC (Heteronuclear Single-Quantum Correlation)

methods have been used. Both experiments correlate coupled heteronuclear spins across a single bond, hence identifying directly connected nuclei, and employ detection of the high-sensitivity nucleus (e.g.  $^1\text{H}$  instead of  $^{13}\text{C}$ ). This inverse detection allows a major improvement in the sensitivity of the experiment.

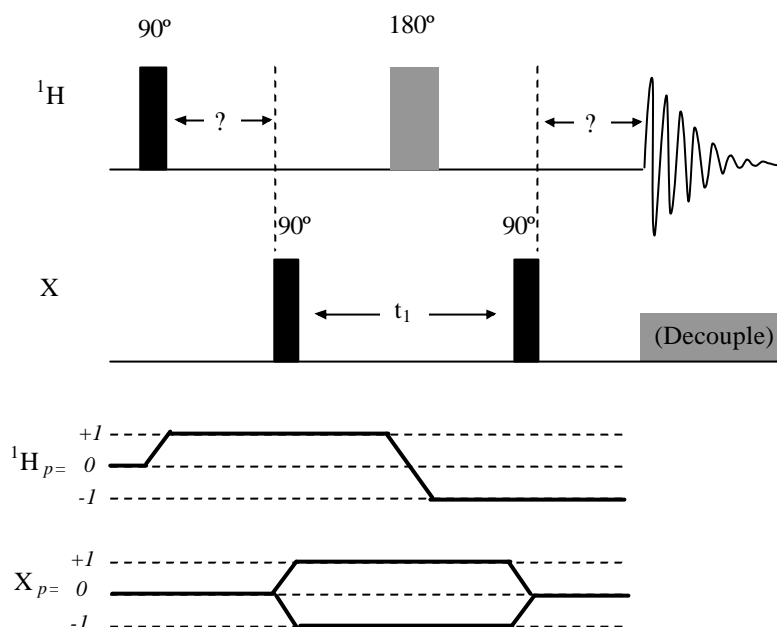


Figure II.9. Basic HMQC pulse sequence and associated coherence transfer pathway (Bax *et al.*, 1983; Claridge, 1999).

The basic HMQC sequence (Bax *et al.*, 1983), shown in Figure II.9, comprises four rf pulses, the operation of which is considered here for a simple  $^1\text{H}$ - $^{13}\text{C}$  spin pair. The sequence starts with proton excitation followed by a period  $\tau$  set to  $1/(2J_{\text{CH}})$ , during which antiphase proton magnetisation develops with respect to  $J_{\text{CH}}$ . Then, the first carbon pulse generates proton-carbon multiple-quantum coherence, the proton magnetisation being transferred to its directly bound carbon. This coherence is, in fact, a combination of both heteronuclear double- and zero-quantum coherence, as represented by the coherence level diagram shown in the Figure. In order for such coherences to evolve during the subsequent period  $t_1$  under the influence of carbon chemical shifts only, a spin-echo is incorporated by placing a  $180^\circ$  proton pulse at the midpoint of  $t_1$ . In this way, at the end of the evolution period  $t_1$ , the proton shifts have refocused and thus have no influence in  $f_1$ . Evolution of the carbon shifts is unaffected by the proton pulse, so these remain to produce the desired frequency labelling. The final carbon pulse then reconverts the multiple-quantum

coherence back to observable single-quantum proton magnetisation. To avoid cancellation of the antiphase proton satellites, a second  $\tau$  period is inserted to refocus the proton-carbon coupling, after which the proton magnetisation is detected. When collecting the proton FID, it is generally desirable to apply broadband decoupling of the carbon spins to remove the  $J_{\text{CH}}$  doublet fine structure, thus doubling the S/N ratio. Conventional quadrature detection in  $f_1$  is implemented by incrementing the phase of the carbon pulse prior to  $t_1$ , according for instance to the TPPI procedure, to yield a phase-sensitive display. The result is a 2D spectrum with  $^1\text{H}$  shifts in  $f_2$  and  $^{13}\text{C}$  shifts in  $f_1$  and crosspeaks indicating one-bond connectivities.

The HSQC experiment (Bodenhausen and Ruben, 1980) differs from HMQC in that only single-quantum transverse magnetisation of the heteronuclear spins evolves during the  $t_1$  period rather than multiple-quantum coherence (Figure II.10). Consequently, the cross peaks in the HSQC spectrum do not contain homonuclear  $^1\text{H}$ - $^1\text{H}$  couplings along  $f_1$ . This results in improved resolution in this dimension, the principal advantage of HSQC over HMQC for small molecules. The most notable disadvantage is the greater number of pulses it utilises, promoting intensity losses from rf inhomogeneity, pulse miscalibration or off-resonance excitation.

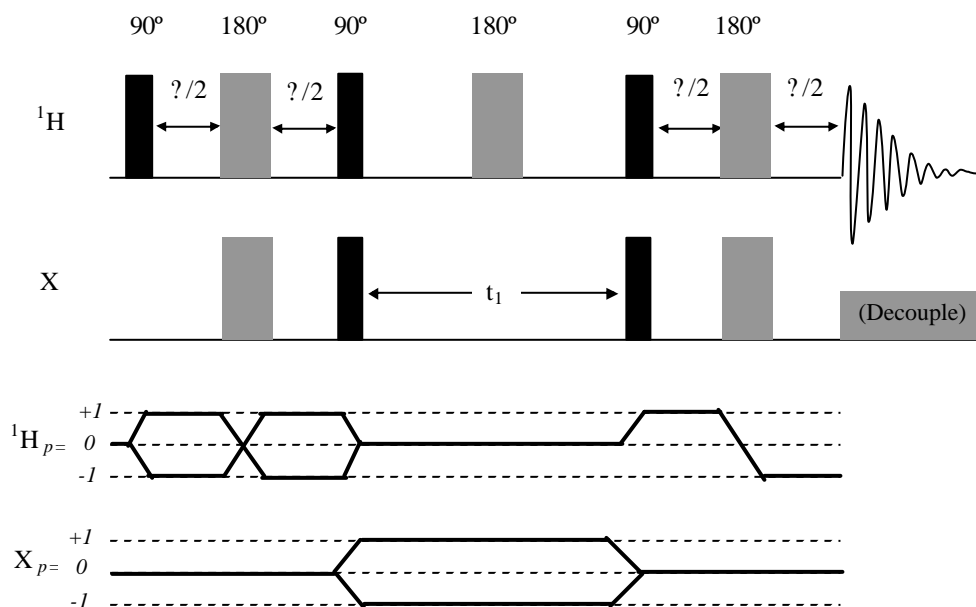


Figure II.10. Basic HSQC pulse sequence and associated coherence transfer pathway (Bodenhausen and Ruben, 1980; Claridge, 1999).

While the correlation methods described above exploit scalar couplings to correlate the chemical shifts of interacting spins,  $J$ -resolved spectroscopy aims to separate chemical shifts from scalar couplings, which may be heteronuclear or homonuclear depending on the details of the experiment. In this work, only homonuclear proton  $J$ -resolved spectroscopy has been employed to provide direct measurement of  $^1\text{H}$ - $^1\text{H}$  coupling constants, and thus only this experiment is described here.

As shown in Figure II.11a, the homonuclear  $J$ -resolved experiment (Aue *et al.*, 1976b) employs a spin-echo sequence during the evolution time  $t_1$  to make the detected FIDs insensitive to chemical shift evolution during  $t_1$ , so that the  $f_1$  dimension only contains coupling information. Indeed, the  $180^\circ$  pulse at the midpoint of the evolution time refocuses proton shifts but not homonuclear couplings, which appear in  $f_1$ . On the other hand, the  $f_2$  dimension contains both chemical shift and coupling constant information, since one cannot simultaneously broadband decouple and observe the proton spectrum. To overcome this feature, which complicates interpretation of the 2D  $J$ -resolve spectra, post-processing techniques are employed, namely by ‘tilting’ the multiplets through an angle of  $45^\circ$  about their midpoints, as illustrated schematically in Figure II.911b.

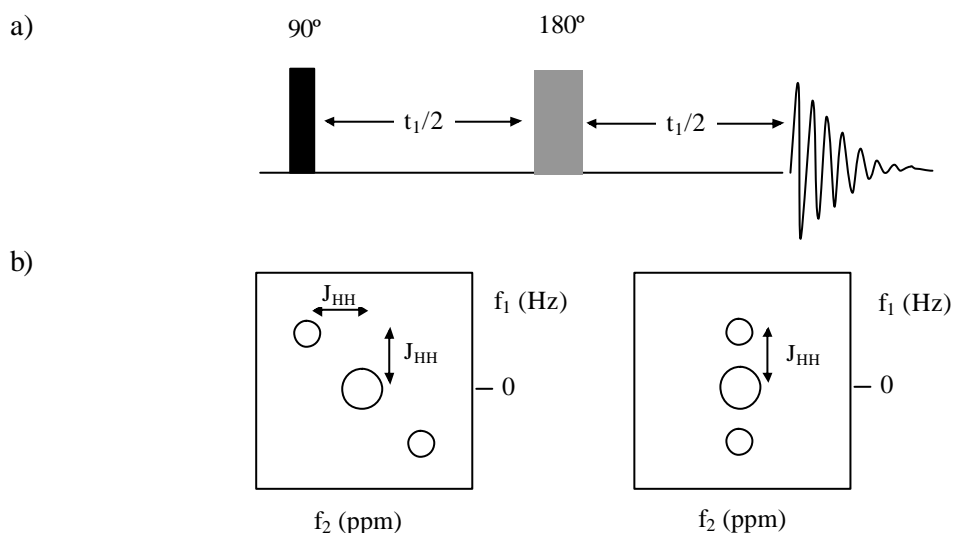


Figure II.11. a) Basic homonuclear  $J$ -resolved pulse sequence and b) schematic representation of the tilting procedure for eliminating homonuclear couplings from the  $f_2$  dimension.

## II.2. NMR Spectroscopy of Solids

### II.2.1. Nuclear Spin Interactions in Solids

Liquid state NMR spectra are dominated by the Zeeman interaction with the external magnetic field  $\mathbf{B}_0$  ( $\hat{H}_Z$ ), the chemical shift interaction ( $\hat{H}_{CS}$ ), and the scalar spin-spin interaction ( $\hat{H}_{SC}$ ) and, thus, the Hamilton operator for a nucleus with spin  $I$  in the liquid domain is defined by the following expression:

$$\hat{H} = \hat{H}_Z + \hat{H}_{CS} + \hat{H}_{SC} \quad \text{II.8?}$$

Due to the rapid tumbling of the molecules, these interactions are isotropic, producing discrete average values for chemical shifts and coupling constants.

In the solid state there are additional mechanisms that have to be considered (Fyfe, 1983; Harris, 1987; Gunther, 1995). These are the anisotropy of the chemical shift interaction ( $\hat{H}_{CS}$ ), dipole-dipole interactions ( $\hat{H}_D$ ) and quadrupolar interactions ( $\hat{H}_Q$ ), the latter occurring only for nuclei with spin  $I > 1/2$  and arising from the interaction of the nuclear electric quadrupole moment with the non spherically symmetrical electric field gradient around the nucleus. Thus, a general Hamiltonian for the interactions experienced by a nucleus of spin  $I$  in the solid state may be written as follows:

$$\hat{H} = \hat{H}_Z + \hat{H}_{CS} + \hat{H}_{SC} + \hat{H}_D + \hat{H}_Q \quad \text{II.9?}$$

The critical feature of these interactions is that they are anisotropic in the solid due to the relatively fixed orientations of the molecules. Consequently, they impose a dependence on the NMR frequency based on the molecular orientation with respect to the main magnetic field direction, and lead to the broadening of spectral lines. The typical magnitudes of these interactions are listed in Table II.2.

Table II.2. Typical magnitudes of nuclear spin interactions in the solid state (Fyfe, 1983).

Type of interaction	Magnitude (Hz)
Zeeman	$10^6 - 10^9$
Chemical Shift	$0 - 10^5$
Scalar Coupling	$0 - 10^4$
Dipole-dipole	$0 - 10^5$
Quadrupolar	$0 - 10^9$

Another important source of line broadening in the spectra of solid samples is the effect of variations in local bulk magnetic susceptibility (Belton and Gil, 1996; Eads, 1999). This is particularly relevant in heterogeneous materials, such as food and biological samples, which contain regions of significantly different bulk magnetic susceptibilities, thus being magnetised to different extents when subject to the applied magnetic field and leading to spectral broadening. This effect is better understood in terms of the simplest case of a thin liquid shell surrounding a spherical particle of higher magnetic susceptibility: nuclear spins in liquid molecules near the surface experience an additional field and thus a higher frequency than distant liquid nuclear spins. Therefore, the liquid NMR spectrum becomes a sum of resonances, whose frequency distribution is given by the field distribution. In this case, the maximum broadening may be approximated by:

$$\Delta\nu \sim 2\chi\gamma\mathbf{B}_0 \quad \text{II.10}$$

where  $\chi$  is the difference in bulk magnetic susceptibilities of particle and liquid (dimensionless),  $\gamma$  is the magnetogyric ratio (Hz/tesla) of the observed nucleus and  $\mathbf{B}_0$  is the magnetic field strength (tesla) (Eads, 1999). This broadening may range from tens to thousands of Hz, depending on the factors shown in equation II.10.

### **II.2.2. High Resolution Solid-State NMR Techniques**

Particular techniques have been developed to obtain highly resolved NMR spectra of solids, which rely on the ability to average the interactions described above on a timescale that is rapid compared to the spectral line widths. The importance of those interactions depends on the nucleus being observed and on the system under study, and the experimental concepts behind the different techniques vary accordingly.

One of the most ingenious techniques especially developed for solid state NMR spectroscopy is the Magic Angle Spinning (MAS) technique, which in this thesis has been used to record  $^1\text{H}$  spectra of mango fruit intact pulp. The basic principle of MAS is to simulate the effect of molecular tumbling in solution state, thus reducing the broadening effects of chemical shift anisotropy (CSA) and dipolar interactions (Fyfe, 1983; Harris,

1987). These interactions have an angular dependence on the factor  $(3\cos^2\theta - 1)$ , where  $\theta$  is the angle between the internuclear vector and the direction of the static field.

The technique of MAS consists of spinning the sample around an axis at an angle  $\theta$  of  $54.74^\circ$  (the magic angle) to the applied magnetic field  $B_0$  (Figure II.12). Since  $3\cos^2\theta - 1 = \frac{1}{2}(3\cos^2\theta - 1)(3\cos^2\theta - 1)$ , and the factor  $(3\cos^2\theta - 1)$  is zeroed for  $\theta = 54.74^\circ$ , the effect of rotation is to average out the CSA and dipolar interactions, as long as the spinning rate is fast enough, thus giving one single value of chemical shift corresponding to the isotropic value observed in solution state.

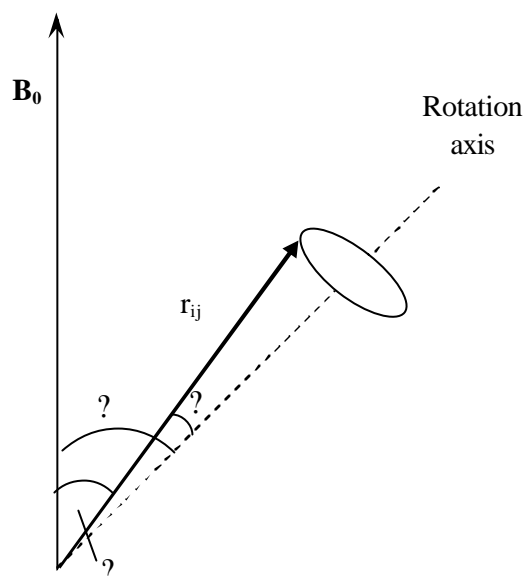


Figure II.12. Macroscopic sample rotation at the magic angle with  $B_0$ .

The averaging of the CSA pattern to only one line by MAS requires spinning rates (SR) of a few KHz, the typical magnitude of CSA line widths (Belton and Gil, 1993). At lower rates, spinning side bands (SSB) are observed on either sides of the isotropic signal, spaced at an interval equal to the SR measured in Hz. The SSB complicate spectral interpretation and have the additional disadvantage of dispersing the intensity of the central band, thus hindering quantitative studies; however, several solutions to this problem exist. MAS at rates of a few KHz also averages the homonuclear dipolar interactions between dilute spins (e.g.  $^{13}\text{C}$ - $^{13}\text{C}$ ), and heteronuclear interactions between abundant and dilute spins (e.g.  $^1\text{H}$ - $^{13}\text{C}$ ). However, in a typical solid, to average out the stronger homonuclear correlations between abundant spins (e.g.  $^1\text{H}$ - $^1\text{H}$ ), spinning rates of several tens of KHz must be employed.

In the case of semi-solid samples, such as the fruit pulps analysed in this work, the fast molecular motion may significantly reduce the strength of anisotropic interactions so that they become of the order or less than the achievable sample spinning rates, thus being effectively averaged out by MAS. In such samples, the main factor contributing to the line broadening is, generally, the magnetic susceptibility inhomogeneity, which in proton

spectra is typically of the order of a few tens of Hz. This magnitude can also be greatly reduced by MAS (Belton and Gil, 1996; Eads, 1999). The reason for this is that susceptibility inhomogeneity also has an angular dependence on the factor  $3\cos^2\theta - 1$  and this factor is zeroed by rotation at the magic angle, as explained above. In addition, the spectral resolution for inherently mobile systems can be further improved by using a high resolution probe together with MAS (HR-MAS probe). This kind of probe is designed to perform solution type experiments and enables the use of a lock system to achieve long-term stability of the magnetic field. As it will be shown in this work, the use of a HR-MAS probe for studying semi-solid samples results in significant resolution enhancement, enabling efficient solvent suppression schemes to be applied and 2D experiments to be carried out.

### **II.3. Hyphenated NMR Methods (HPLC-NMR and HPLC-NMR/MS)**

High-performance liquid chromatography (HPLC) is one of the techniques routinely used for the analysis of complex mixtures, including a wide variety of food samples (Bovanová and Brandsteterová, 2000). However, the ability to obtain structural information on substances separated using HPLC is limited by the on-line detector systems commonly employed, such as refractive index, UV, radiochemical, fluorescence and electrochemical detectors. None of these systems provide detailed structural information and there is always some vagueness as to whether detected peaks are actually those of target compounds or others coeluted with them. This limitation has led to a growing interest in coupling more sophisticated systems to HPLC, namely diode-array UV, IR, mass spectrometry (MS) and, more recently, NMR spectroscopy. HPLC-MS is a particularly well-established analytical tool, since it combines the separation capabilities of HPLC with the ability of MS to detect and identify substances at low concentrations. Applications in food analysis are numerous and have been recently reviewed by Careri *et al.* (1998). In the last years, the new hyphenated method HPLC-NMR has also found its way into the analytical laboratory. The first attempts to couple liquid chromatography with NMR spectroscopy have been carried out in the late 1970s and early 1980s. However, for several years, the technique did not gain importance mainly due to insufficient sensitivity,

the need to use expensive deuterated solvents because of dynamic range problems, and the lack of multiple solvent suppression routines able to cope with mixed solvents and gradient elution. In the last decade, these technical problems have largely been overcome through the development of new specialised hardware and software (Lindon *et al.*, 1996; Spraul *et al.*, 2001). A major technological advance has been the development of dedicated flow probes, where the detection coil is directly fixed on to the outside of the NMR cell, providing an optimal filling factor and improved sensitivity. The efficiency of solvent suppression has also been significantly improved, namely by the introduction of new pulse sequences that can suppress multiple solvents in an automatic fashion, thus making the use of deuterated solvents unnecessary. In addition, HPLC-NMR has benefited from the introduction of oversampling and digital filtering techniques into NMR acquisition systems, which allowed gains in dynamic range and sensitivity.

A further sophistication has been achieved by the combined hyphenation of both NMR and MS to an HPLC system. With the HPLC-NMR/MS set-up, decisions on which LC peaks are interesting for structural analysis can be made with basis on both UV and MS information. Another advantage is the much greater sensitivity of the mass spectrometer compared to the NMR spectrometer, enabling compounds present at concentrations lower than the NMR detection limit to be observed. In addition, NMR and MS data recorded for each fraction provide complementary information which is often sufficient for the unambiguous structural elucidation of a compound.

Figure II.13 shows a schematic representation of a typical instrumental set-up for HPLC-NMR/MS. It includes a standard HPLC equipment, comprising the LC pump, the column and the detector (e.g. UV, DAD, refractive index), a high-resolution NMR spectrometer, equipped with a dedicated flow probe, and a mass spectrometer, attached to the system via a splitter at the output of the HPLC-NMR interface. The effluent from the HPLC column is split immediately after chromatographic detection. Given the relative sensitivities of the two spectrometers, the major proportion (95%) is directed towards the NMR detector and the remaining (5%) to the MS. Coupling of NMR and MS is in parallel mode, so that depending on the length of the capillary to the MS, it is possible to choose MS detection prior to, simultaneous with, or after NMR detection. Besides the flow splitter, the HPLC-NMR/MS interface also comprises a t-piece to allow mixing and push solvents, a double dilutor to mix in ionisation helping agents, to do back exchange of

H<sub>2</sub>O/D<sub>2</sub>O, or to further dilute the flow to the MS, and a special delay loop valve to adjust transfer timing.

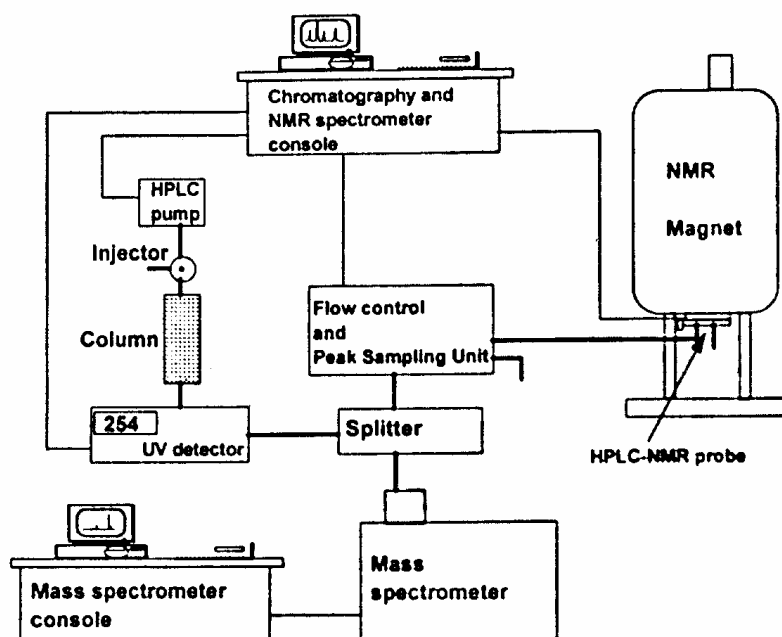


Figure II.13. Schematic representation of a HPLC-NMR/MS system (Hansen *et al.*, 1999).

The heart of the system is the flow control unit, which determines the various patterns of eluent flow. There are currently four main methods of operation which can be employed, with both isocratic and gradient elution: 1) continuous-flow; 2) stop-flow, 3) time-sliced stop-flow and 4) peak collection into capillary loops for posterior analysis. In the continuous-flow mode, NMR and MS data are acquired during chromatography. This method provides a rapid screening of the compounds separated, but the sensitivity is limited by the short acquisition time. Moreover, if gradient elution is used, the shift in the positions of the solvent NMR signals caused by changes in the solvent composition must be taken into consideration for designing solvent suppression schemes. A possible methodology is to carry out a dummy run, determine all frequencies as a function of solvent composition and store them in a list for look-up during the chromatographic run. Alternatively, the solvent suppression frequencies can be determined by measuring a single exploratory scan as soon as a chromatographic peak is detected in real time during the chromatographic run and then apply suppression irradiation at these frequencies as the peak elutes.

In the stop-flow mode, the pump is stopped when the LC-peak has reached the NMR flow cell and started again after the NMR measurement is finished. In this way, 1D spectra with longer acquisition times and also 2D spectra, that may aid spectral assignment and structure determination, can be recorded. The flow may be stopped manually or automatically, using the time-slicing method, which consists of stopping the flow at short intervals over the chromatogram to “time-slice” different parts of a chromatographic peak. This method may be useful if poor chromatographic separation results, if the compounds under study have weak UV chromophores or if the exact chromatographic retention time is poorly defined. However, when operating in the stop-flow mode, the chromatographic resolution is degraded due to diffusion of peaks still sitting on the column or in the transfer capillary when a stop occurs. Furthermore, no MS data can be acquired because of the interruption of the flow during the NMR measurement.

Another operation mode, which overcomes the disadvantages of the stop-flow methods, consists of transferring the LC-peaks of interest into capillary storage loops that retain the LC-peak shape due to small inner diameter (e.g. 0.25 mm). In this case, the flow is not stopped during the chromatography, but only valves are switched to direct the LC-peaks into the loops. After the chromatographic run is finished, the loop contents can be transferred sequentially to the NMR and MS spectrometers for off-line experiments.

## II.4. Fourier Transform Infrared (FTIR) Spectroscopy

Mid-infrared spectroscopy involves the absorption by molecules of radiation in the 4000 to 400  $\text{cm}^{-1}$  range of the electromagnetic spectrum. The absorption arises through transitions between vibrational energy states and rotational substates of the molecule. The rotational substates are not quantised in liquids or in solids, and thus only vibrational transitions are observed. For these transitions to occur, a selection rule states that the vibration must cause a net change in the dipole moment of the molecule (Schrader, 1995; Hesse *et al.*, 1996). The positions of the absorption bands seen in the mid-infrared spectrum depend on the masses of the atoms and on the force constant of the vibrating bonds. Thus, many functional groups in organic molecules show characteristic vibrations, which correspond to absorption bands in defined regions of the infrared spectrum, thus

making infrared spectroscopy a reliable method for assigning a substance to a particular class of compounds. The absorption bands that can be assigned to the individual functional groups, corresponding to fundamental stretching and bending vibrations, lie above  $1500\text{ cm}^{-1}$ . For instance, the stretching vibrations of the group OH of alcohols give strong absorption bands at  $3650\text{--}3200\text{ cm}^{-1}$ , of the group N-H of amines at  $3500\text{--}3200\text{ cm}^{-1}$ , and of the group C=O at  $1800\text{--}1650\text{ cm}^{-1}$  for carboxylic acids,  $1775\text{--}1650\text{ cm}^{-1}$  for ketones,  $1765\text{--}1645\text{ cm}^{-1}$  for aldehydes,  $1745\text{--}1730\text{ cm}^{-1}$  for esters and  $1700\text{--}1650\text{ cm}^{-1}$  for amides (Pretsch *et al.*, 1989). On the other hand, the region below  $1500\text{ cm}^{-1}$  contains overlapping bands that characterise the molecule as a whole and cannot be conclusively assigned to localised vibrations. It is in this region that the pattern of infrared peaks varies most from compound to compound and, therefore, it is known as the fingerprint region. Besides fundamental vibrations, overtones and combination vibrations, which correspond, respectively, to multiple values and combinations of the fundamental vibrations wavenumbers, also arise in this region, although they are generally much weaker than those from fundamental vibrations (Hesse *et al.*, 1996). Besides being useful for structure elucidation, infrared spectroscopy may also be employed in quantitative analysis because the intensity of the infrared absorption band is proportional to the concentration of the absorbing species.

Most infrared spectrometric measurements today are performed with Fourier transform infrared (FTIR) spectrometers, which have largely replaced classical scanning instruments. The basic principle of the FTIR spectrometer is the simultaneous collection of data at all frequencies in the infrared spectrum, thus eliminating the time required for scanning through the different frequencies. The main component of the FTIR instrument is a Michelson interferometer, schematically represented in Figure II.14. The infrared radiation is led into it through a semi-transparent plate (KBr or CsI coated with germanium) which acts as a beam splitter. One half of the light falls onto a fixed mirror, the other

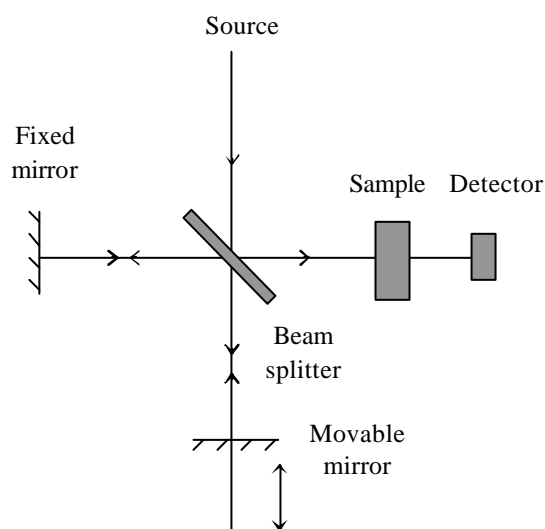


Figure II.14. Schematic representation of a Michelson interferometer

onto a movable mirror, the distance of which from the interferometer can be varied. Both mirrors reflect the light onto the plate, where interference (constructive or destructive) takes place. Since the infrared radiation is polychromatic, the interferogram obtained is a superimposition or summation of the interferograms of all the individual frequencies. The modulated radiation is now passed through the sample, where it is selectively absorbed, depending on the vibrations excited in the sample. The detector records the emerging radiation as an interferogram, converts the optical signals into electrical signals and passes them onto the data storage system. The intensity of the radiation recorded at the detector depends on the moving mirror velocity and varies with time, such that:

$$P(d) = 1/2 P(\nu) \cos 2\pi f t \quad \text{II.11}$$

where  $P(d)$  is the intensity of the radiation detected as a function of  $d = 2L$  ( $L$  being the distance to the beam splitter by which the movable mirror differs from the fixed mirror),  $P(\nu)$  is the intensity of the incident radiation as a function of  $\nu$  (frequency of the incident radiation) and  $f = 2\nu V$ ,  $V$  being the moving mirror velocity. As many frequencies are present in a infrared source, the interferogram is the sum of an infinite number of cosine waves, so that:

$$P(d) = \int_0^{\infty} 1/2 P(\nu) \cos 2\pi f \nu d \nu \quad \text{II.12}$$

In order to extract the frequency information from the interferogram and produce an interpretable band spectrum, Fourier transformation is applied. The Fourier transformation of II.12 is:

$$P(\nu) = \int_{-\infty}^{\infty} 1/2 P(d) \cos 2\pi f \nu d d \quad \text{II.13}$$

Where  $P(\nu)$  represents the intensity of the radiation as a function of frequency, *i.e.*, the spectrum.

There are many sampling methods for measuring infrared spectra of samples in different states of matter and for different applications. The Attenuated Total Reflectance (ATR) method has been the method employed in this thesis to measure the FTIR spectra of mango juice and of beer. This method consists of passing infrared radiation through a high refractive index crystal (e.g. ZnSe, Ge, diamond), coated with the sample under study (Figure II.15). The radiation is reflected off the crystal walls once or many times and, as some of it is absorbed by the sample, its intensity is attenuated. This change in the intensity of radiation totally reflected originates the spectrum of the sample in contact with the crystal.

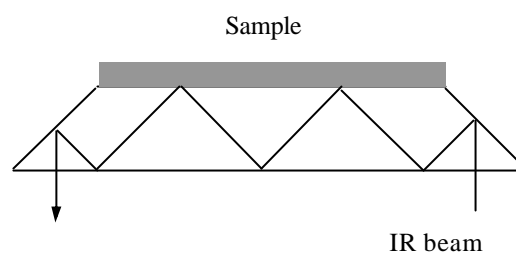


Figure II.15. Horizontal ATR sampling accessory.

The ATR method has the advantages of simplifying sample handling and avoiding problems commonly found in transmission cells, such as filling and cleaning. Liquids, viscous fluids and pastes can be simply poured or spread onto the surface of the ATR accessory and then wiped off after analysis. For this reason, ATR is the sampling method most widely used in the analysis of foods (Wilson and Goodfellow, 1994; Sedman et al., 1998). In the case of powders or other solid samples, the use of a pressure device is recommended to improve the optical contact between the sample and the crystal, which is critical for the quality of the spectrum obtained.

## II.5. Some Multivariate Analysis Methods

Techniques of multivariate data analysis are being increasingly applied to spectral data in order to extract meaningful information from the complex and highly informative spectra and address questions of classification and discrimination. In this thesis, Principal Components Analysis (PCA) is used as a data reduction technique to visualise the main variability aspects of NMR and FTIR data sets, Canonical Correlation Analysis (CCA) is used to establish relationships between two domains (NMR and FTIR), and PLS regression

is applied as a calibration technique to predict concentration values. The basic principles of these chemometric methods are described in the following sections.

### II.5.1. Principal Components Analysis (PCA)

PCA is essentially a descriptive method, often used for data reduction and exploratory analysis on high-dimensional data sets. It helps establishing the presence of any intrinsic class-related patterns or clusters in the data set, without any inclusion of information concerning the classification of samples. The main goal of PCA is to reduce the dimensions of the original data set giving a smaller space that retains the relevant information (Jolliffe, 1986).

Consider the spectra assembled into a  $(n \times d)$  matrix where  $n$  is the number of samples (objects) and  $d$  is the number of data points (variables) per spectrum. It is generally the case with NMR and FTIR spectra that  $d > n$ , since the number of data points may run into many hundreds. PCA reduces the data matrix to  $(n \times p)$ , where  $p$  is the number of principal components (PCs) determined, with  $p < n < d$ . The PCs are orthogonal linear combinations of the original variables calculated in order to maximize the dispersion of the individuals. The sample coordinates on the new PC axes are named scores. Thus, the  $(n \times p)$  matrix contains the PC scores which replace the spectral intensities of the original  $(n \times d)$  matrix. The relationship between new and old axes is expressed in a  $(p \times d)$  matrix of eigenvectors, called loadings. The decomposition of the initial matrix  $\mathbf{X}_{(n, d)}$  is thus formalised by:

$$\mathbf{X}_{(n, d)} = \mathbf{T}_{(n, p)} \mathbf{L}_{(p, d)}^T + \mathbf{E}_{(n, d)} \quad \text{II.14?}$$

where  $\mathbf{T}$  is the scores matrix,  $\mathbf{L}$  the loadings matrix,  $\mathbf{E}$  the error matrix,  $n$  is the number of objects (samples),  $d$  is the number of variables, and  $p$  the number of principal components used.

Successive PCs account for decreasing amounts of variance and are uncorrelated in contrast to the original variables. Therefore, the PCA technique extracts the relevant information (maximizing the variance explained by each new PC), removes the redundancy (uncorrelated new variables) and reduces the dimension of the  $d$ -dimensional space of the original variables. Plots of the scores for different pairs of PCs allow data

patterns to be clearly visualised, since samples with similar properties appear as clusters in the two-dimensional plot. The chemical origin of such clusters can be revealed through the plot of the corresponding loadings, which resemble the spectra and, to some extent, provide interpretable information.

### II.5.2. Partial Least Squares (PLS) Regression

The PLS regression procedure is used to model the relationship between a set of predictor variables  $\mathbf{X}$  ( $n$  objects  $\times k$  variables) and a set of response variables  $\mathbf{Y}$  ( $n$  objects  $\times m$  responses) (Geladi and Kowalski, 1986). In this thesis, PLS is used as a calibration technique to predict the concentration of sugars in juices. There is only one response in  $\mathbf{Y}$  (concentration), and hence  $\mathbf{Y}$  has ( $n$  objects  $\times 1$  response) dimension. This method has the advantage of accepting more variables than objects in the data and of avoiding the problem of collinearity among variables.

The classical PLS regression method is a special case of Non-linear Iterative Partial Least Squares (NIPALS) method, in which the information explained by each dimension is subtracted from the  $\mathbf{X}$  matrix in an iterative process, until all the important variance is extracted. In other words, a PCA is performed on the  $\mathbf{X}$  matrix by means of NIPALS, maximizing at the same time the correlation of the extracted PCs with the response variables vector. The relationship may be formalised as:

$$\mathbf{Y} = \mathbf{X} \mathbf{B} + \mathbf{E} \quad \text{II.15}$$

where  $\mathbf{Y}$  is the vector of dependent variables (in this study, sugar concentration),  $\mathbf{X}$  is the matrix of the independent variables (spectra),  $\mathbf{B}$  is the regression coefficients vector, and  $\mathbf{E}$  represents the error not accounted for by the model. The regression model is generated by calculating the  $\mathbf{B}$  coefficients that minimise the error matrix. The main difference between this and other regression procedures is the way the  $\mathbf{B}$  vector is calculated. In the PLS procedure the information present in the  $\mathbf{Y}$  matrix is used in the calculation of  $\mathbf{B}$  coefficients.

### II.5.3. Canonical Correlation Analysis (CCA)

This multivariate data treatment seeks to identify and quantify the relationships between two sets of variables or domains ( $\mathbf{X}$  and  $\mathbf{Y}$ ) (Robert *et al.*, 1993). The method maximizes the correlation between the linear combination of the variables in one domain with the linear combination of the variables in the other domain. The procedure starts by finding the pair of linear combinations (between both domains) having the largest correlation. Next, it seeks a pair of linear combinations having the largest correlation but uncorrelated to the first pair of linear combinations found. This procedure is repeated until extraction of all canonical factors has been accomplished. The pairs of linear combinations are called canonical variables and their correlations are called canonical correlations. The canonical correlation is a measurement of the strength between the obtained pairs of linear combination between the two domains ( $\mathbf{X}$  and  $\mathbf{Y}$ ). The aim of CCA is to concentrate the information of both domains into a small number of canonical variables that should represent almost the same information present in the initial variables. This method may be useful to characterise one group of variables about which there is little information, by relating it to another group of well-characterised variables.

### References

Aue, W.P.; Bartholdi, E.; Ernst R.R. Two-dimensional spectroscopy. Application to nuclear magnetic resonance. *Journal of Chemical Physics* **1976a**, *64*, 2229-2246.

Aue, W.P.; Karhan, J.; Ernst, R.R.J. Homonuclear broad band decoupling and two-dimensional J-resolved NMR spectroscopy. *Journal of Chemical Physics* **1976b**, *64*, 4226-4227.

Bax, A.; Davis, D.G. MLEV-17 based two-dimensional homonuclear magnetization transfer spectroscopy. *Journal of Magnetic Resonance* **1985**, *65*, 355-360.

Bax, A.; Griffey, R.H.; Hawkins, B.L. Correlation of proton and nitrogen-15 chemical shifted by multiple quantum NMR. *Journal of Magnetic Resonance* **1983**, *55*, 301-315.

Belton, P.S.; Gil, A.M. Proton nuclear magnetic resonance lineshapes and transverse relaxation in a hydrated barley protein. *Journal of the Chemical Society Faraday Transactions* **1993**, *89*, 4203-4206.

Belton, P.S.; Gil, A.M. Magic angle spinning spectra of rare and abundant nuclei in food materials. *Journal of Magnetic Resonance Analysis* **1996**, *2*, 45-52.

Bodenhausen, G.; Ruben, D.J. Natural abundance nitrogen-15 NMR by enhanced heteronuclear spectroscopy. *Chemical Physics Letters* **1980**, *69*, 185-188.

Bovanová, L.; Brandsteterová, E. Direct analysis of food samples by high-performance liquid chromatography. *Journal of Chromatography A* **2000**, *880*, 149-168.

Braun, S.; Kalinowski, H.-O.; Berger, S. *150 and More Basic NMR Experiments*; Wiley-VCH: Weinheim, 1998.

Braunschweiler, L.; Bodenhausen, G.; Ernst, R.R. Coherence transfer by isotropic mixing: application to proton correlation spectroscopy. *Journal of Magnetic Resonance* **1983**, *53*, 521-528.

Careri, M.; Mangia, A.; Musci, M. Overview of the applications of liquid-chromatography-mass spectrometry interfacing systems in food analysis: naturally occurring substances in food. *Journal of Chromatography A* **1998**, *794*, 263-297.

Claridge, T.D.W. *High-Resolution NMR Techniques in Organic Chemistry*; Elsevier Science: Oxford, 1999.

Colquhoun, I.J.; Goodfellow, B.J.; Nuclear magnetic resonance spectroscopy. In *Spectroscopic Techniques for Food Analysis*; Wilson, R.H. Ed.; VCH: New York, 1994; 87-145.

Eads, T. Principles of nuclear magnetic resonance analysis of intact food materials. In *Spectral Method in Food Analysis*; Mossoba, M.M. Ed.; Marcel Dekker, Inc.: New York, 1999; 1-88.

Fan, T.W.-M. Metabolite profiling by one- and two-dimensional NMR analysis of complex mixtures. *Progress in Nuclear Magnetic Resonance Spectroscopy* **1996**, *28*, 161-219.

Fyfe, C.A. *Solid State NMR for Chemists*; CFC Press: Ontario, 1983.

Geladi, P.; Kowalski, B.R. Partial least-squares regression: a tutorial. *Analytica Chimica Acta*, **1986**, *185*, 1-17.

Gunther, H. *NMR Spectroscopy: Basic Principles, Concepts, and Applications in Chemistry*; 2<sup>nd</sup> Ed.; John Wiley & Sons: Chichester, 1995.

Hansen, S.H.; Jensen, A.G.; Cornett, C.; Bjornsdottir, I.; Taylor, S.; Wright, B.; Wilson, I.D. High-performance liquid chromatography on-line coupled to high-field NMR and mass spectrometry for structure elucidation of constituents of *Hypericum perforatum* L. *Analytical Chemistry* **1999**, *71*, 5235-5241.

Harris, R.K. *Nuclear Magnetic Resonance Spectroscopy*; 3<sup>rd</sup> Ed.; John Wiley & Sons: New York, 1987.

Hesse, M.; Meier, H.; Zeh, B. *Spectroscopic Methods in Organic Chemistry*; Georg Thieme Verlag: Stuttgart, 1997.

Jolliffe, I.T. *Principal Component Analysis*; Springer: New York, 1986.

Lindon, J.C.; Nicholson, J.K.; Wilson, I.D. Direct coupling of chromatographic separations to NMR spectroscopy. *Progress in Nuclear Magnetic Resonance Spectroscopy* **1996**, *29*, 1-49.

Martin, G. Analytical performance of high resolution NMR. In *Magnetic Resonance in Food Science*; Belton, P.S., Delgadillo, I., Gil, A.M., Webb, G.A. Eds.; The Royal Society of Chemistry: Cambridge, 1995; 105-119.

Nicholson, J.K.; Foxall, P.J.D.; Spraul, M.; Farrant, R.D.; Lindon, J.C. 750 MHz  $^1\text{H}$  and  $^1\text{H}$ - $^{13}\text{C}$  NMR spectroscopy of human blood plasma. *Analytical Chemistry* **1995**, *67*, 793-811.

Pretsch, E.; Clerc, T.; Seibl, J.; Simon, W. *Spectral Data for Structure Determination of Organic Compounds*; Springer-Verlag: Berlin, 1989.

Robert, P.; Devaux, M.F.; Qannari, A.; Safar, M. Mid and near infrared study of carbohydrates by canonical correlation analysis. *Journal of Near Infrared Spectroscopy* **1993**, *1*, 99-108.

Schrader, B. *Infrared and Raman Spectroscopy: Methods and Applications*; VCH: Weinheim, 1995.

Sedman, J.; Van der Voort, F.R.; Ismail, A.A. Attenuated total reflectance spectroscopy: principles and applications in infrared analysis of food. In *Spectral Methods in Food Analysis*; Mossoba, M.M. Ed.; Marcel Dekker, Inc.: New York, 1999; 397-425.

Spraul, M.; Braumann, U.; Godejohann, M.; Hofmann, M. Hyphenated methods in NMR. In *Magnetic Resonance in Food Science - a View to the Future*; Webb, G.A., Belton, P.S., Gil, A.M. Eds.; The Royal Society of Chemistry: Cambridge, 2001; 54-66.

Wilson, R.H.; Goodfellow, B.J.; Mid-infrared spectroscopy. In *Spectroscopic Techniques for Food Analysis*; Wilson, R.H. Ed.; VCH: New York, 1994; 59-85.

### **III. STUDY OF THE COMPOSITION OF MANGO BY NMR**

III.1. Introduction.....	66
III.2. Materials and Methods.....	67
III.2.1. Sample Preparation.....	67
III.2.2 NMR Measurements.....	68
III.3. High Resolution NMR Study of Mango Juice.....	70
III.3.1. Spectral Assignment.....	70
III.3.2. Compositional Differences Within and Between Cultivars.....	80
III.4. NMR Study of Mango Pulp.....	83
III.4.1. Standard Magic Angle Spinning (MAS) NMR.....	83
III.4.2. High Resolution Magic Angle Spinning (HR-MAS) NMR.....	85
III.4.3. Compositional Differences Between Pulp and Juice.....	90
III.5. Conclusions.....	93
References.....	94

### III.1. Introduction

The increasing trade in mango and the need to develop appropriate technologies to enhance its marketable life and reduce post harvest losses have been accompanied by a growing interest in studying the chemical composition of this fruit. Most data reported in the literature (summarised in Chapter I) have involved separation of the liquid phase of the fruit, followed by analysis by chemical or chromatographic methods. Those methods are usually based on the study of one specific family of compounds and often require extraction procedures to separate the compounds of interest from the complex natural matrix, resulting in laborious and time-consuming sample preparation and analysis. Furthermore, there is the disadvantage that the invasive separation and fractionation methods may interfere with the fruit biochemistry.

High resolution nuclear magnetic resonance (NMR) spectroscopy has the attractive features that structural and quantitative information can be obtained on a wide range of compounds in a single experiment, with minimum sample preparation. In addition, NMR measurements are non-destructive, allowing samples to be subsequently analysed by other methods. For all these reasons, NMR has played an increasingly important role in the compositional study of foods (Alberti *et al.*, 2002).

Since the first attempts to measure  $^1\text{H}$  NMR spectra of fruit juices and other liquid foods (Eads and Bryant, 1986), there have been several instrumental developments that enabled major improvements in spectral resolution and sensitivity (Belton *et al.*, 1998a). In recent years, high resolution  $^1\text{H}$  NMR has been shown to be a valuable method for the analysis of low molecular weight compounds in fruit juices, allowing the identification of several sugars, organic acids, amino acids and other minor components such as phenolic compounds (Vogels *et al.*, 1996; Belton *et al.*, 1996; Belton *et al.*, 1997; Belton *et al.*, 1998b; Le Gall *et al.*, 2001). Moreover, the application of multivariate statistics to NMR spectra has provided promising results, concerning the classification of apple juice according to variety (Belton *et al.*, 1998b) and the detection of adulteration of orange juice (Vogels *et al.*, 1996; Le Gall *et al.*, 2001).

Magic Angle Spinning (MAS) NMR has also been used to characterise the composition of fruits by direct study of intact pulp (Ni and Eads, 1992; Ni and Eads, 1993a; Ni and Eads, 1993b), thus avoiding the use of extraction and separation methods. The  $^1\text{H}$  MAS NMR spectra reported for banana enabled the identification of the three main

sugars present (sucrose, glucose and fructose) and their quantification at different ripening stages (Ni and Eads, 1993b). Recent instrumental developments in MAS NMR equipment have enabled the use of High-Resolution Magic Angle Spinning (HR-MAS) NMR leading to a very significant resolution improvement in the spectra of solid or semi-solid food samples (Gil *et al.*, 1997; Sacco *et al.*, 1998; Alberti *et al.*, 2001) so that components other than the main sugars may become detectable in intact fruits.

The work hereby reported, part of which has already been published (Gil *et al.*, 2000), aims at using liquid state and solid state NMR techniques for characterising the chemical composition of mango juice and intact pulp, respectively. The juice is analysed by high field  $^1\text{H}$  NMR (600 MHz) and assignment strategies based on 2D NMR methods are employed in order to identify as much components as possible. HR-MAS (400 and 500 MHz) is used to obtain highly resolved spectra of fruit pulp, enabling 2D experiments to be carried out. The spectral profiles of juice and pulp are compared to find out if the composition of the juice is fully representative of the composition of the whole fruit, as usually assumed.

## **III.2. Materials and Methods**

### **III.2.1. Sample Preparation**

The juice and pulp samples studied were prepared from three batches of mango fruits: 1) cultivar Tommy Atkins grown in Brazil, 2) cultivar Haden grown in Venezuela, and 3) cultivar Haden grown in Brazil. The nature of these sets of fruits was not chosen to meet particular aims of this work, having been solely conditioned by the fruits found available in the market. Each batch was obtained from a commercial source in Portugal, 3-4 days after harvest and subsequent air shipment, and comprised 40 mature green fruits from the same orchard. Only undamaged fruits having uniform size and colour, and free from visible symptoms of infection, were selected for the study. As thoroughly described in Chapter IV.2.1, these fruits were then ripened for 19-23 days, during which juice and pulp samples were collected for analysis. In the present Chapter, only two stages of ripeness are considered (unripe stage for mature green fruits, and ripe stage for ready-to-eat fruits), whereas the compositional changes occurring during ripening will be discussed in Chapter IV.

The juice was obtained by maceration of the pulp in a domestic juice extractor, followed by centrifugation at 15000 r.p.m. during 15 minutes, and filtration under vacuum through a glass microfiber filter. In order to prevent microbial growth, sodium azide ( $\text{NaN}_3$ ) was added to juices, typically prior to freezing, so that each sample contained 0.05%  $\text{NaN}_3$ . The juice samples were frozen in liquid nitrogen and stored at  $-20^\circ\text{C}$  until NMR analysis. As the chemical shift of many NMR signals is pH dependent, the samples pH (initially varying from 2.9 to 5.3) was adjusted to fall in narrower ranges: the pH of Haden juices was adjusted to  $7.00 \pm 0.05$ , by adding microlitre amounts of NaOH (0.1 M and 1M) and HCl (0.1 M and 1M) solutions, and the pH of Tommy Atkins juices was adjusted to  $5.90 \pm 0.30$ , by mixing 0.500 ml of 0.5 M sodium phosphate buffer with 1.5 ml of juice. Finally, all samples were prepared to contain 7.5-10%  $\text{D}_2\text{O}$ , used as the internal lock, and 0.015-0.020% sodium 3-(trimethylsilyl)propionate (TSP), used as chemical shift and intensity reference, and transferred to 5 mm o.d. NMR tubes.

The pulp samples were collected from the equatorial ring of the fruits, frozen in liquid nitrogen and stored at  $-20^\circ\text{C}$ . The thawed pulps were then packed into 4 mm MAS rotors and, for high-resolution NMR, a few drops of  $\text{D}_2\text{O}$  containing TSP was added, in order to provide a field frequency lock and a chemical shift reference.

### III.2.2. NMR Measurements

The NMR spectra of juices were recorded at  $27^\circ\text{C}$  on a Bruker Avance DRX-600 spectrometer, operating at 599.87 MHz for proton and 150.85 MHz for carbon. The spectrometer was equipped with an automatic sample changer and the data were acquired under an automation procedure that included temperature stabilization (5 minutes), gradient shimming, and acquisition. The quality of the shimming was verified and optimised when necessary so that the maximum line width at half height of the TSP signal at 0.00 ppm was 1.5 Hz. A presaturation sequence ('zgcppr') was used to suppress the water signal by applying low-power selective irradiation at the water frequency during 3 s of the relaxation delay (Bax, 1985). Each  $^1\text{H}$  1D spectrum consisted of 64 scans of 65536 data points with a spectral width of 12019.23 Hz, an acquisition time of 2.73 s, and a relaxation delay of 7 s. This delay was chosen after measuring the spin-lattice relaxation times,  $^1\text{H}$   $T_1$ , so that the recycle time was at least five times the maximum  $T_1$ . In this way, it is possible to carry out a quantitative analysis of the spectra.  $^1\text{H}$   $T_1$  times were measured

using the inversion recovery sequence ( $180^\circ_x$ - $\tau$ - $90^\circ_x$ ) with delays between pulses ( $\tau$ ) in the 100 ms – 30 s range (15 experimental points). The FIDs were Fourier transformed with 0.3 Hz line broadening, phased and baseline corrected using the Bruker XWIN-NMR software.

The TOCSY spectra were acquired in the phase sensitive mode using time proportional phase incrementation (TPPI), and the MLEV17 pulse sequence was used for the spin-lock (Bax and Davis, 1985) (pulse program ‘mlevprtp’). 2048 data points with 16 transients per increment and 200 increments were acquired with a spectral width of 6613.76 Hz in both dimensions. The relaxation delay between successive pulse cycles was 2 s and the mixing time of the MLEV spin lock was 80 ms. The data were zero-filled in the  $f_1$  dimension to 2048 data points and a sine-bell apodization function was applied prior to FT.  $^1\text{H}$ - $^{13}\text{C}$  phase sensitive (echo/antiecho) heteronuclear single quantum correlation (HSQC) spectra were recorded with inverse detection and  $^{13}\text{C}$  decoupling during acquisition (Palmer *et al.*, 1991; Schleucher *et al.*, 1994), using the ‘invieagssi’ pulse program. A relaxation delay of 2.2 s was used between pulses and a refocusing delay equal to  $1/4 J_{\text{C-H}}$  (1.75 ms) was employed. 2048 data points with 64 scans per increment and 300 increments were acquired with spectral widths of 7507.51 and 25000.00 Hz in the proton and carbon dimensions, respectively. The FIDs were weighted using a sine-bell-squared function in both dimensions and zero-filled in the  $f_1$  dimension to 1024 data points. 2D homonuclear  $J$ -resolved spectra (Aue *et al.*, 1976) with water presaturation (pulse program ‘jrespr’) were measured by acquiring 8192 data points with 16 transients per each of 128 increments, using spectral widths of 10000 Hz in the  $f_2$  dimension and 39 Hz in the  $f_1$  ( $J$ -coupling) dimension. Prior to FT, the FIDs were weighted in both dimensions by a sine-bell function and zero-filled in the  $f_1$  dimension to 256 data points. The spectra were tilted by  $45^\circ$  to provide orthogonality of the chemical shift and coupling constant axes and subsequently symmetrized about the  $f_1$  axis.

Standard  $^1\text{H}$  MAS NMR spectra of mango pulps (cv. Tommy Atkins) were recorded on a Bruker MSL 400P NMR spectrometer, operating at 400 MHz for proton, using a 4 mm double bearing MAS probe. The samples were spun at 1.0-1.2 KHz and 3-5 s recycle delays were used. High resolution MAS experiments were carried out on Bruker Avance DRX-400 and DRX-500 spectrometers, operating, respectively, at proton frequencies of 400.13 and 500.13 MHz, and equipped with 4 mm HR-MAS probes. Typically, the samples were spun at 5 KHz, but spinning rates in the range 1-15 KHz were

tried (results presented in section III.4.2). Different rotor configurations were also tested and, preferably, zirconium oxide rotors with a fixed bottom insert and, sometimes, a removable top insert were used. For Haden pulps, 400 MHz  $^1\text{H}$  1D spectra were acquired, consisting of 180 scans of 32768 data points with a spectral width of 6009.62 Hz, an acquisition time of 2.73 s, and a relaxation delay of 6 s. Water suppression was achieved by presaturation during 3 s of the relaxation delay. For Tommy Atkins pulps, 500 MHz  $^1\text{H}$  1D spectra were acquired and consisted of 256/512 scans of 16384 data points with a spectral width of 8012.82 Hz, an acquisition time of 1.02 s, and a relaxation delay of 1.5 s. Water suppression was achieved by presaturation during the relaxation delay. All the FIDs were zero filled to 64K data points and an exponential apodization function was applied, corresponding to a line broadening of 0.3 Hz, before Fourier transformation. TOCSY,  $^1\text{H}$ - $^{13}\text{C}$  correlation and  $J$ -resolved spectra were also recorded for a few samples to aid spectral assignment.

The pulse sequences used in the experiments described above are given in appendix. Some experiments were recorded at the Bruker site of Silberstreifen (Germany), within collaboration with Dr. M. Spraul and Dr. E. Humpfer.

### III.3. High Resolution NMR Study of Mango Juice

#### III.3.1. Spectral Assignment

The  $^1\text{H}$  NMR spectrum of mango juice is shown in Figure III.1. This juice was extracted from a ripe edible fruit (cv. Haden, Venezuela) with a soft texture and a yellow pulp, being characterised by 15.7 % soluble solids and a pH value of 4.95. The spectrum was recorded with presaturation of the water signal, which reduced the water peak (4.80 ppm) to below the intensity of the sugar signals, enabling minor components present at low concentrations to be detected in all spectral regions. The high-field region (0-3 ppm) and the low-field region (6-10 ppm) are vertically expanded in Figure III.1, showing the large number of spectral lines, arising from the many components known to be present in mango juice. Some of the signals were assigned with basis on the 1D spectral profile, by comparison of chemical shifts ( $\delta$  in ppm), spin-spin coupling patterns (multiplicity) and coupling constants ( $J$  in Hz) data with data compiled in the literature for other fruit juices

(Belton *et al.*, 1998a) and for common metabolites found in biological samples (Nicholson *et al.*, 1995; Fan, 1996). Comparison with spectra of reference compounds expected to be present in the juice has also been carried out. However, this approach is seriously hindered by the highly complex and overlapped nature of the spectrum. Thus, in order to aid spectral assignment, 2D NMR spectra, namely TOCSY,  $^1\text{H}$ - $^{13}\text{C}$  correlation and  $J$ -resolved spectra, have been recorded for some mango juice samples. The information obtained from both 1D and 2D spectra is compiled in Table III.1, which shows the list of compounds identified in mango juice.  $^1\text{H}$  chemical shifts are shown in the third column of this Table, while the fourth and fifth columns indicate, respectively, the multiplicity and coupling constants, which could be measured either in the 1D spectrum (for non-overlapped signals) or in the 2D homonuclear  $J$ -resolved spectrum. The last column in Table III.1 provides  $^{13}\text{C}$  chemical shifts for some compounds, which were measured in the  $^1\text{H}$ - $^{13}\text{C}$  correlation spectrum.

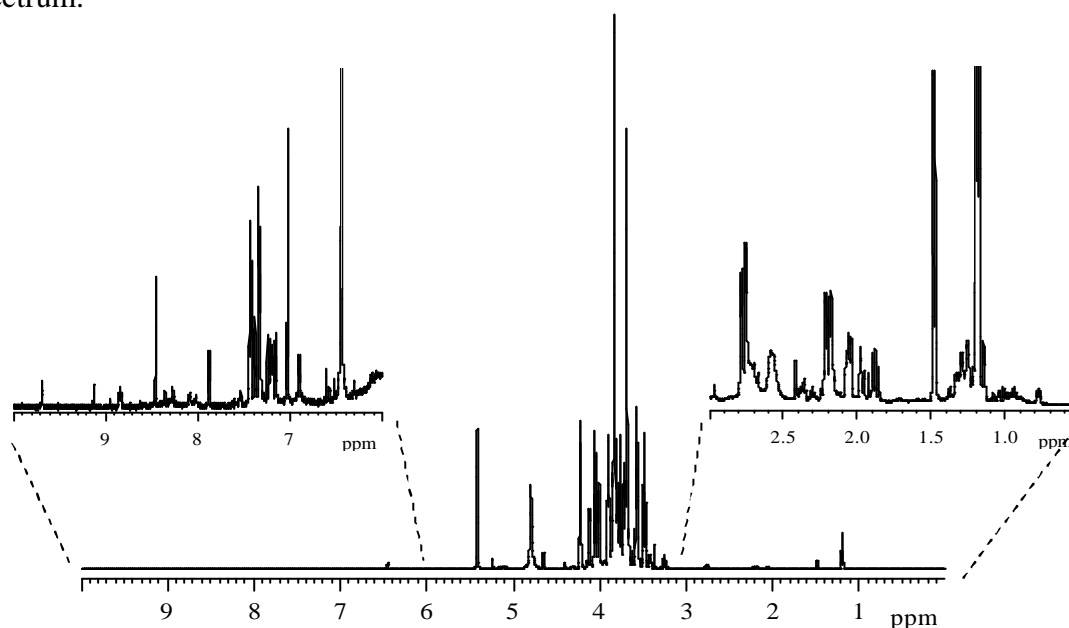


Figure III.1. 600 MHz  $^1\text{H}$  NMR spectrum of ripe mango juice (cv. Haden, Venezuela); NS 64.

Figure III.2 shows the TOCSY spectrum of mango juice (same sample as in Figure III.1). A significant number of cross-peaks are observed in all spectral regions, as clearly illustrated by the expansions shown in Figure III.3. As explained in Chapter II.1.3, the chemical shift coordinates of the cross-peaks correspond to the chemical shifts of scalar coupled nuclei, either directly or through a chain of spin-spin couplings. The following discussion will address the different spectral regions in turn.

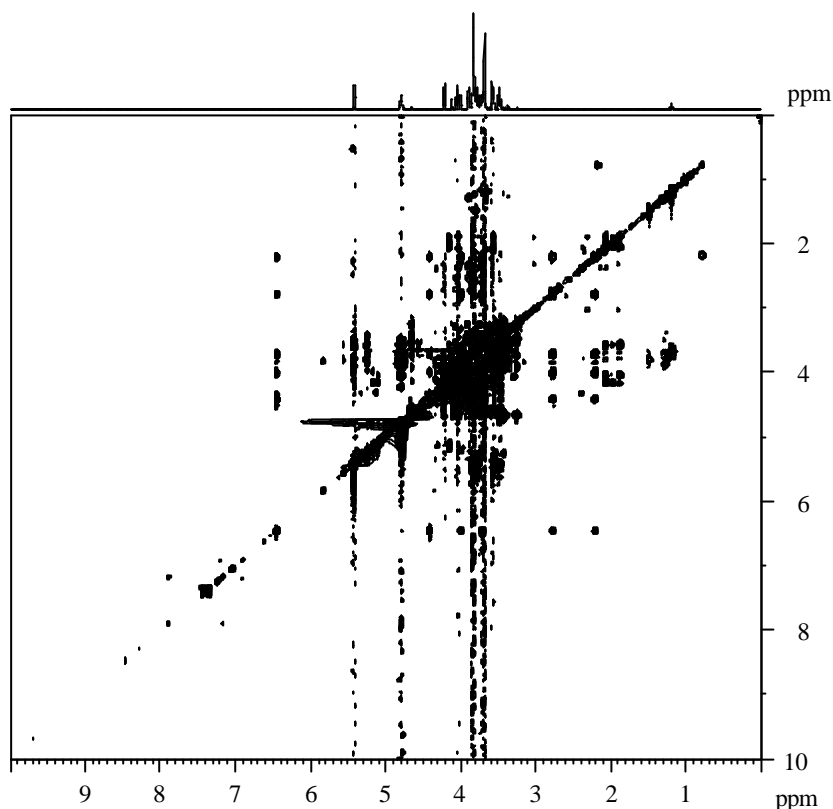


Figure III.2. 600 MHz TOCSY spectrum of ripe mango juice (cv. Haden, Venezuela); NS 16 in  $f_2$ , 80 ms mixing time.

The high-field region (0-3.0 ppm) shows signals arising mainly from aliphatic groups of organic acids and amino acids (Figure III.3a). Shikimic and quinic acids are two of the most prominent organic acids detected and, to our knowledge, this is the first time that these acids are reported to be present in mango juice. Citric, malic and succinic acids, which are generally referred to as the predominant acids in mango fruit (Lizada, 1993), are also visible in the spectrum. As it will be shown later, citric acid is a major component of unripe mango and in the spectrum of unripe juice gives rise to very intense and well-resolved signals. In addition, spin systems for lactic, propionic and 3-hydroxybutyric acids are also identified in the TOCSY spectrum. The structures of the major organic acids detected in mango juice are shown in Figure III.4. In what regards the amino acids identified, alanine is found to be the major aliphatic amino acid present in mango juice, as previously reported for different mango cultivars (Wu *et al.*, 1993). In addition, many other amino acids are detected, such as valine, leucine, isoleucine, threonine, glutamine, glutamic acid and GABA. In juice samples from different batches, shown in section III.3.2, arginine, aspartic acid and asparagine were found to be present at significant levels.

The presence of lipid-type compounds is also detected in the high-field region of the juice spectrum through the TOCSY spin system comprising signals at 0.89, 1.29, 1.55 and 2.21 ppm, which may arise from one or more saturated fatty acids, such as palmitic acid, reported to be one of the most important fatty acids in mango (Wu *et al.*, 1993). Unsaturated fatty acids are not detected in the juice, since correlations to 5.30 ppm, the chemical shift expected for olefinic protons ( $-\text{CH}=\text{CH}-$ ), are not observed.

In the 1.20-1.32 ppm region, there are several overlapped signals, which in the TOCSY spectrum show correlations to resonances in the 3.4-5.2 ppm region, and may tentatively be assigned to protons H6 of fucose (6-deoxy-galactose) and rhamnose (6-deoxy-mannose). The spin systems identified are shown in Table III.1. In the case of  $\beta$ -rhamnose, 4 spin systems may possibly arise from this sugar, which may be free or interspersed with galacturonic acid residues in pectic chains (Tucker, 1993). Indeed, some of the spin systems observed are similar to those reported for rhamnose units of apple pectin (Colquhoun *et al.*, 1990; Schols *et al.*, 1994). However, the high degree of spectral overlap in the mid-field region hinders their distinction and objective assignment.

Other compounds with signals in the high-field region are acetoin, isopropanol/2,3-butanediol and ethanol, which are typical products of fermentation processes and may reflect some microbial activity in this particular juice. Indeed, in other juice samples, ethanol gives rise to much weaker signals and acetoin and isopropanol/2,3-butanediol are not detected at all.

The mid-field region (3.0-5.5 ppm) is dominated by intense and overlapped signals of the major sugars present in mango juice: glucose, fructose and sucrose. Some of their signals are easily recognised in the anomeric region of the 1D spectrum, namely the doublets at 4.64, 5.23 and 5.41 ppm, arising, respectively, from  $\beta$ -glucose (H1),  $\alpha$ -glucose (H1) and sucrose (H1 of the glucose ring). In what regards fructose, the only signal relatively free of overlap is seen at 4.11 ppm (H3 and H4 of  $\beta$ -fructofuranose). The complete spin systems for the three sugars have been measured in the TOCSY spectrum and are listed in Table III.1. In addition, several weak signals are visible in the 4.5-5.5 ppm region of the spectrum (Figure III.3b), indicating the presence of minor sugars. In particular, some spin systems identified in the TOCSY spectrum (Table III.1) seem to be consistent with the presence of xylose and of arabinose and/or galactose, according to  $^1\text{H}$

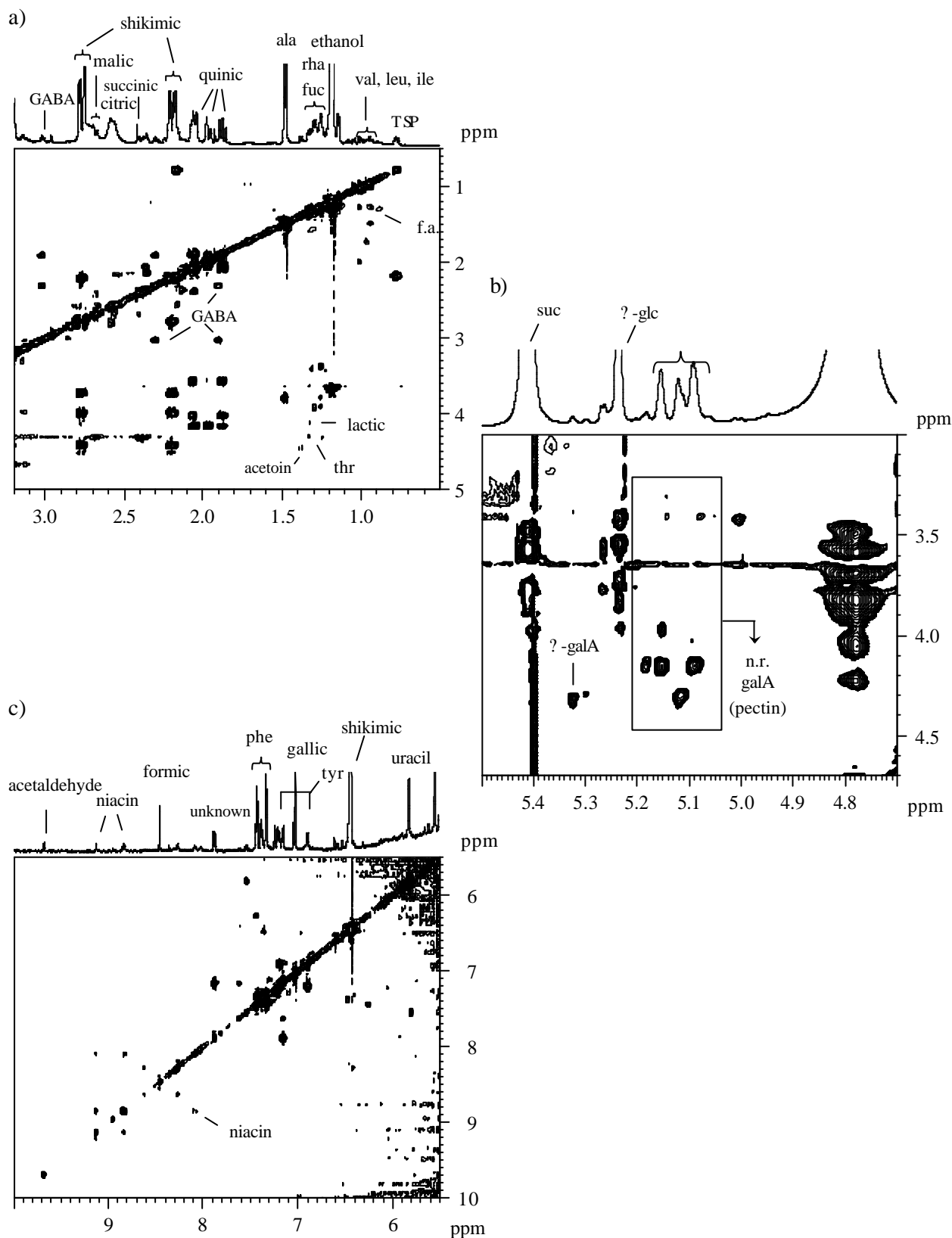


Figure III.3. Expansions of the TOCSY spectrum shown in Figure III.2: a) high-field region, b) mid-field (anomeric) region, and c) low-field region. The three-letter code is used for naming the amino acids; n.r. galA: non-reducing galacturonic acid.

NMR data reported for monosaccharides (Bock and Thøgersen, 1982). Moreover, the relatively broad signals between 5.05 and 5.20 ppm show several couplings to signals in the 3.7-4.3 ppm region and are thought to arise from non-reducing galacturonic acid residues of pectic segments, namely from protons H1 of non-esterified units and from protons H5 of units methyl-esterified at carboxylic groups (Tjan *et al.*, 1974; Neiss *et al.*, 1999). However, their spin systems could not be differentiated due to the high spectral complexity. The proton H1 of free  $\alpha$ -D-rhamnose is also expected to resonate in this region, whereas the signals of pectic  $\alpha$ -D-rhamnose H1 protons are expected to be shifted downfield to about 5.25 ppm, falling under the  $\alpha$ -D-glucose signal. At 5.32 ppm, another relatively broad signal is detected and the respective spin system is consistent with reducing  $\alpha$ -D-galacturonic acid, either free or in the reducing end of pectic segments.

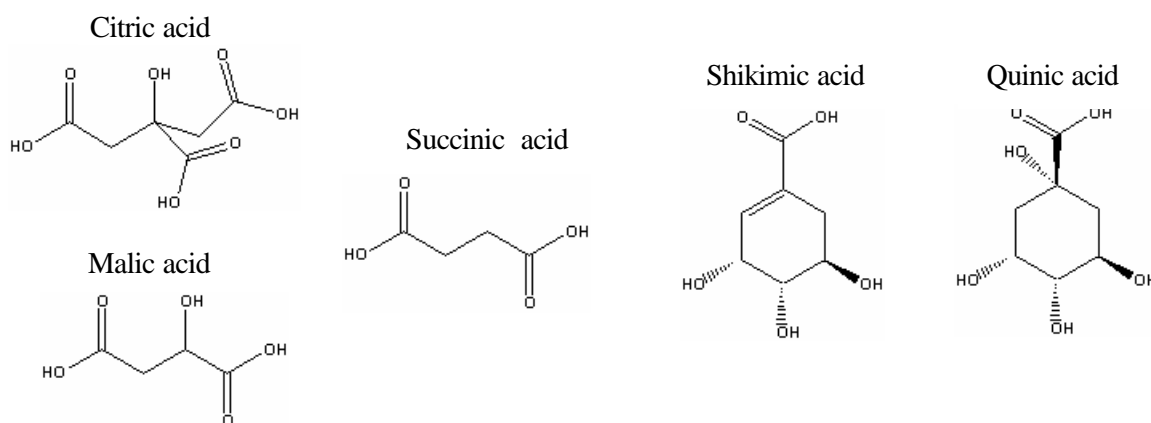


Figure III.4. Structures of the major organic acids found, in this work, to be present in mango juice.

The signals situated in the low-field region (5.5-10 ppm) are the weakest in the spectrum, the most intense signal belonging to shikimic acid (Figure III.3c). Other compounds readily identified are tyrosine, phenylalanine, acetaldehyde and niacin, a vitamin of group B known to occur in mango in approximate quantities of 0.06-0.9 mg per 100 g of fresh weight (Wu *et al.*, 1993). On the other hand, many signals found in this region show no TOCSY correlations, hindering their unambiguous identification. That is the case of several singlets, tentatively assigned to fumaric acid (6.52 or 6.61 ppm), gallic acid (7.03 or 7.04 ppm), adenine or adenosine systems (8.27 and 8.35 ppm) and formic acid (8.45 ppm). Additionally, the spectra of juices from different batches (which will be shown further ahead in Figure III.7) show two broad correlated resonances at 6.89 and 7.61 ppm that suggest the presence of polyphenolic species.

The  $^1\text{H}$ - $^{13}\text{C}$  correlation spectrum has helped confirming some of the assignments. This spectrum shows the correlation between the chemical shifts of protons and carbons that are bonded in a molecule, providing dispersion in the  $^{13}\text{C}$  frequency domain with its much greater chemical shift range. Besides the signals from the major sugars, a significant number of cross peaks are observed for less abundant compounds, particularly in the high-field region (Figure III.5a). In this region,  $^{13}\text{C}$  chemical shifts could be measured for most organic acids and amino acids identified, as well as for C-6 of rhamnose units. In the mid-field region (not shown), besides the cross peaks corresponding to the main sugars,  $^{13}\text{C}$  shifts varying in the 98-108 ppm range are found for the  $^1\text{H}$  signals at 5.05-5.20 ppm, confirming the presence of non-reducing galacturonic acid residues. In the low-field region (not shown), the only cross-peaks detected correspond to shikimic acid, phenylalanine and uridine. The homonuclear 2D  $J$ -resolved spectrum was particularly useful to measure the coupling constants of multiplets that overlap or show poor resolution in the 1D spectrum. An expansion of the high-field region of this spectrum is shown in Figure III.5b to illustrate the information provided.

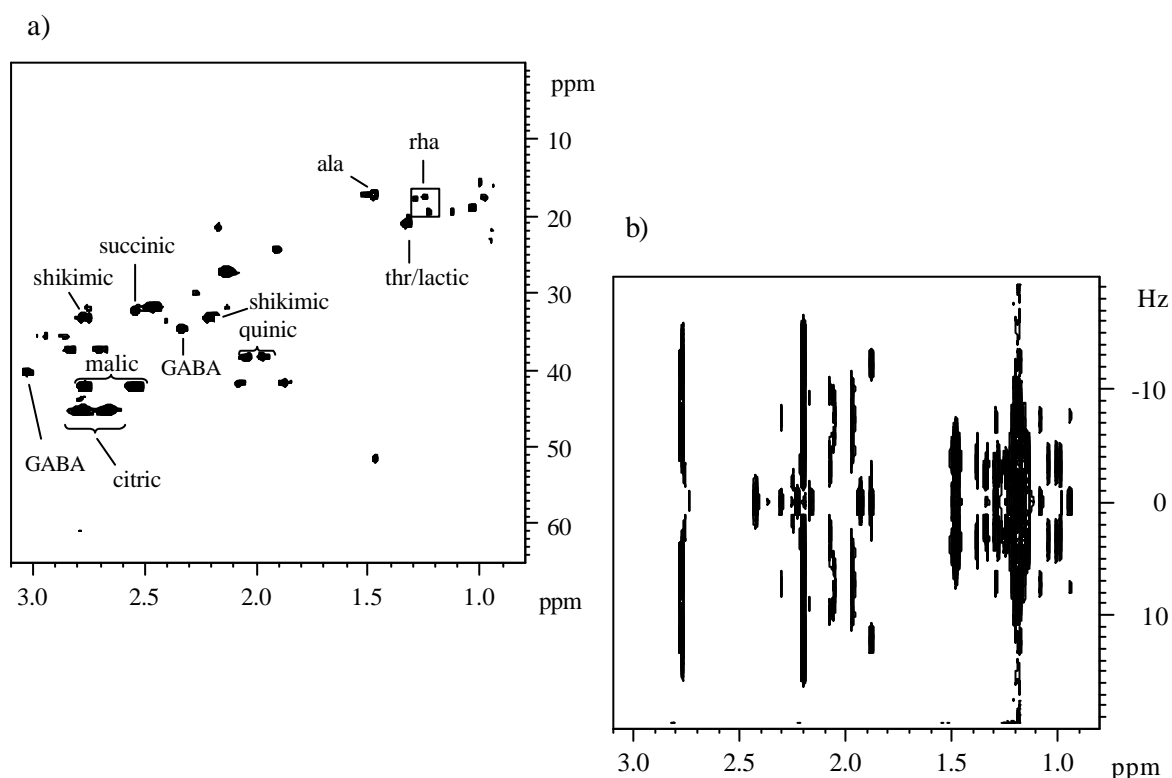


Figure III.5. Expansions of the 600 MHz 2D spectra of ripe mango juice (cv. Haden, Venezuela): a)  $^1\text{H}$ - $^{13}\text{C}$  correlation (HSQC) spectrum (NS 64 in  $f_2$ ) and b)  $J$ -resolved spectrum (NS 16 in  $f_2$ ).

Table III.1.  $^1\text{H}$  and  $^{13}\text{C}$  chemical shifts,  $^1\text{H}$  multiplicity and  $J_{\text{HH}}$  for assigned compounds in mango juice; s: singlet, d: doublet, t: triplet, q: quartet, dd: doublet of doublets, m: multiplet. Most values shown have been measured in the spectra of ripe mango juice (cv. Haden, Venezuela), except those corresponding to compounds marked with <sup>(a)</sup>, which have been measured in the spectra of a different juice sample (cv. Tommy Atkins, Brazil); <sup>(b)</sup> tentative identification; <sup>(c)</sup> the values in square brackets correspond to signals coupled to the 5.0-5.2 ppm signal, but the existence of coupling within them is not clear; <sup>(d)</sup> the  $^{13}\text{C}$  signals indicated are coupled to the  $^1\text{H}$  signals at 1.22-1.25 ppm and arise from C6H; un.: unassigned.

Compound	Assignment	? $^1\text{H}$ (ppm)	Multiplicity	$J$ (Hz)	? $^{13}\text{C}$ (ppm)		
Acetaldehyde	CH <sub>3</sub>	2.24	d	3.0			
	CH	9.68					
Acetaldehyde hydrate	CH <sub>3</sub> , hydrate	1.33					
	CH, hydrate	5.25					
Acetate	?CH <sub>3</sub>	1.92	s				
Acetoin	CH <sub>3</sub>	1.38	d	7.0			
	CH	4.43					
Adenine/Adenosine <sup>(b)</sup>	C8H, ring	8.27	s				
	C2H, ring	8.35	s				
Alanine	?CH <sub>3</sub>	1.48	d	7.2	17.00		
	?CH	3.78			51.53		
?-Aminobutyric acid (GABA)	?CH <sub>2</sub>	1.90			24.14		
	?CH <sub>2</sub>	2.30			t	7.4	34.52
	?CH <sub>2</sub>	3.01			t	7.4	40.20
?-Arabinose/ ?-Galactose <sup>(b)</sup>	C2H	3.80	d	3.4			
	C3H	3.90					
	C1H	5.30					
?-Arabinose/ ?-Galactose/ ?-Galacturonic acid/?-Fucose <sup>(b)</sup>	C1H	3.46, 4.55 3.52, 3.70, 4.57 3.52, 4.51					
	C2H						
	C3H						
Arginine <sup>(a)</sup>	?CH <sub>2</sub>	1.69	m				
	?CH <sub>2</sub>	1.91					
	?CH <sub>2</sub>	3.25					
Asparagine <sup>(a)</sup>	?CH	2.85	dd	7.6;16	35.51		
	?CH	2.95	dd	4.0;16			
	?CH	4.01					
Aspartic acid <sup>(a)</sup>	?CH	2.69	dd	7.6;16	37.29		
	?CH	2.83	dd	3.6;16			
	?CH	3.92					
2,3-Butanediol/ Isopropanol	CH <sub>3</sub>	1.14	d	6.0			
	CH	3.68					
Citric acid	?, ?CH	2.56	d	15.2	45.22		
	?', ?'CH	2.66	d	15.2			
Ethanol	CH <sub>3</sub>	1.18	t	7.1	19.20		
	CH <sub>2</sub>	3.65					
Fatty acids (saturated)	?CH <sub>3</sub>	0.89	t	7.5			
	CH <sub>2</sub> -CH <sub>3</sub>	1.29					
	CH <sub>2</sub> -CH <sub>2</sub> -CH <sub>3</sub>	1.55					
	CH <sub>2</sub> -COOH	2.21					

Table III.1 (cont.)

Compound	Assignment	$\delta$ $^1\text{H}$ (ppm)	Multiplicity	$J$ (Hz)	$\delta$ $^{13}\text{C}$ (ppm)
Formic acid <sup>(b)</sup>	<u>H</u> COOH	8.45	s		
Fructose	C6H	3.68			
( $\beta$ -furanose)	C5H	3.82			
	C3H, C4H	4.11			76.71
$\alpha$ -Fucose <sup>(b)</sup>	C6H	1.20			
	C3H/C4H	3.66			
	C2H	3.76			
	C5H	4.22			
	C1H	5.21			
$\beta$ -Fucose <sup>(b)</sup>	C6H	1.29			
	C4H	3.59			
	C5H	3.77			
Fumaric acid <sup>(b)</sup>	CH	6.52 or 6.61	s		
$\alpha$ -Galacturonic acid	C2H	3.88			
(free/pectic,	C3H	4.00			
reducing end) <sup>(b)</sup>	C4H	4.31			
	C1H	5.32	broad		99.30
$\beta$ -Galacturonic acid	un.	5.06 $\beta$ 3.98/4.09?			98.44
(pectic, non-	un.	5.09 $\beta$ 4.03/4.15/4.23?			100.00/108.35
reducing)/	un.	5.12 $\beta$ 4.09/4.30?			98.56
$\alpha$ -Rhamnose <sup>(b),(c)</sup>	un.	5.15 $\beta$ 3.75/3.97/4.15?			107.95
	un.	5.18 $\beta$ 4.00/4.12?			107.63
Gallic acid <sup>(b)</sup>	C2H, C6H	7.03 or 7.04	s		
$\alpha$ -Glucose	C4H	3.41			
	C2H	3.54			
	C3H	3.71			
	C5H, C6H	3.77-3.88			
	C1H	5.23	d	3.6	93.42
$\beta$ -Glucose	C2H	3.25			76.00
	C4H	3.41			
	C5H	3.45			
	C3H	3.48			
	C6H	3.73, 3.90			
	C1H	4.65	d	8.0	97.52
Glutamic acid	$\alpha$ , $\beta$ 'CH	2.05			
	$\beta$ CH <sub>2</sub>	2.37			
	$\beta$ CH	3.76			
Glutamine	$\beta$ CH <sub>2</sub>	2.13			
	$\beta$ CH <sub>2</sub>	2.35			
	$\beta$ CH	3.76			
$\alpha$ -Hydroxybutyric acid	$\beta$ CH <sub>3</sub>	1.20			
	$\beta$ CH	2.31			
	$\alpha$ 'CH	2.41			
	$\beta$ CH	4.13			

Table III.1 (cont.)

Compound	Assignment	? <sup>1</sup> H (ppm)	Multiplicity	<i>J</i> (Hz)	? <sup>13</sup> C (ppm)
Isoleucine	?CH <sub>3</sub>	0.94	t	7.3	
	?CH <sub>3</sub>	1.01	d	7.0	15.40
	?CH	1.25			
	?CH	1.48			
	?CH	1.98			
Lactic acid	?CH <sub>3</sub>	1.32	d	7.0	20.80
	?CH	4.10			69.00
Leucine	?, ?'CH <sub>3</sub>	0.96			21.61, 22.89
	?CH <sub>2</sub> , ?CH	1.71			
Malic acid	?CH	2.38	dd	7;16.5	42.07
	?CH	2.68	dd		
	?CH	4.30	dd		70.31
Methanol	CH <sub>3</sub>	3.36	s		49.75
Myo-inositol	C5H	3.28			
	C1H, C3H	3.53			
	C4H, C6H	3.63			
	C2H	4.06			
Niacin	C5H	8.08			
	C4H, C6H	8.84			
	C2H	9.12	s		
Phenylalanine	?CH	3.12			
	?CH	3.28			
	?CH	3.97			
	C3H, C5H ring	7.33	m		129.93
	C4H	7.38	m		
Polyphenols <sup>(a)</sup>	C2H, C6H ring	7.43	m		129.74
	un.	6.9	broad		
	un.	7.6	broad		
	un.	7.6	broad		
Propionic acid	?CH <sub>3</sub>	1.08	t	7.1	
	?CH <sub>2</sub>	2.40			
Quinic acid	?CH <sub>2</sub> ?CH <sub>2</sub>	1.84-2.10	m		38.25
	?CH	3.55	dd		
	?CH	4.02	dd		
	?CH	4.14	dd		
?-Rhamnose (free/pectic) <sup>(b), (d)</sup>	un.	1.22, 3.42, 3.88			16.23
	un.	1.24, 3.48, 3.58			17.33
	un.	1.25, 3.36, 3.78, 3.86, 4.03			19.20
	un.	1.29, 3.48, 3.87			
?-Rhamnose <sup>(b)</sup>	C6H	1.31			17.45
	C5H	3.40			
Shikimic acid	C7H	2.19	dd		33.15
	C7H'	2.77	dd		
	C5H	3.70			
	C6H	3.98			
	C4H	4.40	t		72.10
	C3H	6.44	m		132.30
Succinic acid	?, ?CH <sub>2</sub>	2.41	s		32.24

Table III.1 (cont.)

Compound	Assignment	? <sup>1</sup> H (ppm)	Multiplicity	<i>J</i> (Hz)	? <sup>13</sup> C (ppm)
Sucrose	G4H	3.47			
	G2H	3.57			
	G3H	3.78			
	G5H, G6H	3.84			
	G1H	5.41	d	3.6	93.00
	F6H	3.82			
	F5H	3.88			
	F4H	4.05			
Threonine	F3H	4.22	d	8.7	75.47
	?CH <sub>3</sub>	1.32	d	5.2	20.80
	?CH	3.61			
Tyrosine	?CH	4.26			
	C3H, C5H ring	6.90	d	8.5	
Uracil	C2H, C6H ring	7.19	d	8.5	
	C5H	5.80	d		
Uridine <sup>(a)</sup>	C6H	7.54	d		
	C4'H	4.11			
	C3'H	4.21			
	C2'H	4.38			
	C5H ring	5.88	d	8.2	105.00
Valine	C1'H	5.89			90.51
	C6H ring	7.85	d	8.2	144.56
	?CH <sub>3</sub>	0.98	d	7.0	17.39
	?CH <sub>3</sub>	1.04	d	7.0	18.70
?-Xylose <sup>(b)</sup>	?CH	2.27			29.73
	C2H	3.26			
	C3H	3.39			
	C4H	3.64			
	C1H	4.61			

### III.3.2. Compositional Differences Within and Between Cultivars

The chemical composition of mango juice is expected to be strongly dependent on several factors such as the cultivar, cultural and climate conditions of fruit growth, ripeness at harvest, postharvest storage conditions and processing method. The compositional changes taking place during the ripening process are the subject of Chapter IV. The aim of the present section is to evaluate as far as possible the compositional differences within one same cultivar and between different cultivars. For that purpose, only the spectra of unripe juices are compared, so that the influence of ripening and storage conditions on composition is minimised. The similarity of ripening stages among the juices was assessed with basis on identical firmness measurements and chemical parameters, namely the

amount of soluble solids (%SS) and pH, which are often used as maturity indicators. Thus, the three juice samples compared arise from: a) cultivar Haden grown in Venezuela, 12.3 %SS and pH 3.25; b) same cultivar grown in Brazil, 12.6 %SS and pH 3.50; and c) cultivar Tommy Atkins grown in Brazil, 13.0 %SS and pH 3.38. The differences found in the spectra of juices a) and b) of the same cultivar and between these and the spectrum of juice c) of a different cultivar are discussed separately in the following paragraphs.

#### *Comparison Between Juices of the Same Mango Cultivar (Haden)*

The two Haden juices compared (same cultivar, different geographical origin) show similar proportions of the major sugars (sucrose, glucose and fructose) and organic acids (citric, shikimic, quinic and succinic), except for malic acid which is higher in the juice from Brazil (Figure III.6b). Regarding the composition in amino acids, there are some differences to point out, as indicated in Figure III.6 (a and b). The juice from Brazil (sample b) contains notably higher amounts of arginine, glutamic acid/glutamine and aspartic acid/asparagine. The same is observed for tyrosine and phenylalanine in the low-field region of the spectra (Figure III.7). The amount of fatty acids present also differs between the two juices, as indicated by the higher intensity of the broad signals at 0.89, 1.29 and 1.55 ppm in the spectrum of the juice from Venezuela (Figure III.6a). In the low-field region (Figure III.7), further differences are noted, especially in the relative proportions of some compounds, such as uridine- and adenosine-containing compounds, which are higher in the juice from Brazil. Moreover, two weak broad resonances at 6.89 and 7.61 ppm are noted in the spectrum of that sample (indicated with arrows in Figure III.7b), suggesting the presence of condensed phenolic species. These signals have been observed in the  $^1\text{H}$  NMR spectra of apple juices and their presence has been suggested to result from exposure to air and enzymatic oxidation by polyphenoloxidase, which leads to the formation of polymeric condensation products (Belton *et al.*, 1997). As no particular precautions were taken to avoid these effects during the sample preparation procedure, this possibility must be considered. An interesting observation is that the extension of polyphenols formation seems to depend on the ripening degree. The increasing intensity of polyphenolic signals with ripening will be shown in Chapter IV, where the ripening process of mango fruit is discussed. Hence, the Haden juices from Brazil and Venezuela are found to differ mainly in the contents of some amino acids and aromatic compounds.

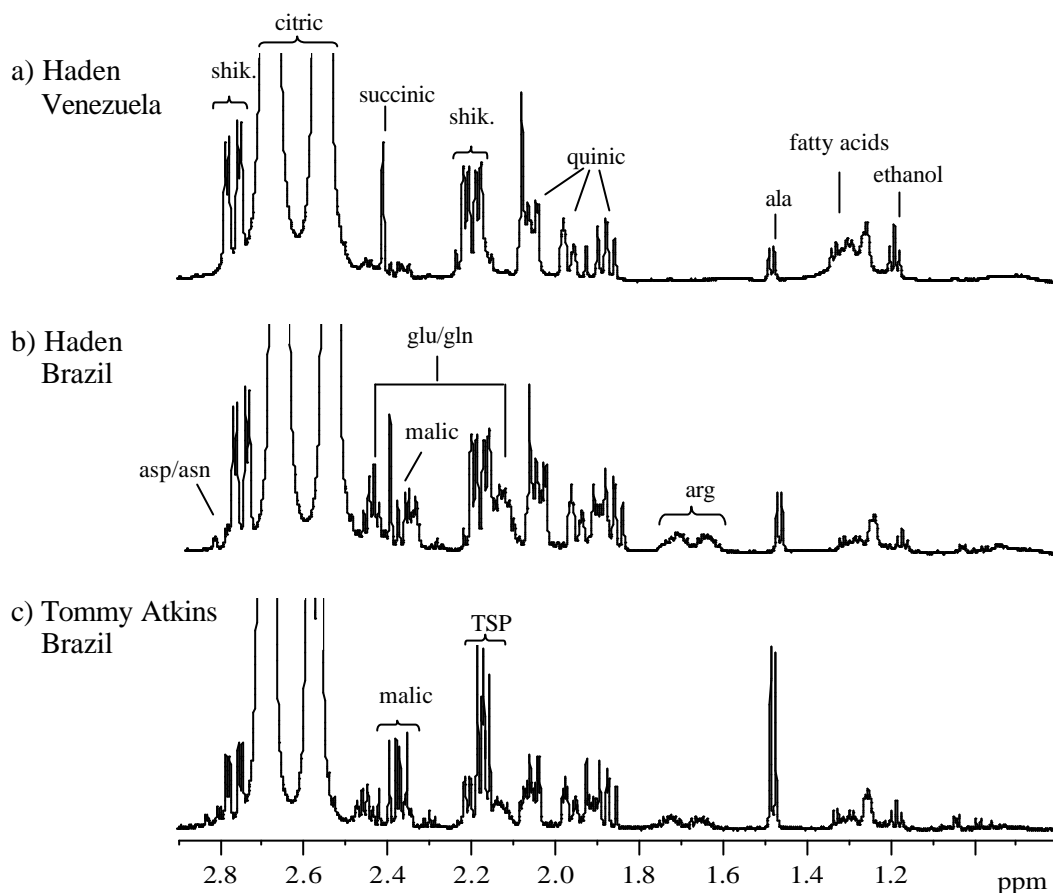


Figure III.6. High-field region of the 600 MHz  $^1\text{H}$  NMR spectra of mango juices from three different batches: a) cv. Haden (Venezuela); b) cv. Haden (Brazil); c) cv. Tommy Atkins (Brazil); NS 64 for all spectra.

#### *Comparison Between Juices of Different Mango Cultivars (Haden and Tommy Atkins)*

Comparing the spectra of the Haden juices discussed in the previous paragraph (samples a and b) with the spectrum of the Tommy Atkins juice (sample c), some of the main differences regard the relative abundances of some organic acids and amino acids. Shikimic and succinic acids are lower in the spectrum of the Tommy Atkins juice, whereas alanine is clearly higher (Figure III.6). On the other hand, phenylalanine is present in very low content in this juice (Figure III.7). Further compositional differences observed in the low-field region (Figure III.7) arise from: uridine and adenosine systems, which are not detected in the Tommy Atkins juice; an unassigned system comprising the doublets at 7.16 and 7.87 ppm also absent in that sample; and a singlet at 7.27 ppm (unassigned) which is much higher in Tommy Atkins than in Haden juices. On the other hand, the broad resonances at 6.89 and 7.61 ppm, suggested to arise from polyphenols, are also detected in the Tommy Atkins juice, similarly to the Haden juice from Brazil.

Hence, the results described above show that the compositional differences between Haden and Tommy Atkins juices, which regard mainly some amino acids and aromatic compounds, are similar in significance to those between Haden juices of distinct geographical origins, thus demonstrating the influence of both cultivar and geographical origin on mango composition.

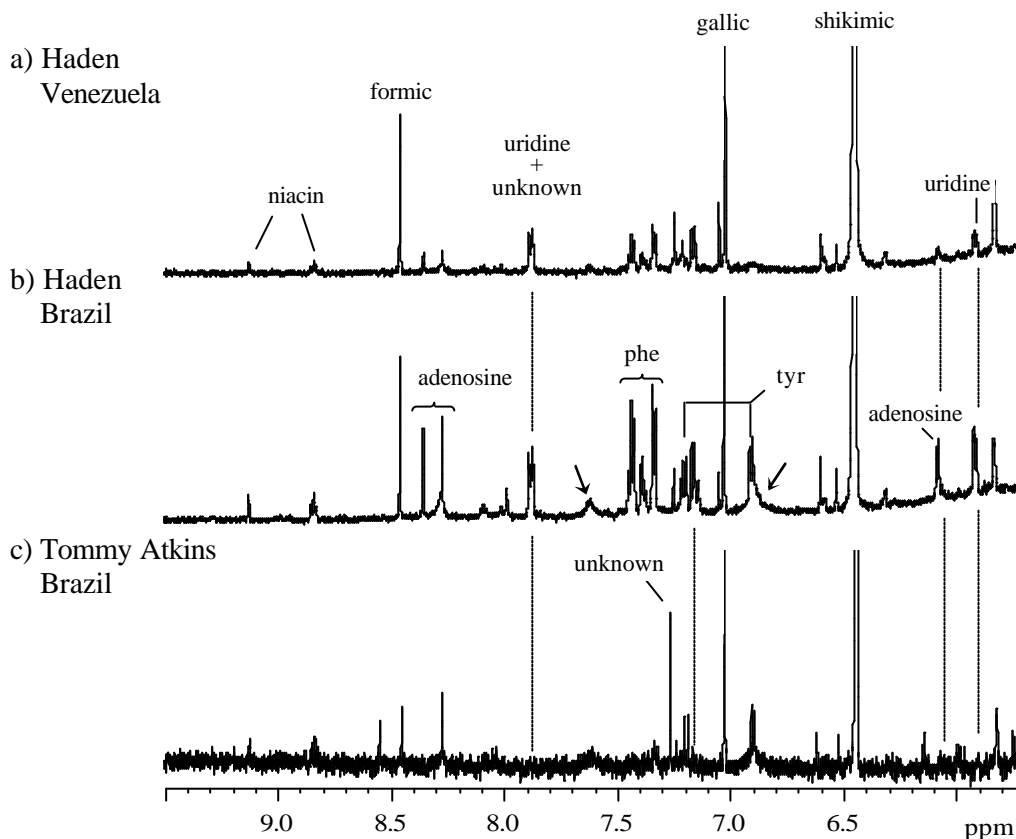


Figure III.7. Low-field region of the 600 MHz  $^1\text{H}$  NMR spectra of mango juices from three different batches: a) cv. Haden (Venezuela); b) cv. Haden (Brazil); c) cv. Tommy Atkins (Brazil); NS 64 for all spectra; the arrows indicate resonances possibly arising from polyphenols; the lower S/N ratio of spectrum c is due to the larger dilution of the Tommy Atkins juice.

### III.4. NMR Study of Mango Pulp Composition

#### III.4.1. Standard Magic Angle Spinning (MAS) NMR

Standard  $^1\text{H}$  MAS NMR spectroscopy was the first approach used to study intact mango pulp. Figure III.8 shows the spectra of mango pulp recorded in static conditions and by spinning the sample at 1.0 or 1.2 KHz. The static  $^1\text{H}$  NMR spectrum (Figure III.8a) is dominated by the intense water signal at 4.7 ppm, showing also a very weak and broad

hump, situated between 3 and 4 ppm, which corresponds to the sugar resonances. The line width at half height ( $\Delta\nu_{1/2}$ ) of the water signal is 108 Hz, which is of the same order of magnitude of the values of 70.9 and 75.9 Hz reported for the water line width in the 200 MHz  $^1\text{H}$  spectra of banana and grape tissues, respectively (Ni and Eads, 1993a). As described in Chapter II.1.4, there are several effects that may contribute to the low resolution of this spectrum, namely the anisotropic interactions typically observed in solids due to their reduced molecular mobility, and the magnetic susceptibility differences within the sample arising from its physical heterogeneity. The former effects (dipolar interactions and chemical shift anisotropy) are expected to be partially averaged by the internal molecular motion characterising the fruit pulp, which is much larger than in a rigid solid. The susceptibility effects, typically of the order of a few tens of Hz for water, have been shown to play an important role in the broadening of the  $^1\text{H}$  spectra of fruit tissues (Cho *et al.*, 1991; Ni and Eads, 1993a; Ni and Eads, 1993b). This may be explained by the heterogeneous nature of the fruit tissues, since the different physical domains have different bulk magnetic susceptibilities and are thus magnetised to different extents when subjected to the strong magnetic field. The magnetised domains then produce position-dependent magnetic field variations in the space around them, giving rise to a spread in resonance frequencies.

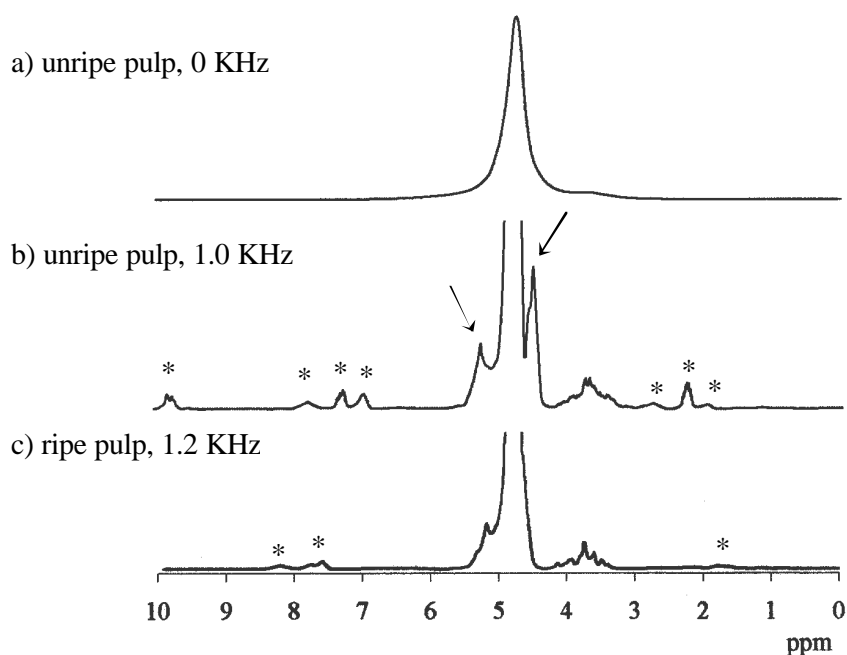


Figure III.8. 400 MHz standard  $^1\text{H}$  NMR spectra of unripe (a and b) and ripe (c) mango pulp (cv. Tommy Atkins) obtained at a) 0 KHz, b) 1.0 KHz spinning rate, and c) 1.2 KHz spinning rate; \*: spinning side bands; the signals indicated with arrows may reflect different water environments.

Spinning the same sample at the magic angle using low speeds (1.0 KHz) results in a significant improvement of the spectral resolution (Figure III.8b), similarly to what has been reported for other fruits (Ni and Eads, 1993a; Ni and Eads, 1993b). The bands identified with an asterisk correspond to spinning side bands, which appear on either sides of the isotropic chemical shift bands, spaced at an interval equal to the spinning rate. These bands reflect the contribution of anisotropic effects, such as chemical shift anisotropy (CSA), to line broadening. Typically, CSA line widths are in the range of a few KHz (Belton and Gil, 1993), and the lines broadened by CSA are expected to be narrowed by MAS rates of the same or larger magnitude. At 1 KHz spinning rate, the  $\Delta\nu_{1/2}$  of the water signal is reduced from 108 to 48 Hz and the sugar resonances centred at 3.7 ppm show much better resolution, compared to the broad hump observed in the static spectrum. The signals indicated with arrows may reflect the different water environments, mostly due to phase separation promoted by sample spinning, although an additional contribution for the peak at 5.2 ppm may arise from sugar anomeric resonances.

Compared to the spectrum of unripe pulp, the  $^1\text{H}$  MAS spectrum of ripe pulp obtained at similar spinning rate (1.2 KHz) shows enhanced resolution (Figure III.8c), the  $\Delta\nu_{1/2}$  of the water signal being 25 Hz. This improvement is related to the softer texture of the ripe pulp, which accounts for the higher internal molecular motion, and thus for the partial averaging of anisotropic interactions. However, the resolution achieved in the standard  $^1\text{H}$  MAS spectra is still not enough to enable objective assignment of the sugar peaks to be made or efficient water suppression techniques to be employed, thus providing limited information about the composition of mango fruit, since no peaks from non-sugar components could be identified. In the following section, the use of a high resolution (HR-MAS) probe to study the mango pulp in more detail is described.

#### **III.4.2. High Resolution Magic Angle Spinning (HR-MAS) NMR**

Figure III.9 shows the  $^1\text{H}$  HR-MAS spectra of ripe mango pulp, obtained in static conditions and by spinning the sample at 1.2 KHz. Comparison with the spectra shown in Figure III.8 demonstrates how the resolution is significantly improved by the use of a HR-MAS probe. The nature of the probe, built so as to incorporate high resolution r.f. parts, and the deuterium lock (by which long term stability of the magnetic field is achieved) are responsible for this enhancement, which can be measured by taking into account the line

widths of the signals. For instance, in the standard  $^1\text{H}$  MAS spectrum of ripe pulp obtained at 1.2 KHz (Figure III.8c), the  $\Delta\nu_{1/2}$  of the most intense sugar peak ( $\delta$  3.82 ppm) is 38 Hz, while in the  $^1\text{H}$  HR-MAS spectrum obtained at the same spinning rate (Figure III.9b) the  $\Delta\nu_{1/2}$  of that signal is 6.4 Hz (about 6 times narrower).

Moreover, the efficient water suppression achieved with the HR-MAS probe enables the detection of many signals in the whole spectrum, similarly to the juice spectrum previously shown. Besides the major sugars, many compounds present at lower concentrations are detected in the high-field and low-field regions of the  $^1\text{H}$  HR-MAS spectrum, as illustrated by the inserts in Figure III.9b. It is also important to stress that the significant resolution improvement obtained allows standard 2D high resolution experiments to be carried out. TOCSY,  $^1\text{H}$ - $^{13}\text{C}$  correlation and  $J$ -resolved spectra have been recorded and enabled the detailed pulp chemical composition to be investigated, as it will be shown further ahead.

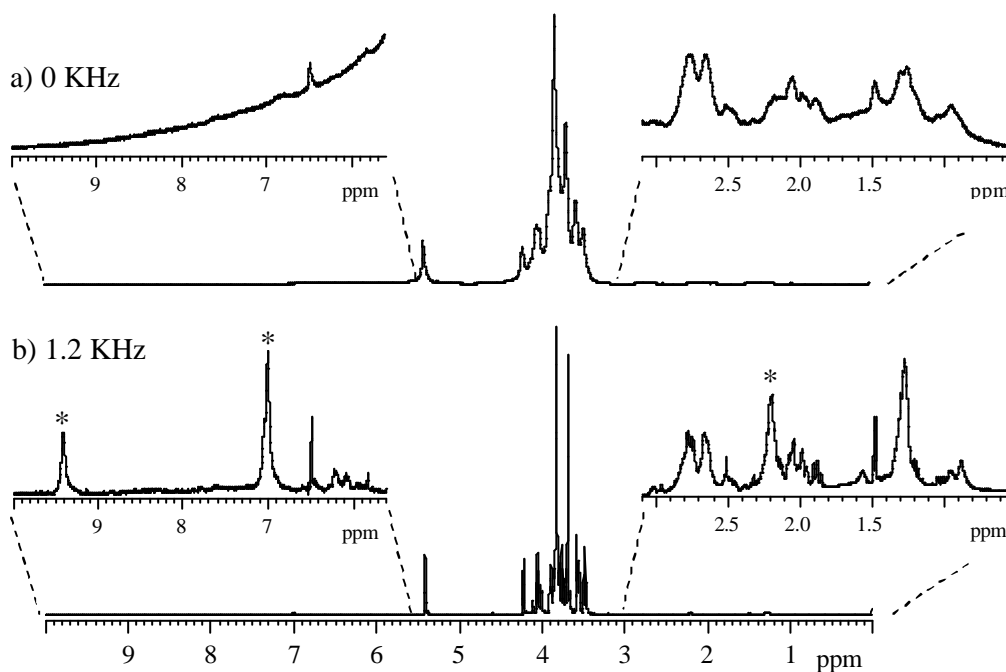


Figure III.9. 500 MHz HR-MAS  $^1\text{H}$  NMR spectra of ripe mango pulp (cv. Tommy Atkins): a) 0 KHz, b) 1.2 KHz. \*: spinning side bands arising from the water peak.

### Effect of Spinning Rate

The effect of using higher spinning rates on the spectral resolution has been investigated by recording  $^1\text{H}$  HR-MAS spectra of ripe mango pulp at spinning rates varying from 3.0 to 15.0 KHz, the maximum rate allowed with the probe used. A rotor with a top spacer, conferring the sample a spherical shape and avoiding water loss during

spinning, has been used to pack the pulp. Most signals show no significant resolution changes with spinning rate. For instance, the values of  $\Delta\nu_{1/2}$  for the sucrose peak at 4.22 ppm are 1.96, 2.00 and 1.83 Hz at 3.0, 7.0 and 15.0 KHz, respectively (not shown). The fact that the resolution of such signals is not improved at higher rates indicates that the broadening factors affecting them have magnitudes smaller than 3.0 KHz (the lowest rate used). This is consistent with sample susceptibility effects being the main broadening mechanism, since they are expected to be of the order of only a few tens of Hz (Ni and Eads, 1993a). On the other hand, the resolution of the signals of lipids and pectins improves consistently with increasing spinning rates. This is illustrated in Figure III.10, which shows the gradual resolution improvement for the signal centred at 1.28 ppm, to which both lipids and pectic sugars (essentially rhamnose) contribute, and also for the less intense signals at 0.89 and 1.55 ppm arising from lipids.

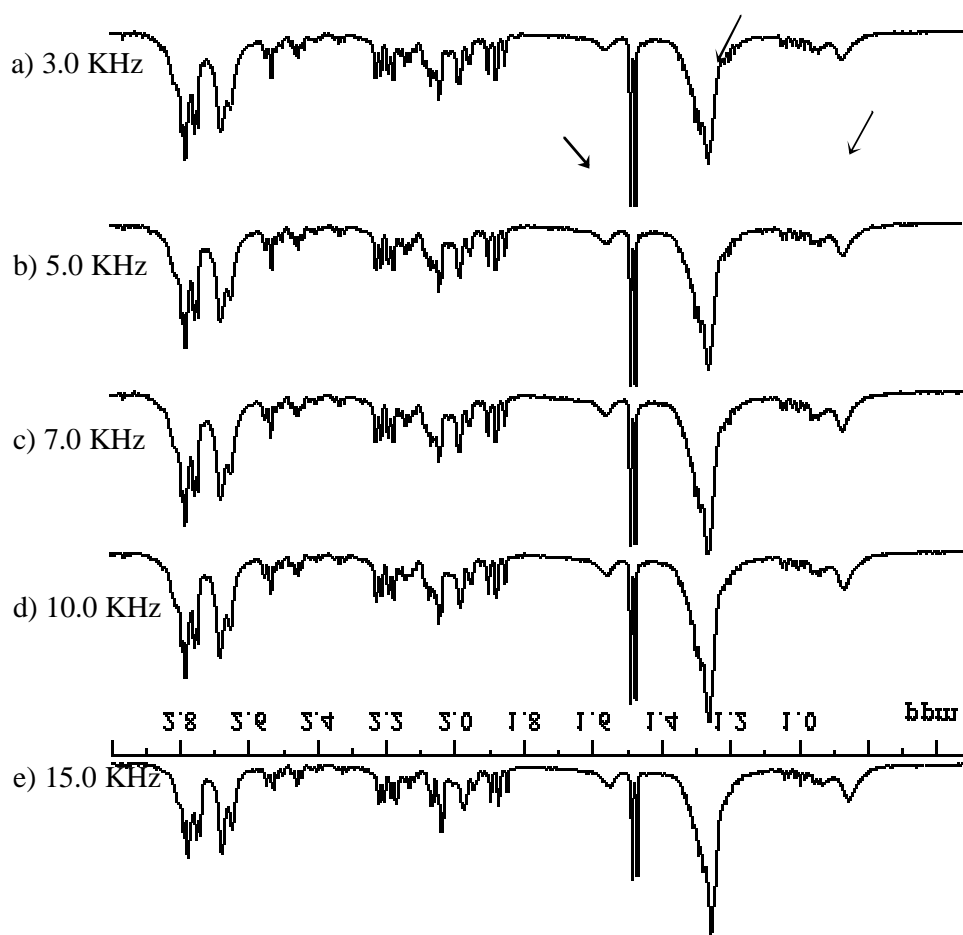


Figure III.10. High-field region of the 500 MHz HR-MAS  $^1\text{H}$  NMR spectra of ripe mango pulp (cv. Tommy Atkins), recorded at different spinning rates (NS 256); the arrows indicate the resonances of lipids and pectic sugars (the latter contributing to the largest signal only).

This result shows that these compounds are under the effect of interactions that are at least of the order of 10-15 KHz, namely dipolar interactions. It is also worth mentioning that for spinning rates higher than 3 KHz, the spinning side bands already have negligible intensity and appear outside the region of interest (0-10 ppm).

An interesting observation regards the behaviour of the broad signals observed in the aromatic region of the spectrum, tentatively assigned to polyphenolic compounds (Figure III.11). These signals are observed at all spinning rates except at 15 KHz (Figure III.11e), and when the spinning rate is decreased back they appear again. Obviously their disappearance does not reflect any chemical change in the sample composition since they

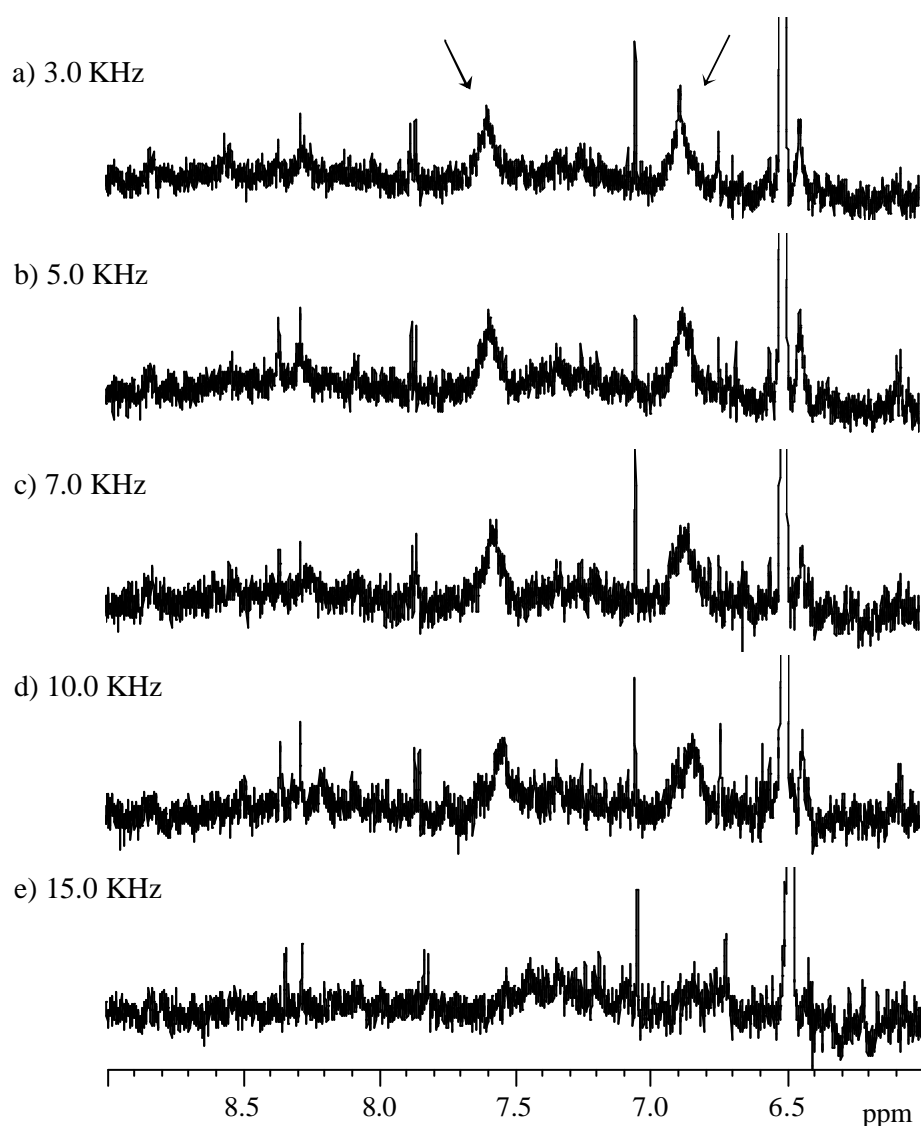


Figure III.11. Low-field region of the 500 MHz HR-MAS  $^1\text{H}$  NMR spectra of ripe mango pulp (cv. Tommy Atkins), recorded at different spinning rates (NS 256); the arrows indicate resonances tentatively assigned to polyphenols.

become visible as soon as the spinning rate is decreased. Instead, it can reflect the interference of molecular motion with spinning rate, which results in loss of the signal from the spectrum. This suggests that the aromatic rings of these polyphenolic compounds may be involved in relatively slow motions of the order of 15 KHz, consistent with their polymeric nature.

#### *Effect of Sample Shape*

The shape of the sample inside the HR-MAS rotor can be cylindrical, semi-spherical (for rotors with one spacer) or spherical (if both bottom and top spacers are provided). The latter rotor types improve spinning stability and reduce magnetic susceptibility variations within the sample, thus potentially improving spectral resolution. Moreover, it has been observed in the present study that the samples packed with spacers generally show less extensive separation of the liquid phase upon spinning than those packed with the cylindrical configuration.

The  $^1\text{H}$  HR-MAS spectra of ripe mango pulp obtained with the three different sample shapes (at 5.0 KHz spinning rate) are shown in Figure III.12. The top spectrum, corresponding to the cylindrical configuration, shows a broad hump in the water region, which prevents the observation of signals in the 4.2-7.2 ppm range. This distortion is likely to be related to the separation of phases seen to occur upon spinning of the cylindrical rotor, which causes water to be present in different magnetic environments, and, hence, to originate a broad signal difficult to suppress by selective irradiation. In what concerns the resolution of most signals, the three spectra are similar. The alanine signal at 1.48 ppm, for instance, shows  $\nu_{1/2}$  of 2.6, 2.3 and 2.5 Hz in the spectra corresponding to cylindrical, semi-spherical and spherical sample shapes, respectively. On the other hand, the  $\nu_{1/2}$  of the signal at 1.28 ppm, attributed to lipids and pectic sugars, decreases from 45.4 Hz in the cylindrical shape, to 43.0 Hz in the semi-spherical shape and to 38.2 Hz in the spherical shape, reflecting a slight resolution increase. This suggests that, at the spinning rate used (5.0 KHz) residual magnetic susceptibility anisotropy contributes to the resolution of the signals from these large molecules.

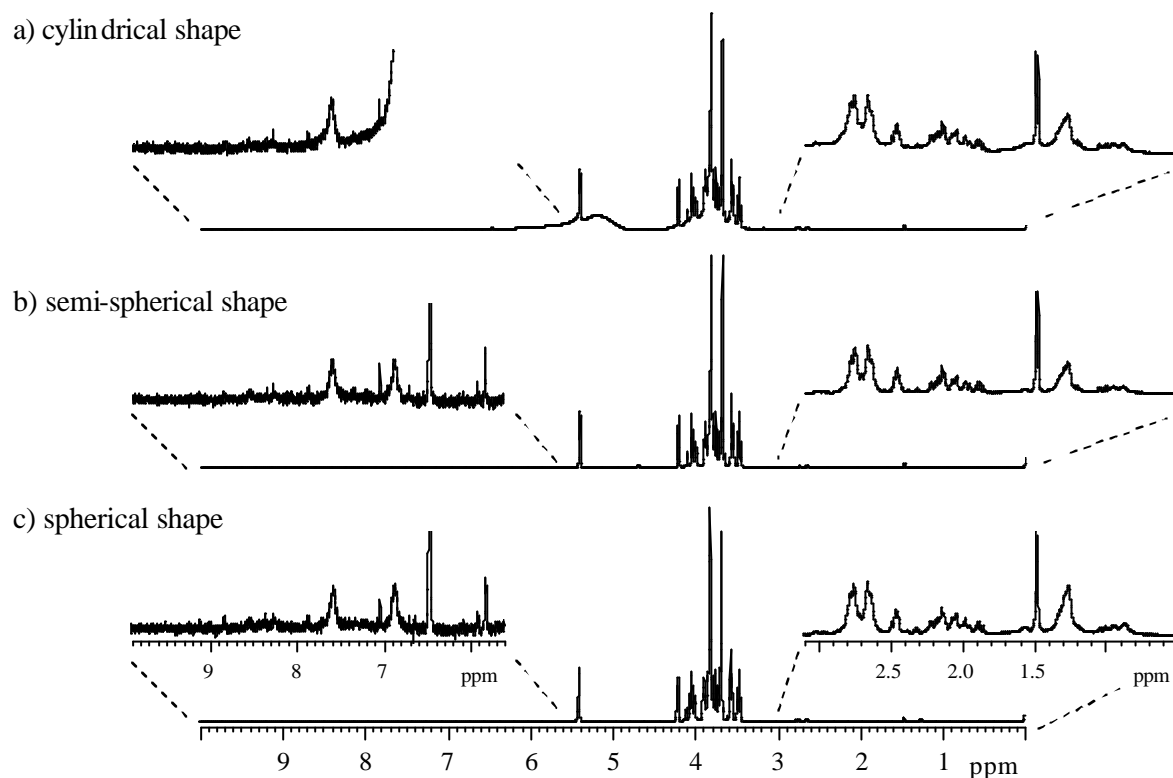


Figure III.12. 500 MHz HR-MAS  $^1\text{H}$  NMR spectra of ripe mango pulp (cv. Tommy Atkins), packed into different rotors: a) cylindrical shape, b) semi-spherical shape, and c) spherical shape; SR 5.0 KHz, NS 256.

### III.4.3. Compositional Differences Between Pulp and Juice

The high resolution achieved in the  $^1\text{H}$  HR-MAS spectra of intact mango pulp enables the detailed study of its composition and comparison with the juice composition, presented in section III.3. The following discussion highlights the spectral differences between a mango pulp and the corresponding juice, reflecting the compositional differences found between the whole fruit and the extracted liquid phase.

Figures III.13 to III.15 show different spectral regions of the  $^1\text{H}$  spectra of pulp and juice, collected from an unripe mango (cv. Haden). As expected, the juice spectrum contains sharper lines and an overall better resolution than the pulp spectrum. For example, the alanine peak at 1.48 ppm shows  $\Delta\nu_{1/2}$  of 2.3 Hz in the pulp spectrum and half of this value in the juice spectrum. The rapid isotropic motions of the molecules in the liquid state, averaging out the anisotropic interactions that are responsible for line broadening, account for the better resolution of the juice spectrum. In addition, the higher field strength ( $B_0$ ) used for recording that spectrum may also contribute to the resolution difference observed, since the dispersion of NMR chemical shifts is linearly related to  $B_0$ . On the

other hand, some signals are only seen in the spectrum of pulp and not in the corresponding juice. This is the case of the relatively broad resonances at 0.89, 1.29 and 1.55 ppm which arise from saturated fatty acids. It must be noted, however, that these signals do appear in some juice samples, particularly in those collected from ripe mangoes, like the one presented in section III.3. In addition, the signals of rhamnose pectic units (overlapping in the 1.2-1.3 ppm region) are more intense in the pulp spectrum than in the corresponding juice. Besides these differences, the TOCSY spectrum of the pulp shows a spin system that is not present in the juice. This system, shown by the dashed lines in Figure III.13c, comprises the resonances at 1.31, 2.02 and 5.31 ppm and possibly arises from unsaturated fatty acids. It is interesting to note that this set of peaks has not been identified in any juice spectrum, not even in the ripe stage, thus showing that these lipids are preferably located in the solid phase of the fruit throughout all ripening stages.

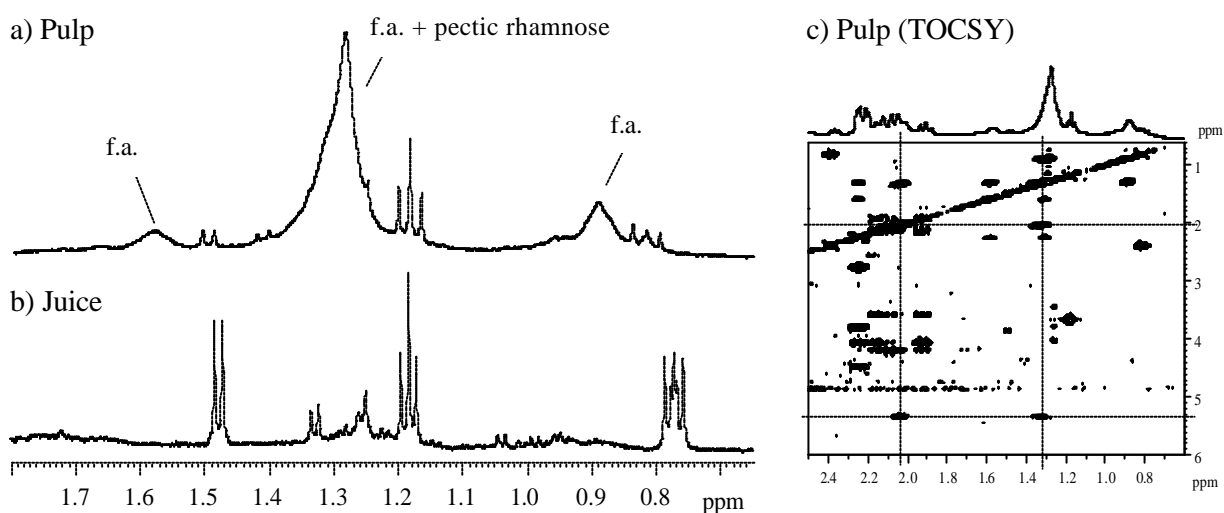


Figure III.13. High-field region of the  $^1\text{H}$  NMR spectra of mango pulp (a and c) and of mango juice (b), collected from an unripe fruit (cv. Haden, Venezuela); the spin system tentatively assigned to unsaturated fatty acids (u.f.a.) is identified in the TOCSY spectrum by the dashed lines. Pulp: 400 MHz, NS 180 for 1D and NS 24 in  $f_2$  for TOCSY; Juice: 600 MHz, NS 64.

Further differences between pulp and juice are found in the sugar anomeric region of the spectra (Figure III.14). The pulp spectrum shows a signal at 5.31 ppm arising from the olefinic protons of unsaturated fatty acids, which is absent in the juice, as previously noted. Moreover, the signals in the 5.05-5.20 ppm range, arising mainly from non-reducing galacturonic acid units of pectic chains, are much more intense in the pulp spectrum, indicating that only a small amount of pectic material is present in the unripe juice. In addition, the TOCSY spectrum of the pulp presents one system comprising the signals at

3.84, 3.95, 4.10, 4.30 and 5.12 ppm (not shown), which may arise from methyl-esterified non-reducing galacturonic acid residues and is not detected in the TOCSY of the juice.

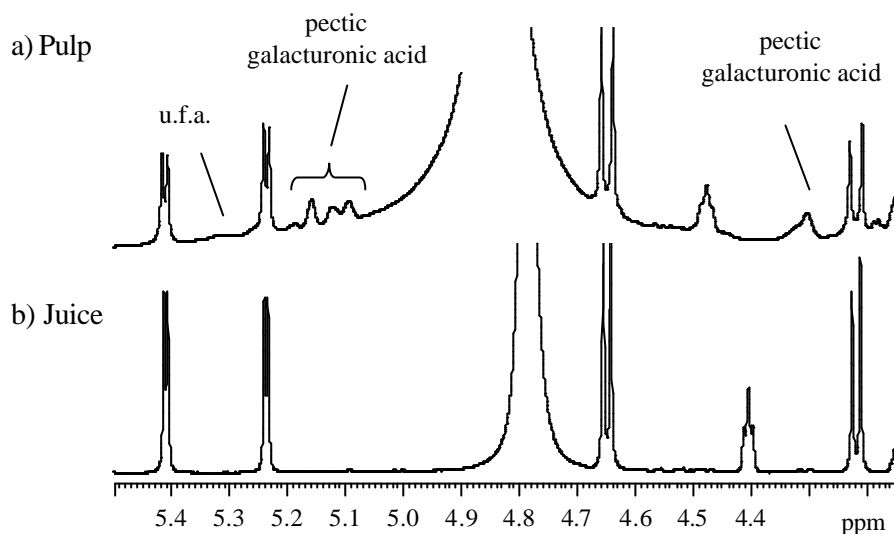


Figure III.14. Mid-field region of the  $^1\text{H}$  NMR spectra of a) mango pulp and b) mango juice, collected from an unripe fruit (cv. Haden, Venezuela); Pulp: 400 MHz, NS 180; Juice: 600 MHz, NS 64.

Finally, in the low-field region, besides the shifts of some signals reflecting the different pH of the samples, there are a few differences between the pulp and juice spectra (Figure III.15). The most significant are the much higher intensity of the unassigned singlet at 7.26 ppm in the pulp spectrum and of the singlet at 8.45 ppm (probably arising from formic acid) in the juice spectrum.

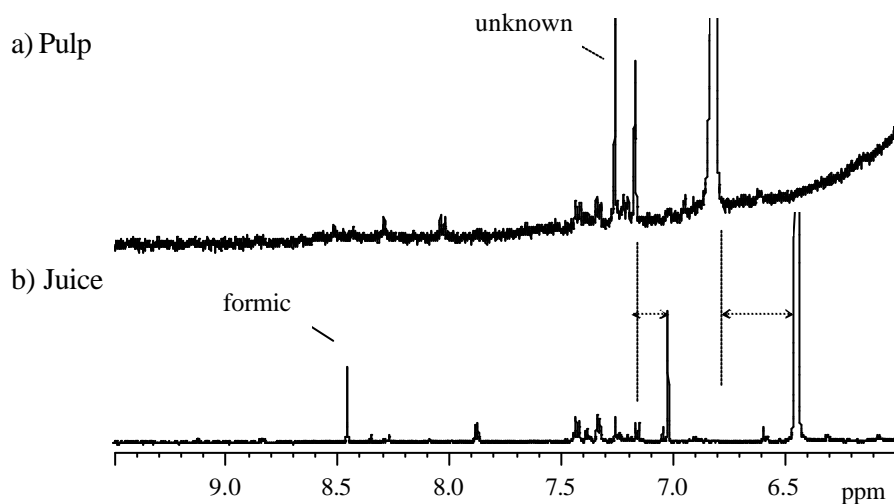


Figure III.15. Low-field region of the  $^1\text{H}$  NMR spectra of a) mango pulp and b) mango juice, collected from an unripe fruit (cv. Haden, Venezuela); the arrows indicate shifts due to pH differences; Pulp: 400 MHz, NS 180; Juice: 600 MHz, NS 64.

### III.5. Conclusions

High resolution  $^1\text{H}$  NMR spectroscopy of mango juice has enabled the identification of just under 50 components, including the 3 main sugars (glucose, fructose, sucrose), 12 organic acids (among which are quinic and shikimic acids, reported for the first time to be present in mango juice), 13 amino acids (including ala, val, leu, arg, tyr, phe), the aliphatic alcohols methanol, ethanol and isopropanol/2,3-butanediol, the cyclic polyalcohol myo-inositol, the vitamin niacin and several other compounds. Resonances of lipid-type components, possibly saturated fatty acids, pectic constituents (rhamnose and galacturonic acid) and polyphenols have also been detected. The spectral assignment was carried out with basis on 1D and 2D NMR spectra (TOCSY,  $^1\text{H}$ - $^{13}\text{C}$  correlation and *J*-resolved) and, besides the compounds identified, about 15 more spin systems have been detected and remain unassigned, requiring further investigation. The main difficulties found in spectral assignment were the low intensity of some signals arising from minor components (particularly noticed in the aromatic region of the spectrum), the high degree of spectral overlap hindering, for instance, the complete assignment of less abundant sugars in the sugar region, and the ambiguity associated with the assignment of singlets and incomplete spin systems. Still, NMR provided a fairly good survey of mango juice components by direct analysis of the juice, requiring minimum sample preparation and without the need of using extraction or separation procedures. The juices of different cultivars (Haden and Tommy Atkins) and geographical origins (Venezuela and Brazil) have been found to differ mainly in the relative abundance of some amino acids, organic acids and aromatic compounds (namely polyphenols).

Solid state NMR techniques have enabled the direct and non-invasive study of intact mango pulp. With a standard probe and MAS at low speeds ( $\sim 1$  KHz) the  $^1\text{H}$  spectrum of the fruit tissue showed enhanced resolution compared to the spectrum recorded in static conditions, enabling detection of the major sugars, but not of other components present in lower amounts. By using a HR-MAS probe, a much more marked resolution improvement has been obtained, the  $^1\text{H}$  HR-MAS spectrum showing signals six fold narrower than the standard  $^1\text{H}$  MAS spectrum. Under such conditions, efficient water suppression could be achieved, enabling the detection of many signals in the whole spectral range. In addition, the spectral resolution achieved enabled 2D NMR spectra to be recorded in order to aid spectral assignment. Interestingly, compositional differences were

found between the intact pulp and the corresponding juice, showing that the composition of the liquid phase is not necessarily fully representative of the composition of the whole fruit. In particular, the pulp showed the presence of fatty acids (both saturated and unsaturated) not detected in the juice and a higher abundance of pectic material.

## References

- Alberti, E.; Belton, P.S.; Gil, A.M. Applications of NMR to Food Science. *Annual Reports of NMR Spectroscopy* **2002**, *47*, 110-148.
- Alberti, E.; Humpfer, E.; Spraul, M.; Gilbert, S.; Tatham, A.S.; Shewry, P.R.; Gil, A.M. A high resolution  $^1\text{H}$  magic angle spinning NMR study of high- $M_r$  subunit of wheat glutenin. *Biopolymers* **2001**, *58*, 33-45.
- Aue, W.P.; Karhan, J.; Ernst, R.R.J. Homonuclear broad band decoupling and two-dimensional J-resolved NMR spectroscopy. *Journal of Chemical Physics* **1976**, *64*, 4226-4227.
- Bax, A. A spatially selective composite 90-degree radiofrequency pulse. *Journal of Magnetic Resonance* **1985**, *65*, 142-145.
- Bax, A.; Davis, D.G. MLEV-17 based two-dimensional homonuclear magnetization transfer spectroscopy. *Journal of Magnetic Resonance* **1985**, *65*, 355-360.
- Belton, P.S.; Delgadillo, I.; Holmes, E.; Nicholls, A.; Nicholson, J.K.; Spraul, M. Use of high-field  $^1\text{H}$  NMR spectroscopy for the analysis of liquid foods. *Journal of Agricultural and Food Chemistry* **1996**, *44*, 1483-1487.
- Belton, P.S.; Delgadillo, I.; Gil, A.M.; Casascelli, F.; Colquhoun, I.J.; Dennis, M.J.; Spraul, M. High field proton NMR studies of apple juices. *Magnetic Resonance in Chemistry* **1997**, *35*, S52-S60.
- Belton, P.S.; Delgadillo, I.; Gil, A.M. High-field solution state proton NMR for food analysis. *Seminars in Food Analysis* **1998a**, *3*, 223-234.
- Belton, P.S.; Colquhoun, I.J.; Kemsley, E.K.; Delgadillo, I.; Roma, P.; Dennis, M.J.; Sharman, M.; Holmes, E.; Nicholson, J.K.; Spraul, M. Application of chemometrics to the  $^1\text{H}$  NMR spectra of apple juices: discrimination between apple varieties. *Food Chemistry* **1998b**, *61*, 207-213.
- Bock, K.; Thøgersen, H. Nuclear magnetic resonance spectroscopy in the study of mono- and oligosaccharides. *Annual Reports on NMR Spectroscopy* **1982**, *13*, 1-57.

Cho, S.I.; Bellon, V.; Eads, T.M.; Stroshine, R.L.; Krutz, G.W. Sugar content measurement in fruit tissue using water peak suppression in high resolution  $^1\text{H}$  magnetic resonance. *Journal of Food Science* **1991**, *56*, 1091-1094.

Colquhoun, I.J.; de Ruiter, G.A.; Schols, A.; Voragen, G.J. Identification by NMR spectroscopy of oligosaccharides obtained by treatment of the hairy regions of apple pectin with rhamnogalacturonase. *Carbohydrate Research* **1990**, *206*, 131-144.

Eads, T.M.; Bryant, R.G. High resolution proton NMR spectroscopy of milk, orange juice, and apple juice with efficient suppression of the water peak. *Journal of Agricultural and Food Chemistry* **1986**, *34*, 834-837.

Fan, T.W.-M. Metabolite profiling by one- and two-dimensional NMR analysis of complex mixtures. *Progress in Nuclear Magnetic Resonance Spectroscopy* **1996**, *28*, 161-219.

Gil, A.M., Alberti, E.; Tatham, A.S.; Belton, P.S.; Humpfer, E.; Spraul, M. Magic angle spinning NMR study of the hydration of the wheat seed storage protein omega-gliadins. *Magnetic Resonance in Chemistry* **1997**, *35*, S101-S111.

Gil, A.M.; Duarte, I.F.; Delgadillo, I.; Colquhoun, I.J.; Casuscelli, J.; Humpfer, E.; Spraul, M. Study of the compositional changes of mango during ripening by use of nuclear magnetic resonance spectroscopy. *Journal of Agricultural and Food Chemistry* **2000**, *48*, 1524-1536.

Le Gall, G., Puaud, M., Colquhoun, I.J. Discrimination between orange juice and pulp wash by  $^1\text{H}$  nuclear magnetic resonance spectroscopy: Identification of marker compounds. *Journal of Agricultural and Food Chemistry* **2001**, *49*, 580-588.

Lizada, C. Mango. In *Biochemistry of Fruit Ripening*; Seymour, G.B., Taylor, J.E., Tucker, G.A., Eds.; Chapman & Hall: London, 1993; 255-271.

Neiss, T.G.; Cheng, H.N.; Daas, P.J.H.; Schols, H.A. Compositional heterogeneity in pectic polysaccharides: NMR studies and statistical analysis. *Macromolecules Symposium* **1999**, *140*, 165-178.

Ni, Q.W.; Eads, T.M. Low-speed magic-angle-spinning carbon-13 NMR of fruit tissue. *Journal of Agricultural and Food Chemistry* **1992**, *40*, 1507-1513.

Ni, Q.W.; Eads, T.M. Liquid-phase composition of intact fruit tissue measured by high resolution proton NMR. *Journal of Agricultural and Food Chemistry* **1993a**, *41*, 1026-1034.

Ni, Q.X.; Eads, T.M. Analysis by proton NMR of changes in liquid-phase and solid-phase components during ripening of banana. *Journal of Agricultural and Food Chemistry* **1993b**, *41*, 1035-1040.

Nicholson, J.K.; Foxall, P.J.D.; Spraul, M.; Farrant, R.D.; Lindon, J.C. 750 MHz  $^1\text{H}$  and  $^1\text{H}$ - $^{13}\text{C}$  NMR spectroscopy of human blood plasma. *Analytical Chemistry* **1995**, *67*, 793-811.

Palmer, A. G.; Cavanagh, J.; Wright, P. E.; Rance, M. Sensitivity improvement in proton detected heteronuclear correlation experiments. *Journal of Magnetic Resonance* **1991**, *93*, 151-170.

Sacco, A.; Bolsi, I.N.; Massini, R.; Spraul, M.; Humpfer, E.; Ghelli, S. Preliminary investigation on the characterization of durum wheat flours coming from some areas of south Italy by means of  $^1\text{H}$  high resolution magic angle spinning nuclear magnetic resonance. *Journal of Agricultural and Food Chemistry* **1998**, *46*, 4242-4249.

Schleucher, J.; Schwendinger, M.; Sattler, M.; Schmidt, P.; Schedletzky, O. A general enhancement scheme in heteronuclear multidimensional NMR employing pulsed field gradients. *Journal of Biomolecular NMR* **1994**, *4*, 301-306.

Schols, H.A.; Voragen, A.G.J.; Colquhoun, I.J. Isolation and characterization of rhamnogalacturonan oligomers, liberated during degradation of pectic hairy regions of rhamnogalacturonase. *Carbohydrate Research* **1994**, *256*, 97-111.

Tjan, S.B.; Voragen, A.G.J.; Pilnik, W. Analysis of some partly and fully esterified oligogalactopyranuronic acids by p.m.r. spectrometry at 220 MHz. *Carbohydrate Research* **1974**, *34*, 15-23.

Tucker, G.A. Introduction. In *Biochemistry of Fruit Ripening*; Seymour, G.B., Taylor, J.E., Tucker, G.A., Eds.; Chapman & Hall: London, 1993; 1-51.

Vogels, J.T.W.E.; Terwel, L.; Tas, A.C.; van den Berg, F.; Dukel, F.; van der Greef, J. Detection of adulteration in orange juices by a new screening method using proton NMR spectroscopy in combination with pattern recognition techniques. *Journal of Agricultural and Food Chemistry* **1996**, *44*, 175-180.

Wu, J.S.; Chen, H.; Fang, T. Mango juice. In *Fruit Juice Processing Technology*; Nagy, S., Chen, C.S., Shaw, P.E. Eds.; Agscience: Auburnadale, 1993; 620-655.

## **IV. STUDY OF THE RIPENING PROCESS OF MANGO: PHYSICAL AND BIOCHEMICAL CHANGES**

IV.1. Introduction.....	98
IV.2. Materials and Methods.....	100
IV.2.1. Sample Preparation.....	100
IV.2.2. Texture, pH, Soluble Solids and Enzymatic Determinations.....	101
IV.2.3. NMR Measurements.....	102
IV.3. Compositional Changes of Mango During Ripening.....	102
IV.3.1. Changes in Texture, pH and Soluble Solids.....	102
IV.3.2. Changes Assessed by NMR.....	104
IV.3.2.1. Qualitative Changes in the Composition of Juices.....	104
IV.3.2.2. Quantitative Analysis of Juices and Pulps.....	108
IV.4. Preliminary Study of the Effect of Refrigeration on Mango Ripening.....	115
IV.4.1. Changes in Texture, pH and Soluble Solids.....	115
IV.4.2. Changes Assessed by NMR.....	117
IV.5. Conclusions.....	119
References.....	120

## IV.1. Introduction

Trade in mango has been limited by the highly perishable nature of this fruit. Ripening cannot be delayed sufficiently to allow for long-distance transport without considerable quality decay. The fruit are also highly susceptible to disease, extremes of temperature and physical injury. Most of the postharvest technologies are designed for disease control and protection against injury during packaging and transport. Technologies for longer-term storage, such as controlled or modified atmospheres, which have been used commercially for temperate fruits, have not been applied successfully to the mango. To improve this situation, a deeper and more detailed knowledge of the biochemistry of ripening is required. This knowledge is also extremely relevant for the processing industry, since the quality of the processed product strongly depends on the quality of the raw materials, defined by a wide range of factors, including the fruit organoleptic properties, nutritional value and safety (e.g. absence of microbial contamination). Therefore, for producing high quality fruit products, it is of utmost importance to monitor the fresh fruit composition and its changes upon ripening and storage, in order to choose the best raw materials for each processing purpose.

Typically, the changes in mango fruit composition during ripening have been followed through physicochemical measurements of firmness, colour, pH, acidity, total solids content, total and reducing sugars (Morga *et al.*, 1979; Krishnamurthy and Joshi, 1989) and through the determination of some individual components by chromatography, such as sugars and organic acids (Medlicott and Thompson, 1985; Medlicott *et al.*, 1986; Selvaraj *et al.*, 1989). In recent years, research has also focused on the development of rapid and non-invasive techniques for monitoring the quality and ripening stage of mango and other fruits. Some studies have established useful relationships between the physicochemical parameters of mango fruit (at different degrees of ripeness) and non-invasive measurements based on X-ray absorption (Barcelon *et al.*, 1999), ultrasonic properties (Mizrach *et al.*, 1997; Mizrach *et al.*, 1999) and near infrared (NIR) spectroscopy (Guthrie and Walsh, 1997). Infrared spectroscopy has also been used to determine individual sugar contents in ripening bananas (Tarkosova and Copikova, 2000), evaluate the effects of cold storage on the lipid composition of apples and pears (Bertoluzza *et al.*, 1994) and follow the changes in the degree of esterification of peach pectins during cold and normal storage (Chatjigakis *et al.*, 1998). Magnetic resonance

techniques have also been increasingly used for monitoring ripening and measuring fruit quality attributes. Magnetic resonance imaging has been applied to detect heat treatment injury of mango fruit (Joyce *et al.*, 1993) and has been shown to provide useful information on the changes of the internal structure of several other intact fruits during storage and ripening (Ishida *et al.*, 1994; Clark and MacFall, 1996; Goodman *et al.*, 1996; Clark *et al.*, 1998). On the other hand, several interesting applications have been reported for low resolution NMR spectroscopy, such as the determination of the sugar content in pears, cherries and grapes (Bellon *et al.*, 1992) and in fresh prunes (Zion *et al.*, 1995), the sensing of the maturity of avocados (Chen *et al.*, 1996), and the measurement of self-diffusion coefficient of water in several fruit juices and apple tissue, which could be related to titratable acidity, insoluble solids and Brix value (Keener *et al.*, 1997). High resolution NMR spectroscopy has been used to characterise the composition of some fruit juices (Vogels *et al.*, 1996; Belton *et al.*, 1996; Belton *et al.*, 1997; Belton *et al.*, 1998; Le Gall *et al.*, 2001) and intact tissues (Ni and Eads, 1992; Ni and Eads, 1993a; Ni and Eads, 1993b), but few studies have reported on the compositional changes occurring during ripening. Ni and Eads (1993b) described the evolution of solid-like components in ripening bananas and detected changes in sugars, lipids and organic acids by  $^1\text{H}$  MAS NMR, which also allowed quantification of glucose, fructose and sucrose. However, this study was limited by the relatively low resolution permitted at the time, and since then, major instrumental developments have significantly increased the potential of high resolution NMR techniques.

The use of high resolution NMR spectroscopy for acquiring a deeper knowledge about the biochemistry of mango ripening is explored in this thesis. The present Chapter describes the systematic study of changes in mango physicochemical parameters (firmness, pH and soluble solids content) and NMR spectral profiles during storage. The high resolution  $^1\text{H}$  spectra of juices are inspected for qualitative variations and, additionally, some components, namely sugars, organic acids and amino acids, are quantified by integration of the corresponding NMR signals. The intact fruit pulps are analysed by HR-MAS  $^1\text{H}$  NMR spectroscopy and a semi-quantitative approach is used to compare the variation of some compounds in pulps with those detected in juices. Moreover, a preliminary study of the effect of refrigeration on mango fruit ripening, assessed by variations in physicochemical properties and in  $^1\text{H}$  NMR spectra of juices, is presented.

## IV.2. Materials and Methods

### IV.2.1. Sample Preparation

Three batches of mango fruits were used for ripening studies: 1) cultivar Tommy Atkins grown in Brazil, 2) cultivar Haden grown in Venezuela, and 3) cultivar Haden grown in Brazil, as these were the fruits commercially available and for which a reliable source was known. All fruits were directly air-freighted to Portugal and obtained from a commercial source, 3-4 days after harvest. Each batch comprised mature green fruits, selected for uniformity of size and colour, and free from apparent infection.

For the detailed study of the ripening process, the Tommy Atkins mangoes grown in Brazil (batch 1) were used. These fruits were ripened at 22±1°C in natural light during 23 days. On day 1, they were characterised by high firmness, green/red peel and light yellow pulp; on day 5, by slightly softer texture, some yellow spots on the peel and yellow pulp; on day 9, by soft texture, yellow/red peel and intensely yellow pulp; from day 11 onwards, by all the latter properties, which gradually increased in intensity. At intervals of two days, three fruits were randomly selected for analysis and their firmness was measured as described in section IV.2.2. For obtaining the juice samples, the pulps of the selected fruits were macerated separately in a domestic juice extractor, centrifuged during 15 minutes at 15000 r.p.m. and filtered through a glass microfiber filter, under vacuum. Samples of average composition (i.e. more representative of each ripening stage) were also prepared by mixing equal portions of the three pulps collected at each ripening day. In order to prevent microbial growth, sodium azide ( $\text{NaN}_3$ ) was added, so that each sample contained an azide concentration of 0.05%. The samples were frozen in liquid nitrogen and stored at -20 °C, until NMR analysis. After thawing, these juices were diluted two times, in order to reduce the excessive viscosity, and their pH was adjusted, in order to decrease shifts in the position of signals that are sensitive to pH. This adjustment was performed by adding a fixed volume of sodium phosphate buffer, containing  $\text{D}_2\text{O}$  and sodium 3-(trimethylsilyl)propionate (TSP), and resulted in making the pH values (initially varying between 3.20 to 5.30) fall in the narrower range of 5.60-6.20. The juice samples prepared in this way contained 7.5%  $\text{D}_2\text{O}$ , used as internal lock, and 0.015% TSP, used as chemical shift and intensity reference. Pulp samples were collected from the equatorial ring of the fruit, frozen in liquid nitrogen and stored at -20°C. For the NMR measurements, the

thawed pulps were packed into 4 mm MAS rotors and a solution of D<sub>2</sub>O containing TSP was added.

Batches 2 and 3 of mango fruits were used to investigate the effect of refrigeration on ripening, taking into account the possible variations arising from their different geographical origins, already discussed in Chapter III.3.2. The Haden fruits grown in Venezuela (batch 2) were obtained in the mature green stage and left to ripen at 22±1°C for 19 days, during which the texture became progressively softer, and the colour of the peel developed from green to yellow-orange with some red and brown spots. At intervals of two days, three fruits were randomly selected from the batch and their firmness measured. Juice samples were obtained by centrifugation and filtration of the macerated pulps, as described for batch 1, and pulp samples were collected from the equatorial ring of each fruit. Juices and pulps were frozen in liquid nitrogen and stored at -20°C. For the NMR analysis, the thawed juices were prepared to contain 10% D<sub>2</sub>O, 0.02% TSP and 0.05% NaN<sub>3</sub>, and their pH was adjusted by addition of microlitre amounts of NaOH (0.1 M and 1M) and HCl (0.1 M and 1M) solutions. The pH values of all juice samples then fell in the range 6.95-7.05. The third batch, comprising mature green Haden mangoes grown in Brazil, was stored at 7°C during 23 days. Compared to the fruits of batch 2, these fruits maintained a higher rigidity and the degreening of the peel was slower. Juice and pulp samples were prepared using the same procedures as for batch 2.

#### **IV.2.2. Texture, pH, Soluble Solids and Enzymatic Determinations**

The changes in texture, pH and soluble solids (%SS) were systematically followed during storage of the three batches of fruits. Firmness measurements were performed on three fruits at each ripening stage using a Texture Analyser TA-Hdi for Tommy Atkins fruits (batch 1) and a universal penetrometer for Haden fruits (batches 2 and 3). The texturometer measured the compression force applied to the unpeeled fruit during 15 seconds. Taking into account the texture differences within the same fruit, this value was recorded in 12 points along the equatorial ring of each fruit and an average value of force (g) was calculated. In the case of the measurements with the penetrometer, a compression force was applied to the unpeeled fruit during 1 minute, using a conical steel needle and a 100 g force gauge, and the depth of penetration (mm) was recorded. Twelve values of firmness were measured along the equatorial ring of each fruit and an average value

calculated. The pH was measured using a Hanna pH meter (precision  $\pm 0.01$ ) and the %SS was measured by refractometry, using an Atago hand refractometer (accuracy  $\pm 0.2\%$ ). Glucose and fructose were quantified enzymatically for a selected set of samples, using the enzymatic tests purchased from Boehringer Mannheim (cat. no. 139106).

### **IV.2.3. NMR Measurements**

The acquisition parameters of the NMR experiments recorded for mango juices and pulps are described in Chapter III.2.2. Regarding spectral processing, additional baseline correction was carried out to improve integration of some signals.

## **IV.3. Compositional Changes of Mango During Ripening**

This section is concerned with the changes occurring during ripening of mangoes of the cultivar Tommy Atkins. The ripening process of the cultivar Haden and the effect of refrigerated storage on these fruits composition is discussed in section IV.4.

### **IV.3.1. Changes in Texture, pH and Soluble Solids**

The variation in firmness during ripening of Tommy Atkins mangoes is illustrated in Figure IV.1a. As expected, there is a progressive softening of the fruits, shown by the decrease of the pulp rupture force, which is more pronounced until day 13, the stage when the fruit attained edible quality. The values obtained for each of the three mango fruits at the same ripening stage (represented in the graph by open symbols) give an indication of the firmness variability within fruits, which, in general, is lower than the overall changes induced by ripening. These results agree with others reported in the literature for this mango cultivar (Medlicott *et al.*, 1986; Mizrach *et al.*, 1997) and confirm the known fact that tissue firmness is closely related to the stage of maturity of mango fruit.

The variations in pH and soluble solids (%SS) during ripening are shown in Figures IV.1b and IV.1c, respectively, and follow the expected trends for most other climateric fruits: acidity decreases and soluble solids (reflecting sugar content) increase. The pH values do not vary much in the first 5 days of ripening (3.25-3.45) and then register a significant increase until day 13, reaching a value of 5.0. After day 13, minimal variations are noted. Similar pH values have been reported for this and other mango cultivars

(Medlicott and Thompson, 1985; Medlicott *et al.*, 1986). The %SS increases just under two-fold until day 9, after which small variations occur, although a slight decreasing trend may be noted. This trend, which has been reported in other studies (Medlicott and Thompson, 1985), may reflect a sugar content decrease during the last stages of ripening. Sugar is constantly being metabolised and initially this would be replenished by starch hydrolysis. At the late stages of ripening, intensification of respiration and starch depletion may cause a net loss in sugar content. On the other hand, the decrease in the acids content, also included in the soluble solids measured, may also contribute to this trend.

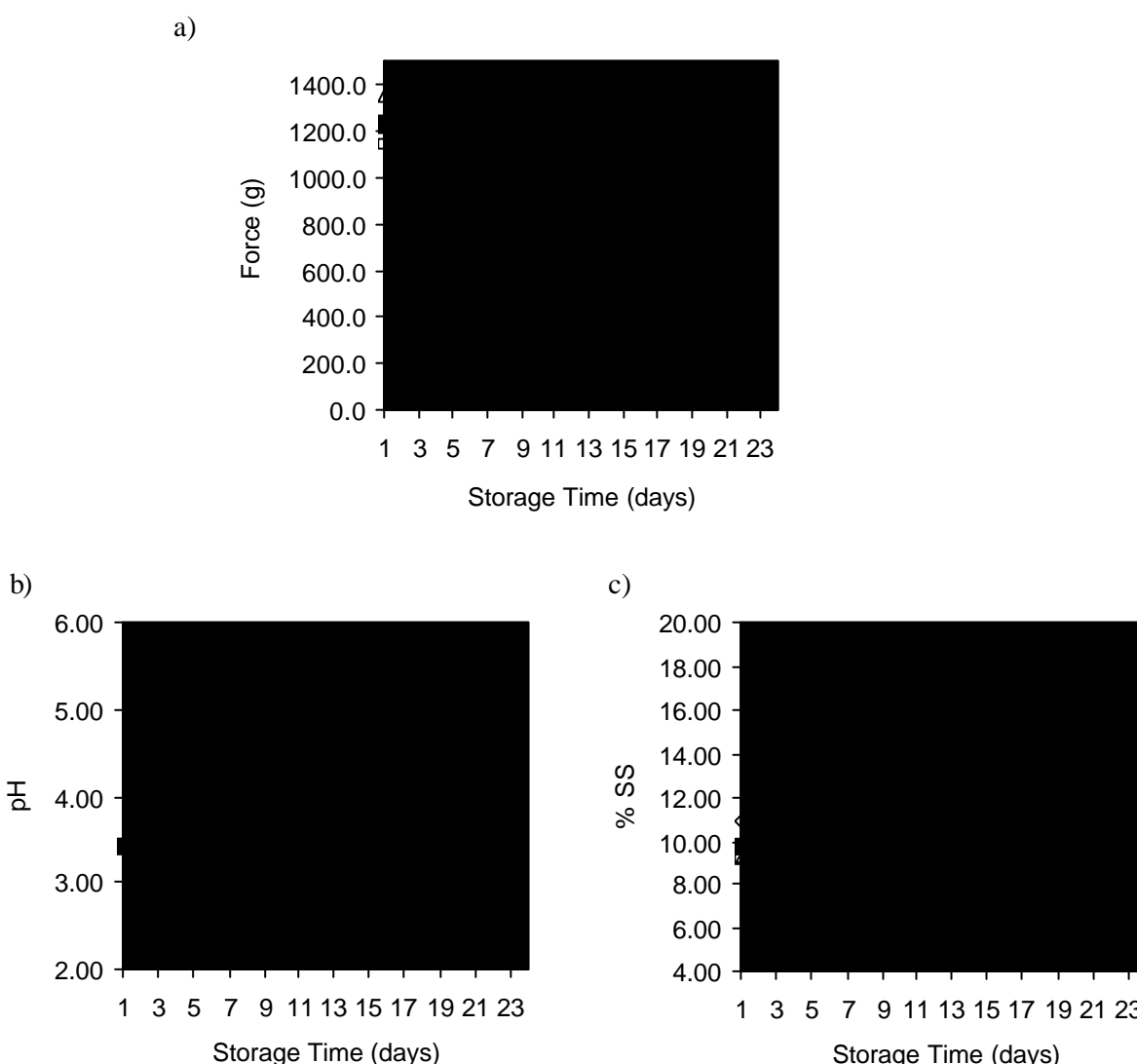


Figure IV.1. Variations in physicochemical properties of mango fruit (cv. Tommy Atkins) during ripening: a) firmness, b) pH and c) soluble solids (% SS). The open symbols correspond to the 3 individual fruits analysed each day, while the asterisk represents average values.

### IV.3.2. Changes Assessed by NMR

#### IV.3.2.1. Qualitative Changes in the Composition of Juices

Figures IV.2 to IV.4 show different regions of the  $^1\text{H}$  spectra of Tommy Atkins juices, collected on days 1, 7, 13 and 19 of the storage period. It is recalled that each of these juices was obtained from the mixed pulps of three fruits at the same ripening stage and hence represents an average composition.

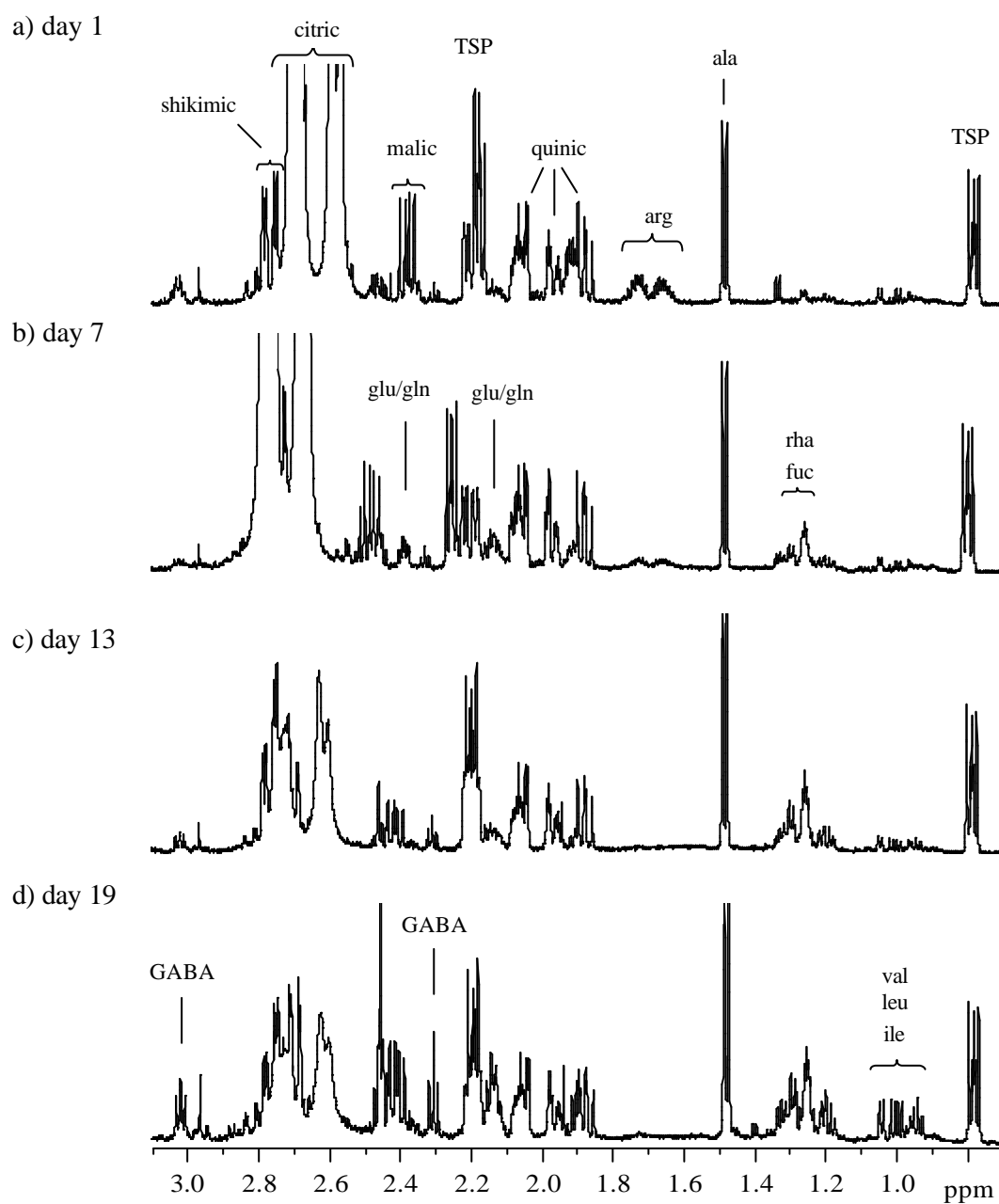


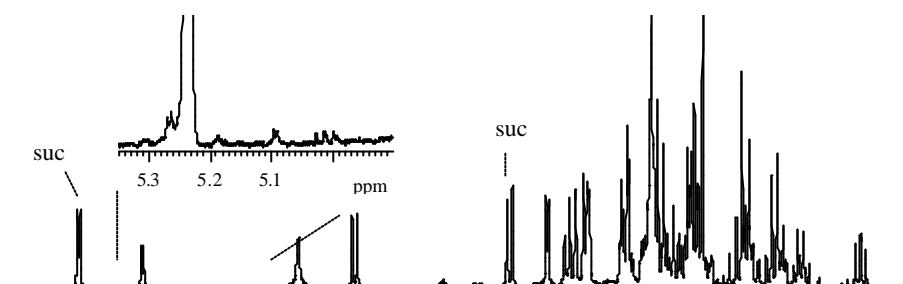
Figure IV.2. High-field region of the 600 MHz  $^1\text{H}$  NMR spectra of Tommy Atkins juices at different ripening stages; NS 64.

The high-field region (Figure IV.2) shows clear variations in the organic acids and amino acids profile. As expected, citric acid decreases drastically during ripening, presumably due to its utilization as a respiratory substrate (Lizada, 1993). This decrease is especially marked after day 7, and in ripe juices (illustrated in Figure IV.2 by the two bottom spectra) citric acid is present in small amounts, showing relatively weak and broad signals. The lower resolution of these signals suggests hindered mobility of residual citric acid in ripe juice, which may be due to some kind of interaction with other components, for instance through the formation of complexes. Quinic, shikimic, malic and succinic acids, the other major organic acids identified in mango juice, are present throughout all ripening stages and show smaller variations, some of which are quantified in section IV.3.2.2. In what regards the amino acids profile, the most drastic change is the decrease of arginine, which is detected until day 9 only (spectrum not shown). On the contrary, valine, leucine, isoleucine, alanine, glutamic acid/glutamine and  $\gamma$ -aminobutyric acid (GABA) are seen to increase, as shown by the quantitative results presented in section IV.3.2.2 for some of them. Moreover, in the 1.20-1.30 ppm region, the signals arising from the deoxy-sugars fucose and rhamnose (both free and pectic) become more noticeable in the spectra of ripe juices.

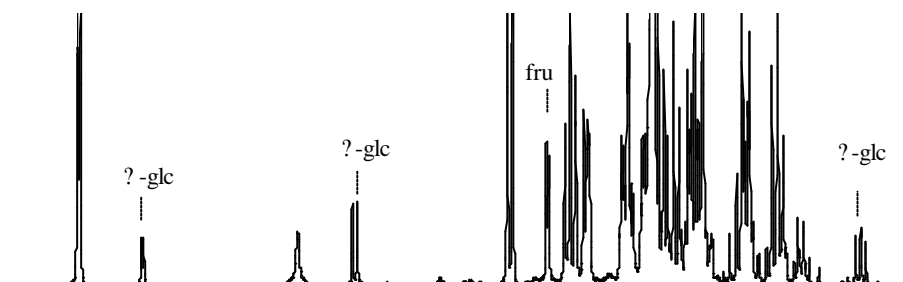
The spectral variations in the sugar region are shown in Figure IV.3. In what concerns the major sugars, it is obvious that different proportions characterise different ripening stages. This difference is easily assessed by comparing the relative intensities of non-overlapped signals. The sucrose peaks at 4.22 and 5.41 ppm show a significant increase relatively to glucose and fructose signals. The peaks at 3.25 and 4.64 ppm arising from  $\beta$ -glucose and the 5.23 ppm peak arising from  $\alpha$ -glucose clearly decrease during ripening, especially during the first 9 days, and, compared to sucrose and fructose, remain quite low in the juices of ripe fruits. Fructose signals show smaller variations in intensity compared to the other sugars. These variations are more clearly shown and further discussed in section IV.3.2.2, where quantification results obtained for the three sugars are presented. Moreover, the inserts in Figure IV.3 show the increasing intensity of non-reducing galacturonic acid signals (5.05-5.20 ppm) during ripening. Along with the increase noted for the rhamnose signals in the high-field region, this observation suggests an increase in the amount of pectic oligosaccharides detected in the juice. Indeed, most

studies reported in the literature state that mango ripening is accompanied by pectin hydrolysis (Tucker and Seymour, 1991; Lizada, 1993; Muda *et al.*, 1995), thus giving rise to smaller oligomers with higher water-solubility, which may be found in the juice extracted from the fruit.

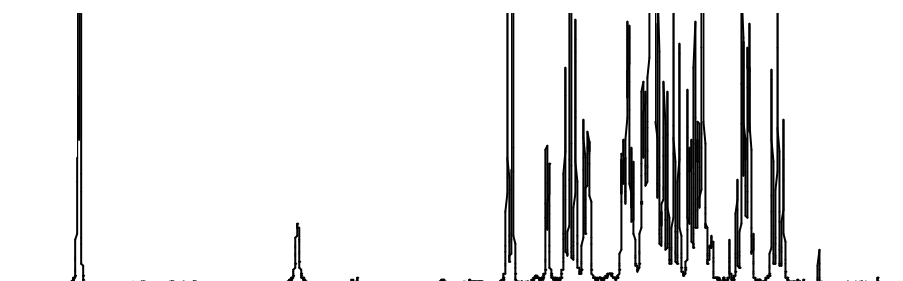
a) day 1



b) day 7



c) day 13



d) day 19

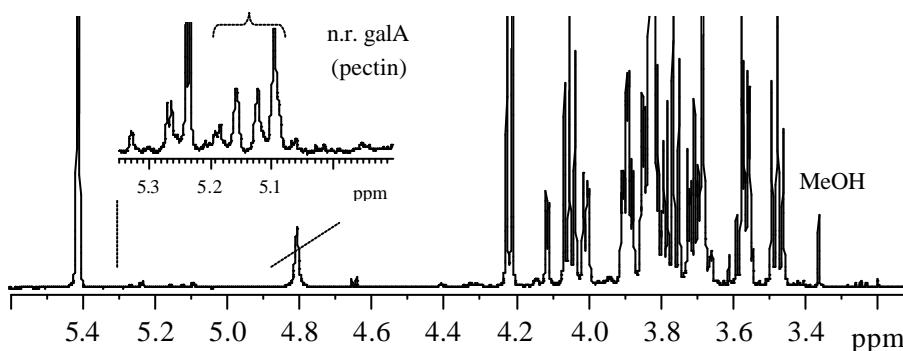


Figure IV.3. Mid-field region of the 600 MHz  $^1\text{H}$  NMR spectra of Tommy Atkins juices at different ripening stages; NS 64.

Figure IV.4 illustrates the changes in the low-field region of the juice spectra. The signals arising from the aromatic protons of phenylalanine and tyrosine are detected only at the early stages of ripening and disappear after days 5 and 7, respectively. In the same period, more precisely from day 5 to day 7, two broad resonances appear at 6.89 and 7.61 ppm (Figure IV.4b), suggesting the formation of condensed phenolic species. The concomitance of these changes suggests that tyrosine and phenylalanine may act as precursors in the polymerisation process of phenolic compounds. In addition, uridine and adenosine systems are seen to increase in the late stages of ripening. Other spectral changes in this region regard unassigned signals (indicated with arrows in Figure IV.4), such as those at 5.82, 6.13 and 7.05 ppm, which increase during ripening and the singlet at 7.26 ppm, which decreases at the latter stages.

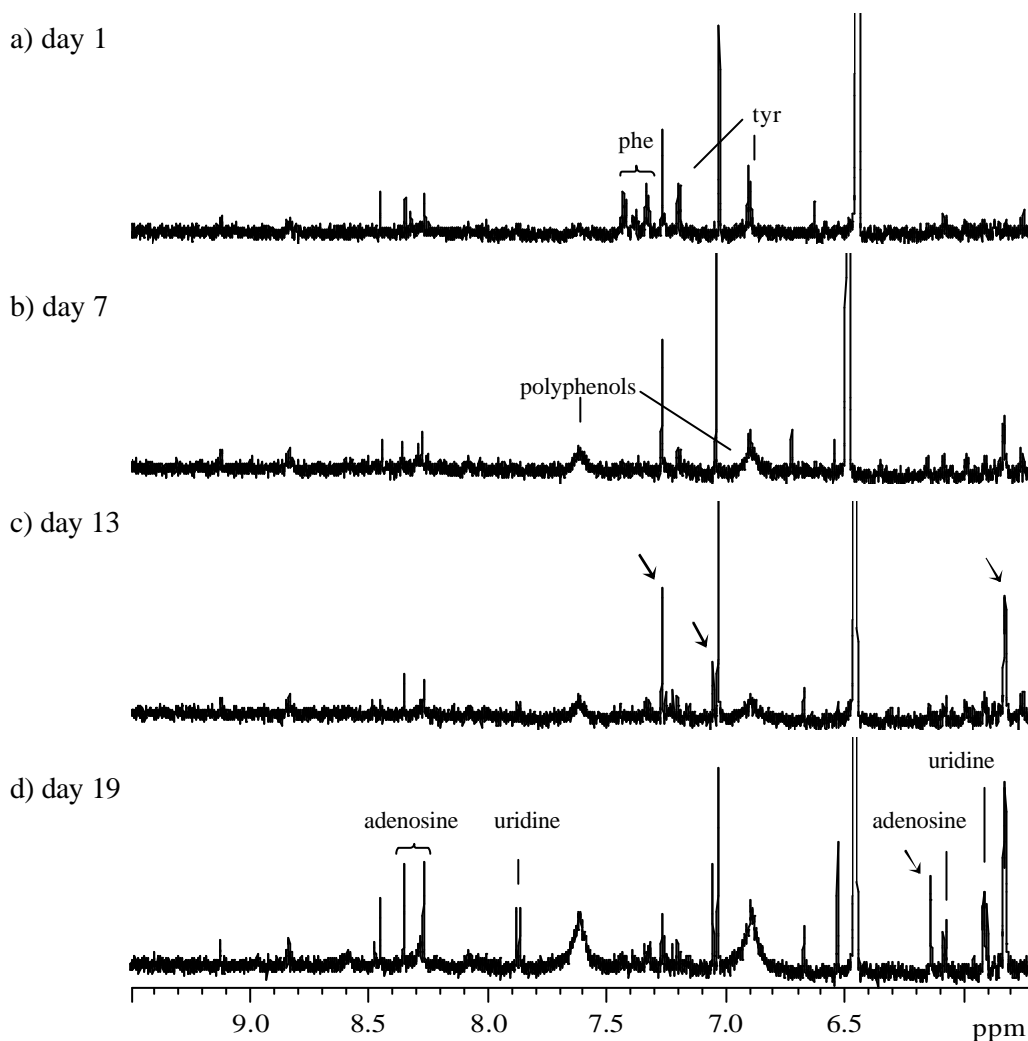


Figure IV.4. Low-field region of the 600 MHz <sup>1</sup>H NMR spectra of Tommy Atkins juices at different ripening stages; NS 64.

### IV.3.2.2. Quantitative Analysis of Juices and Pulps

The variation of some juice components during ripening has been quantified with basis on signal integration. The TSP signal at 0.0 ppm, arising from 9 protons (3 x CH<sub>3</sub>), was used as the intensity reference. The values of this signal area, measured for the different juice spectra, presented a small enough coefficient of variation (5.4%), reflecting the constant concentration of TSP added to the samples. The unknown concentration of a compound Y present in the juices could therefore be calculated according to the equation:  $C_Y = F (A_Y M_Y / n_Y) (C_{TSP} n_{TSP} / M_{TSP} A_{TSP})$ , where  $C$  is the concentration,  $F$  is the dilution factor of the juice sample,  $A$  is the area of the signal integrated,  $M$  is the molecular mass and  $n$  is the number of protons contributing to the signal integrated.

The three main sugars were quantified by integrating the signals that are free from significant overlapping. For sucrose, the areas under the peaks at 4.22 ppm (H3, fructose ring) and at 5.41 ppm (H1, glucose ring) were measured. Both signals arise from one proton and, as expected, their integrals are quite similar. In the case of glucose, the contributions from  $\alpha$ - and  $\beta$ -glucopyranose anomers must be considered. The furanose forms are known to be negligible in aqueous solution at 31°C (Angyal, 1984). For quantifying  $\beta$ -glucose, the doublet at 5.23 ppm was integrated, while for  $\alpha$ -glucose the areas under the signals at 3.24 ppm (H2) and at 4.64 ppm (H1) were measured. For the glucose signal at 4.64 ppm, additional baseline correction was carried out over the integrated region, in order to correct for the baseline offset caused by the proximity of the suppressed water signal. For fructose, the only peak relatively free of overlap is the 4.11 ppm peak arising from H3 and H4 of the  $\beta$ -furanose form. This is, however, a poor indication of the total spectral contribution of fructose since the  $\beta$ -pyranose form is expected to occur in higher abundance, in aqueous solution: 65%  $\beta$ -pyranose and 25%  $\beta$ -furanose, at 31°C (Angyal, 1984). The 25% value was therefore used to estimate the total amount of fructose.

The results of sugar quantification in the Tommy Atkins juices, obtained with basis on the integration measurements described in the previous paragraph, and also on enzymatic determinations, are shown in Figure IV.5a. In the juice of day 1, fructose is the predominant sugar (41.6 g/L), followed by sucrose (31.3 g/L) and glucose (20.3 g/L). After day 5, sucrose becomes the most abundant sugar and continues to increase until day 15,

reaching a concentration that is almost 5 times higher than in the juice of day 1. From day 15 to day 23, sucrose shows a slight decreasing trend. Glucose concentration is steady in the first stages of ripening and then shows a 7.5 times decrease from day 7 to day 11, after which it remains low. Compared to sucrose and glucose, the concentration of fructose does not vary much through the whole ripening period, increasing about 1.4 times until day 9 and decreasing back to initial values afterwards. Fructose amounts calculated with basis on the  $\beta$ -furanose signal area are over-estimated compared to the reference enzymatic values, but both determinations show the same trend. In summary, the first 7-9 days of the storage period are characterised by the accumulation of the three sugars, especially of sucrose, resulting in a two-fold increase of the total sugars content; in the late ripening stages, slight decreasing trends are noted for all sugars.

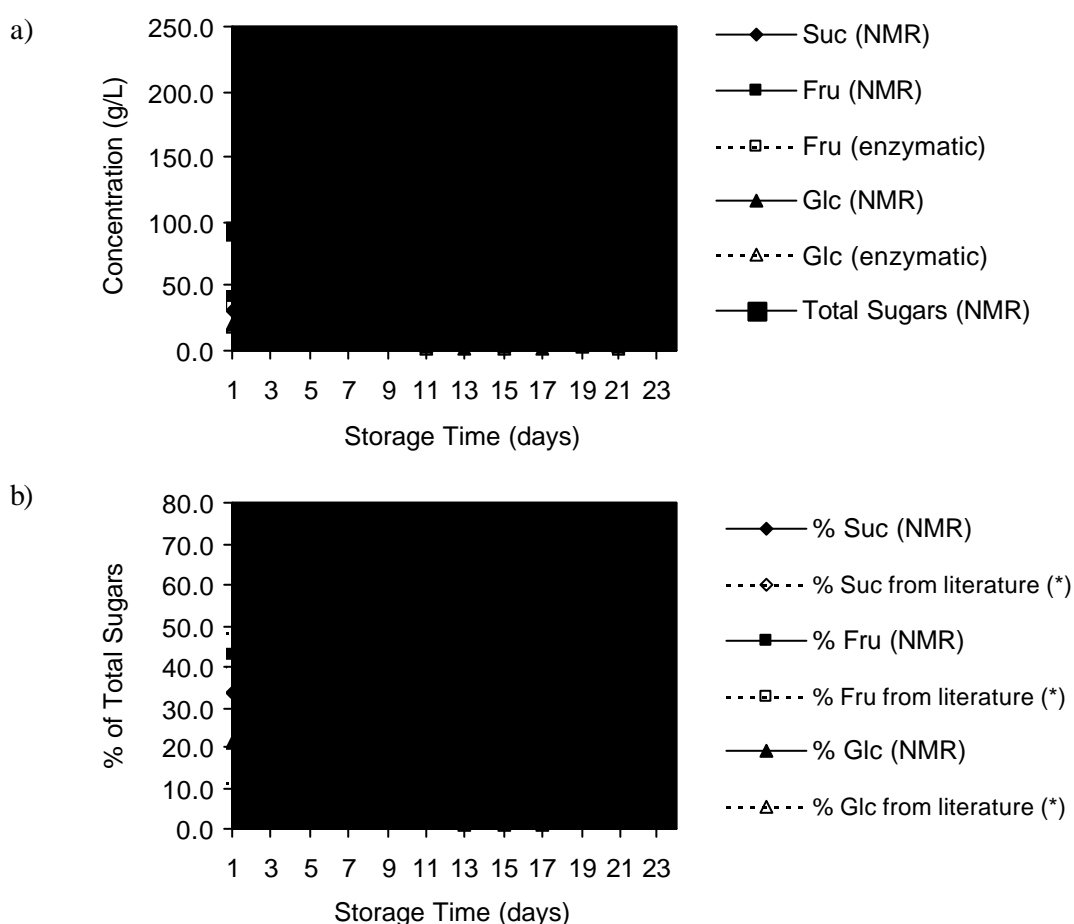


Figure IV.5. Sugars variation in Tommy Atkins juices during ripening: a) concentrations (g/L) determined by integration of NMR signals (suc: 5.41 ppm, fru: 4.11 ppm,  $\beta$ -glc: 5.23 ppm,  $\alpha$ -glc: 4.64 ppm) and by enzymatic methods for glucose and fructose, and b) relative contribution of each sugar to the total sugar content, using the total area of the sugar region (see text). (\*) Results reported by Medlicott *et al.* (1986).

In what concerns the relative contribution of each sugar to the total sugar content, the results are shown in Figure IV.5b. These values have been calculated by using the areas measured for each sugar peak (sucrose: 5.41 ppm, fructose: 4.11 ppm,  $\alpha$ -glucose: 5.23 ppm and  $\beta$ -glucose: 4.64 ppm) multiplied by the appropriate factor (14, 7/2 and 7 for sucrose, fructose and glucose, respectively) to obtain the area corresponding to the total amount of each sugar, and divided by the area measured for the total sugars (area of the 3.20-4.26 ppm region plus the areas of the anomeric signals at 4.64, 5.23 and 5.41 ppm). In the unripe juice, sucrose, fructose and glucose account for approximately 34, 43 and 21 % of total sugars, respectively, whereas in the ripe juice, the sucrose contribution reaches values close to 75 %, fructose accounts for about 20-23 % and glucose contributes less than 2-3% to total sugars. These results reasonably agree with those reported by Medlicott *et al.* (1986) for juices of the same mango cultivar ripened at 22°C (obtained by high-performance liquid chromatography), which are shown by the open symbols in the graph of Figure IV.5b.

The organic acids quantified were citric, malic and shikimic. For citric acid, the doublet at 2.58 ppm arising from two protons was integrated. Malic acid was quantified through integration of the CH<sub>2</sub> signals centred at ~2.4 ppm. In the case of shikimic acid, the signal chosen for integration was the 6.45 ppm peak arising from H<sub>6</sub>. Succinic and quinic acids could not be determined because, in most juice spectra, their signals strongly overlap with other signals and, thus, integration would carry very large errors. The variation of citric and malic acids during ripening is shown in Figure IV.6. In agreement with several studies reported in the literature (Medlicott and Thompson, 1985; Medlicott *et al.*, 1986; Lizada, 1993), citric acid is abundant in unripe juices (cc. ~14 g/L) and consistently declines during ripening to levels below 3 g/L. This high rate of citric acid loss accounts for most of the decrease in acidity observed during ripening. Malic acid contributes with a small loss until day 13, probably due to its utilization as a respiratory substrate, and then increases until the end of the storage period to concentration values close to citric acid amounts in the ripe juice. Medlicott *et al.* (1986) registered a similar variation in the content of malic acid measured by HPLC at six stages during storage for 15 days. Finally, in what regards shikimic acid, its concentration is seen to decrease steadily from 1.9 g/L to 1.2 g/L, as it will be shown further ahead.

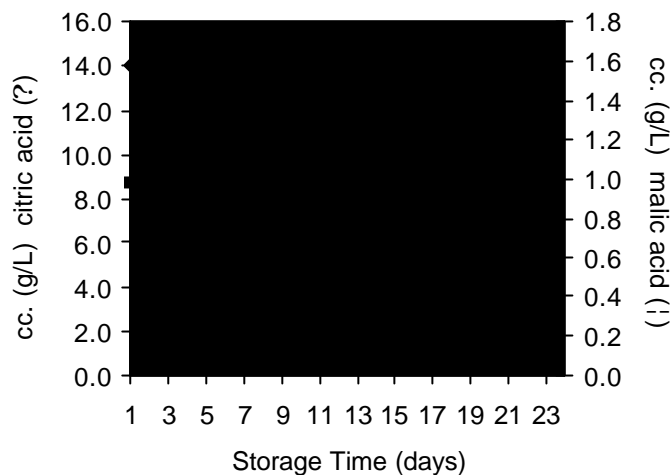


Figure IV.6. Citric and malic acid variation in Tommy Atkins juices during ripening. Concentrations (g/L) determined by integration of NMR signals (citric acid: 2.58 ppm, malic acid: 2.40 ppm).

The amino acids quantified were isoleucine (1.01 ppm, 3 protons), valine (1.04 ppm, 3 protons), alanine (1.48 ppm, 3 protons), GABA (2.30 ppm, 2 protons), arginine (1.60-1.78 ppm, 2 protons), tyrosine (7.19 ppm, 2 protons) and phenylalanine (7.30-7.45 ppm, 5 protons). Their variation during ripening is shown in Figures IV.7 and IV.8.

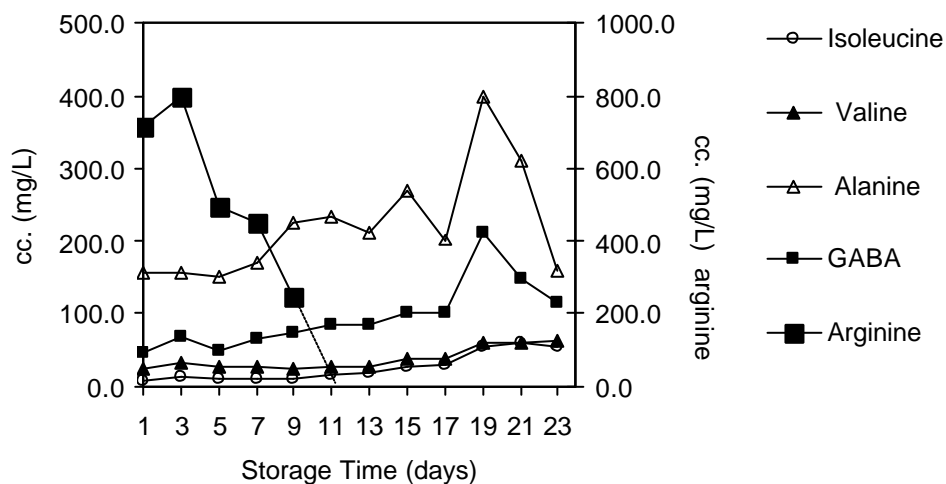


Figure IV.7. Amino acids variation in Tommy Atkins juices during ripening. Concentrations (mg/L) determined by integration of NMR signals (ile: 1.01 ppm, val: 1.04 ppm, ala: 1.48 ppm, GABA: 2.30 ppm, arg:1.60-1.78 ppm). The concentrations of all amino acids except arginine are indicated on the left-hand yy axis; arginine concentration is indicated on the right-hand axis; the dashed line indicates the decrease of arginine to undetectable amounts.

In the juices of days 1-7, arginine predominates, followed by alanine. For subsequent stages, arginine drastically decreases, becoming undetectable from day 9 onwards, and alanine shows a general increasing trend, thus becoming the most abundant amino acid measured. Increases are also noted for valine, isoleucine and GABA, the latter showing a trend similar to alanine. These results generally agree with the variations reported in the literature for two extreme ripening stages (Kalra *et al.*, 1995). The phenylalanine and tyrosine variations are shown in Figure IV.8, along with the variations registered for the area under the signal at 7.61 ppm, possibly arising from polyphenols (for which exact assignment is not known), and for shikimic acid concentration. The results show that polyphenols are being formed while the aromatic amino acids and shikimic acid are being consumed. Therefore, it is possible that tyrosine, phenylalanine and shikimic acid are used as precursors for phenolic polymerisation, the amino acids acting during the first ripening stages and shikimic acid acting more steadily during the whole process.

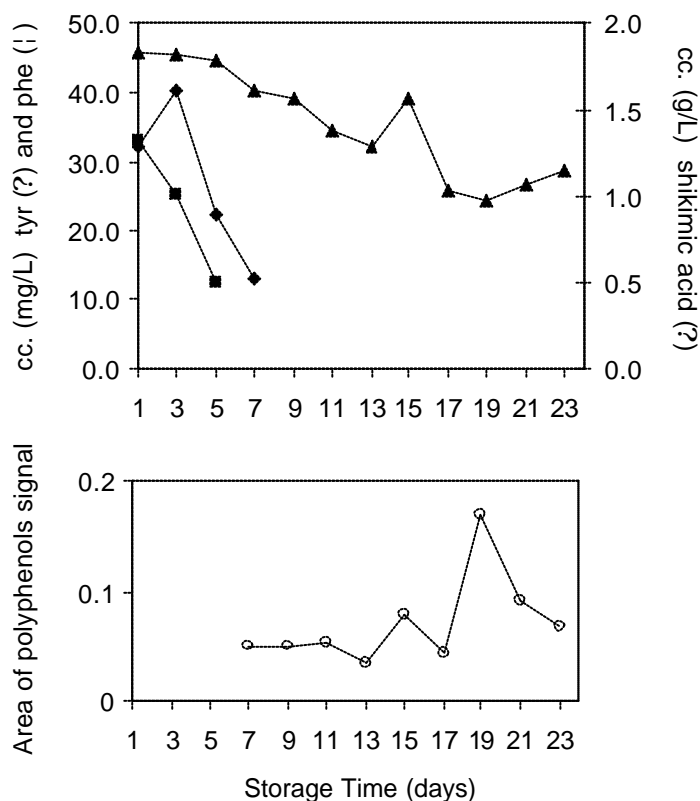


Figure IV.8. Variation of aromatic amino acids, shikimic acid and polyphenols in Tommy Atkins juices during ripening, determined by integration of NMR signals (tyr: 7.19 ppm, phe: 7.30-7.45 ppm, shikimic acid: 6.45 ppm, polyphenols: 7.61 ppm). In the top graph, the dashed lines indicate the decreases of tyrosine and phenylalanine to undetectable amounts; in the bottom graph the dashed line indicates the appearance of polyphenols at day 7.

The use of an intensity reference for carrying out absolute quantification in pulps is not as straightforward as in juices, since it has been found that the relationship between the area of the TSP signal (used for quantification studies in juices) and the concentration added to the pulp samples is not linear. Physical and/or chemical interactions of TSP within the pulp may account for this effect. Moreover, the visible area under the signals arising from pulp components does not always correspond to their total amount but only to the more mobile fraction, thus rendering quantification inaccurate.

In this study, the variations in pulps and juices during ripening are compared through a semi-quantitative approach, which consists of calculating ratios of signals for each spectrum, in order to be able to compare different spectra. These ratios have been obtained by dividing the area of the signal of interest by the area of the sucrose signal at 5.41 ppm, assuming that the concentration of sucrose in a certain juice is the same as in the corresponding intact pulp. Figure IV.9 shows the results obtained for some components. The ratio shikimic acid/sucrose (graph a) is very similar between each intact pulp and the corresponding juice. On the contrary, the ratio polyphenols/sucrose (graph b) shows higher values for pulps, consistent with preferable retention of polyphenols in the pulp. It is also possible that the oxidation reactions leading to the formation of condensed phenolic compounds have occurred more extensively in the pulp than in the juice.

Graph c in Figure IV.9 shows the ratio calculated for the signals in the 5.05-5.20 ppm range, which arise from pectic components, namely from non-reducing galacturonic acid residues. In the unripe fruit of day 1, these signals are much more intense in the spectrum of the intact pulp than in the corresponding juice spectrum, indicating that, as expected, pectins are preferably located in the solid phase of the fruit. From day 5 onwards, the same signals become equally intense in the spectra of pulps and juices, suggesting that the expected pectin hydrolysis has occurred during the first 5 days of ripening, rendering oligomers that are released into the liquid phase.

Finally, graph d in Figure IV.9 shows the ratio calculated for the region 1.10-1.40 ppm, where signals from fatty acids and deoxy-sugars, namely pectic rhamnose, are detected. Ethanol and lactate also resonate in this region, but show small and approximately constant contributions in the spectra compared. In order to evaluate the variation of fatty acids separately from that of pectic rhamnose, the variation of galacturonic acid residues (which are also pectic components), shown in graph c and

discussed above, can be considered. Since, after day 5, those components were seen to be present in similar amounts in pulps and juices, it may be stated that the points shown in graph d for days 5, 9, 13 and 21 correspond mainly to the variation of fatty acids signals. Similarly to what has been observed in the previous Chapter (section III.4.3), these signals are generally more intense in the spectra of pulps than in the corresponding juices. Moreover, the magnitude of this difference is found to be higher for earlier ripening stages (graph d in Figure IV.9). Thus, it is likely that fatty acids are retained in the solid phase of the fruit, especially for early ripening stages.

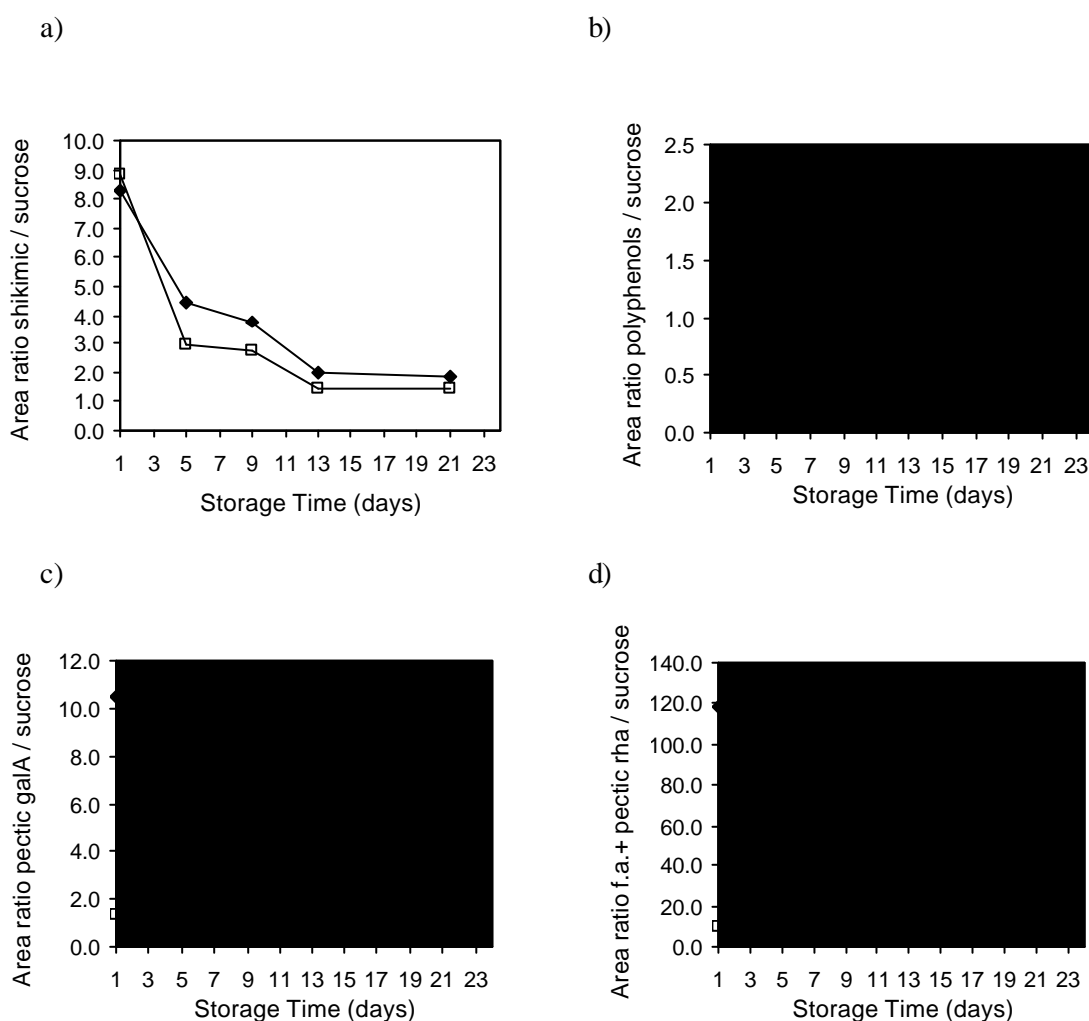


Figure IV.9. Ratios of the areas of some signals relative to the sucrose signal (5.41 ppm) in mango pulp (●) and juice (□) at different ripening stages: a) shikimic acid (6.45 ppm), b) polyphenols (7.61 ppm), c) non-reducing galacturonic acid residues of pectic chains (5.05-5.20 ppm), and d) fatty acids + pectic rhamnose (1.10-1.40 ppm).

#### **IV.4. Preliminary Study of the Effect of Refrigeration on Mango Ripening**

In the present section, the main changes taking place in two batches of mango fruits of the cultivar Haden, stored at different temperatures, are discussed. One of the batches (grown in Venezuela) was stored at 22?1°C, whereas the other batch (grown in Brazil) was stored at 7?1°C. Such low temperature is expected to cause chilling injury on mango fruit, generally assessed by failure to ripen with normal colour, texture and organoleptic properties (Medlicott *et al.*, 1986; Krishnamurthy and Joshi, 1989). Hereby, the effect of refrigeration is monitored not only by usual physicochemical parameters (firmness, pH and % SS), but also by recording <sup>1</sup>H NMR spectra of juices. This is, however, a preliminary study since, in the case of the batch stored under refrigeration, only one fruit could be analysed at each ripening stage. In addition, the comparison between the two batches must account for their different geographical origins and for the subjectivity associated with the initial ripeness stage of each set of mangoes, assessed only with basis on fruit colour and firmness.

##### **IV.4.1. Changes in Texture, pH and Soluble Solids**

The variations of firmness, pH and soluble solids (%SS) during storage of the two batches of fruits are shown in Figure IV.10. On days 1-5, all the fruits show high rigidity, expressed by the small penetration depth achieved by the penetrometer needle (Figure IV.10a). After day 5, the fruits of the batch stored at 22°C show a marked softening until day 13, similarly to what has been observed for the Tommy Atkins fruits (section IV.3.1). On the other hand, the fruits of the batch stored at 7°C show a much less pronounced softening, as viewed by the smaller increase of the penetration depth. Medlicott *et al.* (1986) registered an identical effect for mango fruits ripened at 12°C, compared to those stored at temperatures above 22°C.

The juices collected from the batch ripened at 22°C show the expected pH increase from ~3.0 to a value close to 5.0 for the juice of day 19 (Figure IV.10b). On the other hand, at 7°C, the pH values remain low (3.3-3.7), indicating that the ripe juice is still characterised by high acidity.

The %SS is seen to increase from 8.4 to 15.6% in the batch stored at 22°C (Figure IV.10c), a variation that is similar to the one observed in the Tommy Atkins juices (section

IV.3.1). The juices of the refrigerated batch also reach values around 16%, and thus, this parameter is not a particularly good indicator of mango chilling injury. However, it must be noted that the sugar content of the unripe juice is already high (12.6%) compared to that of the day 1 juice of the other batch. This difference at the initial stage, which is also noted in the pH values, may be related to several factors, namely the different geographical origins of the two batches compared (Venezuela and Brazil) and possible different stages of maturity on harvest. Both pH and %SS results described above fairly agree with those reported in the literature (Medlicott *et al.*, 1986; Krishnamurthy and Joshi, 1989).

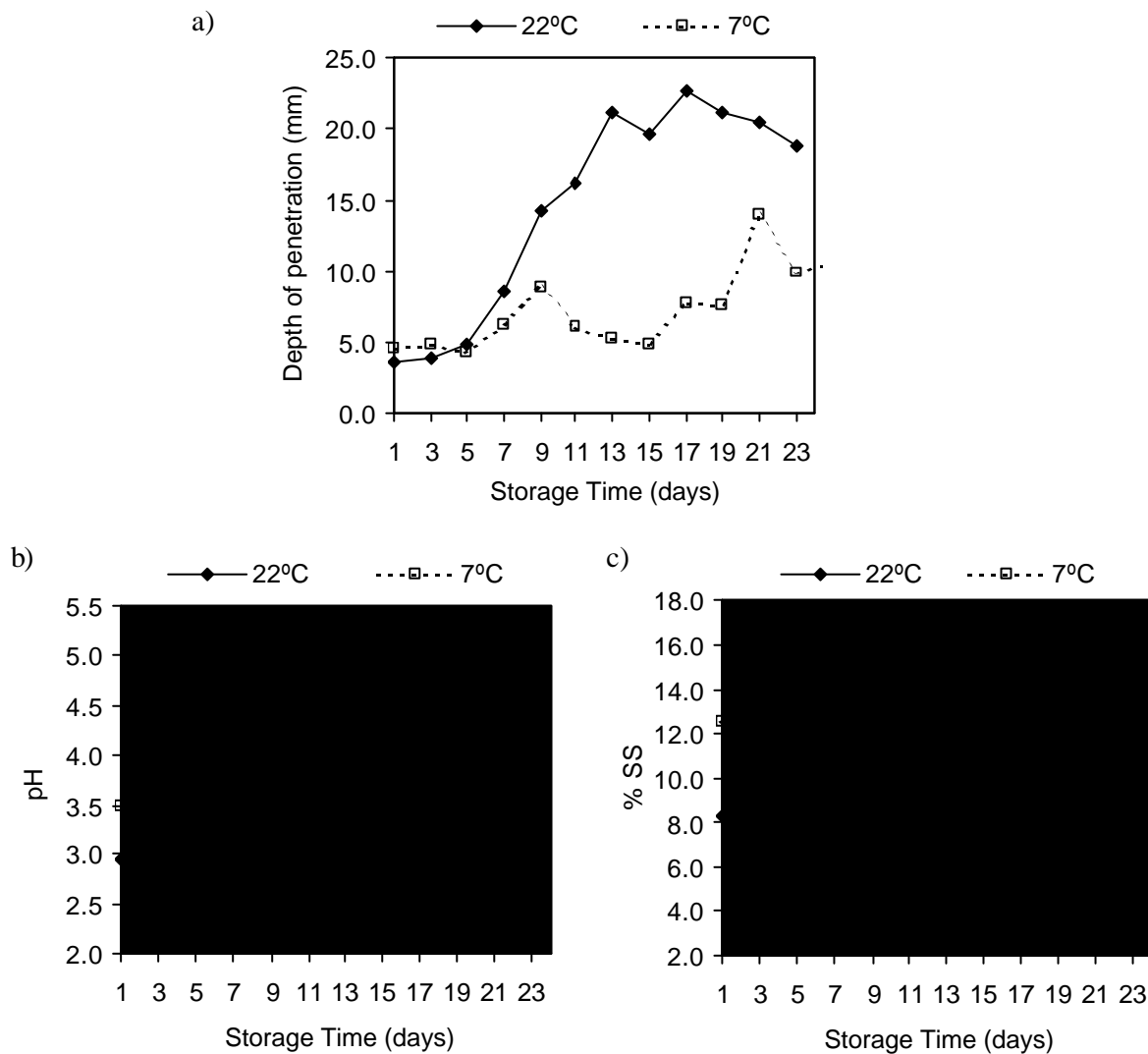


Figure IV.10. Variations in physicochemical properties of mango fruit (cv. Haden) during ripening at 22°C and at 7°C: a) firmness, b) pH and c) soluble solids (%SS). The values shown for the batch stored at 22°C correspond to the averages determined for the three juices analysed each day, while for the refrigerated batch only one juice has been analysed at each ripening stage.

#### **IV.4.2. Changes Assessed by NMR**

The changes observed in the  $^1\text{H}$  NMR spectra of the juices collected at different ripening stages from the two batches of Haden fruits (stored at 22 and a 7°C) are discussed in the present section. However, before investigating the effect of refrigeration, it is interesting to compare the ripening changes taking place at 22°C for the cultivar Haden with those previously reported for the Tommy Atkins cultivar, in order to evaluate the influence of cultivar/origin on the ripening process.

Significant differences are noted regarding some amino acids: a) glutamic acid/glutamine are present in low amounts in Haden juices and do not increase as in Tommy Atkins juices; b) arginine is present in Haden juices throughout ripening until day 17, whereas in Tommy Atkins juices it disappears after day 9; c) phenylalanine and tyrosine are present in all Haden juices and show an increasing trend with ripening, while they are absent in Tommy Atkins juices after 5-7 days of storage. Further differences between the two batches may be noted in the aromatic regions of the spectra. The polyphenolic compounds detected in Tommy Atkins juices (from day 7 onwards) are absent in Haden juices. The synthesis of these compounds has been suggested to be associated with the disappearance of tyrosine and phenylalanine, and, indeed, in Haden juices, these amino acids do not disappear and polyphenols are not formed. Other differences regard uridine and adenosine systems, which do not increase in Haden juices. Hence, ripening at 22°C of the Tommy Atkins and Haden batches differs mainly in the variation of some amino acids (glutamic acid/glutamine, arginine, phenylalanine and tyrosine), polyphenols and other minor components (uridine- and adenosine-containing compounds).

For studying the effect of refrigeration, the changes noted for the two batches of Haden fruits will now be considered. Most spectral changes detected for the Haden juices ripened at 22°C do not occur in the juices of the batch stored at 7°C, which maintain the spectral profile quite unchanged during the whole storage period. The amino acids, for instance, show negligible variations, except for alanine, whose metabolism does not seem to be affected, since it shows the same increasing trend under refrigerated storage and under normal temperature. Similarly, the initial levels of organic acids in the juice remain approximately constant and the variations noted at 22°C, such as the citric acid substantial decrease, are not seen at 7°C.

The major sugars also show relatively small variations in their relative proportions during refrigerated storage, as illustrated in Figure IV.11. However, by comparing the sugar percentages measured for the two batches, significant differences are found, especially in what regards fructose and sucrose (Figure IV.11). Since these differences are noted from the beginning of the storage period, they are likely to arise from factors such as geographical origin and initial ripeness stage, rather than from the effect of the storage temperature. In what concerns aromatic compounds, no significant variations are noted.

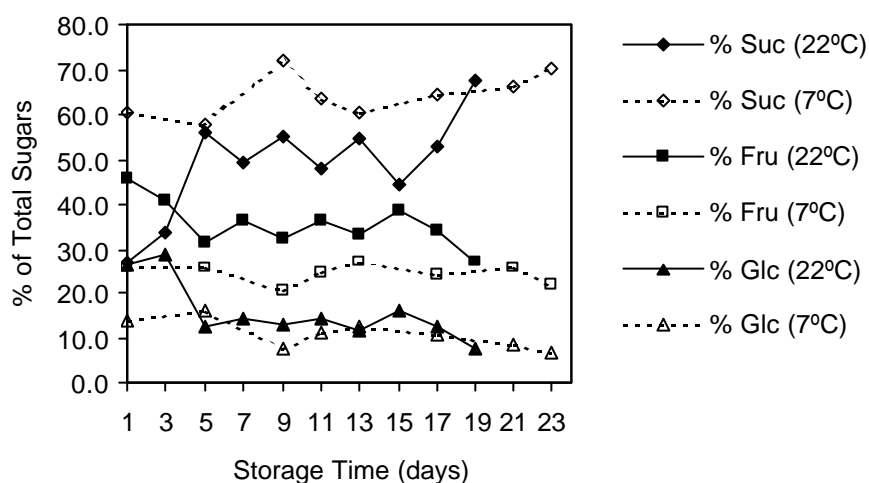


Figure IV.11. Sugars variation in Haden juices during ripening at 22°C and at 7°C: relative contribution of each sugar to the total sugar content, determined by integration of NMR signals (suc: 5.41 ppm, fru: 4.11 ppm,  $\alpha$ -glc: 5.23 ppm,  $\beta$ -glc: 4.64 ppm; total sugars: 3.20-4.26 ppm + 4.64, 5.23 and 5.41 ppm). The values shown for the batch stored at 22°C correspond to the averages determined for the three juices analysed each day, while for the refrigerated batch only one juice has been analysed at each ripening stage.

The small variations in the levels of organic acids and sugars, at 7°C, account for the high acidity and poor edible quality of the refrigerated fruits. Indeed, as shown in Figure IV.12, the ratio of total sugars to citric acid, which is an important indicator of the fruit organoleptic properties, remains low in the juices stored at 7°C, while it significantly increases in the juices collected from mangoes ripened under normal temperature, which developed good flavour. These results agree with those reported by Medlicott *et al.* (1986), who found that, during ripening at 12 and 17°C, although sugars reached levels similar to those accumulated at higher temperatures, citric acid remained high in the juices of refrigerated mangoes, leading to an unfavourable balance between sugars and acids.

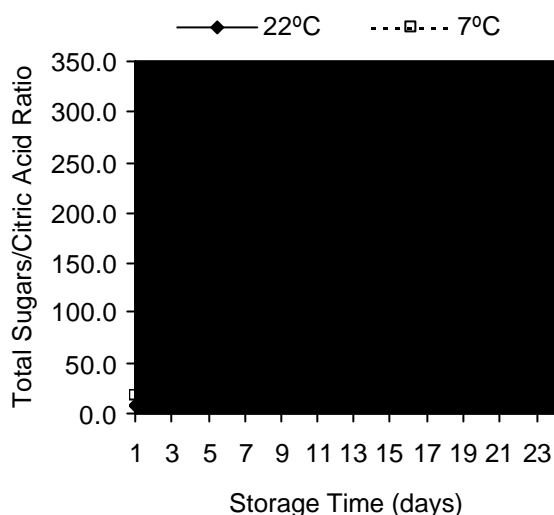


Figure IV.12. Total sugars: citric acid ratio calculated for Haden juices ripened at 22 and 7°C, with basis on integration measurements. The values shown for the batch stored at 22°C correspond to the averages determined for the three juices analysed each day, while for the refrigerated batch only one juice has been analysed at each ripening stage.

In summary, storage at 7°C is found to prevent (or at least to retard) most compositional changes occurring at normal temperature (22°C), within the period studied. In particular, the metabolism of most amino acids and organic acids (namely citric acid) is clearly affected by the low temperature, since these compounds exhibit only small variations throughout storage.

#### IV.5. Conclusions

In this work, the ripening process of mango fruit was found to be characterised by significant changes in many components, as monitored by high resolution <sup>1</sup>H NMR of juices. The major sugars present in mango juice showed different variations upon ripening: sucrose (initial cc. 31 g/L) increased almost 5 times until the mid-stages of the storage period, becoming the most abundant sugar after day 5; fructose, which was the major sugar in the unripe juice (cc. 42 g/L), showed a small increase until day 9 (cc. 60 g/L) and then decreased back to initial concentrations; glucose (initial cc. 20 g/L) significantly decreased after day 7 to 2-3 g/L, constituting only about 2% of the total sugars in the ripe juice. The sum of these variations resulted, as expected, in a two-fold increase of the total sugars content, a slight decreasing trend being noted for late ripening stages. Concerning organic acids and amino acids, different variation patterns were found. As expected, citric acid

(initial cc. 14 g/L) showed a substantial decrease, being largely responsible for the acidity loss reflected by the pH increase of the juice. Shikimic acid also decreased from about 1.8 to 1.1 g/L, whereas malic acid (initial cc. 1 g/L) decreased until mid-stages but then increased back until the end of storage. Some amino acids like alanine, valine and isoleucine were seen to increase during ripening while others such as arginine, tyrosine and phenylalanine were found to decrease. The decrease of the aromatic amino acids, as well as of shikimic acid, was accompanied by the increase in the broad signals attributed to polyphenolic compounds, suggesting the use of the former as precursors of phenolic polymerisation. Another interesting observation regarded the increase in pectic signals, reflecting the process of pectin hydrolysis expected to accompany mango ripening.

For the pulps, a semi-quantitative study has been carried out and the results suggested that polyphenols and fatty acids may be retained in the pulp solid phase, giving rise to signals with relative lower intensities in the spectra of juices. Moreover, pectic components, namely galacturonic acid residues, were detected in higher amounts in the unripe pulp than in the corresponding juice, although this difference was not observed for subsequent ripening stages.

Compared to the Tommy Atkins cultivar, the compositional changes registered for the Haden cultivar, ripened at the same temperature (22°C), differed mainly in the variations of some amino acids, namely glutamic acid/glutamine, arginine, tyrosine and phenylalanine, polyphenols (which were not formed in Haden juices) and other minor components (uridine- and adenosine-containing compounds). The effect of refrigerated storage on the composition of Haden juices has also been investigated and it was found that most juice components showed small variations, compared to the juices stored under normal conditions. Citric acid, for instance, remained high in the juices collected from refrigerated fruits, conferring them a high acidity and an unfavourable balance with sugars, resulting in poor edible quality. Alanine, on the other hand, increased at both storage temperatures, suggesting that its metabolism was not affected by refrigeration.

## References

Angyal, S.J. The composition of reducing sugars in solution. *Advances in Carbohydrate Chemistry and Biochemistry* **1984**, 42, 15-67.

Barcelon, E.G.; Tojo, S.; Watanabe, K. Relating X-ray absorption and some quality characteristics of mango fruit (*Mangifera indica* L.). *Journal of Agricultural and Food Chemistry* **1999**, *47*, 3822-3825.

Bellon, V.; Cho, S.I.; Krutz, G. W.; Davenel, A. Ripeness sensor development based on nuclear magnetic resonance. *Food Control* **1992**, *January*, 45-48.

Belton, P.S.; Delgadillo, I.; Holmes, E.; Nicholls, A.; Nicholson, J.K.; Spraul, M. Use of high-field  $^1\text{H}$  NMR spectroscopy for the analysis of liquid foods. *Journal of Agricultural and Food Chemistry* **1996**, *44*, 1483-1487.

Belton, P.S.; Delgadillo, I.; Gil, A.M.; Casascelli, F.; Colquhou, I.J.; Dennis, M.J.; Spraul, M. High field proton NMR studies of apple juices. *Magnetic Resonance in Chemistry* **1997**, *35*, S52-S60.

Belton, P.S.; Colquhoun, I.J.; Kemsley, E.K.; Delgadillo, I.; Roma, P.; Dennis, M.J.; Sharman, M.; Holmes, E.; Nicholson, J.K.; Spraul, M. Application of chemometrics to the  $^1\text{H}$  NMR spectra of apple juices: discrimination between apple varieties. *Food Chemistry* **1998**, *61*, 207-213.

Bertoluzza, A.; Bottura, G.; Filippetti, P.; Tosi, M.R.; Vasina, M.; Pratella, G.C.; Folchi, A.; Gallerani, G. Vibrational spectroscopy for the evaluation of molecular perturbations induced in fruit lipids by cold storage. *Journal of Molecular Structure* **1994**, *324*, 177-188.

Chatjigakis, A.K.; Pappas, C.; Proxenia, N.; Kalantzi, O.; Rodis, P.; Polissiou, M. FT-IR spectroscopic determination of the degree of esterification of cell wall pectins from stored peaches and correlation to textural changes. *Carbohydrate Polymers* **1998**, *37*, 395-408.

Chen, P.; McCarthy, M.J.; Kim, S.-M.; Zion, B. Development of a high-speed NMR technique for sensing maturity of avocados. *Transactions of the ASAE* **1996**, *39*, 2205-2209.

Clark, C.J.; Drummond, L.N.; MacFall, J.S. Quantitative NMR imaging of kiwifruit (*Actinidia deliciosa*) during growth and ripening. *Journal of the Science of Food and Agriculture* **1998**, *78*, 349-358.

Clark, C.J.; MacFall, J.S. Magnetic resonance imaging of persimmon fruit (*Diospyros kaki*) during storage at low temperature and under modified atmosphere. *Postharvest Biology and Technology* **1996**, *9*, 97-108.

Goodman, B.A.; Williamson, B.; Simpson, E.J.; Chudek, J.A.; Hunter, G.; Prior, D.A.M. High-field NMR microscopic imaging of cultivated strawberry fruit. *Magnetic Resonance Imaging* **1996**, *14*, 187-196.

Guthrie, J.; Walsh, K. Non-invasive assessment of pineapple and mango fruit quality using near infra-red spectroscopy. *Australian Journal of Experimental Agriculture* **1997**, *37*, 253-263.

Ishida, N.; Koizumi, M.; Kano, H. Ontogenic changes in water in cherry tomato fruits measured by nuclear magnetic resonance imaging. *Scientia Horticulturae* **1994**, *57*, 335-346.

Joyce, D.C.; Hockings, P.D.; Mazucco, R.A.; Shorter, A.J.; Brereton, I.M. Heat treatment injury of mango fruit revealed by nondestructive magnetic resonance imaging. *Postharvest Biology and Technology* **1993**, *3*, 305-311.

Kalra, S.K.; Tandon, D.K.; Singh, B.P. Mango. In *Handbook of Fruit Science and Technology. Production, Composition, Storage and Processing*; Salunkhe, D.K., Kadam, S.S. Eds.; Marcel Dekker Inc.: New York, 1995; 123-169.

Keener, K.M.; Stroshine, R.L.; Nyenhuis, J.A. Proton magnetic resonance measurement of self-diffusion coefficient of water in sucrose solutions, citric acid solutions, fruit juices and apple tissue. *Transactions of the ASAE* **1997**, *40*, 1633-1631.

Krishnamurthy, S.; Joshi, S.S. Studies on low temperature storage of Alphonso mango. *Journal of Food Science and Technology* **1989**, *26*, 177-180.

Le Gall, G., Puaud, M., Colquhoun, I.J. Discrimination between orange juice and pulp wash by <sup>1</sup>H nuclear magnetic resonance spectroscopy: Identification of marker compounds. *Journal of Agricultural and Food Chemistry* **2001**, *49*, 580-588.

Lizada, C. Mango. In *Biochemistry of Fruit Ripening*; Seymour, G.B., Taylor, J.E., Tucker, G.A., Eds.; Chapman & Hall: London, 1993; 255-271.

Medlicott, A.P.; Thompson, A.K. Analysis of sugars and organic acids in ripening mango fruits (*Mangifera indica* L. var Keitt) by high performance liquid chromatography. *Journal of the Science of Food and Agriculture* **1985**, *36*, 561-566.

Medlicott, A.P.; Reynolds, S.B.; Thompson, A.K. Effects of temperature on the ripening of mango fruit (*Mangifera indica* L. var Tommy Atkins). *Journal of the Science of Food and Agriculture* **1986**, *37*, 469-474.

Mizrach, A.; Flitsanov, U.; Fuchs, Y. An ultrasonic nondestructive method for measuring maturity of mango fruit. *Transactions of the ASAE*. **1997**, *40*, 1107-1111.

Mizrach, A.; Flitsanov, U.; Schmilovitch, Z.; Fuchs, Y. Determination of mango physiological indices by mechanical wave analysis. *Postharvest Biology and Technology* **1999**, *16*, 179-186.

Morga, N.S.; Lustre, A.O.; Tunac, M.M.; Balagot, A.H.; Soriano, M.R. Physico-chemical changes in Philippine Carabao mangoes during ripening. *Food Chemistry* **1979**, *15*, 225-234.

Muda, P.; Seymour, G.B.; Errington, N.; Tucker, G.A. Compositional changes in cell wall polymers during mango fruit ripening. *Carbohydrate Polymers* **1995**, *26*, 255-260.

- Ni, Q.W.; Eads, T.M. Low-speed magic-angle-spinning carbon-13 NMR of fruit tissue. *Journal of Agricultural and Food Chemistry* **1992**, *40*, 1507-1513.
- Ni, Q.W.; Eads, T.M. Liquid-phase composition of intact fruit tissue measured by high resolution proton NMR. *Journal of Agricultural and Food Chemistry* **1993a**, *41*, 1026-1034.
- Ni, Q.X.; Eads, T.M. Analysis by proton NMR of changes in liquid-phase and solid-phase components during ripening of banana. *Journal of Agricultural and Food Chemistry* **1993b**, *41*, 1035-1040.
- Selvaraj, Y.; Kumar, R.; Pal, D.K. Changes in sugars, organic acids, amino acids, lipid constituents and aroma characteristics of ripening mango (*Mangifera indica* L.) fruit. *Journal of Food Science and Technology* **1989**, *26*, 308-313.
- Tarkosova, J.; Copikova, J. Determination of carbohydrate content in bananas during ripening and storage by near infrared spectroscopy. *Journal of Near Infrared Spectroscopy* **2000**, *8*, 21-26.
- Tucker, G.A.; Seymour, G.B. Cell wall degradation during mango fruit ripening. *Acta Horticulturae* **1991**, *291*, 454-460.
- Vogels, J.T.W.E.; Terwel, L.; Tas, A.C.; van den Berg, F.; Dukel, F.; van der Greef, J. Detection of adulteration in orange juices by a new screening method using proton NMR spectroscopy in combination with pattern recognition techniques. *Journal of Agricultural and Food Chemistry* **1996**, *44*, 175-180.
- Zion, B.; Chen, P.; McCarthy, M.J. Nondestructive quality evaluation of fresh prunes by NMR spectroscopy. *Journal of the Science of Food and Agriculture* **1995**, *67*, 423-429.



## **V. SUGAR QUANTIFICATION IN MANGO JUICE BY MULTIVARIATE ANALYSIS OF FTIR AND NMR DATA**

V.1. Introduction.....	126
V.2. Materials and Methods.....	128
V.2.1. Sample Preparation.....	128
V.2.2. FTIR Measurements.....	130
V.2.3. NMR Measurements.....	130
V.2.4. Enzymatic Determinations.....	130
V.2.5. Multivariate Analysis.....	131
V.3. Sugar Quantification by Partial Least Squares (PLS)-FTIR.....	131
V.3.1. Application to Sugar Standard Solutions.....	131
V.3.2. Application to Mango Juices as a Function of Ripening.....	135
V.4. Sugar Quantification by Partial Least Squares (PLS)-NMR.....	138
V.4.1. Application to Sugar Standard Solutions.....	138
V.4.2. Application to Mango Juices as a Function of Ripening.....	142
V.5. Conclusions.....	144
References.....	144

## V.1. Introduction

The sugar composition and its dependence upon the ripening process has been studied for many fruits, including mango. As reported in Chapters III and IV of this thesis, glucose, fructose and sucrose are the most abundant components of mango juice and show large variations with ripening. Indeed, total sugar content is commonly used as a ripening indicator and is one of the most important criteria for evaluating the edibility of fruits and the quality of their processed products. Traditionally, sugar contents of foods (particularly in juices and beverages) are estimated with basis on refractive index measurements and volumetric procedures, which provide information about the total sugar content and the amount of reducing sugars (glucose and fructose), respectively (Pomeranz and Meloan, 1994). For quantifying each sugar separately, enzymatic analysis and chromatographic methods (Corradini *et al.*, 1997; Lee and Coates, 2000) are usually employed. In recent years, spectroscopic methods have become alternative techniques for the analysis of sugars in food samples, having the attractive features of being non-invasive and potentially more rapid than the above methods.

Many authors have illustrated the applicability of mid-infrared spectroscopy, in conjunction with chemometric methods, to the quantification of sugars in natural samples. Most studies used the Attenuated Total Reflectance (ATR) technique for measuring the infrared spectra, which is very convenient for analysing liquid and semi-solid samples. In a comparative study of a horizontal ATR cell and a Cylindrical Internal Reflection cell (CIRCLE cell), Garrigues *et al.* (1998) demonstrated the superiority of ATR in terms of the sensitivity achieved in the determination of sugars in fruit juices and soft drinks by PLS regression of the FTIR data. ATR FTIR measurements have been employed to determine glucose, fructose and sucrose in aqueous standards (Kemsley *et al.*, 1993), glucose syrups (Mirouze *et al.*, 1993), raw sugar cane juices (Cadet and Offmann, 1997; Cadet, 1999) and fruit juices (Garrigues *et al.*, 1998; Rambla *et al.*, 1998; Tewari *et al.*, 1999), using multivariate data analysis. Good results have been reported when samples employed as standards in the calibration set were of the same type as those to be analysed, as evaluated by comparison with reference methods such as HPLC and polarimetry (Mirouze *et al.*, 1993; Cadet and Offmann, 1997; Cadet, 1999). Although the use of real samples for calibration may aid in taking into account possible contributions from other components in the system, the choice of the reference analytical method may, for the same reason, be

hindered by possible interferences. In addition, a calibration set based on real samples will be specifically applicable to the particular sample under study whereas, if a suitable model can be built based on simpler laboratory samples, such robust model may be applicable to other systems. Therefore, some studies have been carried out based on external calibration sets prepared from aqueous standard solutions (Garrigues *et al.*, 1998; Rambla *et al.*, 1998; Tewari *et al.*, 1999). Tewari *et al.* (1999) quantified sugars and citric acid in synthetic mixtures and in apple juices, using PLS and PCR of FTIR ATR data. The calibration set comprised 24 standard mixtures of glucose, fructose, sucrose and citric acid, in which concentrations were gradually increased for all components simultaneously. Internal cross-validation indicated good agreement between known and predicted concentrations and some results of the application to apple juices were shown. However, comparison with a reference method to evaluate their accuracy was lacking. Garrigues *et al.* (1998) and Rambla *et al.* (1998) proposed the use of a reduced calibration set, comprising 8 ternary mixtures of glucose, fructose and sucrose at two concentration levels, for quantification of sugars in aqueous synthetic mixtures and several fruit juices and soft drinks. Recovery studies indicated good accuracy of the procedure.

In this work (Duarte *et al.*, 2002), a recently developed single reflectance ATR cell is employed to record the FTIR spectra of sugar standard solutions and mango juices at different ripening stages. This cell enables very small sample amounts to be analysed (enough to cover a 2 mm diameter crystal surface) and is of easy-handling relating to cell cleaning between experiments. The PLS calibration is constructed with a set of synthetic mixtures of glucose, fructose and sucrose, comprising six concentrations for each sugar, and the contents of each sugar in ripening mango juices are predicted and compared to the values obtained by enzymatic determinations.

Nuclear magnetic resonance (NMR) spectroscopy is also potentially valuable for quantitative analysis, provided that adequate experimental conditions are employed, as described in Chapter II.1.2. However, there are not many studies in the literature reporting the quantification of food components using high resolution NMR. Cho *et al.* (1991) measured the total sugar content in muskmelon tissue by correlating the  $^1\text{H}$  NMR sugar peak height with the sugar content measured by refractometry. Subsequently, using the technique of Magic Angle Spinning (MAS), Ni and Eads (1993) were able to estimate the concentrations of individual sugars (glucose, fructose and sucrose) in banana tissue, by

first measuring the standard NMR spectra on separate samples of aqueous solutions of each sugar at known concentrations, and then simulating an observed banana spectrum through the addition of appropriate fractions of standard spectra until the shape of the observed spectrum was reproduced. More recently, there has been a report in which some amino acid ratios observed in the NMR spectra of fruit juices have been compared to published values obtained by HPLC (Belton *et al.*, 1996). In Chapter IV.3.2.2 of this thesis, the concentrations of sugars and other mango juice constituents have been determined by integration of the NMR signals, using the signal of a standard material (TSP) as an intensity reference. However, in the case of strongly overlapped signals, this approach is clearly misleading and unsatisfactory. Moreover, when a large number of samples are to be quantified, signal integration may be a tedious process. Therefore, the use of multivariate methods becomes desirable.

The work described in section V.4 of this Chapter makes use of multivariate analysis, namely PLS regression, applied to the  $^1\text{H}$  NMR spectra of standard solutions and mango juices to predict the concentrations of glucose, fructose and sucrose, similarly to the approach used for the FTIR data. The procedure is tested here for sugars, which are major components in juices, but it would be important to apply it to other components, particularly those whose signals show strong overlap in the NMR spectrum.

## V.2. Materials and Methods

### V.2.1. Sample Preparation

**Standard Solutions:** Standard aqueous solutions of glucose, fructose and sucrose were prepared from analytical grade reagents, obtained from Sigma-Aldrich and dried under vacuum at 35°C until constant weight ( $\pm 0.0002$  g). These standards comprised one solution of each sugar, nine binary mixtures and ten ternary mixtures, with concentrations varying according to a triangular experimental design; six concentration levels were chosen for each sugar, based on the concentration ranges commonly found in mango juices at different ripening stages (Hulme, 1971; Medlicott *et al.*, 1986): sucrose, 4-148 g/L, glucose, 3-59 g/L, fructose, 4-99 g/L. Table V.1 lists the standard mixtures prepared and respective sugar concentrations. In order to prevent microbial growth, sodium azide was added, so that each solution contained 0.05%  $\text{NaN}_3$ . The solutions, found to have pH values of 6.9-7.0, were frozen in liquid nitrogen and stored at -20°C until FTIR and NMR

measurements. For NMR analysis, the thawed solutions were prepared to contain 10% D<sub>2</sub>O (field-frequency lock) and 0.02% sodium 3-(trimethylsilyl)tetradeutero propionate (TSP-*d*<sub>4</sub>, chemical shift and intensity reference), by mixing 900  $\mu$ l of sample with 100  $\mu$ l of TSP-*d*<sub>4</sub> 0.2% in D<sub>2</sub>O.

Table V.1. Concentrations (g/L) of the three sugars in the standard solutions of the calibration set.

Standard solution no.	Sugar concentration (g/L)		
	Glucose	Fructose	Sucrose
1	2.96	4.45	88.90
2	7.41	4.45	59.26
3	2.96	29.64	59.26
4	14.82	4.45	29.63
5	7.41	29.64	29.63
6	2.96	44.46	29.63
7	29.64	4.45	4.45
8	14.82	29.64	4.45
9	7.41	44.46	4.45
10	2.96	59.28	4.45
11	-	4.45	118.53
12	-	29.64	88.90
13	-	59.28	29.63
14	2.96	74.10	-
15	7.41	59.28	-
16	29.64	29.64	-
17	44.46	-	4.45
18	29.64	-	29.63
19	7.410	-	88.90
20	-	-	148.16
21	-	98.80	-
22	59.28	-	-

**Mango Juices:** Juices prepared from Tommy Atkins mangoes as described in Chapter IV.2.1 were used for this study. For FTIR, the thawed juices were measured directly. For NMR, sample preparation consisted of adding water (to reduce excessive viscosity) and phosphate buffer containing D<sub>2</sub>O and TSP, so that the juices pH, initially varying between 3.20 to 5.30, were adjusted to fall in the narrower range of 5.60-6.20, as previously explained in Chapter IV.2.1.

### V.2.2. FTIR Measurements

Fourier transform infrared spectra of standard solutions and of juice samples were collected on a Bruker IFS55 FTIR spectrometer. A single reflectance horizontal ATR cell (Golden Gate, equipped with a diamond crystal) was used. The data were recorded at 20±1°C, in the spectral range of 4000-700 cm<sup>-1</sup>, by accumulating 512 scans with a resolution of 4 cm<sup>-1</sup>. The choice of these conditions was based on a study of FTIR acquisition parameters and their effect on the mean errors of prediction reported by Rambla *et al.* (1998). For each standard solution and juice sample, a total of five spectra were recorded (named here as replica spectra), each spectrum obtained for a different sample batch. Between consecutive spectra, the crystal was carefully cleaned with water and, to avoid memory effects, the replica spectra were recorded randomly, i.e. intermingled with the spectra of other samples. In this way, a total of 110 spectra of standard solutions and 40 spectra of juices were recorded. These spectra were converted into JCAMP format and transferred to a PC workstation for statistical analysis.

### V.2.3. NMR Measurements

The 1D<sup>1</sup>H NMR spectra of mango juices have been recorded using the acquisition parameters described in Chapter III.2.2. The spectra of sugar standard solutions were acquired under the same conditions. The FIDs were Fourier transformed with different line-broadening factors, varying in the range 0.3-100 Hz, as it will be described in section V.4.1. The spectra were then phased, baseline corrected and calibrated by the TSP signal at 0.0 ppm. The resulting spectra were converted into JCAMP format and transferred to a PC workstation for statistical analysis.

### V.2.4. Enzymatic Determinations

In order to evaluate the predictive ability of sugar quantification in mango juices by multivariate analysis of FTIR and NMR data, each sugar was quantified enzymatically for a selected set of samples, using the triple enzymatic test for sucrose/D-glucose/D-fructose (cat. no. 716260) and the single test for D-glucose (cat. no. 716251), both purchased from Boehringer Mannheim. For ripening stages later than day 13, the glucose-specific test had to be used along with the triple test, since glucose content becomes significantly lower than those of the other sugars.

### **V.2.5. Multivariate Analysis**

Partial-Least Squares (PLS1) regression was the method employed to build calibration models and predict the concentration of sugars in juice samples. Principal Components Analysis (PCA) was also used. The calculations were performed using the program developed by Dr. A. Barros in the ‘Institut National Agronomique Paris-Grignon’ in collaboration with the University of Aveiro (Barros, 1999). The basic principles of PCA and PLS methods are described in Chapter II.5.

For multivariate analysis of the FTIR data, the spectral region between 1250 and 900  $\text{cm}^{-1}$  (‘fingerprint’ region) was selected. Each spectrum was autoscaled (mean centred and standardised), and the first and second derivatives of the spectra were calculated by the Savitsky-Golay procedure (Savitsky and Golay, 1964). PLS regression was applied to the three sets of spectra (autoscaled, first and second derivatives), as discussed in section V.3.1. For multivariate analysis of the NMR spectra, the 2.9-5.7 ppm region was used, excluding the segment containing the suppressed water signal at 4.80 ppm. Each spectrum was normalised by adjusting the total area to unity. This procedure helps removing the potential intensity variation caused by the NMR equipment.

The prediction errors of the PLS models developed for the estimation of sugars in mango juices were evaluated by the Root Mean Square Error of Prediction (RMSEP), in percentage, defined as:

$$\text{RMSEP}(\%) = \frac{100}{\bar{y}} \sqrt{\frac{\sum_{i=1}^N (y_i - \hat{y}_i)^2}{N}}$$

where N is the number of samples,  $y_i$  is the actual concentration,  $\hat{y}_i$  is the predicted concentration, and  $\bar{y}$  is the average of actual concentration values.

## **V.3. Sugar Quantification by Partial Least Squares (PLS)-FTIR**

### **V.3.1. Application to Sugar Standard Solutions**

Glucose, fructose and sucrose show intense and characteristic bands in the fingerprint region (1250-900  $\text{cm}^{-1}$ ) of the mid-infrared wavelength range (Figure V.1), reflecting mainly C-O stretching vibrations. Although each sugar has a characteristic set of absorption bands in this region, these bands are severely overlapped in the spectrum of a

mixture of sugars, thus hindering individual sugar identification/quantification by univariate calibration strategies.

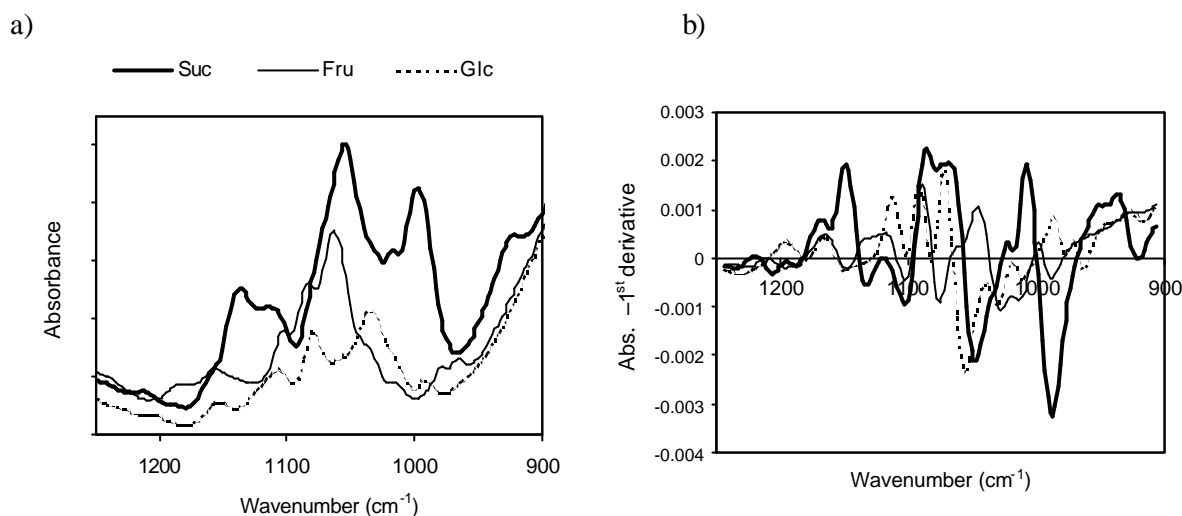


Figure V.1. a) FTIR-ATR spectra (1250-900 cm<sup>-1</sup>) of standard aqueous solutions of sucrose, fructose and glucose, recorded using a Golden Gate single reflectance ATR cell, with 4 cm<sup>-1</sup> resolution and 512 scans; b) first derivative functions of the FTIR spectra shown in a).

In order to build a multivariate calibration model for determining sugars in mango juices, the set of 22 standard solutions shown in Table V.1 was measured by FTIR and PLS1 regression was applied to the autoscaled spectra, to the first derivatives and to the second derivatives of the spectra. Table V.2 shows the statistical parameters obtained for the three models. Each model was tested by internal cross-validation, also called the leave-k-out procedure, k being the 5 replica spectra of each sample. The objective function used to find the "best" model was the Root Mean Square Error of Cross-Validation (RMSECV), in percentage. It is clear from the results shown in Table V.2 that the RMSECV (%) values and the model dimensionalities (or latent variables) corresponding to the first derivative treatment are lower than those obtained for the other models, in particular for the model constructed with the autoscaled spectra. Therefore, the underlying variations present in the FTIR spectra of sucrose, glucose and fructose mixtures are most suitably identified with the use of the first derivatives of the spectra, shown in Figure V.1b. Rambla *et al.* (1998) have also reported lower prediction errors for PLS regression of first-derivative spectra compared to absorbance spectra. In addition, it also becomes clear from Table V.2 that the error obtained for glucose (4.9%) is higher than that obtained for sucrose and fructose (1.4%). This may be a reflection of the relatively low glucose concentrations, spread within

a narrower range (3-59 g/L) than those of sucrose and fructose (4-148 g/L and 4-99 g/L, respectively).

Table V.2. Statistical results of the application of PLS1 to the three sets of FTIR data: autoscaled spectra, first derivative spectra and second derivative spectra.

	Latent Variables	RMSECV (%)
<b>autoscaled spectra</b>		
Fructose	8	9.3
Glucose	5	10.1
Sucrose	7	14.9
<b>1<sup>st</sup> derivative spectra</b>		
Fructose	4	1.4
Glucose	4	4.9
Sucrose	4	1.4
<b>2<sup>nd</sup> derivative spectra</b>		
Fructose	4	3.0
Glucose	6	5.7
Sucrose	6	1.8

Figure V.2 shows the **b** vectors as obtained from the PLS1 regression applied on the first derivatives of the spectra. These vectors establish the profile of each sugar and enable its amount to be predicted in test or real samples. All the three obtained PLS1 models (each with 4 latent variables) explained 99% of the total variability present in the concentration vectors (sugars amount).

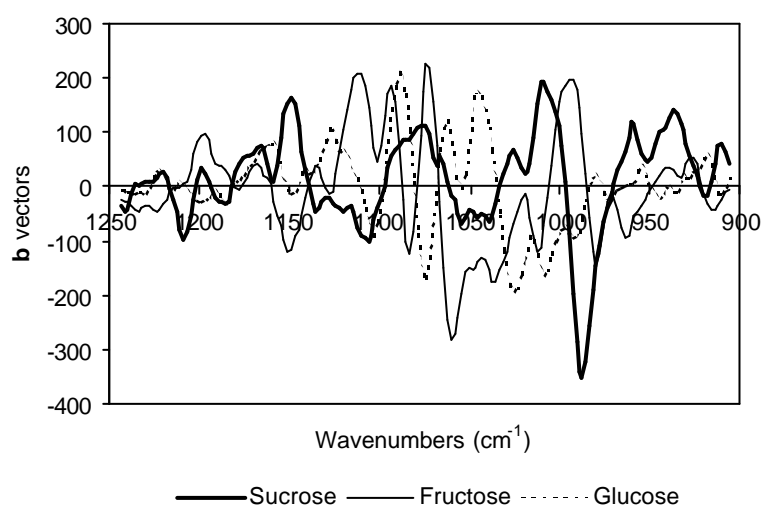


Figure V.2. **b** vectors obtained with the PLS1 model (4 latent variables) applied on the first derivatives of the FTIR-ATR spectra (1250-900  $\text{cm}^{-1}$ ) of the standard sugar solutions.

For a better understanding of the main sources of variability affecting the FTIR spectra of the standard sugar solutions in the calibration set, Principal Component Analysis (PCA) was performed in the 1250-900  $\text{cm}^{-1}$  region of the corresponding first derivative spectra. Figure V.3a shows the scores scatter plot of the two first Principal Components (PCs), which together account for 99% of the total variability present in the spectra.

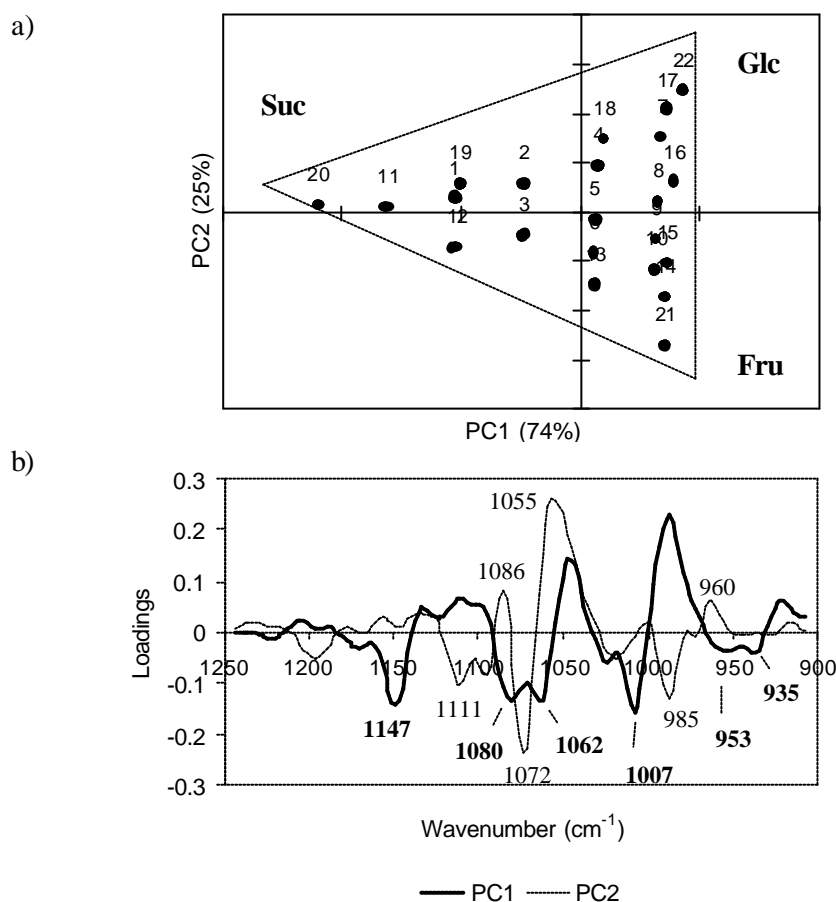


Figure V.3. PCA of the first derivative FTIR-ATR spectra (1250-900  $\text{cm}^{-1}$ ) of the standard sugar solutions: a) Scores scatter plot of PC1 vs. PC2 and b) PC1 and PC2 loadings profiles.

The plot obtained shows that the samples are suitably distributed along a concentration gradient, according to their sugar composition determined by the triangular experimental design employed. As expected, the three individual sugar solutions at maximum concentration levels are located at the vertices of the “triangle”: sucrose (sample 20) is located in the negative side of PC1 axis while fructose (sample 21) and glucose (sample 22) are located in the positive side of PC1. This distinction can be further interpreted by inspecting the loadings profile corresponding to PC1 (Figure V.3b). It can

be seen that the bands related to sucrose (negative PC1 loadings) are those located at 935, 953, 1007, 1022, 1062, 1080 and 1147  $\text{cm}^{-1}$ . Comparison with the first derivative spectra shown in Figure V.1b confirms that these values correspond to maxima in the sucrose spectral profile. The scores scatter plot (Figure V.3a) also shows a distinction between fructose and glucose along the PC2 axis: the positive bands located at 960, 1055 and 1086  $\text{cm}^{-1}$  (Figure V.3b) appear to be more related to glucose variation, whereas the negative bands located at 985, 1016, 1072, 1095 and 1111  $\text{cm}^{-1}$  (Figure V.3b) should be more related to fructose variation.

### V.3.2. Application to Mango Juices as a Function of Ripening

The FTIR spectra of four mango juices collected at different ripening stages are shown in Figure V.4. From day 1 to day 19, these spectra show a tendency for total area increase, reflecting the increase in total sugars, as well as changes in the spectral profile due to changes in the proportion of the three main sugars, sucrose, fructose and glucose.

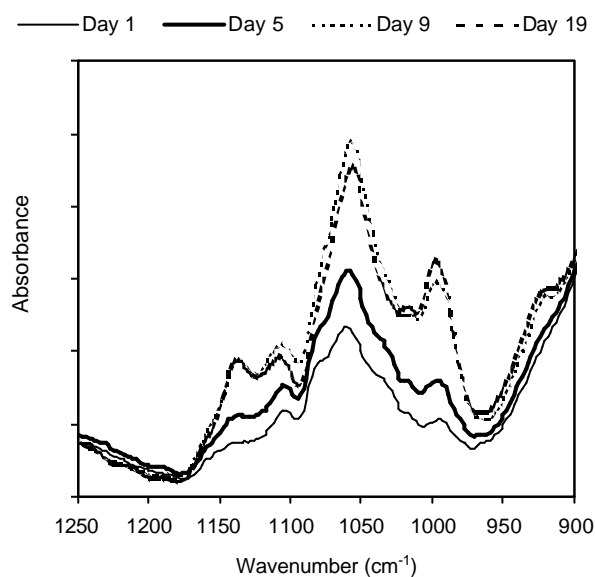


Figure V.4. FTIR-ATR spectra (1250-900  $\text{cm}^{-1}$ ) of four mango juices at different ripening stages, recorded using a Golden Gate single reflectance ATR cell, with 4  $\text{cm}^{-1}$  resolution and 512 scans.

In order to quantify each of the three sugars at different ripening stages, the PLS1 calibration model developed for the standard sugar solutions was applied to the first derivative functions of the mango juices spectra. Sucrose, glucose and fructose were also quantified by specific enzymatic tests so that the accuracy of the estimated concentrations

could be verified. The results are shown in Table V.3. Firstly, it should be noted that some discrepancy occurs between FTIR and enzymatic results for sucrose and fructose in day 1. This may relate to the fact that the 5 replica spectra taken for the juice of day 1 show poorer reproducibility than the replica measured for the other samples, therefore limiting the accuracy of the values obtained by PLS-FTIR. For days 3 to 9, both sets of data are in very good agreement for all sugars. For stages later than day 13, good agreement is shown for sucrose and fructose but, for glucose, concentrations determined enzymatically are consistently lower than those predicted by FTIR. This arises from the drastic glucose decrease, at late ripening stages, to concentration levels lower than those observed in previous studies (Medlicott and Thompson, 1985; Medlicott *et al.*, 1986). Since the glucose concentration levels found here (0.6-1.5 g/L) are well below the minimum glucose concentration present in the standard solutions used to build the PLS-FTIR model (3.0 g/L), such low concentrations could not be adequately predicted by this model.

Table V.3. Concentrations (g/L) of the three sugars in mango juices at different ripening stages, estimated by PLS1 applied on the first derivative FTIR-ATR spectra and measured by enzymatic tests. The uncertainties of each PLS-FTIR estimated values are indicated; the precision of the enzymatic tests was found to be 1.5-1.6% for each type of test employed.

Ripening stage	Glucose		Fructose		Sucrose	
	PLS1	Enzymatic	PLS1	Enzymatic	PLS1	Enzymatic
Day 1	20.36 ±1.00	19.34	34.28 ±0.48	39.10	27.84 ±0.40	38.15
Day 3	18.27 ±0.90	16.03	36.14 ±0.51	35.70	31.48 ±0.44	32.00
Day 5	19.58 ±0.96	17.13	37.17 ±0.52	36.07	47.17 ±0.66	47.63
Day 9	11.71 ±0.57	10.84	42.72 ±0.60	43.64	98.59 ±1.40	97.00
Day 13	2.46 ±0.12	0.58	42.68 ±0.60	38.90	117.69 ±1.65	118.02
Day 17	2.49 ±0.12	0.94	32.13 ±0.45	32.67	109.40 ±1.53	111.31
Day 19	4.20 ±0.21	1.29	26.40 ±0.37	25.87	111.30 ±1.56	110.80
Day 21	4.46 ±0.22	1.47	26.51 ±0.37	n.d.	104.64 ±1.46	n.d.

n.d.: not determined

In summary, the present PLS-FTIR model is able to predict sugar contents in mango juices with different ripening degrees with the following RMSEP (%) values: 5.1% for sucrose (down to 1.3% if spectral dispersion in day 1 is improved); 6.7% for fructose (down to 4.8% if spectral dispersion in day 1 is improved); 8.0 % for glucose until mid-stages of ripening, beyond which prediction errors may reach about 25%.

The juices first derivative spectra, obtained as a function of ripening, were also treated by PCA and the resulting scores scatter plot is shown in Figure V.5a. The juices of days 1 to 5 are clearly separated from the remaining samples, along the PC1 dimension.

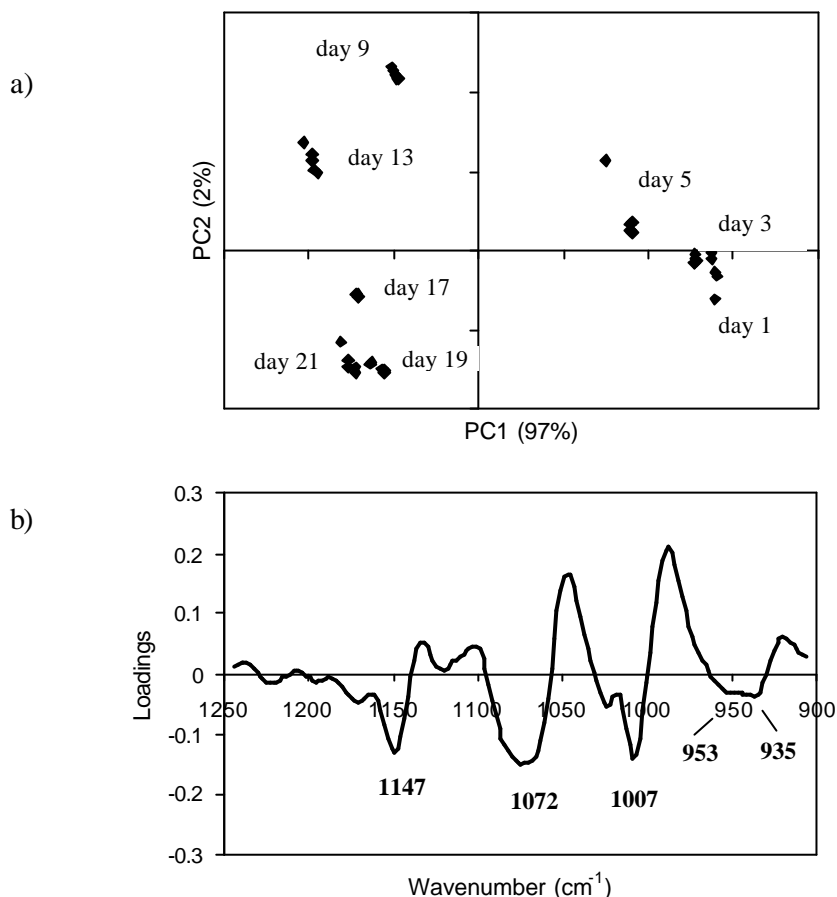


Figure V.5. PCA of the first derivative FTIR-ATR spectra (1250-900  $\text{cm}^{-1}$ ) of mango juices: a) Scores scatter plot of PC1 vs. PC2 and b) PC1 loadings profile.

The PC1 loadings profile (Figure V.5b) indicates that the samples with scores located in the negative side of PC1 are richer in sucrose, since loading values are negative at the wavenumbers 935, 953, 1007, 1022, 1072 and 1147  $\text{cm}^{-1}$ , already seen to be characteristic of sucrose. Indeed, the quantification results presented in Table V.3 show that the sucrose content is below 50 g/L from day 1 to day 5 and increases to concentrations close to or higher than 100 g/L in the remaining days. Moreover, since citric acid is known to decrease drastically during the first stages of ripening (Medlicott and Thompson, 1985; Medlicott *et al.*, 1986), the possibility that this variation may contribute

to the PC1 loadings profile shown in Figure V.5b was also considered. However, the fact that this profile shows no significant contributions in regions of strong citric acid absorbance such as at  $1180\text{ cm}^{-1}$  or  $1220\text{ cm}^{-1}$  indicates that the results obtained do not depend significantly on the citric acid variations. The variability within the PC2 dimension is not as significant as that in PC1, since it accounts for only 2% of the total variability in the spectra. However, some distinction between juices of day 9 and those of the latest ripening stages (days 19 and 21) may be suggested from the plot (Figure V.5a), probably reflecting variations in the proportion of glucose and fructose.

## V.4. Sugar Quantification by Partial Least Squares (PLS)-NMR

### V.4.1. Application to Sugar Standard Solutions

Similarly to the approach used for the FTIR data, PLS1 regression was applied to the  $^1\text{H}$  NMR spectra of standard sugar solutions, aiming at building a model to predict the concentrations of glucose, fructose and sucrose in real juice samples. The model was tested by internal cross-validation and extremely large errors (RMSECV%) resulted for the three sugars: 50.8% for glucose, 37.1% for fructose and 52.3% for sucrose. A first approach to investigate possible sources for such large errors consisted of carrying out integration measurements in the spectra of sugar solutions, in order to find out if the signals areas correctly represented the known concentrations. The signals integrated were: 5.41 ppm for sucrose, 5.23 ppm for  $\alpha$ -glucose, 3.24 ppm for  $\beta$ -glucose and 4.11 ppm for fructose. PLS1 regression was applied to these signals areas taking into account the known sugars concentrations. The values of RMSECV (%) obtained were: 2.1% for sucrose, 2.9% for  $\alpha$ - and  $\beta$ -glucose, and 1.8 % for fructose (3 latent variables used for each sugar). These values are notably low, showing the good predictive power of this model and thus the correct correspondence between the areas of the signals and the known concentrations. Therefore, possible sources of error arising from sample preparation or from saturation effects in the vicinity of the suppressed water signal may be discarded.

One of the critical factors known to affect the multivariate analysis of NMR data is the alignment of the spectra, in which peak position may shift due to changes in pH, concentration and/or temperature. In the case of the sugar solutions studied, small shifts of about 0.004 ppm were found for some signals probably due to the concentration/temperature effects rather than pH effects, since pH values fell between 6.9

and 7.0, and the positions of the sugar signals are not expected to be affected by such small pH variations. In order to mask these shifts, LB factors higher than 0.3 Hz were tentatively employed for processing the spectra. Figure V.6 shows the 2.5-6.0 ppm region of the spectrum of a sugar mixture processed with LB 0.3, 25, 50, 75 and 100 Hz and illustrates, for the sucrose signal at 5.4 ppm, how the differences in peak position are masked.

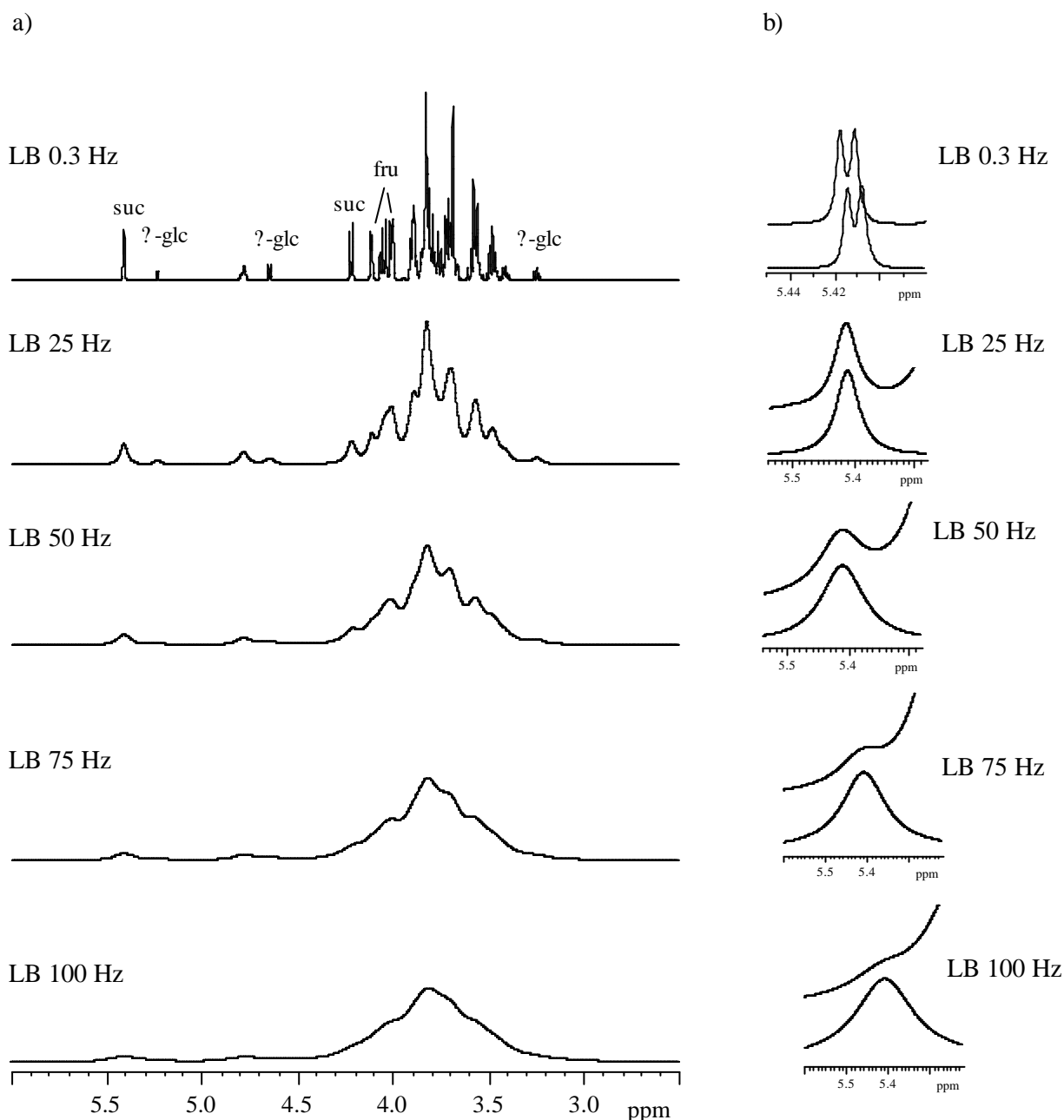


Figure V.6. a) 600 MHz <sup>1</sup>H NMR spectrum of a ternary sugar mixture (solution 5 in Table V.1) processed with different LB factors (NS 64) and b) sucrose signal at 5.4 ppm in two sugar solutions spectra, processed with different LB's.

New PLS1 models were built for the sets of normalised spectra processed with LB factors up to 100 Hz. Table V.4 shows the statistical parameters obtained. The prediction errors (RMSECV %) significantly decrease for the sets processed with LB 25 and 50 Hz, increasing again for higher LB values, probably due to the great loss of spectral information. These results show that increasing the LB factor in order to mask spectral shifts is a possible way to improve the predictive ability of a calibration model based on NMR spectra of sugar standards, suggesting that low field instruments may be adequate for this use. However, this matter requires further investigation, as the results are far from optimum.

Table V.4. Statistical results of the application of PLS1 to the sets of NMR spectra processed with different LB factors.

	Latent Variables	RMSECV (%)
<b>LB 0.3 Hz</b>		
Fructose	5	37.1
Glucose	3	50.8
Sucrose	4	52.3
<b>LB 25 Hz</b>		
Fructose	6	13.5
Glucose	5	26.4
Sucrose	4	9.4
<b>LB 50 Hz</b>		
Fructose	5	12.4
Glucose	6	15.6
Sucrose	4	9.7
<b>LB 75 Hz</b>		
Fructose	7	13.9
Glucose	7	25.0
Sucrose	5	11.7
<b>LB 100 Hz</b>		
Fructose	3	36.7
Glucose	2	34.1
Sucrose	5	11.6

With basis on the lowest prediction errors, the set processed with LB 50 Hz was chosen for building the calibration curves and for calculating the **b** vectors, shown in Figure V.7, which were used to predict the amounts of each sugar in the juice samples.

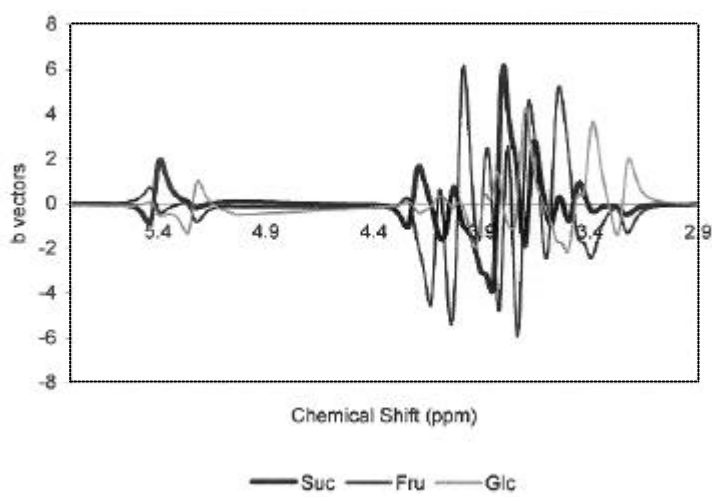


Figure V.7. **b** vectors obtained with the PLS1 model (4 latent variables for sucrose, 5 for fructose and 6 for glucose) applied on the normalised  $^1\text{H}$  NMR spectra (sugar region) of the standard sugar solutions.

Indeed, PCA of the sugar spectra showed that the scores distribution closer to the triangular design was the plot obtained for the spectra processed with LB 50 Hz, shown in Figure V.8a.

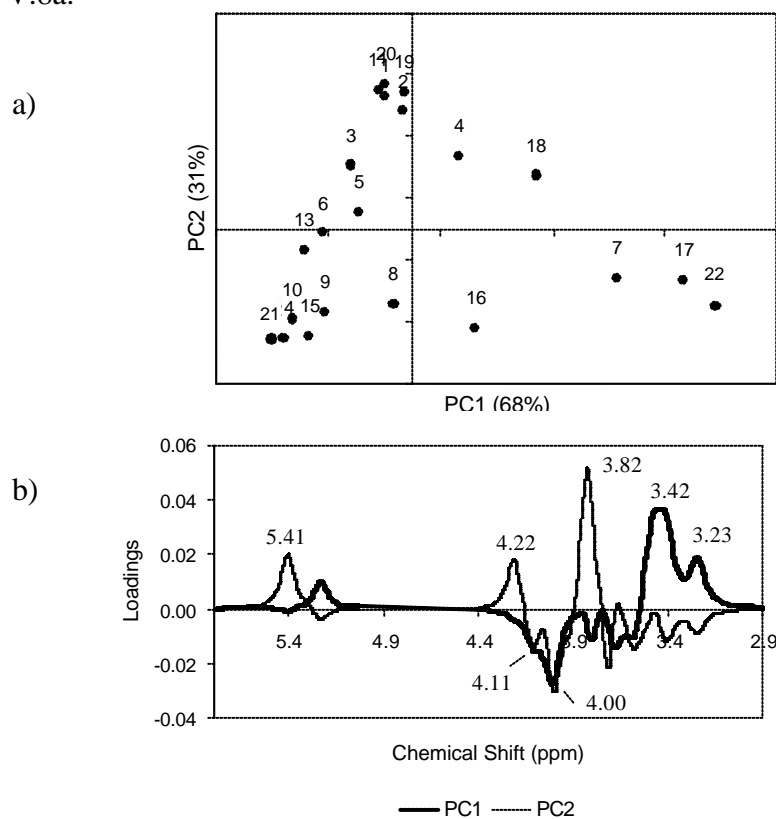


Figure V.8. PCA of the normalised  $^1\text{H}$  NMR spectra (sugar region) of the standard sugar solutions: a) Scores scatter plot of PC1 vs. PC2 and b) PC1 and PC2 loadings profiles.

As expected, the single sugar solutions (samples 20, 21 and 22) are located at the vertices of the ‘triangle’, with sucrose separated from glucose and fructose with basis on PC2, and the two monosaccharides distinguished from each other by PC1. Indeed, the PC2 loadings profile (Figure V.8b) shows positive signals at positions corresponding to sucrose (3.82, 4.22, 5.41 ppm), whereas the PC1 loadings profile (Figure V.8b) shows positive values for glucose peaks (3.24, 3.42, 5.23) and negative values for fructose peaks (4.00, 4.11). However, the scores scatter plot in Figure V.8a is a poor version of the plot obtained by PCA of the FTIR spectra (Figure V.3a).

#### V.4.2. Application to Mango Juices as a Function of Ripening

Although the PLS calibration model discussed in the previous section has large prediction errors, it was applied to the  $^1\text{H}$  NMR spectra of mango juices, processed with LB 50 Hz, in order to estimate the concentrations of the three sugars and compare them to the values determined by enzymatic assays. The results of this exploratory quantification are presented in Table V.5. For juices of days 1 and 5, the PLS1 and enzymatic values show relatively good agreement, but for the samples of later ripening stages, large discrepancies are noted. The prediction errors (RMSEP %) obtained are 25.5% and 32.3% for glucose and fructose, respectively, and such high errors reflect the little accuracy of the PLS-NMR method.

Table V.5. Concentrations (g/L) of the three sugars in mango juices at different ripening stages, predicted by PLS1-NMR and measured by enzymatic tests. The precision of the enzymatic tests was found to be 1.5-1.6% for each type of test employed, whereas the uncertainties of the PLS-NMR results are shown.

Ripening stage	Glucose		Fructose		Sucrose	
	PLS1	Enzymatic	PLS1	Enzymatic	PLS1	Enzymatic
Day 1	16.69 $\pm$ 2.60	18.04	35.69 $\pm$ 4.43	34.33	30.90 $\pm$ 3.00	n.d.
Day 5	18.15 $\pm$ 2.83	17.06	39.77 $\pm$ 4.93	35.71	56.18 $\pm$ 5.45	n.d.
Day 9	6.72 $\pm$ 1.05	10.10	26.21 $\pm$ 3.25	46.23	64.46 $\pm$ 6.25	n.d.
Day 11	2.73 $\pm$ 0.43	1.62	37.36 $\pm$ 4.63	42.82	113.82 $\pm$ 11.04	n.d.
Day 15	2.85 $\pm$ 0.44	0.87	18.73 $\pm$ 2.32	39.19	66.61 $\pm$ 6.46	n.d.
Day 21	4.14 $\pm$ 0.65	1.55	22.92 $\pm$ 2.84	27.26	100.39 $\pm$ 9.74	n.d.

n.d.: not determined

The  $^1\text{H}$  NMR spectra of the juice samples processed with LB 50 Hz were also analysed by PCA. The scores scatter plot of PC1 vs. PC2 is shown in Figure V.9a. As in the case of the FTIR data (Figure V.5a), the juices collected at early ripening stages are separated from the juices collected after day 9 along the PC1 axis, which explains 93% of the total variability present in the NMR data. The PC1 loadings profile (Figure V.9b) shows positive values at chemical shifts characteristic of sucrose and negative values at positions corresponding to glucose and fructose, thus indicating that the observed separation of samples is determined essentially by the proportions of these sugars: the juices of days 9 to 23, with scores lying in the positive side of PC1, are characterised by the predominance of sucrose, while the contributions of glucose and fructose are more important in the juices of days 1 to 7.

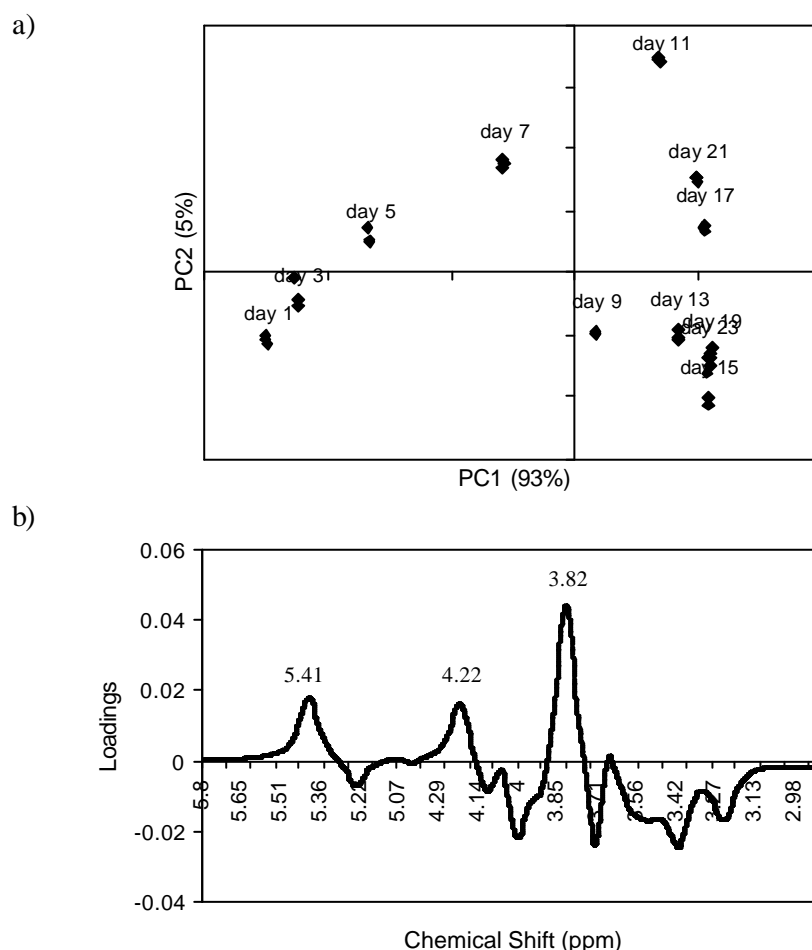


Figure V.9. PCA of the normalised  $^1\text{H}$  NMR spectra (sugar region) of mango juices: a) Scores scatter plot of PC1 vs. PC2 and b) PC1 loadings profile.

## V.5. Conclusions

The PLS-FTIR method, calibrated by a triangular model of standard sugar solutions, has been shown to be suitable for the determination of sucrose, fructose and glucose in mango juices obtained from fruits differing in ripening degree. Sucrose and fructose were accurately quantified throughout the ripening process, whereas glucose determination carried a prediction error of up to 25% after day 9. It was shown that the FTIR spectrum of a juice may, in this way, be used as a rapid indicator of ripening degree, particularly when pH and %SS of the fresh juice are not very sensitive to ripening degree (after the mid-stages of ripening, as shown in Chapter IV.3.1) or when, in the case of commercial juices, they are affected by other factors e.g. addition of pH regulators or sweeteners. The present work refers to a particular mango cultivar, however, the method and model developed should be applicable to other cultivars and possibly even to other fruits, as long as the sucrose/glucose/fructose proportion is sensitive to ripening degree and the sugar concentrations fall within the concentration ranges used in the sugar calibration model. In any case, for a new system (fruit of different cultivar or type) the trends of sugar variation should be characterised and the model concentration values checked/optimised.

On the other hand, the prediction errors obtained by the PLS-NMR method were much higher. It was found that spectral alignment was determinant in the magnitude of these errors and that increasing the line broadening factor used to process the spectra could improve the predictive ability of the calibration model. Still, the results were far from optimum and this matter requires further investigation.

## References

- Barros, A.S. Contribution à la sélection et la comparaison de variables caractéristiques. *Ph.D. Thesis*, Institut National Agronomique Paris-Grignon, France, 1999.
- Belton, P.S.; Delgadillo, I.; Holmes, E.; Nicholls, A.; Nicholson, J.K.; Spraul, M. Use of high-field  $^1\text{H}$  NMR spectroscopy for the analysis of liquid foods. *Journal of Agricultural and Food Chemistry* **1996**, *44*, 1483-1487.
- Cadet, F. Measurement of sugar content by multidimensional analysis and mid-infrared spectroscopy. *Talanta* **1999**, *48*, 867-875.
- Cadet, F.; Offmann, B. Direct spectroscopic sucrose determination of raw sugar cane juices. *Journal of Agricultural and Food Chemistry* **1997**, *45*, 166-171.

Cho, S.I.; Bellon, V.; Eads, T.M.; Stroshine, R.L.; Krutz, G.W. Sugar content measurement in fruit tissue using water peak suppression in high resolution <sup>1</sup>H magnetic resonance. *Journal of Food Science* **1991**, *56*, 1091-1094.

Corradini, C.; Canali, G.; Nicoletti, I. Application of HPAEC-PAD to carbohydrate analysis in food products and fruit juices. *Seminars in Food Analysis*, **1997**, *2*, 99-111.

Duarte, I.F.; Barros, A.; Delgadillo, I.; Almeida, C.; Gil, A.M. Application of FTIR spectroscopy for the quantification of sugars in mango juice as a function of ripening. *Journal of Agricultural and Food Chemistry* **2002**, *50*, 3104-3111.

Garrigues, S.; Rambla, F.J.; de la Guardia, M. Comparative study of reflectance cells for PLS-FTIR determination of sugars in soft drinks. *Fresenius Journal of Analytical Chemistry* **1998**, *362*, 137-140.

Hulme, A.C. The Mango. In *The Biochemistry of Fruits and their Products*; Hulme, A.C. Ed.; Academic Press: London, 1971; 233-254.

Kemsley, E.K.; Wilson, R.H.; Poulter, G.; Day, L.L. Quantitative analysis of sugars solutions using a novel fiber-optic-based sapphire ATR accessory. *Applied Spectroscopy* **1993**, *47*, 1651-1654.

Lee, H. S.; Coates, G. A. Quantitative study of free sugars and myo-inositol in citrus juices by HPLC and a literature compilation. *Journal of Liquid Chromatography and Related Techniques* **2000**, *23*, 2123-2141.

Medlicott, A.P; Reynolds, S.B.; Thompson, A.K. Effects of temperature on the ripening of mango fruit (*Mangifera indica* L. var Tommy Atkins). *Journal of the Science of Food and Agriculture* **1986**, *37*, 469-474.

Medlicott, A.P; Thompson, A.K. Analysis of sugars and organic acids in ripening mango fruits (*Mangifera indica* L. var Keitt) by high performance liquid chromatography. *Journal of the Science of Food and Agriculture* **1985**, *36*, 561-566.

Mirouze, F. L.; Boulou, J.C.; Dupuy, N.; Meurens, M.; Huvenne, J.P.; Legrand, P. Quantitative analysis of glucose syrups by ATR/FT-IR spectroscopy. *Applied Spectroscopy* **1993**, *47*, 1187-1191.

Ni, Q.X.; Eads, T.M. Analysis by proton NMR of changes in liquid-phase and solid-phase components during ripening of banana. *Journal of Agricultural and Food Chemistry* **1993**, *41*, 1035-1040.

Pomeranz, Y.; Meloan, C.E.; Refractometry and Polarimetry. In *Food Analysis*; Pomeranz, Y.; Meloan, C. E. Eds.; Chapman & Hall: New York, 1994; 430-447.

Rambla, F. J.; Garrigues, S.; Ferrer, N.; de la Guardia, M. Simple partial least squares-attenuated total reflectance Fourier transform infrared spectrometric method for the

determination of sugars in fruit juices and soft drinks using aqueous standards. *Analyst* **1998**, *123*, 277-281.

Savitsky, A.; Golay, M.J.E. Smoothing and differentiation of data by simplified least squares procedures. *Analytical Chemistry* **1964**, *36*, 1627-1639.

Tewari, J.; Joshi, M.; Gupta, A.; Mehrotra, R.; Chandra, S. Determination of sugars and organic acid concentration in apple juices using infrared spectroscopy. *Journal of Scientific & Industrial Research* **1999**, *58*, 19-24.

## VI. STUDY OF SPOILAGE, HEAT TREATMENT AND MICROBIAL CONTAMINATION IN MANGO JUICES BY NMR SPECTROSCOPY

VI.1 Introduction.....	148
VI.2. Materials and Methods.....	150
VI.2.1. Sample Preparation.....	150
VI.2.1.1. Culture of Microorganisms.....	150
VI.2.1.2. Preparation of Spores Suspensions.....	150
VI.2.1.3. Preparation and Inoculation of Juices.....	151
VI.2.2. Soluble Solids, pH and Enzymatic Determinations.....	152
VI.2.3. NMR Measurements.....	152
VI.3. Natural Mango Juice: Changes Upon Spoilage, Heat Treatment and Microbial Contamination.....	153
VI.3.1. Changes Assessed by Soluble Solids and pH.....	153
VI.3.2. Changes Assessed by NMR Spectroscopy.....	154
VI.3.2.1. Effect of Natural Spoilage.....	154
VI.3.2.2. Effect of Heat Treatment.....	163
VI.3.2.3. Effect of Inoculation with <i>Penicillium expansum</i> .....	164
VI.4. Commercial Mango Juice: Changes Upon Microbial Contamination.....	170
VI.4.1. Changes Assessed by Soluble Solids and pH.....	171
VI.4.2. Changes Assessed by NMR Spectroscopy.....	172
VI.4.2.1. Effect of Inoculation with <i>Penicillium expansum</i> .....	172
VI.4.2.2. Effect of Inoculation with <i>Neosartorya fischeri</i> .....	177
VI.5 Conclusions.....	181
References.....	183

## VI.1. Introduction

Microbial growth in fruits and fruit products is a serious concern, as it may cause decay, loss of nutritive and organoleptic properties and production of toxic substances. The low pH of fruits is the major factor that influences the composition of their microflora. In general, most yeasts and moulds grow well under acid conditions, and thus fungi are often the predominant microorganisms in fruit products, while only a few bacteria are sufficiently aciduric to be important (Frazier and Westhoff, 1988; Splittstoesser, 1996).

The traditional methods of detecting microbial growth in fruit and fruit products consist of plating procedures based on culturing the fruit sample in adequate medium, incubating and counting the microbial populations after 3-5 days. This is often too long for quality control management to initiate prompt corrective action if product contamination is detected. Therefore, research efforts have focused on developing more rapid methods for detecting microbial contamination. Examples of these methods are the bioluminescent procedure that measures the quantity of adenosine triphosphate (ATP) in living yeasts (Littel and LaRocco, 1986), the impedimetric detection, which correlates the microbial population with the time required to produce a change in impedance (Schaertel *et al.*, 1987), and some specific immunoassays (Lin *et al.*, 1986; Notermans *et al.*, 1992). Another approach is to detect specific metabolic products of microorganisms. For instance, the degree of mouldiness in grapes may be related to the glycerol content of the must, and the amounts of ethanol have long been used to monitor yeast growth in bulk-stored grape juice (Splittstoesser, 1996). Acetylmethyl carbinol (acetoin) and diacetyl are suggested to be indicators of the growth of various fungi and certain bacteria, conferring characteristic off-flavours to the contaminated fruit products (Singhal *et al.*, 1997). Organic acids are also indicators of microbial growth. Succinic, acetic, formic and lactic acids have been found to be produced in tomatoes by mould and bacteria, whereas citric acid has been seen to disappear (Singhal *et al.*, 1997). The pattern of volatile amines in apple fruits has also been reported to be a good indication of contamination by different moulds. It has been observed that butylamine and isobutylamine, not present in healthy fruits, occur in contaminated ones and could therefore be used as an index of mould contamination (Singhal *et al.*, 1997). Another common response of plant tissue to infection by microorganisms is an increase in the synthesis of characteristic phenolic compounds (Singhal *et al.*, 1997).

High resolution NMR spectroscopy has been shown to be a powerful method for the elucidation of metabolic pathways of microorganisms. In particular, the technique has been applied to study the metabolism of lactic acid bacteria, which are involved in wine fermentation, through *in vivo*  $^1\text{H}$ ,  $^{13}\text{C}$  and  $^{31}\text{P}$  NMR experiments that provide information on metabolite levels and fluxes through metabolic pathways (Santos, 1995; Ramos and Santos, 1999). The strength of applying NMR towards this aim resides on its non-destructive nature and its broad screening capability, *i.e.* the ability to simultaneously detect a wide range of species and potentially enable the identification of novel, unexpected compounds.

The work presented in this Chapter makes use of high resolution NMR to follow the compositional changes of natural and commercial mango juice subject to natural spoilage and to inoculation with two moulds; the effect of heat treatment on a natural juice is also investigated to a lesser extent. Indeed, the principal aim of the work described here is to explore the potential of the technique to detect and identify indicators of spoilage, either occurring naturally or caused by specific microorganisms. The natural juice prepared from fresh mangoes was tested for the effects of spoilage (resulting from chemical, enzymatic and/or microbial processes), heat-treatment, and deliberate contamination with spores of *Penicillium expansum*. This mould is the most common apple-rotting fungus and can be commonly found in the processing lines of fruit products. It infects the intact fruit through the wounds caused during handling and packing operations and is responsible for high postharvest losses. Moreover, although *P. expansum* is destroyed by the pasteurisation treatment given to the juices or other fruit products, it produces the mycotoxin patulin, which is resistant to thermal destruction between pH 3.5 and 5.5, and thus may be present in pasteurised products, constituting a health concern (Splittstoesser, 1996). The effect of microbial contamination was also investigated for a commercial juice, in order to evaluate its susceptibility to spoilage after the processing treatment given at the industrial scale. For this purpose, *P. expansum* and a second mould, *Neosartorya fischeri*, have been used to inoculate the juice. The choice of the *N. fischeri* was based on the knowledge that this mould is heat resistant, thus, in many instances, surviving the commercial pasteurisation treatment given to most fruit products (e.g. 90°C, 3 minutes) and being able to induce spoilage by germination and subsequent outgrowth during storage. There are a few studies reporting the presence of this fungus in processed juices (Obeta and Ugwuanyi, 1995), and

investigating its thermal resistance in fruit products, by determining the number of spores that survive heat treatment at various temperatures (Beuchat, 1986; Rajashekhara *et al.*, 1998; Rajashekhara *et al.*, 2000). Moreover, the growth of *N. fischeri* on mango, orange and pineapple juices has been monitored by microbial counts and by observing the changes in the juices colour, odour and body (Obeta and Ugwuanyi, 1997). However, the information on the compositional changes induced by this mould is scarce, and the present work aims at identifying possible chemical indicators of the *N. fischeri* growth on a processed juice, in particular, mango juice.

## **VI.2. Materials and Methods**

### **VI.2.1. Sample Preparation**

#### **VI.2.1.1. Culture of Microorganisms**

The mould *Penicillium expansum* used in this study was kindly provided by the 'Instituto Nacional de Engenharia e Tecnologia Industrial', in Lisbon, from its culture collection (strain 310 isolated from apple juice). The mould *Neosartorya fischeri* was purchased from DSMZ ('Deutsche Sammlung von Mikroorganismen and Zellkulturen GmbH') culture collection (strain DSM 3700). Both cultures were maintained on slants of freshly prepared potato dextrose agar (PDA) and stored at 4°C until used.

#### **VI.2.1.2. Preparation of Spores Suspensions**

In order to produce sufficient mature spores, *P. expansum* and *N. fischeri* cultures were inoculated into slants of PDA and incubated at 25-28 °C for 5 and 20 days, respectively. For each mould, spores were harvested from the slants by flooding with 5-6 ml of sterile deionised water containing 0.1% Tween 80 and collecting the aliquots to an Erlenmeyer flask, until 20-30 ml were obtained. A 10 minutes sonication treatment was followed by filtration of the suspension through sterile glass wool to remove hyphal fragments. Microscopic examination of the filtrate revealed free spores. Each suspension was then diluted to give spores concentrations of  $10^6$ /ml,  $10^5$ /ml and  $10^4$ /ml, measured by using a Newbauer chamber for counting spores. The spores of heat-resistant moulds are in a state of dormancy which requires heat treatment to induce germination. Therefore, the *N.*

*fischeri* suspension was activated by heating a 10 ml portion, in a screw capped test tube, at 70°C for 1 hour in a water bath, as described by Obeta and Ugwuanyi (1997).

### **VI.2.1.3. Preparation and Inoculation of Juices**

**Natural Mango Juice:** Ripe edible mangoes of the cultivar Haden grown in Brazil were used for this study. The fruits were washed, peeled and their pulps macerated in a domestic juice extractor. The resulting puree was centrifuged (at 15000 r.p.m. during 15 minutes) to give the juice. Aliquots of 20.0 ml were poured into 27 sterile bottles of 100 ml, which were treated/stored in the following conditions: one group of 6 bottles was stored at 25°C without any treatment, in order to follow the changes occurring during natural spoilage of the juice, while the other bottles were heat-treated in a water bath at 80°C during 15 minutes, in order to eliminate most of the natural microflora existing in the juice (Ejechi *et al.*, 1998), similarly to the pasteurisation treatment commonly applied at industrial level; five of these bottles containing heated juice were then stored under refrigeration (4°C) for maximum preservation and other six were stored at 25°C. The remaining 10 bottles of heat-treated juice were inoculated with spores of *P. expansum*, in order to investigate the changes induced by this mould in the juice composition: 5 bottles were inoculated with 0.500 ml of suspension containing  $10^5$  spores per ml, and 5 bottles were inoculated with 0.500 ml of suspension containing  $10^4$  spores per ml, to give spores concentrations in the juice of about 2500/ml (batch A) and 250/ml (batch B), respectively.

During a period of 132 hours (5.5 days), one bottle was withdrawn every 24 hours from each group and the juice samples prepared. The juice was filtered through a glass microfiber filter under vacuum and through a 0.45  $\mu$ m filter with a syringe, and both pH and soluble solids (%SS) were measured. For NMR analysis, the filtered juice was mixed with a solution of D<sub>2</sub>O containing 3-(trimethylsilyl)propionate sodium salt (TSP) and sodium azide (NaN<sub>3</sub>), in order to give samples with 10% D<sub>2</sub>O (field-frequency lock), 0.02% TSP (chemical shift and intensity reference) and 0.05% NaN<sub>3</sub> (to prevent microbial growth in the stored samples). The pH of the juices was adjusted to 7.00 $\pm$ 0.05 with microliter amounts of sodium hydroxide solutions (NaOH 3M, 1M, 0.1M), in order to reduce pH-related shifts in the positions of NMR signals. The juice samples were frozen in liquid nitrogen and stored at -20°C until the NMR measurements.

**Commercial Mango Juice:** One-litre packages were aseptically opened and their contents dispensed into sterile flasks of 4L capacity to have 2L of juice in each flask (plugged with cotton). For each experiment, one flask was used as control (juice without inoculation) and inoculation was performed on the second flask. For the experiment with *Penicillium expansum*, 1.00 ml of spore suspension ( $10^6$ /ml) was inoculated into 2L of juice to give approximately 500 spores per ml. For the experiment with *Neosartorya fischeri*, the flasks were heated in a water bath at 75°C for 15 minutes and one flask containing 2L of juice was inoculated with 1.00 ml of the heat-activated spores suspension ( $10^6$ /ml), to give 500 spores per ml.

All the flasks were stored at 25°C, during 310 hours (13 days) for the experiment with *P. expansum* and during 465 hours (24 days) for the experiment with *N. fischeri*. At regular time intervals, 25 ml samples of juice were withdrawn, centrifuged (15000 r.p.m., 15 min), filtered through a glass microfiber filter under vacuum and through a 0.45  $\mu$ m filter with a syringe, and both pH and %SS were measured. The filtered juices were frozen in liquid nitrogen and stored at -20°C until the NMR measurements. The preparation of samples for NMR consisted of adding D<sub>2</sub>O containing TSP and NaN<sub>3</sub>.

For additional information on the commercial juice, the composition shown on the package label (per 100 ml of juice) follows: 10 g sugars, 0.1 g proteins, traces of lipids and 30 mg vitamin C (ascorbic acid).

### VI.2.2. Soluble Solids, pH and Enzymatic Determinations

The soluble solids (%SS) were measured by refractometry, using an Atago hand refractometer (accuracy  $\pm$ 0.2%) and the pH values were measured using a Hanna pH meter (precision  $\pm$ 0.01). Sucrose, glucose and fructose were quantified enzymatically for a selected set of samples (commercial juices only), using enzymatic tests purchased from Boehringer Mannheim (cat. no. 716260).

### VI.2.3. NMR Measurements

The NMR spectra of natural juices were recorded on a Bruker Avance DRX-600 spectrometer, operating at 599.87 MHz for proton and 150.85 MHz for carbon, while the spectra of commercial juices were recorded on a Bruker Avance DRX-500 spectrometer, operating at 500.13 MHz for proton and 125.77 MHz for carbon. Typically, each <sup>1</sup>H 1D

spectrum consisted of 64 scans of 65536 data points with a spectral width of 12019.23 Hz, an acquisition time of 2.73 s, and a relaxation delay of 7 s. A presaturation sequence was used to suppress the water signal by applying low-power selective irradiation at the water frequency during 3 s of the relaxation delay (pulse program 'zgcppr'). All the FIDs were Fourier transformed with 0.3 Hz line broadening, phased and baseline corrected using the Bruker XWIN-NMR software. TOCSY spectra were also recorded for a few samples to aid spectral assignment.

### **VI.3. Natural Mango Juice: Changes Upon Spoilage, Heat Treatment and Microbial Contamination**

#### **VI.3.1. Changes Assessed by Soluble Solids and pH**

The variations of soluble solids (%SS) and pH in natural mango juice submitted to different treatments and storage conditions are shown in Figures VI.1a and VI.1b, respectively. The %SS showed an increasing trend during storage of the non-treated juice and of the not inoculated heated juices. The increase from 14.1 to 15.8% noted by heating the juice may simply reflect some water evaporation. On the other hand, hardly any change is observed for the inoculated juices. The pH did not vary much in heated juices stored either at 25 or 4°C, but decreased for the juice naturally spoiled and for the juices inoculated with *P. expansum*. As it will be shown later, this decrease in pH should be related to the accumulation of several organic acids in the spoiled and contaminated juices.

Changes in the juice colour have also been registered: the colour of the non-treated juice was seen to change from yellow to light brown in the first 36 hours of storage and to darken until the end of the experiment time; moreover, from 36 hours onwards, the juice presented small particles in suspension; heat treatment was seen to cause a slight darkening of the yellow colour at the time of heating, but the heated juices did not subsequently change in appearance during storage; on the other hand, after 84 hours, the inoculated juices presented a lighter colour and a higher viscosity than the control juice stored in the same conditions, these changes being more marked in the juice of batch A, inoculated with higher spores concentration.

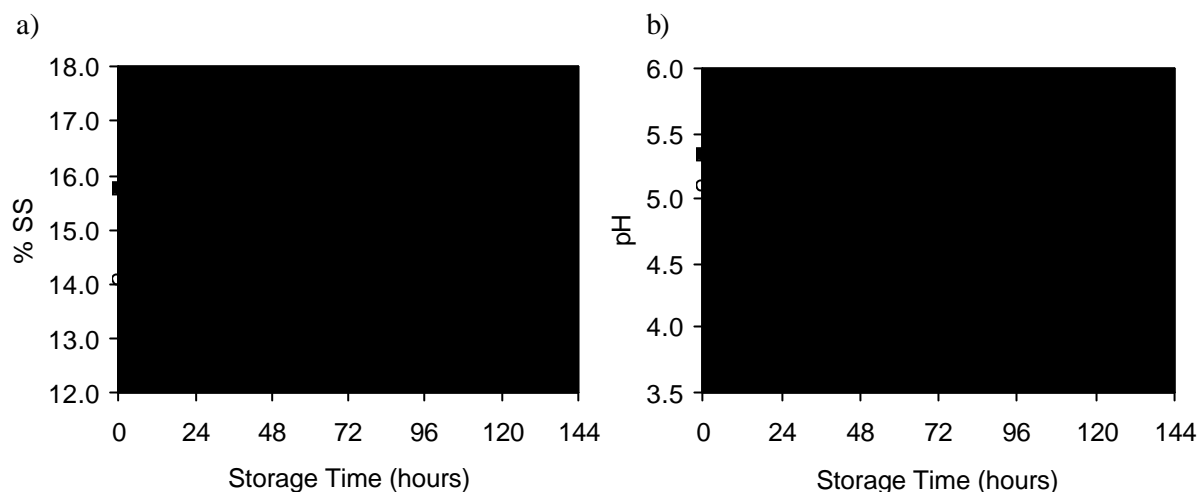


Figure VI.1. Variation of a) %SS and b) pH in natural mango juices submitted to different treatments/storage conditions: (○) non-treated juice stored at 25°C, (●) heated juice stored at 25°C, (□) heated juice stored at 4°C, (◇) batch A of heated and inoculated juice (spores cc. 2500/ml), stored at 25 °C and (△) batch B of heated and inoculated juice (spores cc. 250/ml), stored at 25 °C.

### VI.3.2. Changes Assessed by NMR Spectroscopy

#### VI.3.2.1. Effect of Natural Spoilage

Figures VI.2a, VI.5a and VI.6a show, respectively, the high-field, mid-field and low-field regions of the 1D spectra of the non-treated juices, freshly prepared (time 0), and after storage during 132 hours, the final time of the experiment. Many differences may be observed in the whole spectral range, reflecting drastic changes in the juice composition upon natural degradation. These changes may have many different sources, since many types of chemical, enzymatic and microbial processes are expected to occur, and, hence, the biochemical interpretation of the spectral changes is obviously very difficult due to the high complexity of the system and the great diversity of reactions and metabolic pathways present. Table VI.1 summarises the spectral changes observed within the period of the experiment and the time when they are first noted. Some of the signals that vary are still unassigned and, in cases for which the corresponding spin systems were identified in the TOCSY spectra, this is indicated on Table VI.1. The most significant variations are discussed in the following paragraphs. In the case of some major compounds, a semi-quantitative study has been carried out through integration of the 1D spectra. For a given signal, the areas measured at different storage times have been divided by the area measured in the time 0 spectrum, thus providing the magnitude of variation of that signal from time 0 to the end of the experiment.

Table VI.1. Changes in the <sup>1</sup>H NMR spectra of non-treated mango juice, after storage at 25°C during 132 hours; (\*) possibly 3,4,5-trihydroxycyclohexane carboxylic acid; <sup>(a)</sup> tentative identification; <sup>(b)</sup> additional information provided in Figure VI.5b; the values in square brackets correspond to other chemical shifts belonging to the same spin system.

Compound undergoing change	<sup>1</sup> H ppm (multiplicity)	Type of variation ?: increase ?: decrease	Time when variation is first noted
<b>High-field region (0-3 ppm)</b>			
Acetate	1.92 (s)	?	36 h
Acetoin	1.37 (d) 2.22 (s) 4.42	?	36 h
Alanine	1.47 (d) 3.79	?	36 h
Cyclic acid (*)	1.38 1.62 1.99 2.13 2.58 3.43 3.79 4.13	Appears	36 h
Isoleucine	0.93 (t) 1.00 (d)	?	36 h
Isopropanol / 2,3-butanediol	1.14 (d) 3.67	?	36 h
Lactic acid	1.32 (d) 4.12	?	36 h
Leucine	0.95 (t) 1.72	?	36 h
Quinic acid	1.87 1.95 2.06 3.55 4.02 4.14	?	36 h
Shikimic acid	2.19 2.77 3.70 3.98 4.40 6.45	?	36 h
Succinic acid	2.41 (s)	?	36 h
Valine	0.98 (d) 1.04 (d)	?	36 h
<i>Unassigned:</i>			
1	2.96 (s)	?	36 h
<b>Mid-field region (3-5.5 ppm)</b>			
Fructose	4.11	(b)	
Glucose	4.64, 5.23	(b)	
Sucrose	5.41	(b)	
<i>Unassigned:</i>			
1	4.90 ?3.95?	Appears	60 h
2	4.96 ?3.75 4.01?	Appears	60 h
3	5.37 ?3.59 3.77 4.02?	Appears	60 h
<b>Low-field region (5.5-10 ppm)</b>			
Acetaldehyde	9.67	Disappears	36 h
Adenine / Adenosine <sup>(a)</sup>	8.30 (s), 8.31 (s), 8.35 (s), 8.38 (s)	Disappear	36 h
Adenosine (ribose moiety) <sup>(a)</sup>	6.07 (d) ?4.43?	Disappears	36 h
Catechol <sup>(a)</sup>	6.86 6.94	Appears	60 h
Fumaric acid <sup>(a)</sup>	6.52 (s)	Disappears	36 h
Gallic acid <sup>(a)</sup>	7.04 (s)	Disappears	36 h
Nicotinamide	7.57 8.27 8.63 8.96	Disappears	36 h
NAD <sup>+</sup>	8.99 9.09 9.34	Appears	36 h
Shikimic acid	6.45	?	36 h
Tyrosine	6.89 (d) 7.19 (d)	Disappears	36 h
Uracil <sup>(a)</sup>	5.80 (d) 7.54 (d)	?	36 h
<i>Unassigned:</i>			
1	6.11 (d) ?3.77 4.35?	?	36 h
2	7.24 (s)	Disappears	36 h

In the high-field region (Figure VI.2a), prominent increases are detected for several signals, namely the doublet at 1.14 ppm (which shows a TOCSY correlation to 3.67 ppm, and may arise from isopropanol or from 2,3-butanediol), the lactic acid doublet (1.32 ppm), the singlet at 1.92 ppm assigned to acetate, the signals of acetoin (1.37 ppm doublet and 2.22 ppm singlet), and the singlet at 2.41 ppm attributed to succinic acid with basis on the shift of this peak with the variation in the sample's pH. Other compounds like pyruvic acid, diacetyl and oxaloacetic acid may also originate a singlet at about 2.4 ppm but show a lower sensitivity to pH changes, and thus the assignment to succinic acid is favoured. The quantitative variation of these compounds is shown in Figure VI.2b. The largest increase is registered for the signal at 1.14 ppm arising from isopropanol/2,3-butanediol (100 times/84 hours). Acetate increases 25 times/132 hours, while lactic acid, acetoin and succinic acid increase 18 times/84 hours, 10 times/84 hours and 6 times/84 hours, respectively.

All the compounds indicated above are typical products of different types of fermentation, possibly undergone by the microorganisms present in the juice. To illustrate this, Figure VI.3 shows the wealth of products that may result from the bacterial fermentation of glucose. The extension of each metabolic flux and the proportions of the products formed depend on the nature of the microorganisms present and on a number of factors such as aeration, pH, temperature and water activity. In the case of our experiment, the formation of acetoin, isopropanol/2,3-butanediol, acetate, lactic acid and succinic acid have been favoured, in detriment of other fermenting pathways like those producing ethanol. Indeed, the alcoholic fermentation that is typical of yeasts does not seem to be important here since ethanol is not accumulated in significant quantities (Figure VI.2b).

Other changes in the high-field region of the spectra (Figure VI.2a) regard the decrease of some amino acids, namely valine, leucine, isoleucine and alanine, and of the acids quinic and shikimic, which progressively decrease to residual amounts. Interestingly, the marked decrease of these organic acids is accompanied by the formation of a new compound, not present in the initial juice, which gives rise to the signals marked with arrows in Figure VI.2a. Besides this group of resonances (1.38, 1.62, 1.99, 2.13, 2.58 ppm), the spin system of the new compound includes signals at 3.43, 3.79 and 4.13 ppm, as shown by the TOCSY expansion in Figure VI.2c, where dashed lines highlight the identified correlations. The observed spin system is consistent with the structure shown in

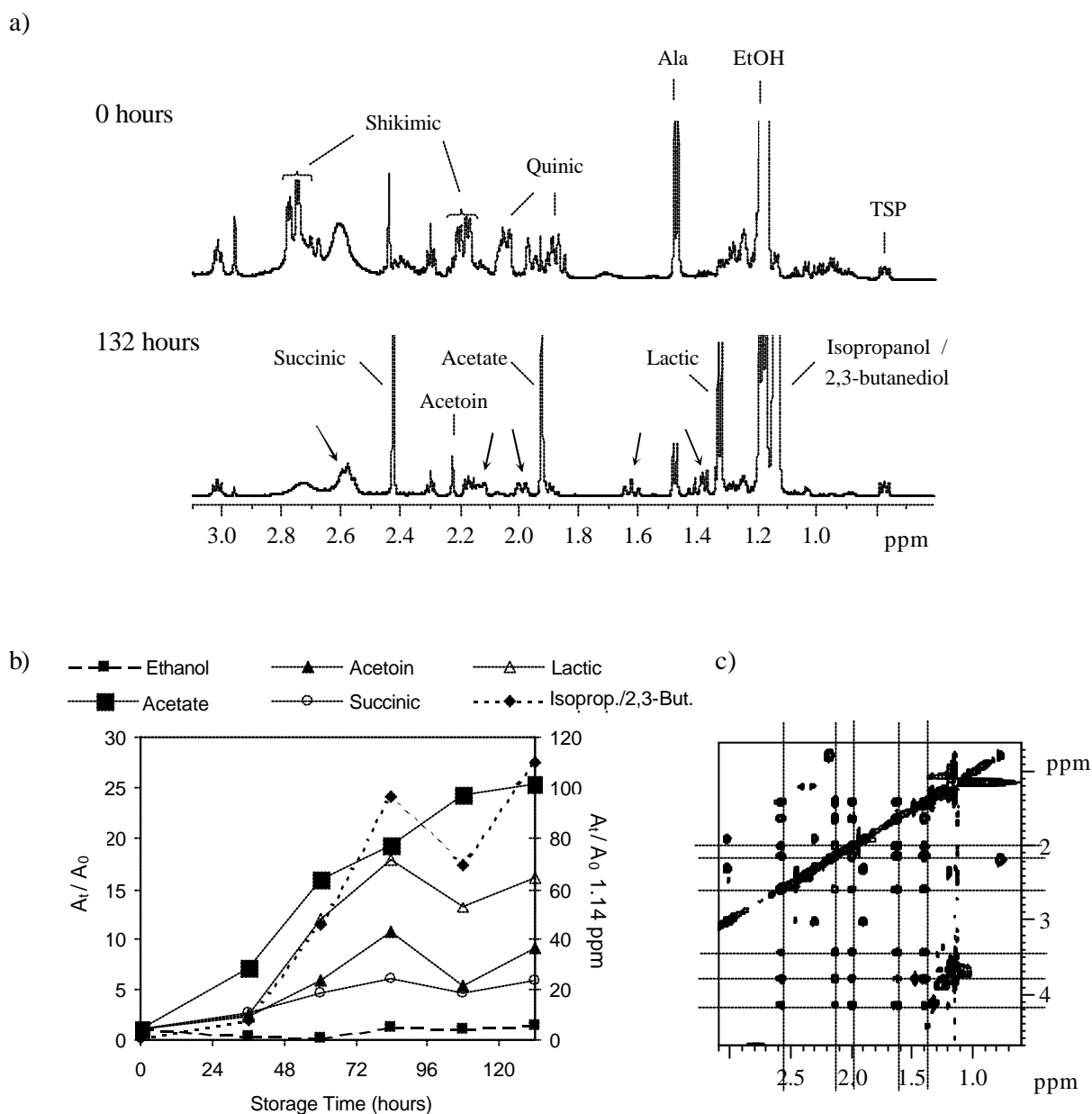


Figure VI.2. a) High-field region of the 600 MHz  $^1\text{H}$  NMR spectra of non-treated natural mango juice, freshly prepared (time 0) (top spectrum) and after storage during 132 hours (bottom spectrum), NS 64. The arrows indicate the signals of the new cyclic acid formed (see Figure VI.4); b) Relative variation of some compounds determined by integration of NMR signals ( $A_t$  = area at time t,  $A_0$  = area at time 0): ethanol-1.17 ppm, acetoin-2.22 ppm, lactic acid-1.32 ppm, acetate-1.92 ppm, succinic acid-2.41 ppm and isopropanol/2,3-butanediol-1.14 ppm; c) Expansion of the TOCSY spectrum of the non-treated juice stored for 132 hours, where the spin system of the new cyclic acid is highlighted by dashed lines.

Figure VI.4, corresponding to 3,4,5-trihydroxycyclohexane carboxylic acid (or to a similar structure substituted in the hydroxyl groups). The similarity of the proposed structure with the structures of quinic and shikimic acids (also shown in Figure VI.4) suggests that the variations of these compounds may indeed be correlated. However, the nature of the reactions occurring is, at this stage, not known. Specific enzymes (naturally present in the juice or carried by microorganisms) might be involved, since the conversion of either quinic or shikimic acids to the new cyclic acid is not expected to occur spontaneously. In addition, one may also speculate that quinic and shikimic acids may be inter-converted, with basis on the scheme shown in Figure VI.4, where several enzymes (identified in the enzymatic complex of plants, bacteria, fungi and yeasts) are involved (Dewick, 1998).

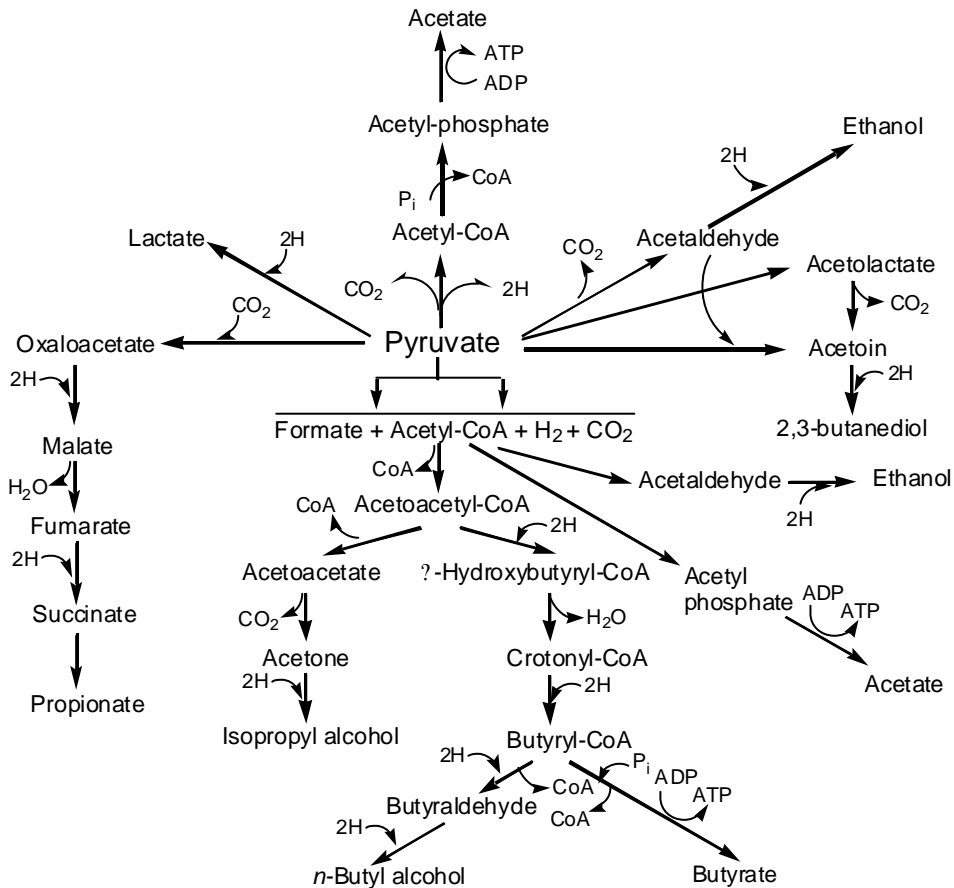


Figure VI.3. Diagram illustrating the major fates of pyruvate in various bacterial fermentations of glucose (Morris, 1985).

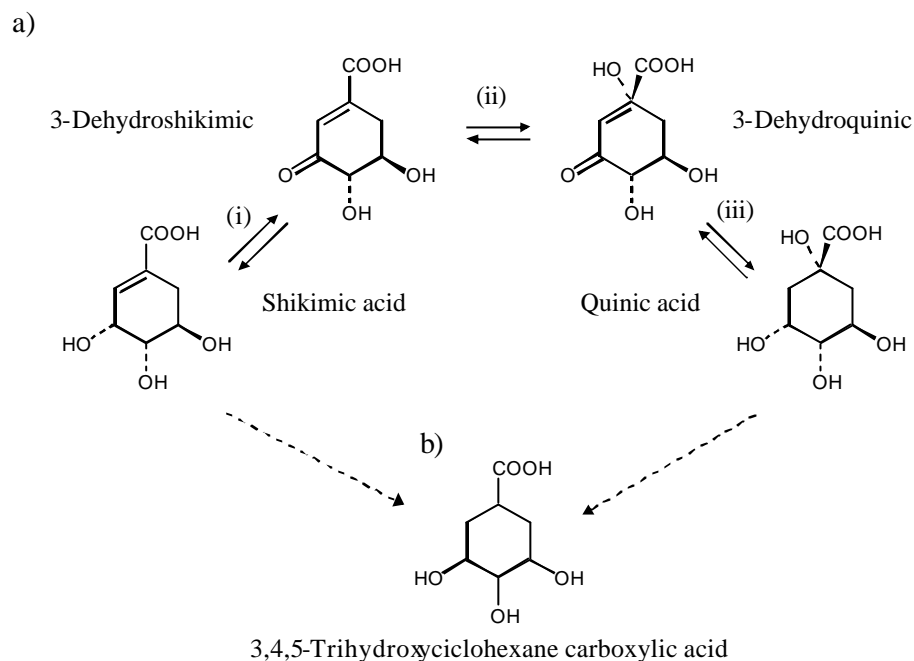


Figure VI.4. a) Scheme showing a possible pathway for the inter-conversion of quinic and shikimic acids (adapted from Dewick, 1998). The enzymes involved are: (i) shikimate dehydrogenase, (ii) 3-dehydroquininate synthase, (iii) quinate dehydrogenase; b) structure proposed for the new cyclic acid formed upon spoilage of natural mango juice (3,4,5-trihydroxycyclohexane carboxylic acid).

The mid-field regions of the spectra are shown in Figure VI.5a. Although no significant changes are seen in the profile of the major sugars, some quantitative variation is noted, as shown in Figure VI.5b. Relatively to the initial contents (0 hours), sucrose decreases while glucose and fructose increase. In order to better evaluate the real magnitude of these variations, the approximate absolute concentrations of each sugar expected to be present in the initial juice should be considered. These concentrations were not measured but may be estimated with basis on the values reported for ripe mango juice in Chapter IV.3.2.2: sucrose ~140 g/L, fructose ~45 g/L and glucose ~3 g/L. With basis on these values, the sugars variation upon spoilage may be represented in terms of approximate concentrations, as shown in Figure VI.5c. From 0 to 132 hours of storage, sucrose decreases ~45 g/L, while ~20 g of fructose and ~3 g of glucose are accumulated. These numbers suggest that sucrose is hydrolysed into fructose and glucose and that most glucose is metabolised, since only a small amount of this sugar is accumulated, resulting from the balance between its production (from sucrose hydrolysis) and its utilization. The glucose catabolism is likely to be related to the accumulation of the typical fermentation products identified in the aliphatic region of the juice spectra.

In addition to the major sugars variations, other changes detected in the same spectral region concern the appearance of signals at 4.90, 4.96 and 5.37 ppm, corresponding to the formation of new carbohydrates in the juices stored for more than 60 hours. Their corresponding spin systems are listed in Table VI.1. The broad nature of the new signals at 4.90 and 4.96 ppm (compounds 1 and 2 shown by the insert in Figure VI.5a) suggests that the carbohydrates formed consist of relatively large molecules.

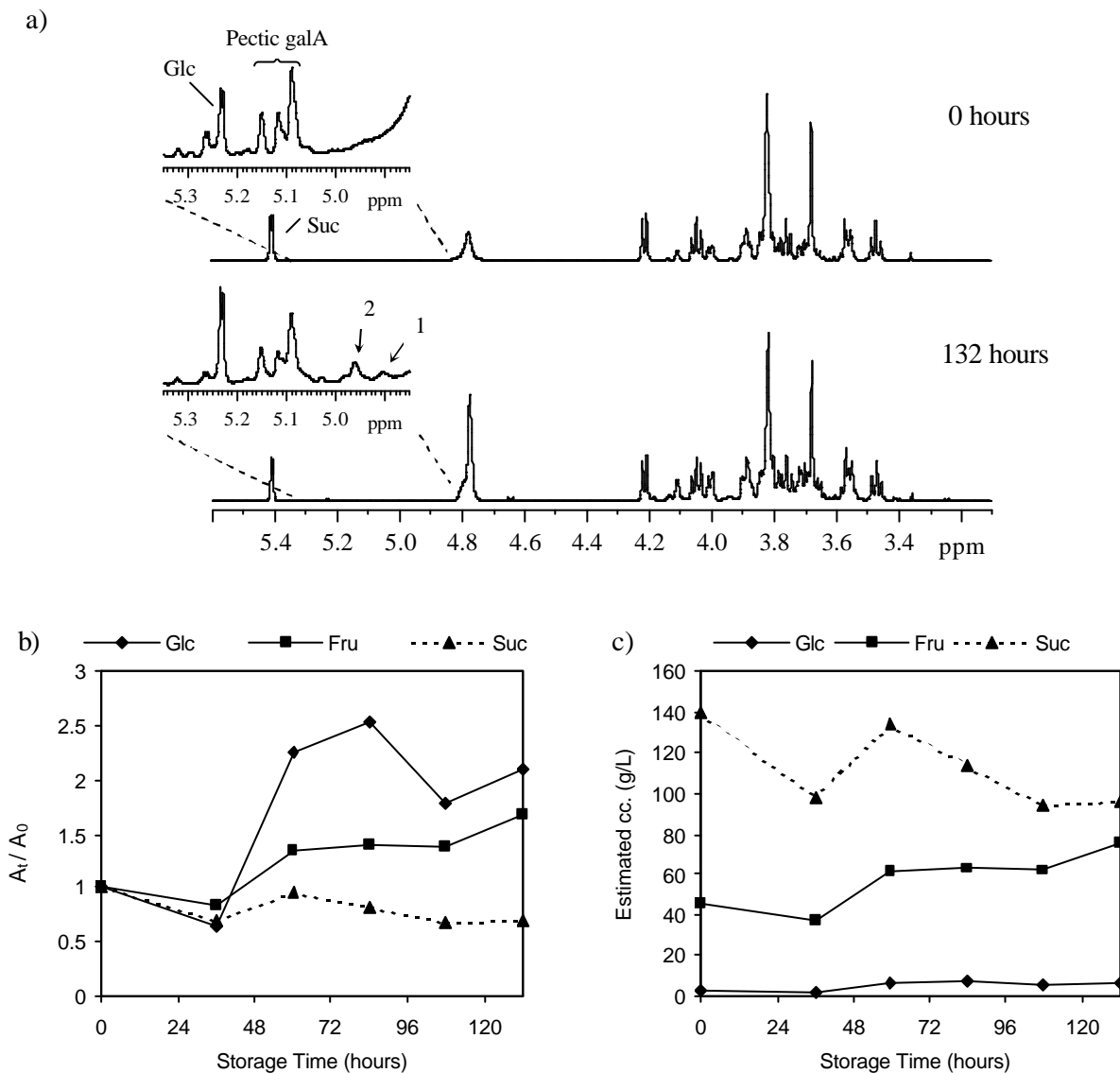


Figure VI.5. a) Mid-field region of the 600 MHz  $^1\text{H}$  NMR spectra of non-treated natural mango juice, freshly prepared (time 0) (top spectrum) and after storage during 132 hours (bottom spectrum), NS 64. The peak numbers correspond to unassigned carbohydrates listed in Table VI.1; b) Relative variation of sugars determined by integration of NMR signals ( $A_t$  = area at time  $t$ ,  $A_0$  = area at time 0): glucose-5.23 ppm, fructose-4.11 ppm and sucrose-5.41 ppm; c) Variation of sugars in terms of absolute concentrations, estimated with basis on the values expected to be present in ripe mango juice at time 0 (see text).

In the low-field region, there are many differences between the spectra of juices collected at different storage times, as summarised in Table VI.1 and illustrated in Figure VI.6a for the extreme times. Several signals are seen to decrease/disappear in the spectrum of the spoiled juice, while others are seen to increase/appear. The assignment of most signals is not straightforward either because they show no TOCSY correlations (e.g. singlets proposed to belong to fumaric and gallic acids) or because they may arise from molecules with similar structures. For instance, the singlets between 8.3 and 8.4 ppm, which are seen to disappear, may correspond to protons H2 and H8 of adenine or of an adenosine system, either free or as part of adenosine mono-, di-, or tri-phosphate molecules (Figure VI.6b), but a more certain assignment is not possible only with basis on the 1D and TOCSY spectra. The disappearance of these singlets is accompanied by the disappearance of the small doublet at 6.07 ppm (spin system 4.43, 6.07), which may arise from a ribose moiety of an adenosine system. Other interesting changes regard the disappearance of the spin system comprising the signals at 7.57, 8.27, 8.63 and 8.96 ppm, concomitantly with the appearance of the system 8.99, 9.09 and 9.34 ppm. The former may arise from nicotinamide, while the latter is assignable to NAD<sup>+</sup> (nicotinamide adenine dinucleotide) (structures shown in Figure VI.6b). Nicotinic acid (niacin), on the other hand, shows no significant variation. Additional changes in the aromatic region of the spectra consist of decreases in shikimic acid, already noted in the aliphatic region of the spectra, tyrosine, uracil and acetaldehyde signals. On the other hand, a significant increase is noted for the unassigned doublet at 6.11 ppm probably arising from a sugar moiety (compound 1 in Figure VI.6a), and for the multiplets at 6.86 and 6.94 ppm arising from an aromatic ring, possibly catechol.

Regarding the timing of the changes viewed by NMR, it is noted that most of them have been observed at 36 hours of storage. During that period, the juice also changed its colour and a small increase in the soluble solids content was already noticed. Therefore, in order to better evaluate the ability of high resolution NMR to detect indicators of natural spoilage earlier than simpler methods, collection and analysis of samples between 0 and 36 hours of storage would be required. However, these results have already been useful to demonstrate the complex amalgam of compositional changes that NMR is able to detect and identify.

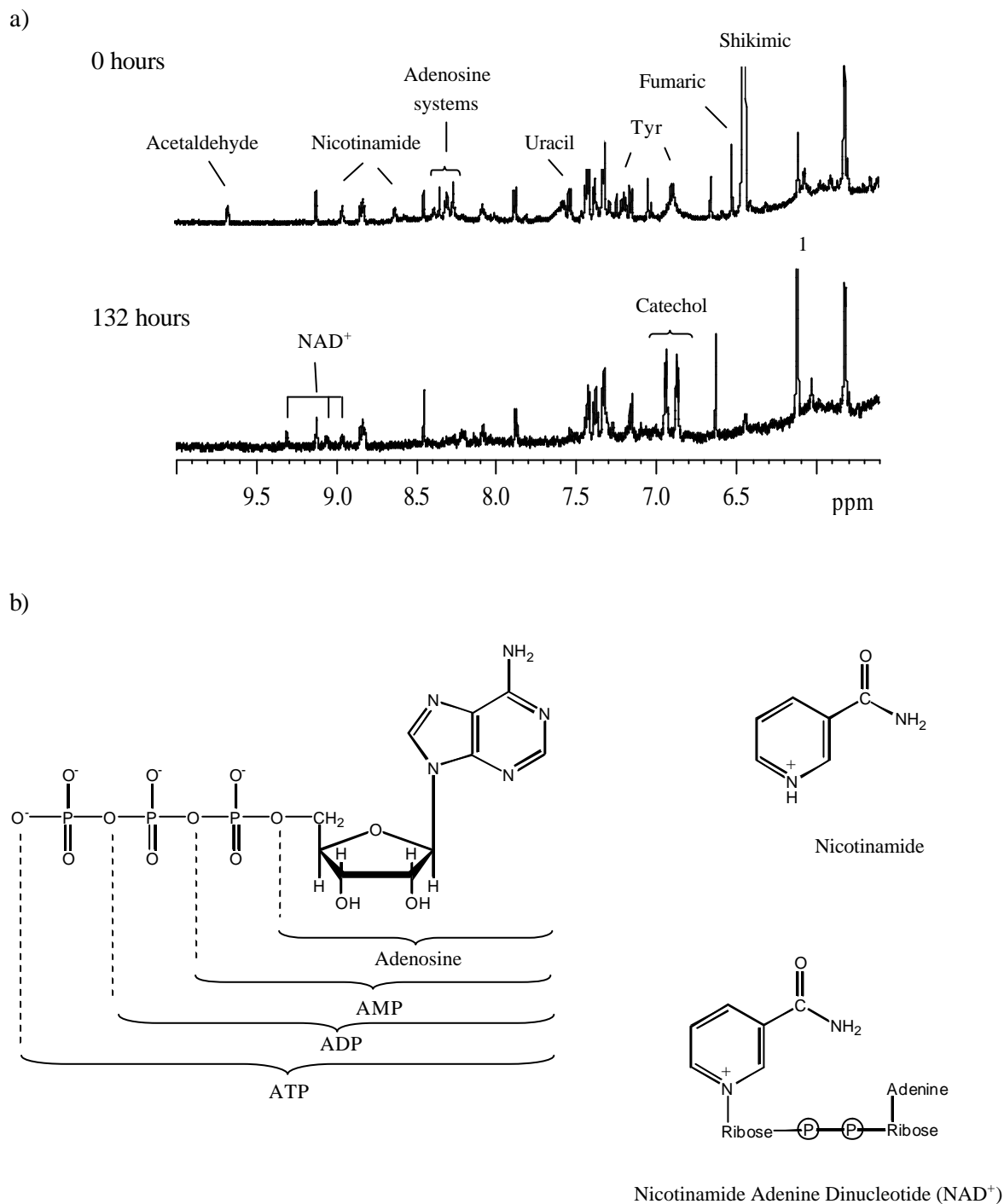


Figure VI.6. a) Low-field region of the 600 MHz  $^1\text{H}$  NMR spectra of non-treated natural mango juice, freshly prepared (time 0) (top spectrum) and after storage during 132 hours (bottom spectrum), NS 64. Peak no. 1 corresponds to an unassigned compound (?’s listed in Table VI.1); b) Structures of some compounds undergoing changes in the low-field region of the spectra.

### VI.3.2.2. Effect of Heat Treatment

The spectra of non-treated and heat-treated juices collected at time 0 are generally similar, showing that the heat treatment applied (80°C, 15 min) does not cause drastic changes in the juice composition. However, there are some differences to point out in the low-field region of the spectra, indicated with arrows in Figure VI.7. Acetaldehyde disappears (due to evaporation) and so do the signals tentatively assigned to uracil and to an adenosine system, and the unassigned signals at 6.11 (spin system 3.77, 4.35, 6.11 ppm) and 7.28 ppm. On the other hand, a uridine system is detected in the heat-treated juice.

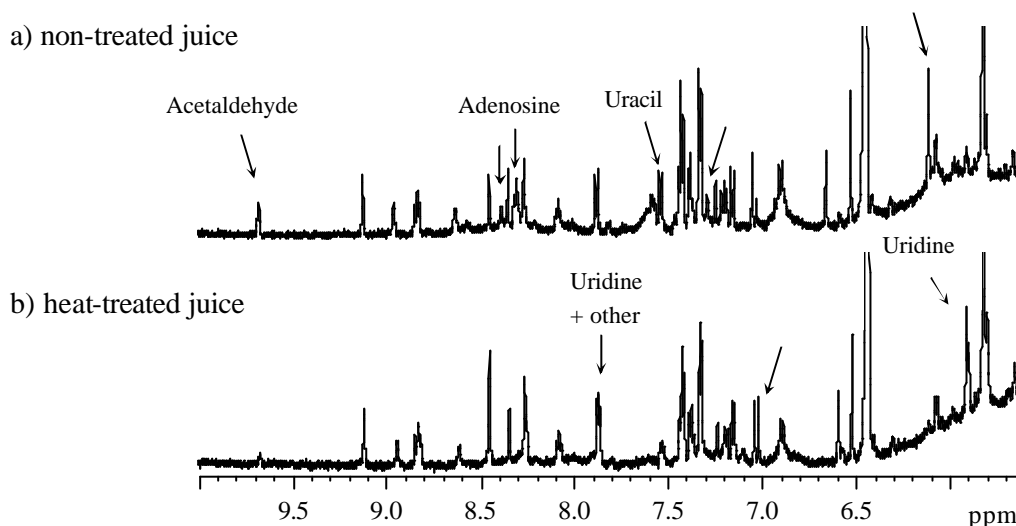


Figure VI.7. Low-field region of the 600 MHz  $^1\text{H}$  NMR spectra (NS 64) of a) non-treated natural mango juice and b) the same juice immediately after heat treatment (80°C, 15 min). The arrows indicate signals undergoing changes.

In what regards the changes in the composition of the heat-treated juice during storage at 25°C, only a few changes are noted, namely in the low-field region of the spectra (marked with arrows in Figure VI.8). In the juice stored at 25°C, tyrosine, the singlet at 7.04 ppm (possibly gallic acid), and the singlet at 7.24 ppm (unassigned) are seen to gradually decrease and disappear. In the juice stored at 4°C, tyrosine and the singlet at 7.24 ppm decrease at a lower rate than in the juice stored at 25°C, and are still detected at the final time of the experiment.

These results confirm the effectiveness of heat treatment in preserving the composition of the juice, especially if refrigerated storage is employed, since almost all the changes seen to occur throughout storage of the non-treated juice (described in the previous section) have been prevented in the heated juice. Therefore, since the heated juice practically doesn't change its composition over time, it may be taken as 'control' for evaluation of the changes caused by the presence of the mould *P. expansum* (inoculated after heat-treatment), discussed in the following section. Indeed, these changes can be assumed to be due specifically to the *P. expansum* growth, since the natural juice microflora has been eliminated by heating the juice prior to inoculation.

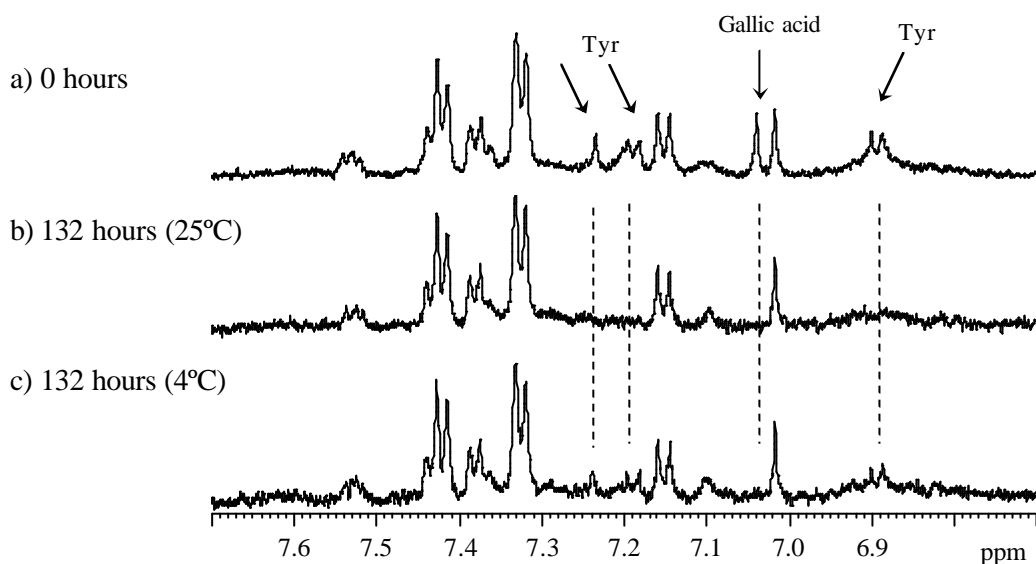


Figure VI.8. 600 MHz  $^1\text{H}$  NMR spectra (6.7-7.7 ppm region) of heat-treated natural mango juices collected at time 0 (a) and after 132 hours of storage at 25°C (b) and at 4°C (c); NS 64. The arrows indicate signals undergoing changes.

### VI.3.2.3. Effect of Inoculation with *Penicillium expansum*

The changes induced by *P. expansum* growth were followed by recording  $^1\text{H}$  NMR spectra of the juices collected at different times after inoculation, in order to find out which features may be pointed out as indicators of the natural juice contamination. The magnitude of variation of some major compounds has been determined by signal integration, as described in section VI.3.2.1.

Figures VI.9, VI.10 and VI.11 show, respectively, the high-field, mid-field and low-field regions of the 1D spectra of the control juice and of the juice inoculated with

2500 spores/ml (batch A), after 132 hours of storage. It is important to stress that the control juice showed only minor variations over time in the aromatic region of the spectra, as described in the previous section. The spectral variations in the contaminated juices are summarised in Table VI.2. The data shown refers to the juices of batch A, but it has been observed that the juices of batch B, inoculated with smaller spores concentration (250 spores/ml) show the same qualitative changes, occurring at a slower rate. In the following paragraphs, the most prominent changes observed in the different spectral regions are discussed sequentially.

In the high-field region (Figure VI.9a), the signals for which most significant increases are noted arise from isopropanol/2,3-butanediol, lactic acid, acetoin, acetate and succinic acid, similarly to the changes registered for natural spoilage (Figure VI.2a). However, the magnitude of these increases is now different, reflecting differences in the metabolic processes that lead to the formation of these products. The largest accumulations in the juices contaminated with *P. expansum* are observed for acetoin (120-160 times/84 hours), lactic acid (85-95 times/60 hours) and isopropanol/2,3-butanediol (50-75 times/132 hours), as shown graphically in Figure VI.9c, for both batches of inoculated juice. The effect of the higher spores concentration in the juice of batch A is reflected by the larger accumulation of the compounds mentioned above, except for lactic acid, which increases at approximately the same rate independently of the inoculum concentration.

On the other hand, citric and malic acids are seen to decrease and it is possible that their catabolism contributes to the aliphatic compounds accumulated. Concerning the utilization of citric acid, it is interesting to note the spectral variation shown in Figure VI.9b. From 0 to 36 hours, the broad resonances give place to the well-resolved signals of citric acid, which disappear afterwards. The broad nature of the signals in the first spectrum suggests hindered mobility of citric acid in the initial juice, which may be related to the formation of complexes. The next steps seem to consist of rendering the citric acid free and of its subsequent utilization. In addition to citric and malic acids, several amino acids, listed in Table VI.2, are seen to decrease. These compounds may be used as organic sources of nitrogen, which is required by the fungus to synthesize proteins to build protoplasm.

Table VI.2. Changes in the  $^1\text{H}$  NMR spectra of heat-treated mango juice, after inoculation with spores of *P. expansum* and storage at 25°C during 132 hours; (\*) variation specific of *P. expansum* growth (compared to natural spoilage); <sup>(a)</sup> tentative identification; <sup>(b)</sup> additional information provided in Figure VI.10b; the values in square brackets correspond to other chemical shifts belonging to the same spin system.

Compound undergoing change	$^1\text{H}$ ppm (multiplicity)	Type of variation ?: increase ?: decrease	Time when variation is first noted
<b>High-field region (0-3 ppm)</b>			
Acetate	1.92 (s)	?	36 h
Acetoin	1.37 (d) 2.22 (s) 4.42	?	36 h
Alanine	1.47 (d) 3.79	?	36 h
Isoleucine	0.93 (t) 1.00 (d)	?	36 h
Isopropanol / 2,3-Butanediol	1.14 (d) 3.67	?	36 h
Lactic acid	1.32 (d) 4.12	?	36 h
Leucine	0.95 (t) 1.72	?	36 h
Citric acid (*)	2.57 2.70	Disappears	60 h
Glu / Gln (*)	2.13 2.46 3.77	?	36 h
Malic acid (*)	2.38 2.68 4.29	?	36 h
Succinic acid	2.41 (s)	?	36 h
Valine	0.98 (d) 1.04 (d)	?	36 h
<i>Unassigned:</i>			
1 (*)	0.83 (d) 0.96	Appears	36 h
2 (*)	1.43 (d) 4.11	Appears	36 h
3 (*)	1.51 (s)	Appears	36 h
4	2.96 (s)	?	36 h
<b>Mid-field region (3-5.5 ppm)</b>			
Fructose	4.11	(b)	
Glucose	4.64, 5.23	(b)	
Sucrose	5.41	(b)	
<i>Unassigned:</i>			
1	4.91 ?3.71 3.95?	Appears	36 h
2	4.98 ?3.57 3.71 3.89?	Appears	36 h
3 (*)	5.11 ?3.41 3.54 3.77 3.89?	Appears	36 h
4	5.37 ?3.80 4.01?	Appears	36 h
<b>Low-field region (5.5-10 ppm)</b>			
Acetaldehyde	9.67	Disappears	36 h
Adenine / Adenosine <sup>(a)</sup>	8.26 (s), 8.35 (s)	Disappear	36 h
Adenosine (ribose moiety) <sup>(a)</sup>	6.07 (d) ?4.43?	Disappears	36 h
Fumaric acid <sup>(a)</sup>	6.52 (s)	Disappears	60 h
Gallic acid <sup>(a)</sup>	7.04 (s)	Disappears	36 h
Tyrosine	6.89 (d) 7.19 (d)	Disappears	36 h
Uridine	5.90 7.86 (d)	Disappears	36 h
<i>Unassigned:</i>			
1 (*)	5.79 ?3.71 4.26?	?	60 h
2	6.12 (d) ?3.73 4.35?	?	36 h
3	7.24 (s)	?	60 h

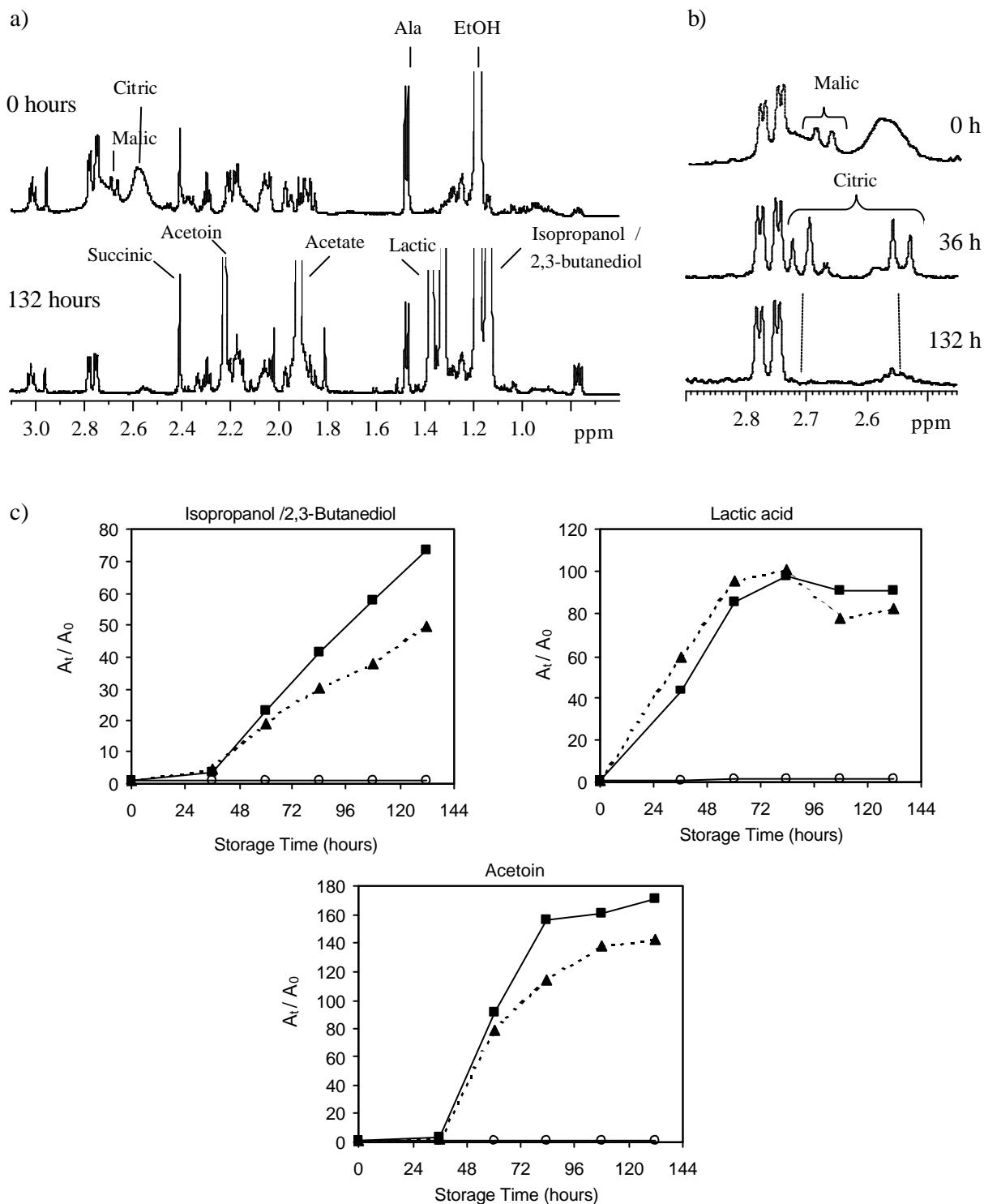


Figure VI.9. a) High-field region of the 600 MHz <sup>1</sup>H NMR spectra of heat-treated natural mango juice at time 0 (top spectrum) and of the juice inoculated with *P. expansum* after 132 hours of storage (bottom spectrum), NS 64; b) 2.45-2.90 ppm region of the spectra at time 0 (top), 36 hours (middle) and 132 hours (bottom); c) Relative variation of some compounds determined by integration of NMR signals ( $A_t$  = area at time t,  $A_0$  = area at time 0): isopropanol/2,3-butanediol-1.14 ppm, lactic acid-1.32 ppm and acetoin-2.22 ppm; (○) control juice, (△) inoculated juice (batch A), (□) inoculated juice (batch B).

The sugar profile of the juice contaminated with *P. expansum* is significantly different from that of the control juice, as shown in Figure VI.10a. The drastic decreases of glucose and sucrose largely contribute for this difference. The relative variations of these sugars and of fructose are shown in Figure VI.10b. The results indicate that sucrose is hydrolysed to glucose, which is rapidly consumed, and to fructose, which is seen to increase while the amounts of glucose available are still high. When the glucose levels become low, fructose also decreases, reflecting its utilization by *P. expansum*. These observations support the preferential utilization of glucose by the mould, which is in agreement with glucose being the substrate most commonly oxidized by fungi (Moore-Landecker, 1982). The inoculum concentration clearly influences the rate of glucose depletion, which is higher for larger concentration of spores (batch A). Besides the variations mentioned above, many other changes are noted in the anomeric region of the spectra, most of which are still unassigned (Table VI.2). Among the new signals detected, the broad signal at 4.98 ppm, possibly arising from a relatively large carbohydrate (compound 2) and the doublet at 5.11 ppm (compound 3) are the most intense, as shown by the insert in Figure VI.10a.

In the low-field region (Figure VI.11), the signals tentatively assigned to adenine/adenosine, fumaric and gallic acids, as well as the signals of uridine, tyrosine and acetaldehyde are seen to disappear. On the other hand, the unassigned signals at 5.79 ppm (compound 1) and at 6.12 ppm (compound 2) register clear increases. Some of these changes, namely the disappearance of gallic acid and tyrosine, are likely to be unrelated to the *P. expansum* contamination since they also occur in the control juice. The remaining of the changes noted above were also noted in the naturally spoiled juice, except for the increase of compound 1, which seems to be a specific indicator of *P. expansum* growth.

In summary, it is noted that, although most changes caused by the *P. expansum* growth are common to those registered for the juices subject to natural spoilage (section VI.3.2.1), there are some variations exclusively detected in the juice contaminated with *P. expansum*, thus being potential indicators of the presence of this mould. These changes are marked with (\*) in Table VI.2 and include, among others, the use of citric and malic acids

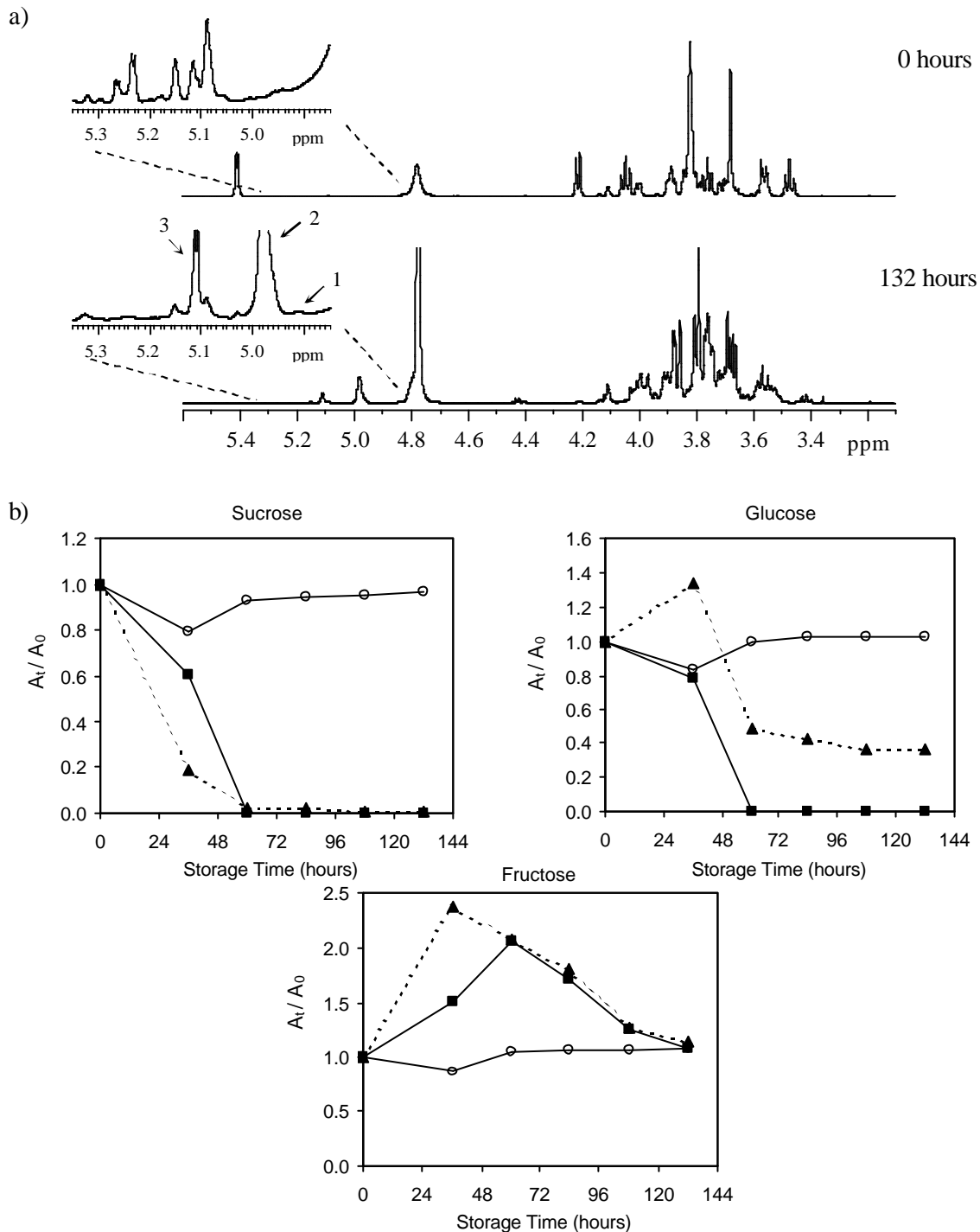


Figure VI.10. a) Mid-field region of the 600 MHz  $^1\text{H}$  NMR spectra of heat-treated natural mango juice at time 0 (top spectrum) and of the juice inoculated with *P. expansum* after 132 hours of storage (bottom spectrum), NS 64. The peak numbers correspond to unassigned carbohydrates listed in Table VI.2; b) Relative variation of sugars determined by integration of NMR signals ( $A_t$  = area at time  $t$ ,  $A_0$  = area at time 0): glucose-5.23 ppm, fructose-4.11 ppm and sucrose- 5.41 ppm. (○) control juice, (■) inoculated juice (batch A), (▲) inoculated juice (batch B).

and the increase of some new unidentified sugars (not detected in the initial juice). On the other hand, some alterations detected during natural spoilage did not occur in the juice contaminated with *P. expansum*. Some examples are the marked decreases of quinic and shikimic acids, probably related to the formation of a new cyclic acid (proposed to be 3,4,5-trihydroxycyclohexane carboxylic acid), and several changes in the low-field region. Those alterations reflect the action of the microorganisms and enzymes present in the non-treated juice, which were inactivated by the heat-treatment that preceded inoculation with *P. expansum*.

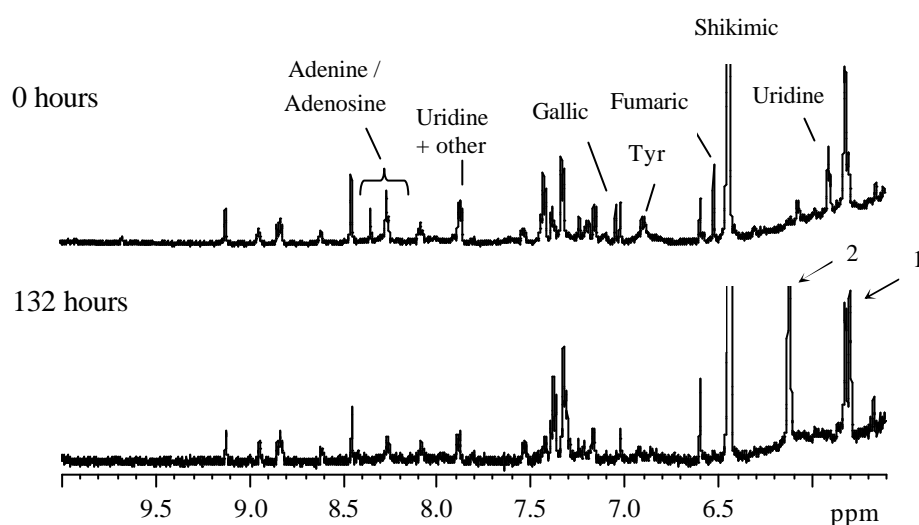


Figure VI.11. Low-field region of the 600 MHz  $^1\text{H}$  NMR spectra of heat-treated natural mango juice at time 0 (top spectrum) and of the juice inoculated with *P. expansum* after 132 hours of storage (bottom spectrum), NS 64. The peak numbers correspond to unassigned compounds listed in Table VI.2.

#### VI.4. Commercial Mango Juice: Changes Upon Microbial Contamination

It has been shown in the last sections that natural mango juice suffers significant changes in composition by the effect of microbial activity. The present sub-chapter is concerned with the susceptibility to microbial spoilage of a commercial mango juice. This study is important because contamination can also occur after the juice has been processed and, in addition, some microorganisms, like the mould *Neosartorya fischeri* used in this work, may survive the processing treatment commonly given to fruit products.

#### VI.4.1. Changes Assessed by Soluble Solids and pH

Both the control juice and the juice inoculated with *P. expansum* showed no significant variations of the soluble solids content, which was found to be in the range 11.7-12.3% until the end of the experiment (Figure VI.12a). The pH of the control juice was  $3.95 \pm 0.05$ , whereas for the inoculated juice a slight decreasing trend may be suggested, the final value being  $3.75 \pm 0.05$  (Figure VI.12b). It is also important to note that the inoculated juice started to show alterations in appearance after 72 hours. The colour developed from intense to light yellow, and at 120 hours the juice presented a modified aroma. After 144 hours, the juice showed solid aggregates in suspension and at the end of the experiment (310 hours), there was a dense fungal colony at the surface.

The %SS and the pH showed also no significant changes in the juice inoculated with *N. fischeri* (Figures VI.12c and VI.12d). Alterations in appearance were noted after 168 hours. The colour developed from intense to light yellow, and at 240 hours, the contaminated juice presented solid aggregates in suspension and a modified aroma.

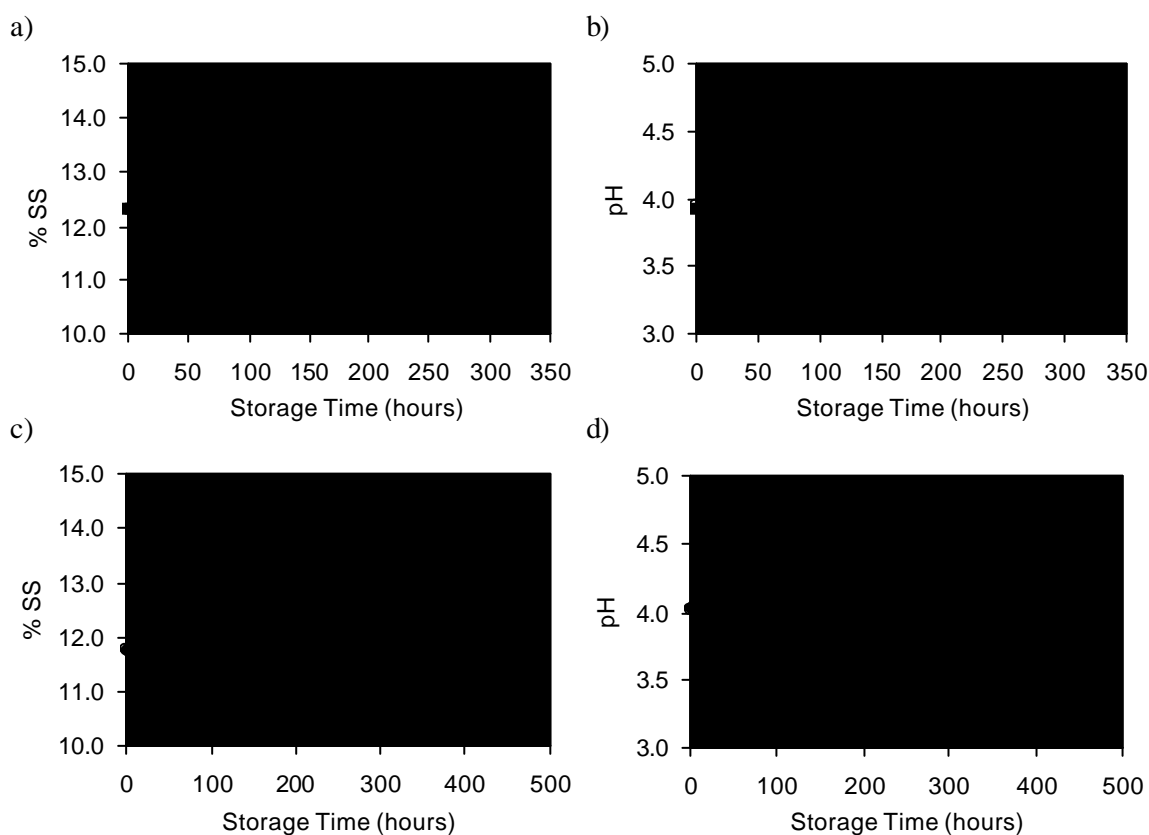


Figure VI.12. Variation of %SS (a and c) and pH (b and d) in commercial mango juices: (●) control juice, (○) juice inoculated with *P. expansum*, (□) juice inoculated with *N. fischeri*.

## VI.4.2. Changes Assessed by NMR Spectroscopy

### VI.4.2.1. Effect of Inoculation with *Penicillium expansum*

The  $^1\text{H}$  NMR spectra of commercial juice samples contaminated with *P. expansum* showed several changes during the storage period after inoculation, contrarily to the spectra of control juice (not inoculated and stored under the same conditions). Figures VI.13, VI.14 and VI.15 show, respectively, the high-field, mid-field and low-field regions of the spectra corresponding to the control juice and to the contaminated juice stored for 310 hours. The spectral differences detected within that period are summarised in Table VI.3, including the changes not yet assigned. The following paragraphs will address each spectral region separately.

In the high-field region (Figure VI.13a), the main variation is detected for ethanol, which increases significantly from 20 hours onwards (28 times/310 hours), as shown graphically in Figure VI.13b. This is accompanied by smaller increases of isopropanol / 2,3-butanediol (doublet at 1.14 ppm) and succinic acid (singlet at 2.61 ppm), illustrated in the same figure. Propionic acid (triplet at 1.05 ppm) is seen to appear and increase after 150 hours of storage. On the other hand, contrarily to what has been observed for the natural juice inoculated with *P. expansum*, the accumulations of other fermentation products like lactic acid, acetate and acetoin are not registered. Differences between the initial compositions and pH values of natural and commercial juices, as well as differences in the experimental setups employed may account for the different variations observed. For instance, the commercial juice was subject to more anaerobic conditions during storage than the natural juice (larger volume, less exposure to air), which is likely to influence the metabolism of the mould.

In what regards the compounds that are used up, some amino acids, namely alanine and GABA, are seen to decrease in the latter stages of the experiment. Moreover, fatty acids, which contribute with resonances at 0.88, 1.25-1.30 and 1.57 ppm in the spectrum of the initial juice, significantly decrease, possibly indicating their utilization by the fungus as carbon and energy sources. Interestingly, this decrease is accompanied by the increase in the signals of TSP, the reference that has been added to the juices. It is possible that, at the beginning of the experiment, TSP (namely the more hydrophobic part of the molecule, consisting of the  $\text{CH}_3$  groups attached to Si) is interacting with the lipid fraction of the

juice, originating broader and less intense signals; as the fatty acids are used, TSP is rendered free and gives rise to well-resolved signals.

Table VI.3. Changes in the  $^1\text{H}$  NMR spectra of commercial mango juice, after inoculation with spores of *P. expansum* and storage at 25°C during 310 hours; <sup>(a)</sup> tentative identification; <sup>(b)</sup> additional information provided in Figure VI.14b; the values in square brackets correspond to other chemical shifts belonging to the same spin system.

Compound undergoing change	$^1\text{H}$ ppm (multiplicity)	Type of variation ?: increase ?: decrease	Time when variation is first noted
<b>High-field region (0-3 ppm)</b>			
Alanine	1.47 (d) 3.79	?	198 h
Succinic acid	2.61 (s)	?	70 h
Propionic acid <sup>(a)</sup>	1.05 (t)	?	150 h
Fatty acids	0.88 1.25-1.30 1.57	?	44 h
GABA	1.90 2.40 (t) 3.01	?	198 h
Ethanol	1.18 (t) 3.65	?	44 h
Isopropanol / 2,3-Butanediol	1.14 (d)	?	70 h
<i>Unassigned:</i>			
1	1.31 (t)	?	150 h
2	1.49 (s)	Appears	310h
3	2.11 (s)	?	150 h
<b>Mid-field region (3-5.5 ppm)</b>			
Fructose	4.11	(b)	
Glucose	4.64, 5.23	(b)	
Sucrose	5.41	(b)	
<i>Unassigned:</i>			
1	4.18 ?3.83 4.07?	Appears	44 h
2	4.26 ?3.79 4.03?	Appears	44 h
3	4.91 ?3.71 3.93?	Appears	44 h
4	4.96 ?3.72 4.00?	Appears	44 h
5	5.42	Appears	44 h
<b>Low-field region (5.5-10 ppm)</b>			
<i>Unassigned:</i>			
1	5.85 ?3.80?	?	100 h
2	6.12 ?3.76?	Appears Disappears	44 h 198 h
3	6.40 6.85 7.35	Appears	44 h
4	6.56 7.03 7.62	Appears	44 h
5	7.13 (s)	?	70 h
6	7.18 (s)	?	70 h
7	7.26 (s)	?	100 h

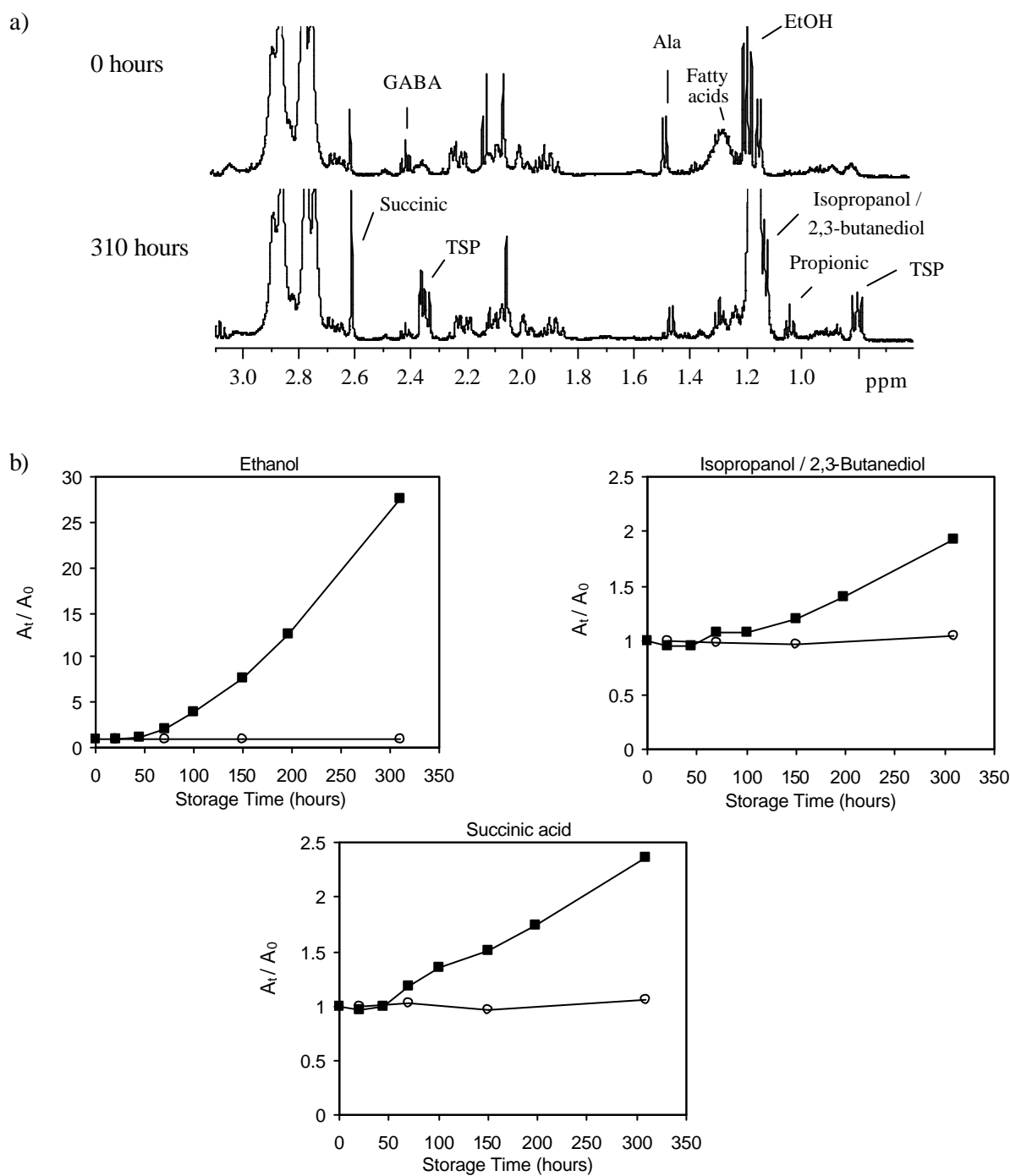


Figure VI.13. a) High-field region of the 500 MHz  $^1\text{H}$  NMR spectra of commercial mango juice at time 0 (top spectrum) and of the juice inoculated with *P. expansum* after 310 hours of storage (bottom spectrum), NS 64; b) Relative variation of some compounds determined by integration of NMR signals ( $A_t$  = area at time t,  $A_0$  = area at time 0): ethanol-1.17 ppm, isopropanol/2,3-butanediol-1.14 ppm, succinic acid-2.61 ppm. (■) control juice, (○) inoculated juice.

The sugar profiles of the spectra (Figure VI.14a) show drastic changes in the carbohydrate composition of the inoculated juice. The quantitative variations of the major sugars are shown in Figure VI.14b. In the case of sucrose and fructose, only the enzymatic results are presented because integration measurements in the 1D spectra are affected by large errors arising from strong signal overlapping. For glucose, the values measured by signal integration and by enzymatic tests agree, indicating a glucose increase of about 2.5-2.8 times/198 hours. The enzymatic determinations of the three sugars show that, from 0 to 198 hours of storage, sucrose decreases almost 55 g/L, while glucose suffers an increase of 22.6 g/L and fructose shows a small decrease (4.4 g/L). These results suggest that while the amount glucose resulting from sucrose hydrolysis remains in the juice, fructose is used by the mould more extensively than it is produced, thus showing an absolute decrease. The proposal that fructose is preferentially being utilized by *P. expansum* is, however, discrepant with the general observation that glucose is the substrate most commonly oxidized by fungi. Furthermore, these results are quite different from those registered for the natural juice contaminated with the same mould (Figure VI.10). It should be reminded that differences have also been noted concerning the aliphatic compounds formed, thus supporting the idea that the metabolism of *P. expansum* is significantly different in natural and commercial juices, under the experimental conditions employed. A more detailed discussion of this matter would require, however, further investigation.

Other spectral changes detected in the mid-field region of the spectra regard the appearance and increase of signals at 5.42, 4.26 and 4.18 ppm (overlapping with sucrose) and at 4.07 ppm (overlapping with fructose). These signals (numbered in Figure VI.14a and listed in Table VI.3) probably arise from new carbohydrates formed by the mould, but their identity could not be established at this stage.

In the low-field region, several variations are detected, involving the signals numbered in Figure VI.15, which arise from compounds not yet identified. Compound 1 (5.85 ppm) increases from 100 hours onwards, while compound 2 (6.12 ppm) appears at 44h, but then disappears again after 198 hours of storage; compounds 3 and 4 appear after 44 hours and show very weak signals until the end of storage; in addition, the singlets at 7.13, 7.18 and 7.26 ppm (peak numbers 5, 6 and 7 in Figure VI.15) vary in intensity. These unknown compounds may correspond to numerous aromatic species, synthesised by the

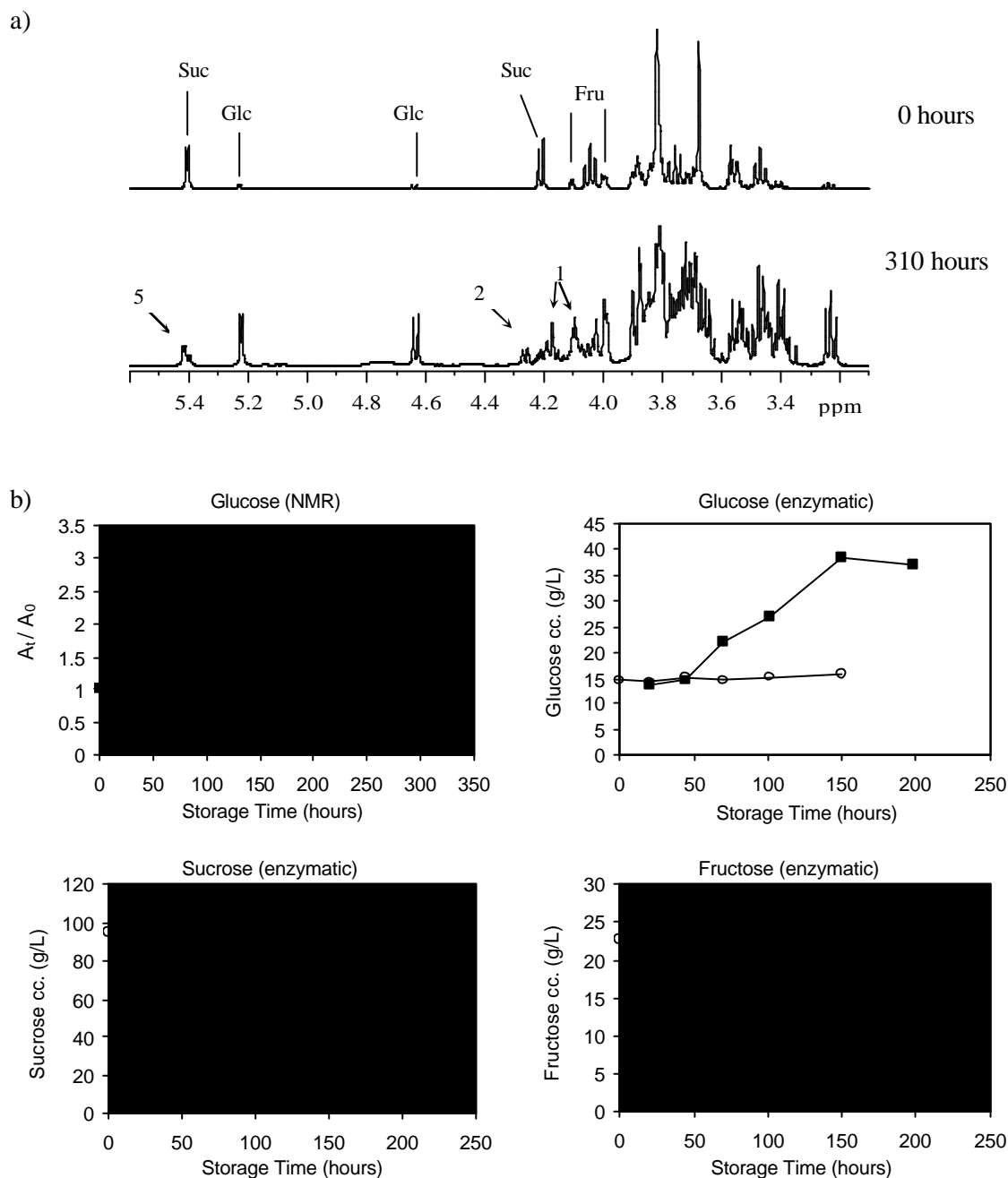


Figure VI.14. a) Mid-field region of the 500 MHz  $^1\text{H}$  NMR spectra of commercial mango juice at time 0 (top spectrum) and of the juice inoculated with *P. expansum* after 310 hours of storage (bottom spectrum), NS 64. The peak numbers correspond to unassigned compounds listed in Table VI.3 (peaks 3 and 4 are not visible in the expansion shown); b) Variation of sugars in not inoculated, commercial mango juice (?) and in juice inoculated with *P. expansum* (■), determined by integration of NMR signals ( $A_t$  = area at time t,  $A_0$  = area at time 0) and by enzymatic tests.

mould in very low amounts, and their identification by standard  $^1\text{H}$  NMR is obviously very difficult, calling for the use of improved analytical methods. In addition, it should be noted that these changes clearly differ from those detected for the natural juice contaminated with the same mould (Figure VI.11), similarly to what has been observed in the other spectral regions. The distinct aromatic compositions of natural and commercial juices (shown by comparing the top spectra in Figures VI.11 and VI.15) are likely to greatly account for that difference.

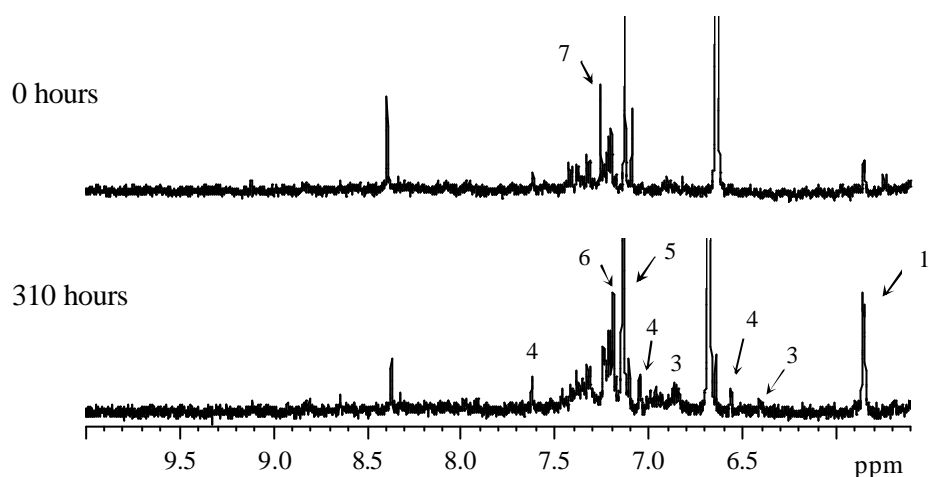


Figure VI.15. Low-field region of the 500 MHz  $^1\text{H}$  NMR spectra of commercial mango juice at time 0 (top spectrum) and of the juice inoculated with *P. expansum* after 310 hours of storage (bottom spectrum), NS 64. The peak numbers correspond to unassigned compounds listed in Table VI.3 (peak 2 is detected between 44 and 198 hours only, thus it is not seen in the spectra shown).

#### VI.4.2.2. Effect of Inoculation with *Neosartorya fischeri*

The heat-resistant mould *N. fischeri* has been inoculated into the commercial juice and the compositional changes followed by  $^1\text{H}$  NMR over a storage period of 465 hours. While the control juice spectra did not change within the time of the experiment, the spectra of the contaminated juices showed several variations with time, as illustrated in Figures VI.16 to VI.18 for the extreme times. Those variations are summarised in Table VI.4 and discussed in the following paragraphs for the different spectral regions.

In the high-field region (Figure VI.16), most signals show no pronounced variation. The most significant change, first noted at 128 hours, is the decrease of the signals of fatty acids, accompanied by the increase of the TSP signals, similarly to what was registered for the commercial juice inoculated with *P. expansum*. In addition, alanine and GABA show

slight decreasing trends from 226 hours onwards, while the signals of valine, leucine and isoleucine show increased intensities in the last spectrum recorded (465 hours), although no variations have been noted before that. Finally, it should be noted that the production of alcohols (ethanol, isopropanol/2,3-butanediol) and acids (propionic, succinic) seen to occur in the juice contaminated with *P. expansum* is not detected here, reflecting an important difference in the metabolism of the two moulds.

Table VI.4. Changes in the  $^1\text{H}$  NMR spectra of commercial mango juice, after inoculation with spores of *N. fischeri* and storage at 25°C during 465 hours; <sup>(a)</sup> tentative identification; <sup>(b)</sup> additional information provided in Figure VI.17b.

Compound undergoing change	$^1\text{H}$ ppm (multiplicity)	Type of variation ?: increase ?: decrease	Time when variation is first noted
<b>High-field region (0-3 ppm)</b>			
Alanine	1.47 (d) 3.79	?	226 h
Fatty acids	0.88 1.25-1.30 1.57	?	128 h
GABA	1.90 2.40 (t) 3.01	?	226 h
Valine	0.98 (d) 1.04 (d)	?	465 h
Leucine	0.95 (t) 1.72 (m)	?	465 h
Isoleucine	0.93 (t) 1.00 (d)	?	465 h
<i>Unassigned:</i>			
1	2.06 (s)	?	226 h
2	2.11 (s)	?	226 h
<b>Mid-field region (3-5.5 ppm)</b>			
Fructose	4.11	(b)	
Glucose	4.64, 5.23	(b)	
Sucrose	5.41	(b)	
<i>Unassigned:</i>			
1	4.91 ?3.70 3.99?	Appears	145 h
2	4.96 ?3.75 4.02?	Appears	145 h
3	4.98 ?3.75?	Appears	145 h
4	5.37	Appears	193 h
<b>Low-field region (5.5-10 ppm)</b>			
Tyrosine	6.89 (d) 7.19 (d)	?	273 h
<i>Unassigned:</i>			
1	6.12 ?3.79 4.35?	Appears	145 h
2	7.13 (s)	?	145 h
3	7.26 (s)	?	226 h
4	7.92 (s)	Appears	273 h
5	8.65 (s)	Appears	273 h

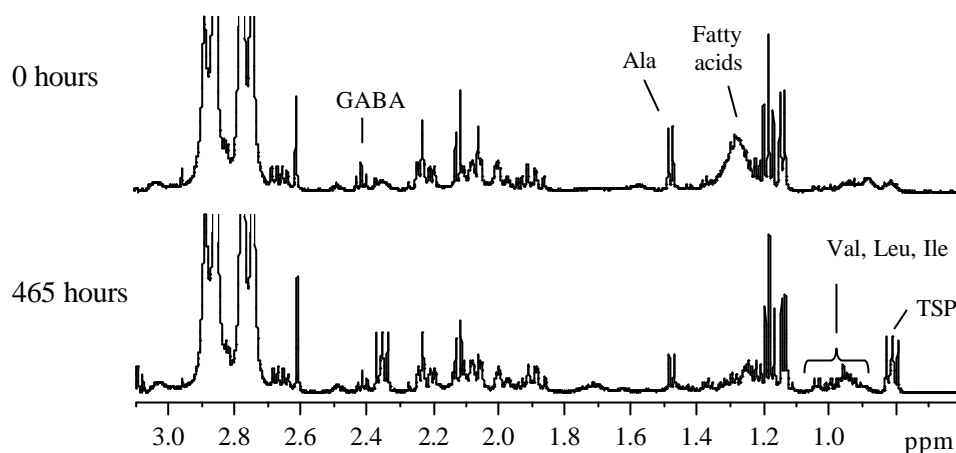


Figure VI.16. High-field region of the 500 MHz  $^1\text{H}$  NMR spectra of commercial mango juice at time 0 (top spectrum) and of the juice inoculated with *N. fischeri* after 465 hours of storage (bottom spectrum), NS 64.

In the mid-field region (Figure VI.17a), it is clear that while the juice spectrum corresponding to time 0 is dominated by sucrose, the spectrum of contaminated juice stored for 465 hours is dominated by glucose and fructose. The variation of these sugars with time is shown in Figure VI.17b. The results obtained by integration of the NMR signals agree with those obtained by enzymatic assays and suggest that sucrose starts being hydrolysed into glucose and fructose after 226 hours of storage. Both monosaccharides are accumulated and there is no evidence of their use by the microorganism, thus suggesting that the growth of *N. fischeri* was still at an early stage at the end of the storage period studied. Further changes detected in this region regard the appearance of new weak signals (listed in Table VI.4) arising from unidentified carbohydrates.

In the low-field region (Figure VI.18), the most prominent change concerns the signal at 6.11 ppm (peak 1), which appears in the spectrum recorded for 128 hours and increases from that time onwards. This variation is distinct from that observed in the juice contaminated with *P. expansum*. Other important changes are the increase of the singlet at 7.13 ppm (peak 2), which is one of the first alterations to be noted in the whole spectral range, and the disappearance of the unassigned singlet at 7.26 ppm (peak 3). There is still to point out the appearance of weak signals at 7.92 and 8.65 ppm (peaks 4 and 5, respectively) and the increase of tyrosine, changes that did not occur in the juice inoculated with *P. expansum*. Again, further interpretation of these changes is hindered by the unknown identity of the compounds giving rise to them.

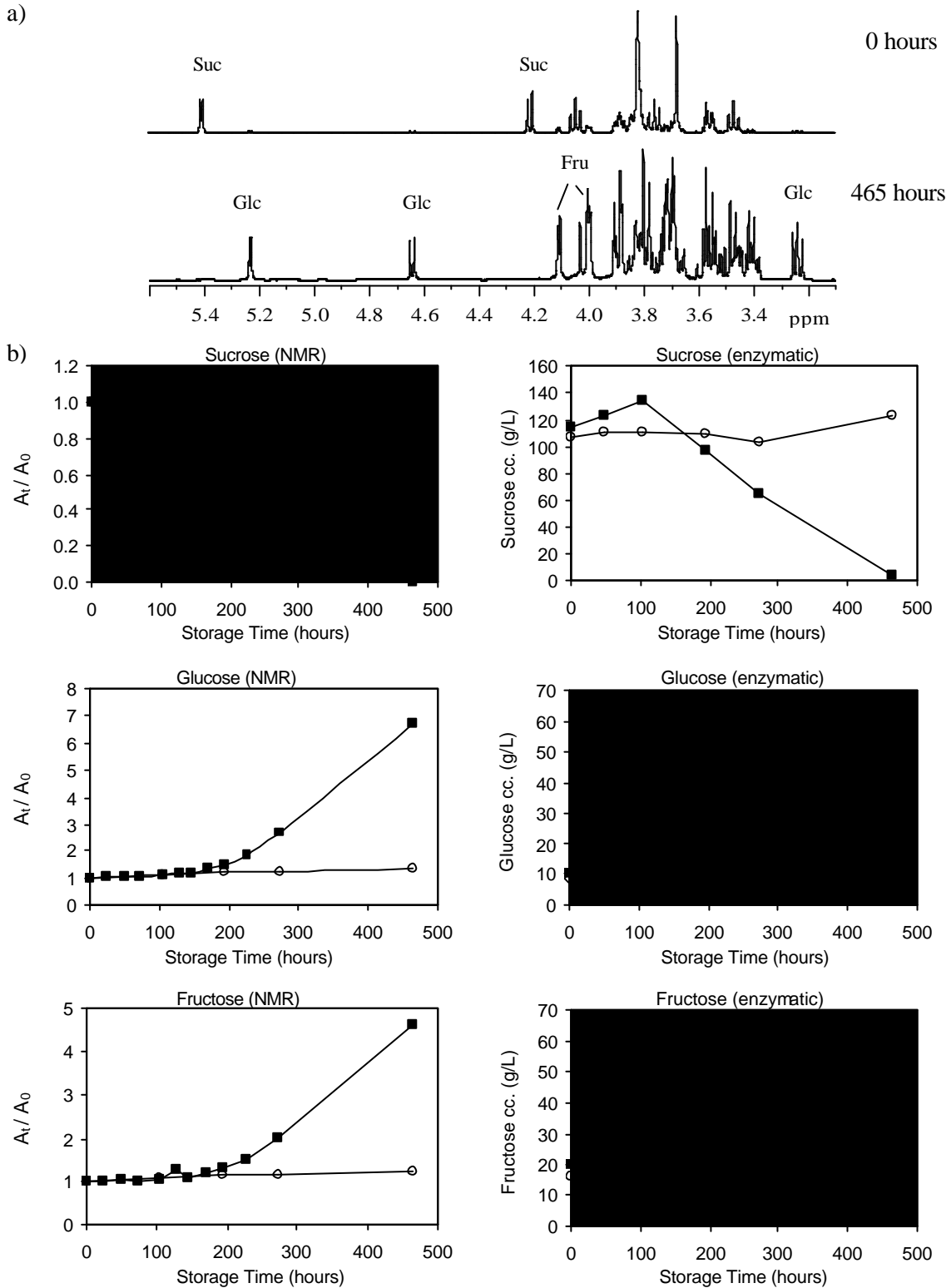


Figure VI.17. a) Mid-field region of the 500 MHz  $^1\text{H}$  NMR spectra of commercial mango juice at time 0 (top spectrum) and of the juice inoculated with *N. fischeri* after 465 hours of storage (bottom spectrum), NS 64; b) Variation of sugars in not inoculated commercial mango juice (?) and in juice inoculated with *N. fischeri* (◻), determined by integration of NMR signals ( $A_t$  = area at time t,  $A_0$  = area at time 0) and by enzymatic tests.

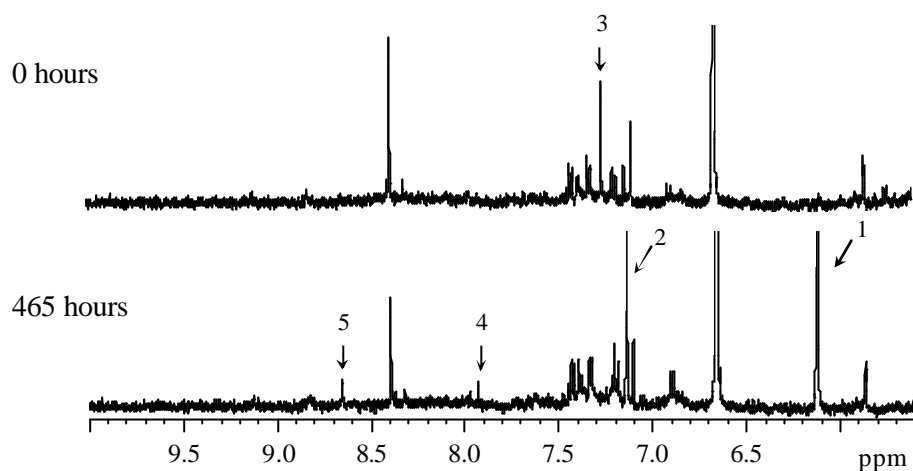


Figure VI.18. Low-field region of the 500 MHz  $^1\text{H}$  NMR spectra of commercial mango juice at time 0 (top spectrum) and of the juice inoculated with *N. fischeri* after 465 hours of storage (bottom spectrum), NS 64. The peak numbers correspond to unassigned compounds listed in Table VI.4.

## VI.5. Conclusions

High resolution  $^1\text{H}$  NMR has been used for detecting compositional changes in mango juices subject to different treatments and microbial contaminations, and has enabled the simultaneous screening of a wide range of compounds, including their quantitative variation through time.

In the case of the natural juice prepared from fresh mangoes and stored at 25°C without any treatment, the components that have been found to decrease were mainly organic acids (e.g. quinic, shikimic and fumaric) and amino acids (e.g. alanine and tyrosine). The decreases of shikimic and quinic acids were suggested to be related to the formation of a new compound in the spoiled juice, proposed to be 3,4,5-trihydroxycyclohexane carboxylic acid. In what regards the main sugars, sucrose showed a decrease, possibly reflecting its partial hydrolysis into fructose and glucose, which were accumulated in the spoiled juice. The amount of glucose accumulated, however, was much smaller than the expected to result from sucrose hydrolysis, indicating the utilization of this sugar. Indeed, the glucose catabolism is consistent with the increases found for typical fermentation products, namely acetate, lactic acid, acetoin, isopropanol/2,3-butanediol and succinic acid. The spoiled juice was also characterised by the presence of relatively large carbohydrates, suggested with basis on the appearance and increase of broad signals in the

4.9-5.0 ppm region, with spin systems characteristic of sugars. Finally, the aromatic region of the spectra showed changes involving adenosine and nicotinamide systems, which may be related to variations in the levels of ADP/ATP and NAD<sup>+</sup>.

Heat treatment of the natural juice (80°C, 15 min) was seen to cause some compositional changes detected in the low-field region of the spectra. After heat-treatment, the juice preserved its general composition throughout storage and only slight changes concerning a few aromatic compounds were noted. On the other hand, the heat-treated juice inoculated with spores of *Penicillium expansum* showed several changes over time. The compounds catabolised by the mould included organic acids such as citric and malic acids, amino acids (e.g. alanine, tyrosine, glutamic acid/glutamine), the three major sugars (especially glucose), and others like uridine- and adenosine-containing compounds. On the other hand, the main metabolic products were acetate, lactic acid, acetoin, isopropanol/2,3-butanediol, succinic acid and some unassigned sugars possibly including oligosaccharides. Many of these changes are common to those detected in the naturally spoiled juice but occur at different rates, while others have only been detected in the juice contaminated with *P. expansum* (e.g. decrease of citric and malic acids, increase of some unidentified carbohydrates). It should also be noted that most changes were detected by NMR at 36 hours of storage, whereas soluble solids and pH showed negligible variations in that period, and the colour of the juice only started to change after 84 hours.

The susceptibility of a commercial mango juice to the contamination with *P. expansum* has been evaluated and the results were significantly different from those obtained for the natural juice. The different composition of the juices, their different pH values and the distinct experimental setups employed are expected to contribute to this fact. Ethanol was one of the main metabolic products, while the accumulations of lactic acid, acetate and acetoin were not observed. In what regards the main sugars, the hydrolysis of sucrose and the utilization of fructose, rather than of glucose, were suggested. In addition, fatty acids were consumed and several unassigned changes were detected in the aromatic region of the spectra. The time when some of the spectral changes were first noted has been at 44 hours of storage, much earlier than changes in appearance (noticed after 72 hours) or in pH (slight decreasing trend after 98 hours) were observed.

Finally, in what concerns the effects of the heat-resistant mould *Neosartorya fischeri* on the composition of the commercial mango juice, less significant alterations

were found within the time of the experiment, reflecting the slower metabolism of this mould compared to *P. expansum*. In the aliphatic region of the spectra, the major change was the decrease of fatty acids. The sugar composition changed from the predominance of sucrose to the predominance of glucose and fructose, suggesting the occurrence of sucrose hydrolysis. The aromatic regions of the spectrum have also been found to change with *N. fischeri* growth, but most variations are still unassigned at this stage. Again, NMR enabled earlier detection of microbial contamination, since the first spectral change was noticed at 128 hours, whereas no significant changes in pH or %SS were registered and the changes in the juice appearance were visible after 168 hours only.

In summary, it can be concluded that, although many questions need to be further investigated, NMR is a powerful tool for monitoring the complex compositional changes of juices spoiled by microbial activity and other effects, being potentially useful for quality control purposes, for instance, in terms of detecting contamination at early times. In the future, this study would obviously benefit from a more complete assignment of the spectral changes, particularly in what regards carbohydrates and aromatic compounds, and from accurate absolute quantitative determinations.

## References

- Beuchat, L.R. Extraordinary heat resistance of *Talaromyces flavus* and *Neosartorya fischeri* ascospores in fruit products. *Journal of Food Science* **1986**, *51*, 1506-1510.
- Dewick, P.M. The biosynthesis of shikimate metabolites. *Natural Products Reports* **1998**, *15*, 17-58.
- Ejechi, B.O.; Souzey, J.A.; Akpomedaye, D.E. Microbial stability of mango (*Mangifera indica* L.) juice preserved by combined application of mild heat and extracts of two tropical species. *Journal of Food Protection* **1998**, *61*, 725-727.
- Frazier, W.C.; Westhoff, D.C. Contamination, preservations and spoilage of vegetables and fruits. In *Food Microbiology*; Frazier, W.C., Westhoff, D.C. Eds.; McGraw-Hill: Singapore, 1988; 196-217.
- Lin, H.H.; Lister, R.M.; Cousin, M.A. Enzymes-linked immunosorbent assay for detection of mold in tomato puree. *Journal of Food Science* **1986**, *51*, 180-192.

Littel, K.J.; LaRocco, K.A. ATP screening method for presumptive detection of microbiologically contaminated carbonated beverages. *Journal of Food Science* **1986**, *51*, 474-476.

Moore-Landecker, E. *Fundamentals of the Fungi*; Prentice-Hall: New Jersey, 1982.

Notermans, S.; Heuvelman, C.J.; Van Egmond, H.P.; Paulsch, W.E.; Besling, J.R. Detection of mold in food by enzyme-linked immunosorbent assay. *Journal of Food Protection* **1986**, *49*, 786-791.

Morris, J.G. Anaerobic Metabolism of Glucose. In *Comprehensive Biotechnology: The Principles, Applications and Regulations of Biotechnology in Industry, Agriculture and Medicine*; Moo-Young, M., Bull, A.T., Dalton, H., Eds.; Pergamon Press: 1985; 357-378.

Obeta, J.A.N.; Ugwuanyi, J.O. Heat-resistant fungi in Nigerian heat-processed fruit juices. *International Journal of Food Science and Technology* **1995**, *30*, 587-590.

Obeta, J.A.N.; Ugwuanyi, J.O. Shelf life study of some Nigerian fruit juices inoculated with ascospores of *Neosartorya* spp.. *Plant Foods for Human Nutrition* **1997**, *50*, 325-331.

Rajashekhara, E.; Suresh, E.R.; Ethiraj, S. Thermal death rate of ascospores of *Neosartorya fischeri* ATCC 200957 in the presence of organic acids and preservatives in fruit juices. *Journal of Food Protection* **1998**, *61*, 1358-1362.

Rajashekhara, E.; Suresh, E.R.; Ethiraj, S. Modulation of thermal resistance of ascospores of *Neosartorya fischeri* by acidulants and preservatives in mango and grape juice. *Food Microbiology* **2000**, *17*, 269-275.

Ramos, A.; Santos, H. NMR studies of wine chemistry and wine bacteria. In *Annual Reports on NMR Spectroscopy*; Webb, G.A. Ed.; Academic Press: London, 1999; 179-202.

Santos, H. NMR studies of lactic acid bacteria involved in wine fermentation. In *Magnetic Resonance in Food Science*; Belton, P.S., Delgadillo, I., Gil, A.M., Webb, G.A. Eds.; The Royal Society of Chemistry: Cambridge, 1995; 127-135.

Schaertel, B.J.; Tsang, N.; Firstenberg-Eden, R. Impedimetric detection of yeast and mold. *Food Microbiology* **1987**, *4*, 155-163.

Singhal, S.; Kulkarni, P.R.; Rege, D.V. Fruit and vegetable products. In *Handbook of Indices of Food Quality and Authenticity*; Singhal, S., Kulkarni, P.R., Rege, D.V. Eds.; Woodhead Publishing Limited: Cambridge, 1997; 79-130.

Splittstoesser, D.F. Microbiology of fruit products. In *Processing Fruits: Science and Technology*; Somogyi, L.P., Ramaswamy, H.S., Hui, Y.H., Eds.; Technomic: Basel, 1996; 261-292.

## **VII. APPLICATION OF HYPHENATED NMR (HPLC-NMR AND HPLC-NMR/MS) FOR THE DETECTION OF MINOR COMPONENTS IN FRUIT JUICES AND WINE**

VII.1. Introduction.....	186
VII.2. Materials and Methods.....	187
VII.2.1. Sample Preparation.....	187
VII.2.2. Instrumentation and Measurements.....	187
VII.3. Characterisation of Carbohydrates in Mango Juice.....	190
VII.3.1. Application to Fresh Mango Juices.....	190
VII.3.2. Application to Spoiled and Contaminated Mango Juices.....	196
VII.4. Characterisation of Aromatic Compounds in Grape Juice.....	200
VII.5. Characterisation of Aromatic Compounds in a Wine Phenolic Extract.....	212
VII.6. Conclusions.....	216
References.....	217

## VII.1. Introduction

Over the last years, HPLC-NMR and HPLC-NMR/MS have been established as standard analytical tools, especially in the area of pharmaceutical research (Lindon *et al.*, 2000). The numerous works reporting on the identification of endogenous and drug metabolites in biofluids (Schockor *et al.*, 1996; Sidemann *et al.*, 1997; Daykin *et al.*, 2001) and on the investigation of natural products (Bringman *et al.*, 1999; Hansen *et al.*, 1999) have demonstrated the outstanding advantages of these techniques for the analysis of complex mixtures, that may offset the high cost of the equipment and the relatively low sensitivity of NMR spectroscopy. These advantages may be summarised as the speed of analysis and the high structural information obtained concurrently as the chromatography proceeds, thus avoiding the need to obtain perfect chromatographic separations, which often requires a time-consuming and laborious process, and providing the possibility of detecting and identifying novel structures. In the area of food analysis, however, only a few applications have been reported. These include an example of on-flow HPLC-NMR of a wine concentrate, showing the potential interest of the method to study wine oligosaccharides (Spraul and Hoffman, 1995), the investigation of the detailed structures of hop and beer bitter acids by HPLC-NMR (Pusecker *et al.*, 1999), and the identification of several quercetin and phloretin glycosides differing in the state of glycosilation in an apple peel extract by HPLC-NMR/MS (Lommen *et al.*, 2000).

In this work, HPLC-NMR and HPLC-NMR/MS are applied to the investigation of minor components in different food samples, namely mango and grape juices and a wine phenolic extract. The mango juice analysis is focused on the characterisation of carbohydrates other than the main sugars commonly found in the juice (sucrose, glucose and fructose), which have been found difficult to characterise by NMR alone. In particular, a pectic fraction is separated and characterised for two ripening stages, with basis on the spectroscopic data obtained. Furthermore, the structural elucidation of the sugars formed during spoilage and microbial contamination of mango juice is attempted by using the HPLC-NMR method. In the case of the grape juice and of the wine extract samples, HPLC-NMR/MS analysis is carried out to characterise their aromatic composition, giving particular emphasis to the investigation of phenolic components. As previously described in Chapter I.2, grape juice and wine are usually rich sources of phenolic compounds, which, besides contributing significantly to the sensory qualities of these products, are

suspected to have important beneficial properties to human health (Bravo, 1998). There is extensive literature on the isolation and identification of the phenolic constituents of grape and wine, as briefly reviewed in Chapter I.2.2. Among the various methods available, HPLC-MS is regarded as one of the most valuable tools for polyphenols analysis. In this work, the potential usefulness of HPLC-NMR/MS is discussed.

## **VII.2. Materials and Methods**

### **VII.2.1. Sample Preparation**

The mango juices analysed by hyphenated NMR consisted of natural fresh juices and of spoiled/contaminated juices. The fresh samples were a ripe juice of the cultivar Tommy Atkins and two juices of the cultivar Haden at unripe and ripe stages. These samples have been prepared as described in Chapter IV.2.1 (batches 1 and 2, respectively) and kept frozen at  $-20^{\circ}\text{C}$  until analysis. The thawed samples were then directly injected onto the HPLC column for HPLC-NMR and HPLC-NMR/MS measurements. Some of the natural mango juices described in Chapter VI were also analysed by HPLC-NMR, namely the non-treated juices stored for 0 and 132 hours at  $25^{\circ}\text{C}$  and the juice inoculated with spores of *Penicillium expansum*, stored under the same conditions.

The grape juice sample was kindly provided by the University of Santa Catarina, Brazil, within a work collaboration. The pulp and seeds from red grapes (variety Isabel) were used to prepare the juice, which was then freeze-dried. Before analysis, 315 mg of sample were dissolved in 1.0 ml of distilled water.

The wine phenolic extract was also provided by the University of Santa Catarina, Brazil. The extract was prepared from red wine produced from grapes of the variety Bordo, by phase partitioning with ethyl acetate, followed by chromatographic separation using sequential elution with hexane, chloroform, ethyl acetate, methanol and water. The detailed extraction procedure is described by Maraschin *et al.* (2001).

### **VII.2.2. Instrumentation and Measurements**

1D and 2D NMR spectra of grape juice and wine extract samples were recorded on a Bruker Avance DRX-500 spectrometer, operating at 500.13 MHz for proton and 125.77 MHz for carbon. For acquiring the  $^1\text{H}$  1D spectra, a presaturation sequence was used to

suppress the water signal by applying low-power selective irradiation at the water frequency during the relaxation delay. Each  $^1\text{H}$  1D spectrum consisted of 512 scans of 16384 data points with a spectral width of 8012.82 Hz, an acquisition time of 1.02 s, and a relaxation delay of 7 s. The TOCSY spectra were acquired in the phase sensitive mode using time proportional phase incrementation (TPPI) and the MLEV17 pulse sequence. 32 transients were collected for each of the 400 increments, using a spectral width of 5482.46 Hz in both dimensions, 8192 data points, a mixing time of 100 ms and a relaxation delay of 1.5 seconds.

HPLC-NMR/(MS) experiments were performed using the following instrumentation: The HPLC system consisted of a HP 1100 solvent delivery pump with vacuum degasser (Agilent, Waldbronn, Germany), a manual injector from Rheodyne, Model 7725i (Cotati, CA, USA), equipped with a 1-ml sample loop, and a diode array detector from Bruker, Rheinstetten, Germany. HPLC-NMR measurements were carried out using a BPSU-36 interface coupled to a DRX-500 NMR spectrometer equipped with a  $^1\text{H}$ - $^{13}\text{C}$  inverse-detection flow probe (cell of 4 mm i.d. with a volume of 120  $\mu\text{l}$ ) from Bruker (Rheinstetten, Germany). The temporary sample storage unit (BPSU-36) was used for automated multiple NMR experiments overnight. For on-line MS detection, an ESQUIRE-3000 ion trap mass spectrometer, equipped with an electrospray ion source, from Bruker Daltonics (Bremen, Germany) was used. Five percent of the eluent was split into the MS using a splitter from LC Packings, San Francisco, CA, USA. Both UV as well as MS were used to trigger the transfer of the HPLC fractions to the BPSU (for temporary storage) or directly to the NMR.

For the study of mango juice carbohydrates, chromatographic separation was carried out at 35°C, using a 300 x 7.8 mm ION-300 column, containing a cation-exchange polymer in the hydrogen ionic form, with a particle size of 50  $\mu\text{m}$ . The mobile phase consisted of 0.0085N  $\text{H}_2\text{SO}_4$  in  $\text{D}_2\text{O}$ . Injection volumes of 50-100  $\mu\text{l}$  and flow rates of 0.15-0.30 ml/min were used. The diode array detector was operated at 200 and 220 nm, for detection of sugars and organic acids, respectively.

$^1\text{H}$  NMR spectra were obtained at 500 MHz using the continuous-flow and the loop-sampling methods. For continuous-flow experiments, successive NMR spectra were

acquired automatically, each spectrum comprising a total of 16 transients summed into 8192 data points with an acquisition time of 0.82 s and a spectral width of 5000 Hz. A pulse sequence with presaturation during relaxation delay (1.0 s) was used (program 'lc2pr' from the Bruker library). 1D  $^1\text{H}$  NMR spectra of loops were recorded by accumulating 64 transients with 16384 data points, a spectral width of 10000 Hz and an acquisition time of 0.82 s. The TOCSY spectra of loops consisted of 4096 data points with 24 transients per each of 128 increments acquired with a spectral width of 3000 Hz in both dimensions. The mixing time of the MLEV spin lock was 60 ms.

Electrospray ionisation (ESI) was carried out in positive mode and mass spectra were acquired up to  $m/z$  1500 after adding 50  $\mu\text{l}/\text{min}$  of 20 mM aqueous sodium acetate solution to the split ratio of the eluent via a T-piece with a syringe pump.

For the studies of aromatic compounds, chromatographic separation was carried out at 35°C, using a 250 x 4 mm Purospher reverse phase (RP18) column from Merck, with a particle size of 5.0  $\mu\text{m}$ . The mobile phase consisted of a mixture of  $\text{D}_2\text{O}$  (containing 0.06% formic acid) and acetonitrile, changing in composition according to the following gradient: 0 min - 3% acetonitrile, 40 min - 40 % acetonitrile, 60 min - 100 % acetonitrile, 70 min - 3% acetonitrile. Injection volumes were 20  $\mu\text{l}$  (in the case of the wine phenolic extract, due to the small volume available) and 500  $\mu\text{l}$  (for grape juice). The flow rate was typically 1.00 ml/min. The diode array detector was operated at 280 nm (for detection of catechins, proanthocyanidins and benzoic acids), 320 nm (for detection of hydroxycinnamic acids) and 365 nm (for detection of flavonols).

$^1\text{H}$  NMR spectra were obtained at 500 MHz using the continuous-flow mode for both grape juice and wine extract samples and also the loop-sampling method for the grape juice. In continuous-flow experiments, data were recorded with double solvent suppression of water and acetonitrile signals (pulse program 'lc1wetdw'). Each spectrum consisted of 16 transients of 8192 data points with a spectral width of 7002.8 Hz and an acquisition time of 0.6 s. 1D  $^1\text{H}$  NMR spectra of loops were recorded with 64 transients, 16384 data points, a spectral width of 10000 Hz and an acquisition time of 0.82 s.

ESI-MS experiments were carried out in positive and negative modes with a scan range from 100 to 1000  $m/z$ . For loop analysis, automatic switch between MS and MS/MS was performed in order to identify fragment ions.

### VII.3. Characterisation of Carbohydrates in Mango Juice

#### VII.3.1. Application to Fresh Mango Juices

The typical carbohydrate composition of mango juice viewed by NMR has been presented in Chapter III.3.1. Besides sucrose, glucose and fructose, identified as the major sugars, other resonances arising from less abundant carbohydrates have been detected, namely the signals at 5.0-5.4 ppm, expanded in Figure VII.1, showing very low intensity and poor resolution compared to the major sugars. Some of these signals are thought to arise from galacturonic acid units of pectin chains. In this Chapter, a more complete characterisation of these less abundant carbohydrates is attempted by combining the separation ability of liquid chromatography with NMR and mass spectrometry.

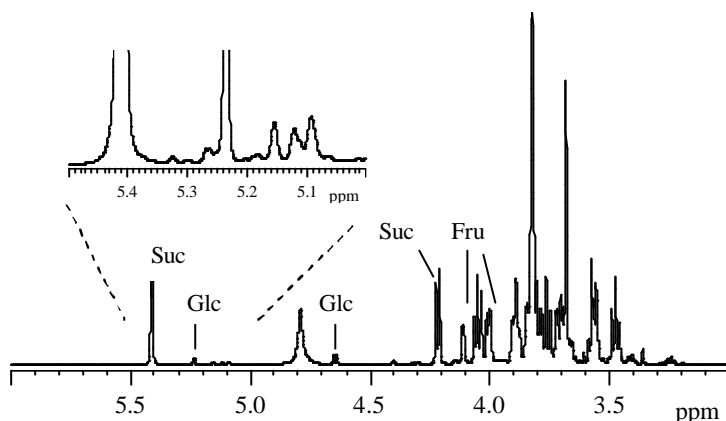


Figure VII.1. Mid-field region of the 600 MHz  $^1\text{H}$  NMR spectrum of mango juice; NS 64.

Figure VII.2 shows the continuous-flow NMR chromatogram obtained by the elution of ripe mango juice (cv. Tommy Atkins) in the ION-300 column, using the conditions described in section VII.2.2. The NMR chemical shifts are represented on the horizontal axis and the chromatographic retention times (RT) on the vertical axis; therefore, the rows of this type of diagram correspond to  $^1\text{H}$  NMR spectra of the fractions separated during chromatography. The vertical lines at about 4.7 and 2.0 ppm arise, respectively, from continuous flow of water and acetonitrile (residual amount existing on the system). Along the RT axis, the different rows reveal the separation of different sugars and organic acids present in mango juice. Figure VII.2b shows some of these rows and Figure VII.2c shows the MS spectra corresponding to rows 2 to 5, recorded during the continuous-flow experiment. Row 1 did not give a measurable MS spectrum.

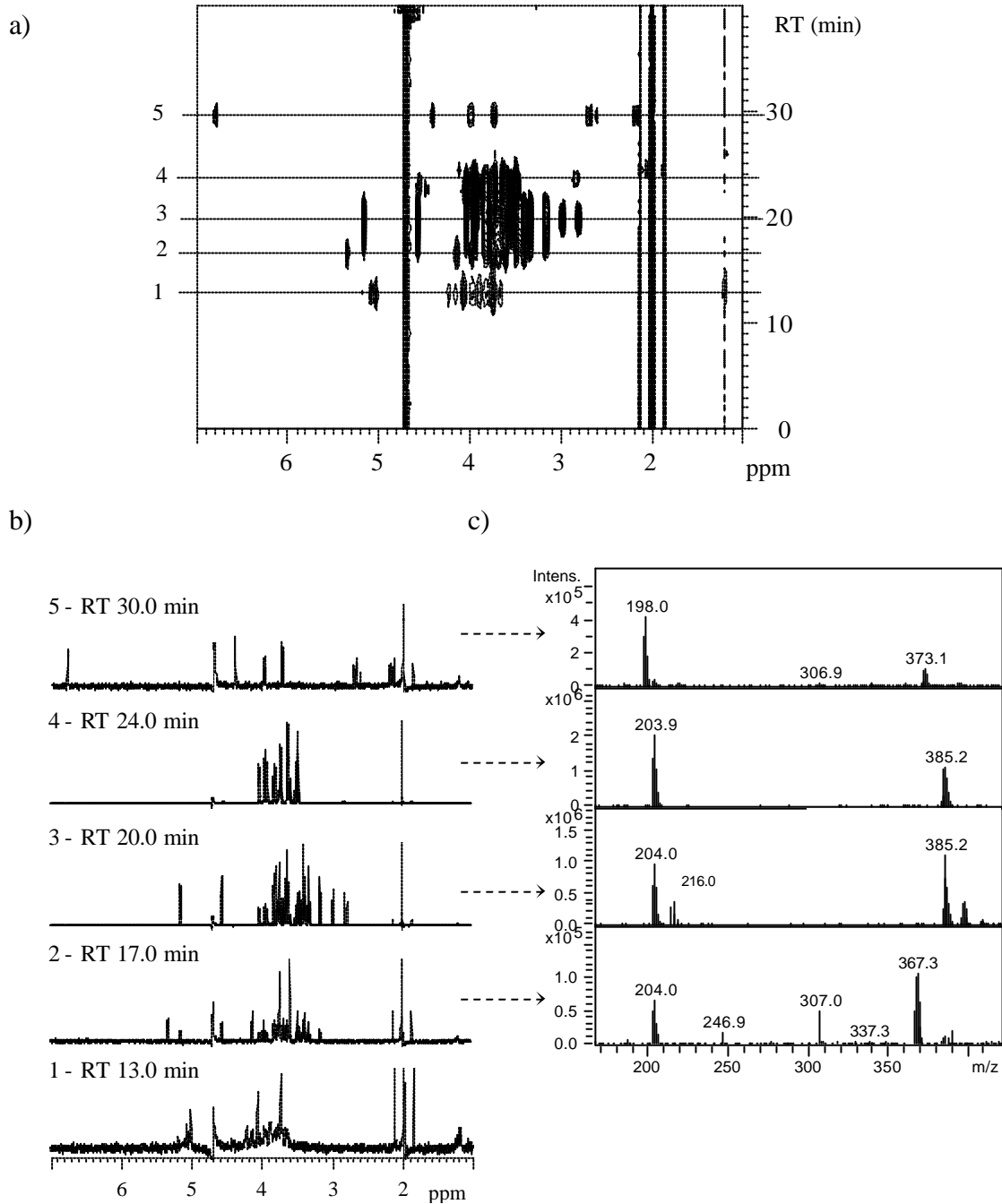


Figure VII.2. a) Continuous-flow NMR chromatogram resulting from the elution of mango juice on the column ION-300 (flow rate 0.3 ml/min); b) rows extracted from the NMR chromatogram; c) MS spectra acquired concurrently with the NMR data in positive-ionisation mode. Identification of compounds in spectra 1 to 5: 1 - pectic fraction (no MS ionisation), 2 - sucrose + glucose, 3 - glucose + fructose + citric acid, 4 - fructose + malic acid, and 5 - shikimic acid.

Between 15 and 30 minutes, the NMR chromatogram shows the elution of the major sugars and organic acids present in mango juice. Sucrose starts eluting at about 15.0 min and is immediately followed by glucose (spectrum 2), which later co-elutes with

fructose and citric acid (spectrum 3). Fructose and malic acid are eluted at 24.0 min (spectrum 4), followed by shikimic acid (spectrum 5). Although NMR data is sufficient for the unequivocal identification of these compounds, confirmation is provided by the corresponding MS spectra (Figure VII.2c). It must be noted that, since sodium acetate was added to the eluent fraction sent to the mass spectrometer, in order to facilitate ionisation, the  $m/z$  values detected are those due to  $M + Na^+$  ions. Moreover,  $M$  includes exchangeable hydrogen-to-deuterium substitutions, since  $D_2O$  was used for HPLC. The deuteration to different extents justifies the multiplet nature of the MS peaks observed for sugars and organic acids, which have several exchangeable protons in OH and COOH groups. Therefore, the MS data is interpreted as follows: at 17.0 min, the peaks at  $m/z$  204 and 367 correspond, respectively, to the molecular ions  $M + Na^+$  of glucose and sucrose; at 20.0 min, the peak at  $m/z$  385 indicates the formation of a noncovalent dimer of glucose and/or fructose  $M + (M + Na)^+$  and  $m/z$  216 corresponds to citric acid; at 24.0 min,  $m/z$  204 is detected again, but it now corresponds to fructose only, as shown by the NMR spectrum; finally, at 30.0 min, shikimic acid gives a peak at  $m/z$  198 and the noncovalent dimer  $M + (M + Na)^+$  is detected at  $m/z$  373.

The pectic fraction in which we are especially interested in is seen to elute at earlier retention times (spectrum 1 in Figure VII.2b), separated from the major components, thus enabling, potentially, a more detailed characterisation of these carbohydrates. Unfortunately, no MS data is available, because this fraction showed no ionisation under the conditions used (positive mode). In order to improve the S/N of the 1D NMR spectrum shown, a second chromatographic run has been carried out, during which the pectic fraction has been collected into a capillary loop of a storage unit, for subsequent transfer to the NMR spectrometer. The 1D spectrum acquired by accumulation of 64 scans and the TOCSY spectrum of the same fraction are shown in Figure VII.3.

Before analysing those spectra, it is useful to recall the general structure of pectins. Pectins are a family of complex, highly heterogeneous polysaccharides found in the cell walls and intercellular regions of higher plants. They consist of an  $\alpha$ -(1-4)-linked galacturonic acid homopolymer (smooth region) interrupted by rhamnose units carrying neutral sugar side-chains (hairy regions) (Tucker, 1993). Galacturonic acid units in both regions are partially methyl-esterified (at carboxylic groups) and acetylated (at hydroxyl groups). Figure VII.4 shows a schematic representation of pectin structure.

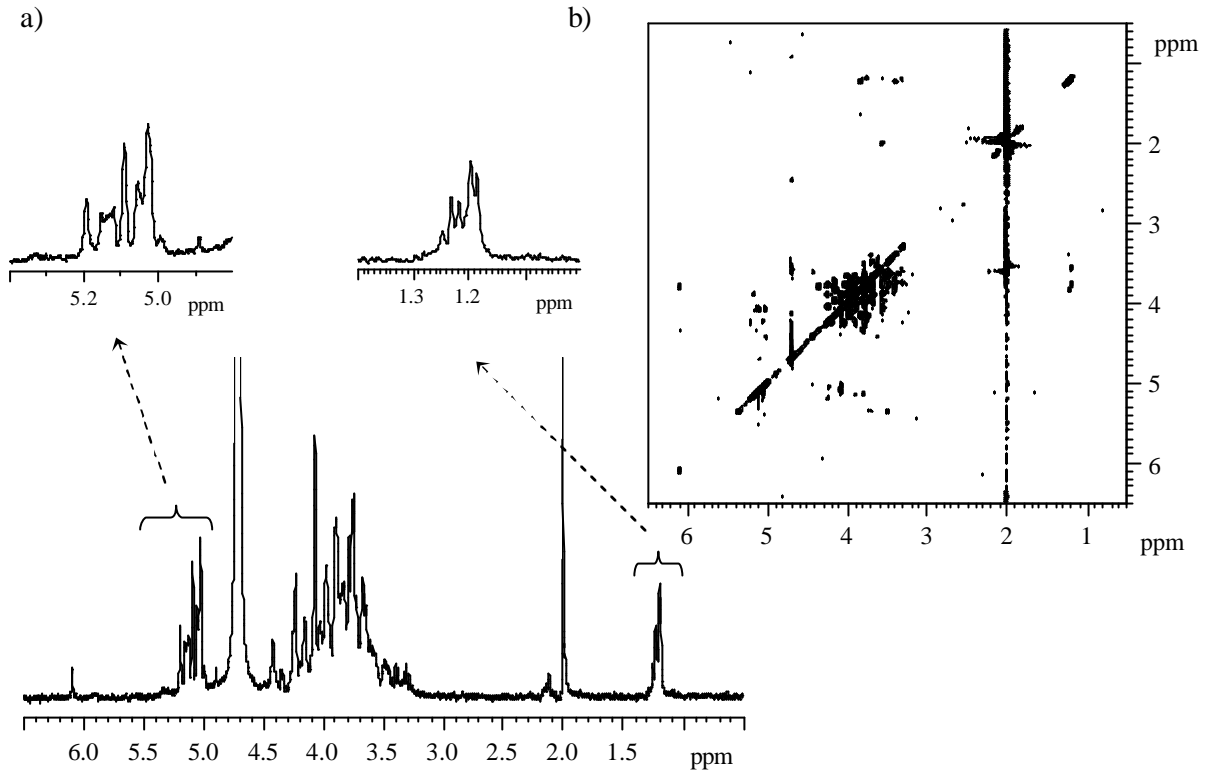


Figure VII.3. a)  $^1\text{H}$  NMR spectrum (NS 64) and b) TOCSY spectrum obtained for the pectic fraction of mango juice, collected into a loop after injection of 50  $\mu\text{l}$  of juice into the column ION-300.

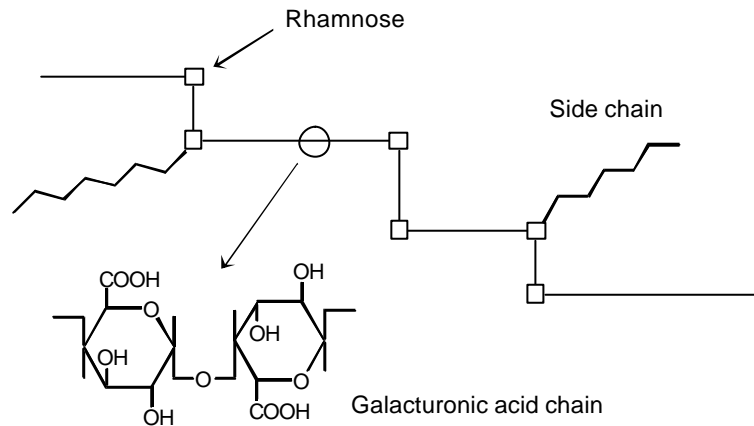


Figure VII.4. Schematic representation of the pectin structure (Tucker, 1993). The side chains (branched polymers of galactose and arabinose) constitute the neutral pectin which is attached to the rhamnogalacturonan acidic pectin polymers via the rhamnose residues.

The spectrum obtained for the pectic fraction of mango juice (Figure VII.3) will now be considered. The doublets at 1.19 and 1.22 ppm, shown in the Figure insert, can be readily assigned to methyl protons (H-6) of rhamnose units. Furthermore, a third signal at 1.23 ppm, overlapping in the 1D spectrum, could be identified in the TOCSY spectrum as being part of another spin system also characteristic of rhamnose. With basis on the  $^1\text{H}$

chemical shifts reported in the literature for sugars (Bock and Thøgersen, 1982) and for rhamnogalacturonan oligosaccharides (Colquhoun *et al.*, 1990; Schols *et al.*, 1994), these systems have been tentatively assigned to  $\alpha$ - and  $\beta$ - forms of rhamnose in the terminal position of the chain (reducing moiety) and to non-reducing rhamnose, as indicated in Table VII.1. Another highly informative region is the 4.9-5.4 ppm region, also expanded in Figure VII.3a, which contains signals of galacturonic acid residues. More specifically, protons H5 of esterified galacturonic acid units are expected to fall in the 5.0-5.1 ppm region and to show a correlation with H4 at about 4.3-4.4 ppm, while protons H1 of esterified and non-esterified residues are expected to resonate in the 4.9-5.0 ppm and 5.1-5.2 ppm ranges, respectively (Tjan *et al.*, 1974; Neiss *et al.*, 1999). The spin systems identified in the TOCSY spectrum for different galacturonic acid units that compose the pectic fraction studied are shown in Table VII.1. Although many resonances could not be assigned due to the still high complexity of the 2D spectrum in the 3.0-4.5 ppm region, it may be suggested that at least five different galacturonic acid residues are present in the fraction separated. At least two of these residues are thought to be non-esterified (as indicated in Table VII.1), with basis on the H-1 shifts falling in the range 5.1-5.2 ppm; the other galacturonic acid residues are possibly esterified, with basis on the correlations of 5.0-5.1 ppm with 4.3-4.4 ppm, attributed to H-5 and H-4, respectively, and on the H-1 shifts at about 5.0 ppm. Moreover, it also becomes apparent that galacturonic acid is not present as a reducing moiety, since the H-1 signals expected to arise at 5.3 and 4.6 ppm for  $\alpha$ - and  $\beta$ -GalA, respectively, are not observed. In what regards other neutral sugars other than rhamnose, there is no clear evidence of their presence.

Table VII.1.  $^1\text{H}$  NMR chemical shifts (ppm) from the 1D and TOCSY spectra of the pectic fraction of mango juice; r.e.: reducing end; n.r.: non-reducing; n.i.: not identified.

		H-1	H-2	H-3	H-4	H-5	H-6
Rha (r.e.)	$\alpha$	5.12	4.06	3.80	3.41	3.83	1.22
	$\beta$	4.88	n.i.	3.62	3.85	3.37	1.23
Rha (n.r.)		5.19	4.23	3.76	3.32	3.56	1.19
GalA possibly esterified		n.i.	n.i.	3.61	4.41	5.01	
		n.i.	n.i.	3.78	4.34	5.13	
		4.99	4.05	n.i.	n.i.	n.i.	
		5.02	4.05	n.i.	n.i.	n.i.	
		5.04	4.22	n.i.	n.i.	n.i.	
GalA non-esterified		5.09	4.06	3.87	n.i.	n.i.	
		5.15	4.09	3.88	n.i.	n.i.	

In order to investigate the effect of ripening on the pectic fraction of mango juice, HPLC-NMR data have also been collected for unripe and ripe juices of the cultivar Haden. The  $^1\text{H}$  NMR spectra of the fractions separated in each juice are shown in Figure VII.5. The profile of the bottom spectrum, corresponding to the ripe juice, is generally similar to the one shown in Figure VII.3a for the ripe juice of the Tommy Atkins cultivar, except for the more intense signal at 3.74 ppm. This signal appears to be a singlet and may arise from methyl groups ( $-\text{OCH}_3$ ) esterifying the carboxylic groups of galacturonic acid residues, thus suggesting a higher degree of methylation for the pectic fraction of the Haden juice. In what concerns the effect of ripening, there are clear differences in the spectral profiles of the two fractions shown in Figure VII.5. The top spectrum shows lower S/N ratio (for equal sample amounts and number of transients), which is indicative of the smaller amount of pectic material in the unripe juice. Moreover, this spectrum has an overall poorer resolution, indicating the presence of larger molecules. These observations may be interpreted in light of pectin hydrolysis reported to occur during mango ripening (Lizada, 1993). Indeed, it is expected that, as the fruit ripens, smaller and more soluble oligomers are released from the pectin complex, being present in the liquid phase in higher amounts. Furthermore, the spectra reveal differences in the monomer composition of the two fractions. In the 1.0-1.4 ppm region of the unripe juice spectrum, only the doublet at 1.19 ppm, previously assigned to non-reducing rhamnose, is observed, whereas the other signals identified in the ripe juice as belonging to  $\alpha$ - and  $\beta$ -rhamnose (reducing moiety) are absent. In the 3.0-4.5 ppm region, some of the most prominent signals in the unripe juice spectrum (3.48, 3.61, 3.86, 3.90 and 4.42 ppm doublet with  $J$  7.8 Hz) may possibly arise from  $\beta$ -galactose and/or  $\beta$ -arabinose, although further confirmation by 2D spectra would be useful. On the other hand, the signals assigned to galacturonic acid residues are much weaker in the unripe juice spectrum, as clearly shown by comparison of the 4.9-5.4 ppm regions expanded in the Figure inserts. These observations suggest that the pectic fraction of the unripe juice is characterised by lower contents of galacturonic acid and higher contents of neutral sugars (galactose/arabinose). This agrees with previous studies on the cell wall polysaccharides of mango fruit. Brinson *et al.* (1988) reported that the ripe tissue fraction contained approximately 90% galacturonic acid whereas the unripe material possessed only 7% and was particularly rich in galactose and arabinose. The marked loss of galactose

from the pectic polysaccharides during ripening has also been reported by Tucker and Seymour (1991).

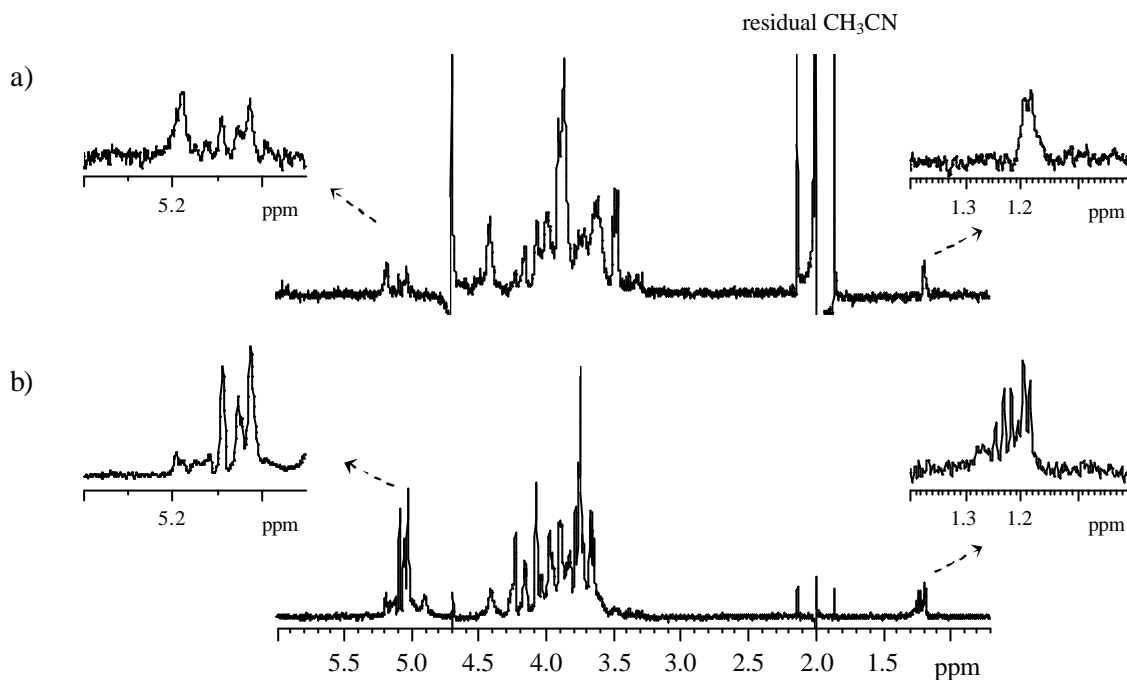


Figure VII.5. <sup>1</sup>H NMR spectra of pectic fractions obtained after elution of a) unripe and b) ripe mango juices on the column ION-300 (injection volume 50  $\mu$ l); NS 128.

### VII.3.2. Application to Spoiled and Contaminated Mango Juices

It has been shown in Chapter VI.3.2 that spoilage and microbial contamination of mango juice induce drastic changes in the carbohydrate composition, although most of the new sugars formed could not be identified. In this Chapter, the HPLC-NMR analysis of three of these samples is described, in order to investigate further the nature of the changes detected. The continuous-flow NMR chromatograms obtained for the control juice (freshly prepared), for the spoiled juice (non-treated and stored for 132 hours at 25°C) and for the juice inoculated with *P. expansum* and stored for 132 hours (25°C) are shown in Figure VII.6. The compounds eluting in some of the rows are identified in the Figure. It must be noted that the flow rate used is not the same for the three juices, as indicated in the Figure caption, thus requiring careful comparison of retention times.

Compared to the continuous-flow NMR chromatogram of fresh mango juice (Figure VII.6a), the NMR chromatogram of spoiled juice (Figure VII.6b) shows several differences, reflecting some of the compositional changes discussed in Chapter VI.3.2.1.

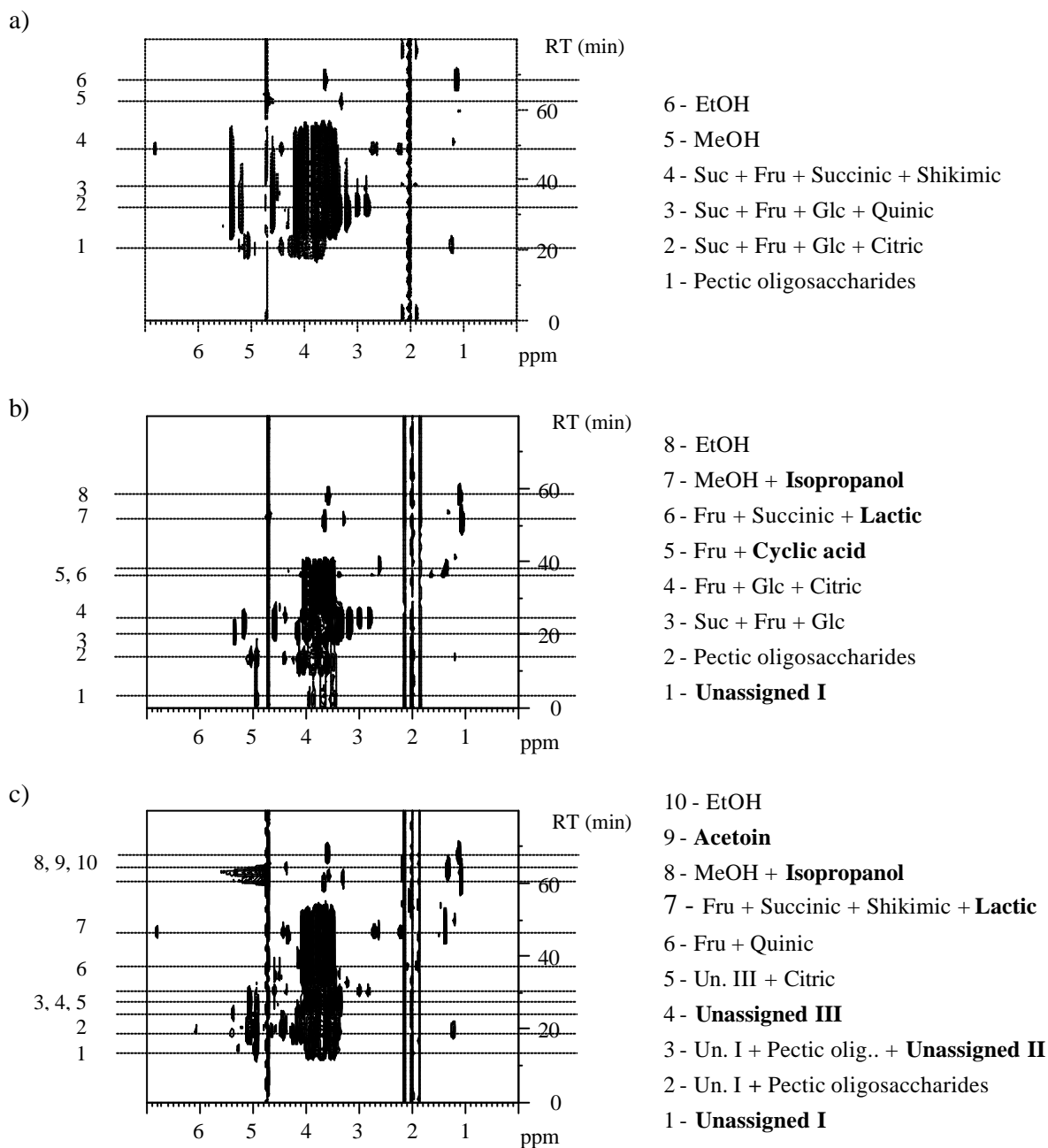
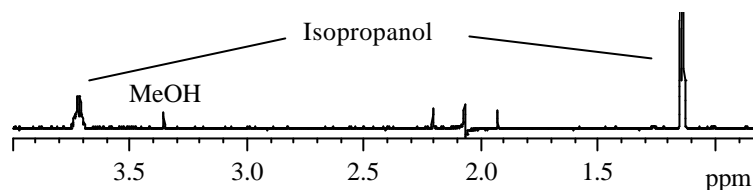


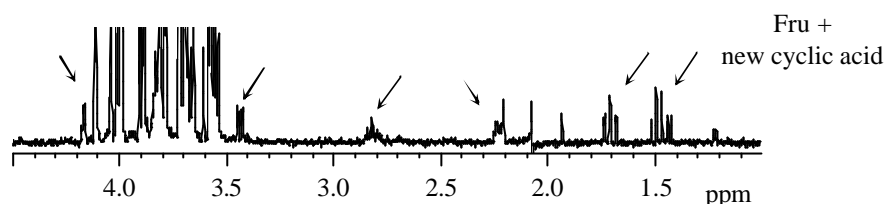
Figure VII.6. Continuous-flow NMR chromatograms obtained for mango juices eluted on the column ION-300: a) fresh juice, b) naturally spoiled juice (non-treated, stored for 132 hours at 25°C) and c) juice inoculated with *P.expansum* and stored for 132 hours (25°C). Flow rates: a) and c) 0.15 ml/min.; b) 0.2 ml/min.

A major difference regards the detection of a new compound in the spoiled juice eluting in the first 4 min of chromatography, before the other juice components. Spectrum 1 in Figure VII.7 shows the corresponding row extracted from the NMR chromatogram. Comprising three groups of signals at about 3.55, 3.73, 3.95 ppm and a doublet at 4.97 ppm ( $J$  2.3 Hz), this spectrum shows a profile which is typical of a carbohydrate-type molecule, but its

3 - RT 51.0 min



2 - RT 36.5 min



1 - RT 3.0 min

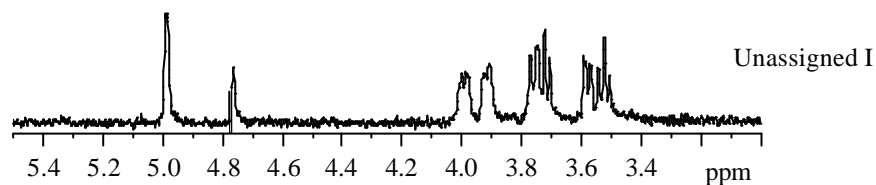


Figure VII.7. Rows extracted from the NMR chromatogram of the spoiled juice shown in Figure VII.6b.

structure has not been determined yet (compound named as 'Unassigned I'). As it elutes very early in the chromatography, even before the pectic fraction, it should arise from a relatively large compound with low affinity for the cation-exchange polymer contained in the chromatographic column used. Later in the chromatography, at about 36.5 min, another new compound is detected in the NMR chromatogram of the spoiled juice, co-eluting with fructose. The corresponding  $^1\text{H}$  spectrum (spectrum 2 in Figure VII.7) shows the signals of fructose and six weak signals (marked with arrows) that have been identified in Chapter VI.3.2.1 to belong to the spin system of a cyclic acid, possibly derived from quinic and/or shikimic acids and proposed to be 3,4,5-trihydroxycyclohexane carboxylic acid. The absence of quinic and shikimic acids in the spoiled juice is indeed clearly visible by comparing the continuous-flow diagrams shown in Figures VII.6a and VII.6b. Other compounds that have been seen to increase by the effect of spoilage (Figure VI.2b in Chapter VI.3.2.1) and are clearly detected in the NMR chromatogram of the spoiled juice (Figure VII.6b) are succinic and lactic acids, co-eluting at 39.0 min, and isopropanol, co-eluting with methanol at about 51.0 min. This latter row is shown in Figure VII.7 (spectrum 3). In this spectrum, the ratio between the area of the doublet at 1.14 ppm and

the area of the multiplet at 3.72 ppm is 6.0, thus confirming the identification of isopropanol. This is a useful finding, since, when the spectrum of the whole juice has been analysed in the previous Chapter, these signals, which were partially or totally overlapped, could not be conclusively assigned because the chemical shifts observed were consistent with either isopropanol or 2,3-butanediol.

The continuous-flow NMR chromatogram of juice contaminated with *P. expansum* (Figure VII.6c) also shows marked differences compared to the diagram in Figure VII.6a. Again, there is a new compound eluting before the pectic fraction. The row in which this compound is detected is shown in Figure VII.8 (spectrum 1) and is identical to the row separated in the spoiled juice at early retention times, indicating that the same unassigned carbohydrate-like compound ('Unassigned I') is formed in the contaminated juice, as already noted in Chapter VI.3.2.3.

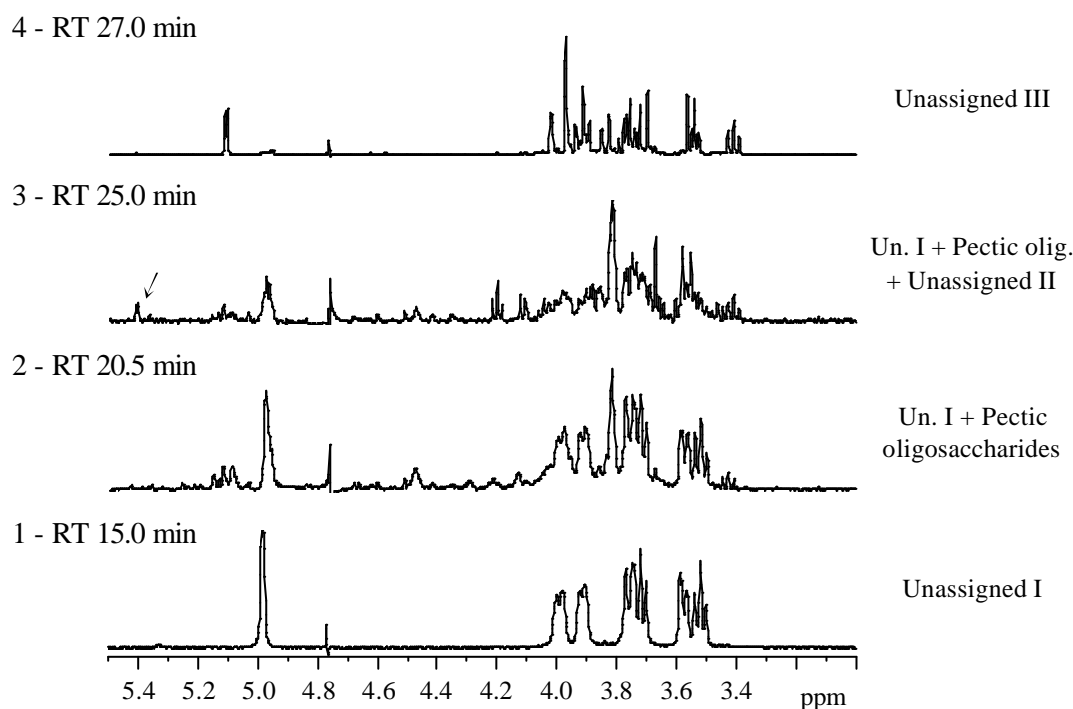


Figure VII.8. Rows extracted from the NMR chromatogram of the juice contaminated with *P. expansum* shown in Figure VII.6c.

The following rows of the contaminated juice NMR chromatogram are distinct from those found in the fresh juice, especially due to the absence of sucrose and glucose. Moreover, new sugars are detected in those rows, as shown in Figure VII.8 (spectra 3 and 4). Spectrum 3 (RT 25.0 min) contains signals from the compounds eluting earlier (spectra 1

and 2), but also some other signals, such as the doublet at 5.40 ppm, which must arise from a different sugar, the identity of which is still unknown. At 27.0 min (spectrum 4), another unidentified new sugar is seen to elute, giving rise to signals at 3.41, 3.56, 3.71-4.06 and 5.11 ppm, which have already been identified to be part of the same spin system in the TOCSY spectrum of the contaminated juice, analysed in the previous Chapter. This sugar has now been separated from the other juice components, and additional information may be obtained from its spectrum. For instance, the fact that the doublet at 5.11 ppm ( $J$  3.8 Hz) is the only signal detected in the anomeric region of the spectrum suggests that the anomeric proton is not free and that this sugar is non-reducing, since, otherwise, two signals for the  $\alpha$ - and  $\beta$ -configuration would be observed. Obviously, further structural elucidation of this compound needs to be carried out in and, in the future, it would be useful to acquire MS data in addition to NMR spectra. Other differences detected in the NMR chromatogram of the contaminated juice (Figure VII.6c) compared to the fresh juice (Figure VII.6a) are: the detection of lactic acid, co-eluting with shikimic and succinic acids, the increased intensity of the isopropanol signals, and the appearance of acetoin, eluting right before ethanol. Indeed, all these compounds have been previously shown to suffer significant increases by the effect of the *P. expansum* growth in the natural mango juice (Chapter VI.3.2.3, Figure VI.9).

Hence, the main advance obtained by HPLC-NMR relatively to the NMR analysis carried out in Chapter VI consisted of separating some of the carbohydrates formed upon spoilage and microbial contamination, thus providing additional structural information, although not having enabled their full assignment yet.

#### VII.4. Characterisation of Aromatic Compounds in Grape Juice

Figure VII.9 shows the  $^1\text{H}$  NMR spectrum of red grape juice. As expected, the most intense signals arise from the sugars glucose and fructose, known to be the major components of grape juice (Peynaud and Ribéreau-Gayon, 1971). The other regions of the spectrum, vertically expanded in the Figure, show many lines, revealing the great chemical complexity of the sample. It is beyond the aim of this work to pursue extensive assignment or give an exhaustive description of grape juice composition. Nevertheless, partial assignment based on the analysis of 1D and TOCSY spectra, and on the assignment of

mango juice, previously carried out in Chapter III, is given in Table VII.2. Some signals are also labelled in Figure VII.9.

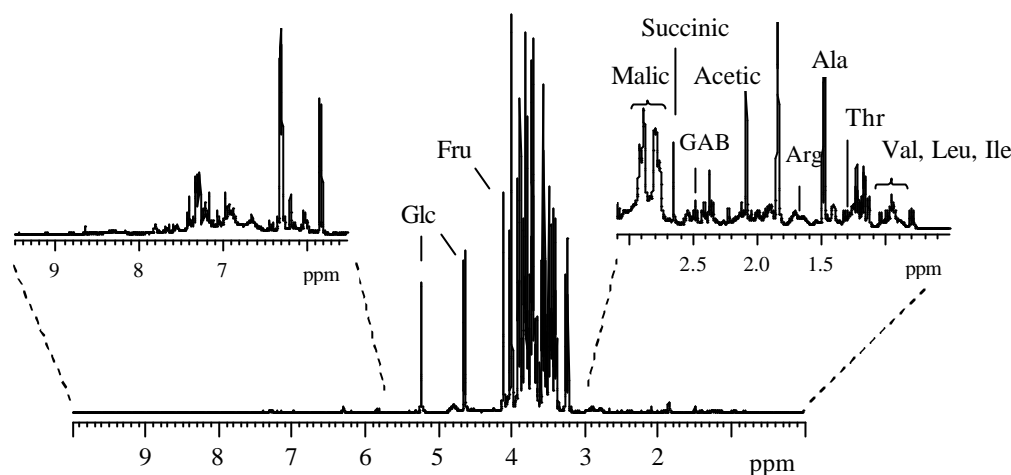
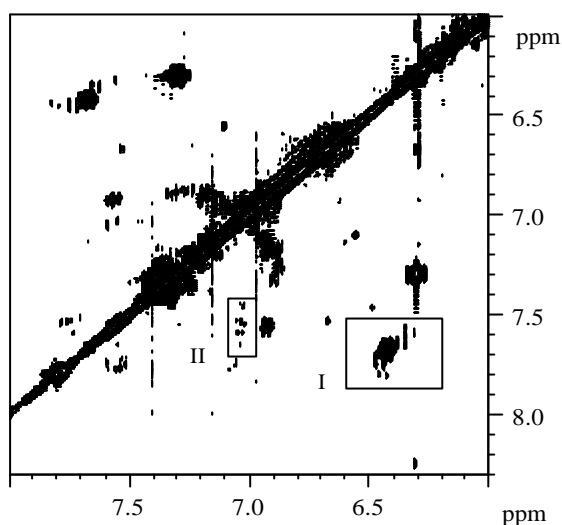


Figure VII.9. 500 MHz  $^1\text{H}$  NMR spectrum of red grape juice; NS 512.

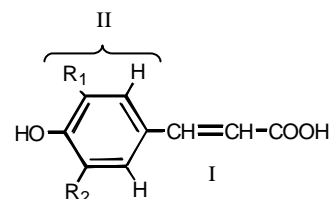
In the aliphatic region, ten amino acids have been identified (e.g. valine, threonine, alanine, proline, arginine, glutamine), as well as the acids malic, succinic and acetic, ethanol and rhamnose. In the sugar region, besides glucose and fructose, signals from pectic galacturonic acid units and tartaric acid have been detected. In the aromatic region, the TOCSY spectrum (Figure VII.10a) shows a great number of cross peaks, but their assignment is not straightforward because most spin systems are described by two chemical shifts only, and no more couplings are observed. For instance, the cross-peaks outlined by box I in Figure VII.10a correspond to at least five pairs of doublets with similar chemical shifts and coupling constants ( $J$  16 Hz), without any other TOCSY correlations. These signals may arise from olefinic protons of *trans*-cinnamic acids or their derivatives, known to be present in grape juice in reasonable concentrations (Spanos and Wrolstad, 1992), either free or esterified. In addition, the signals in box II (Figure VII.10a) correspond to another five spin systems (with two chemical shifts each) that may arise from the ring protons of those compounds. However, due to the structure of cinnamic derivatives (Figure VII.10b), the olefinic protons (I) have no TOCSY correlation with the phenyl protons (spin system II), and in the esterified form there are no correlations with the protons of the ester radical (III). Consequently, only fragments of spin systems are visible in the TOCSY spectrum, hindering the identification of the different cinnamic compounds.

a)



b)

## Cinnamic acids

*p*-Coumaric acid: R<sub>1</sub>, R<sub>2</sub>=HCaffeic acid: R<sub>1</sub>=H, R<sub>2</sub>=OHFerulic acid: R<sub>1</sub>=H, R<sub>2</sub>=OCH<sub>3</sub>

## Cinnamic esters

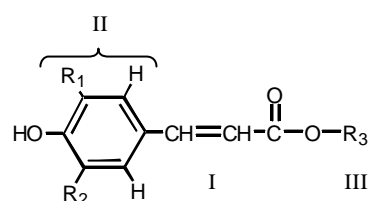
R<sub>3</sub> = tartaric acid, quinic acid, sugars, etc.

Figure VII.10. a) 500 MHz TOCSY spectrum of red grape juice; b) Structure of some cinnamic compounds commonly found in grapes; I, II and III indicate different spin systems.

The identification of this kind of phenolic acids by high resolution NMR has been reported in the literature. Gerothanassis *et al.* (1998) investigated the phenolic composition of oregano extracts by using a combination of 2D methods (COSY, TOCSY and NOESY/ROESY), and, in particular, by making use of the NOE/ROE effect between spatially close but uncoupled <sup>1</sup>H nuclei to establish the connection between the olefinic and the phenyl protons. Further work has been carried out by Exarchou *et al.* (2001), who performed COSY experiments at low temperature and <sup>1</sup>H-<sup>13</sup>C heteronuclear multiple-bond correlation (HMBC) experiments to resolve the signals of caffeic and rosmarinic acid in plant extracts. These approaches show clear advantages over classical analysis, where individual phenolic acids require isolation and purification prior to structural identification, but have the disadvantages of involving long experimental times for acquisition of 2D NMR spectra, and a demanding work of spectral interpretation. The work hereby reported aims at showing the potential of the HPLC-NMR/MS method for separating and identifying these phenolic acids and other aromatic compounds present in grape juice.

Table VII.2.  $^1\text{H}$  chemical shifts, multiplicity and  $J_{\text{HH}}$  for assigned compounds in grape juice; s: singlet, d: doublet, t: triplet, dd: doublet of doublets, m: multiplet; <sup>(a)</sup> tentative identification; un.: unassigned.

Compound	Assignment	$^1\text{H}$ (ppm)	Multiplicity	$J$ (Hz)
Acetic acid	?CH <sub>3</sub>	2.08	s	
Alanine	?CH <sub>3</sub>	1.48	d	7.2
	?CH	3.83		
?-Aminobutyric acid (GABA)	?CH <sub>2</sub>	1.94	t	7.4
	?CH <sub>2</sub>	2.48		
	?CH <sub>2</sub>	3.04		
Arginine	?CH <sub>2</sub>	1.68	m	
	?CH <sub>2</sub>	1.90		
	?CH <sub>2</sub>	3.22		
	?CH	3.79		
Ethanol	CH <sub>3</sub>	1.18	t	7.1
	CH <sub>2</sub>	3.65		
Fructose (?-furanose)	C6H	3.67		
	C5H	3.80		
	C3H, C4H	4.11		
Fumaric <sup>(a)</sup>	CH	6.65	s	
?-Galacturonic acid (pectic, non-reducing) / ?-Rhamnose <sup>(a)</sup>	un.	4.00, 4.12, 5.08		
	un.	3.92, 4.28, 5.11		
?-Galacturonic acid (free/pectic, reducing end) <sup>(a)</sup>	un.	4.13, 5.15	broad	
	un.	3.92, 5.18		
	C2H	3.82		
	C3H	3.92		
	C4H	4.33		
Gallic acid <sup>(a)</sup>	C1H	5.31	s	
	C2H, C6H	7.06 or 7.15		
?-Glucose	C4H	3.40	d	3.7
	C2H	3.53		
	C3H	3.70		
	C6H	3.77		
	C5H	3.82		
	C1H	5.23		
	C2H	3.24		
?-Glucose	C4H	3.40	dd	
	C5H	3.46		
	C3H	3.49		
	C6H	3.72, 3.89		
	C1H	4.64		
	C1H	4.64		
Glutamic acid	?,?'CH	2.10	d	7.9
	?CH <sub>2</sub>	2.51		
	?CH	4.28		
Glutamine	?CH <sub>2</sub>	2.15		
	?CH <sub>2</sub>	2.54		
	?CH	3.82		

Table VII.2 (cont.)

Compound	Assignment	$\delta$ $^1\text{H}$ (ppm)	Multiplicity	$J$ (Hz)
Isoleucine	$\delta\text{CH}_3$	0.93		
	$\delta'\text{CH}_3$	1.00		
	$\delta\text{CH}$	1.98		
	$\delta\text{CH}$	3.71		
Leucine	$\delta, \delta'\text{CH}_3$	0.95		
	$\delta\text{CH}_2, \delta\text{CH}$	1.71		
	$\delta\text{CH}$	3.77		
Malic acid	$\delta\text{CH}$	2.78	dd	6.5, 16.5
	$\delta'\text{CH}$	2.90		
	$\delta\text{CH}$	4.53		
Niacin	C5H	8.06		
	C4H, C6H	8.82		
	C2H	9.12	s	
Phenylalanine	C3H, C5H	7.32		
	C4H	7.37		
	C2H, C6H	7.41		
Proline	$\delta\text{CH}_2$	2.00	m	
	$\delta\text{CH}_2$	2.06		
	$\delta\text{CH}_2$	2.33		
	$\delta\text{CH}_2$	3.33		
	$\delta\text{CH}_2$	3.41		
	$\delta\text{CH}$	4.14		
Succinic acid	$\delta, \delta\text{CH}_2$	2.65	s	
Tartaric acid	CH	4.52	s	
Threonine	$\delta\text{CH}_3$	1.32	d	6.4
	$\delta\text{CH}$	3.63		
	$\delta\text{CH}$	4.27		
Tyrosine	C3H, C5H	6.89		
	C2H, C6H	7.17		
Uridine	C5H, C1'H	5.89		
	C6H	7.85	d	8.3
Valine	$\delta\text{CH}_3$	0.98	d	
	$\delta'\text{CH}_3$	1.03	d	
	$\delta\text{CH}$	2.27		
	$\delta\text{CH}$	3.65		

The UV chromatogram obtained by HPLC elution of the grape juice, using the conditions previously described in section VII.2.2, shows the detection of many peaks at 280, 320 and 365 nm (Figure VII.11a), which are major absorption wavelengths for a wide range of phenolic compounds (Revilla and Ryan, 2000). Some peaks are not very well resolved, but this is not of great concern, since they are subsequently analysed by NMR and MS, which are potentially capable of distinguishing between co-eluting compounds.

Figures VII.11b and VII.11c show the Total Ion Current (TIC) MS chromatograms obtained in negative and positive ionisation modes, respectively, during two chromatographic runs. For most retention times, the TIC obtained in negative mode (Figure VII.11b) shows higher intensity than the one obtained in positive mode (Figure VII.11c). Therefore, data obtained by negative ionisation are preferably reported, as in most studies reporting the analysis of phenolic compounds by ESI-MS (Pérez-Margariño *et al.*, 1999; Lazarus *et al.*, 1999; Fulcrand *et al.*, 1999). Indeed, Fulcrand *et al.* (1996) found that, generally, the response of polyphenols is better in the negative ionisation mode than in the positive mode.

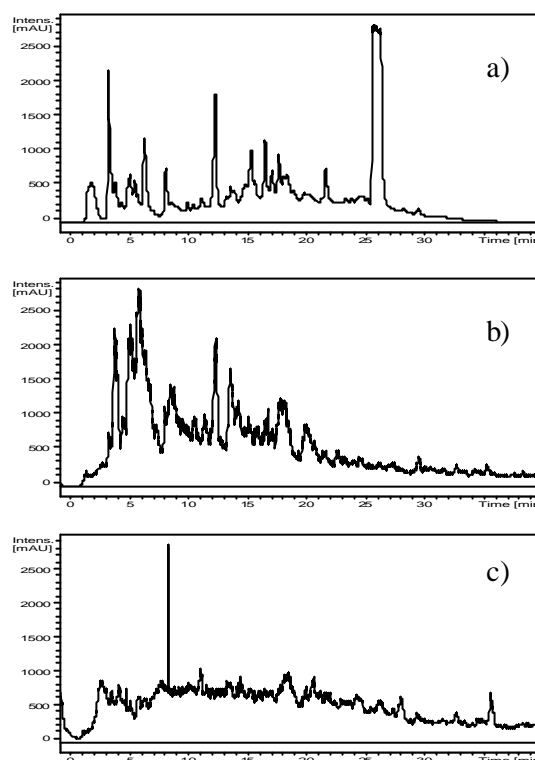


Figure VII.11. a) UV chromatogram (280, 320, 365 nm), b) MS TIC (negative mode) and c) MS TIC (positive mode), resulting from the elution of grape juice on the column RP18 (flow rate 1.00 ml/min).

The continuous-flow NMR chromatogram is shown in Figure VII.12a. At early retention times, the most polar metabolites elute together, giving rise to the series of bands that appear at the start of the chromatogram. Among these are the sugars glucose and fructose, several amino acids (e.g. val, leu, ala, gln, glu), organic acids (e.g. malic, succinic, citric) and ethanol. With respect to aromatic components, at least 14 rows containing signals in the 6.0-10.0 ppm region are detected, which is indicative of the rich aromatic composition of the grape juice.

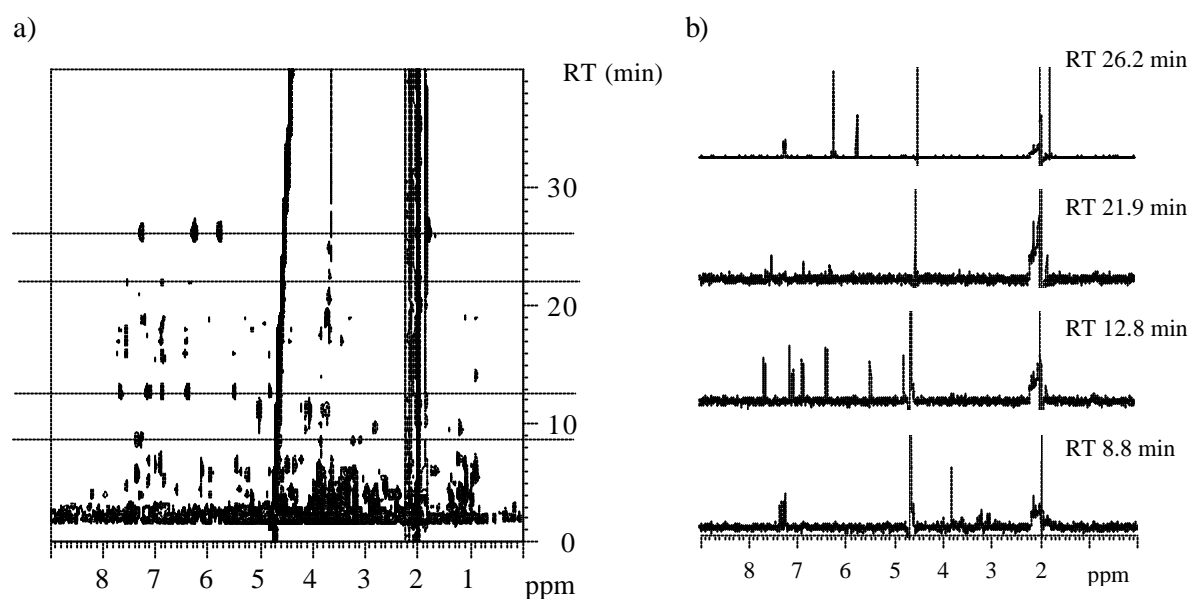


Figure VII.12. a) Continuous-flow NMR chromatogram resulting from the elution of red grape juice on the column RP18 (flow rate 1.00 ml/min) and b) rows extracted from the NMR chromatogram.

Compared to the grape juice spectrum (Figure VII.9), the spectra of the rows, such as those shown in Figure VII.12b, are easier to assign, since they arise from much simpler fractions. In some cases, however, the S/N of the spectra registered during the on-flow experiment (with only 16 scans each) is too low. In order to improve the results, a loop-sampling experiment was performed. 1D spectra with 64 scans and in some cases TOCSY spectra were recorded for the fractions collected. Moreover, automatic switch between positive and negative ionisation was employed and MS/MS experiments were carried out to identify fragment ions. In this way, several aromatic compounds could be identified in grape juice and Table VII.3 summarises the results, putting together the UV, MS and NMR data registered in each case; the structure of some of the compounds listed is not completely elucidated, for reasons that will be explained further ahead, and their tentative identification is marked with <sup>(a)</sup>. The following paragraphs discuss the results obtained in more detail.

Figure VII.13 shows the <sup>1</sup>H NMR spectra in the aromatic region of four fractions collected into loops during the first 10 min of chromatography. Spectrum 1 (RT 4.6 min) is rather complex as it shows many signals, appearing to reflect the coelution of several compounds. Among the signals detected, the doublets overlapping at 5.83 ppm and the

doublet at 7.81 ppm may be assigned to a uridine system. Spectrum 2 (RT 6.4 min) is probably a compound related to epicatechin, but its structure is still not clear. Spectrum 3 (RT 7.0 min) shows the compound detected in spectrum 2 and a singlet arising from gallic acid (? 7.12 ppm). The identification of this phenolic acid ( $M_w$  170) is confirmed by the respective mass spectrum, which shows a peak at  $m/z$  172, corresponding to the fully deuterated molecular ion  $[M - D]^+$  of gallic acid. Spectrum 4 (RT 8.8 min) shows the presence of phenylalanine. The additional high-field signals and the MS peak at  $m/z$  170 (in positive-ionisation mode) provide unambiguous confirmation of the presence of this aromatic amino acid, which is overlapped in the 1D spectrum.

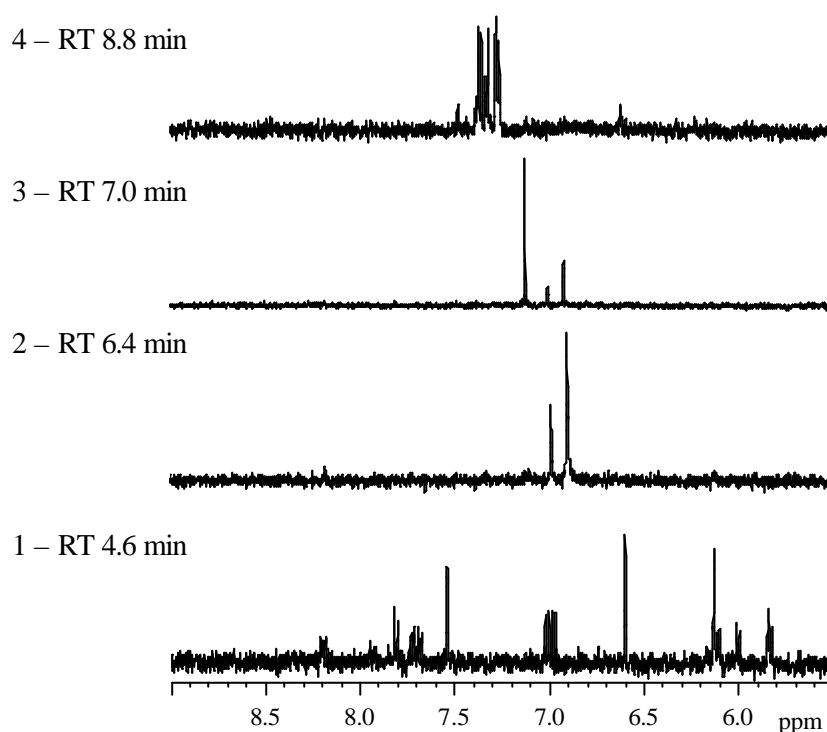
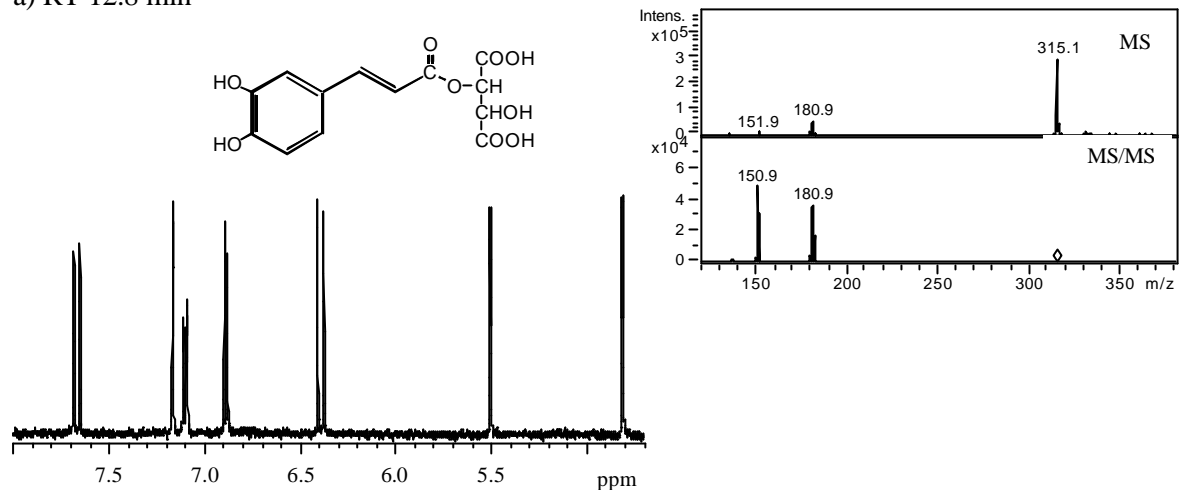


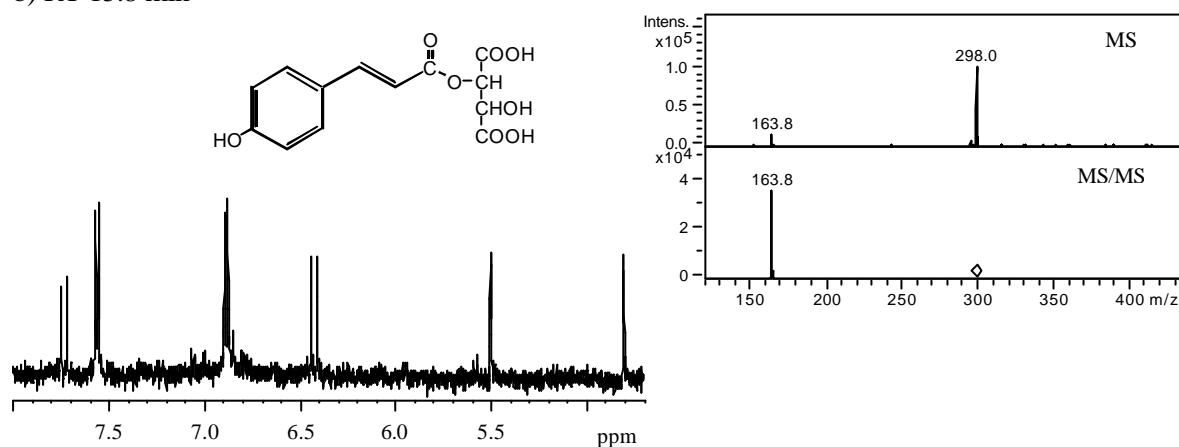
Figure VII.13.  $^1\text{H}$  NMR spectra of four fractions of grape juice collected into loops.

Between 10 and 30 min, good separation is noted for several aromatic compounds. The compounds eluting at 12.8, 15.8 and 21.9 min are unequivocally identified as cinnamic constituents, with basis on the comparison of their NMR spectra with published data (Gerothanassis *et al.*, 1998; Lu and Foo, 1999), and also with basis on the corresponding MS spectra (Figure VII.14). The data shown in Figure VII.14a is consistent with the presence of *trans*-caftaric acid (*trans*-caffeoyltartaric acid), the most abundant cinnamic compound known to occur in grapes (Singleton *et al.*, 1986). The signals found

a) RT 12.8 min



b) RT 15.8 min



c) RT 21.9 min

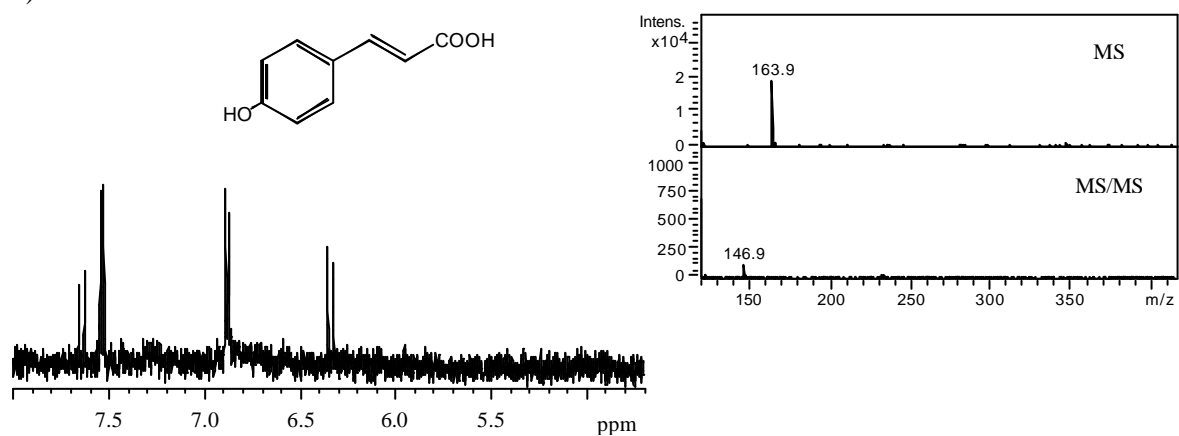


Figure VII.14. <sup>1</sup>H NMR and MS spectra of three fractions of grape juice collected into loops: a) RT 12.8 min, *trans*-caftaric acid; b) RT 15.8 min, *trans*-coutaric acid; and c) RT 21.9 min, *p*-coumaric acid.

in the 6.0-8.0 ppm region of the  $^1\text{H}$  NMR spectrum are consistent with a *trans*-caffeoyl moiety: the aromatic ring protons originate an ABX spin system at 6.89 ( $J$  8.3 Hz), 7.10 ( $J$  8.3 Hz) and 7.17 ppm and the olefinic protons give rise to a pair of doublets at 6.39 and 7.67 ppm ( $J$  16.0 Hz). The doublets seen at 4.81 and 5.50 ppm indicate that this caffeoyl moiety is esterified with tartaric acid, thus being *trans*-caftaric acid. Further confirmation is given by the MS data recorded for this fraction, as the mass spectrum shows a peak at  $m/z$  315, corresponding to the molecular ion  $[\text{M} - \text{D}]^+$  for *trans*-caftaric acid with the 3 OH and the 2 COOH groups all deuterated. The fragmentation of this ion, seen in the MS/MS spectrum, originates, as expected, the ions corresponding to caffeic ( $m/z$  181) and tartaric ( $m/z$  151) acids. The  $\lambda_{\text{max}}$  322 nm observed in the UV spectrum also agrees with the expected value for *trans*-caftaric acid (Revilla and Ryan, 2000). Figure VII.13b shows the data obtained for the fraction of grape juice collected at 15.8 min, which indicates the presence of *trans*-coutaric acid (*trans*-coumaroyltartaric acid). The *trans*-coumaroyl group is identified by the AB resonance system (6.89 and 7.56 ppm,  $J$  8.6 Hz) and by the doublets arising from the olefinic protons (6.43 and 7.73 ppm,  $J$  16.2 Hz). Again, the doublets at 4.81 and 5.50 ppm are detected, indicating esterification with tartaric acid. This assignment is corroborated by MS, as the mass spectrum of this fraction shows a peak at  $m/z$  298 corresponding to the molecular ion  $[\text{M} - \text{D}]^+$  of coutaric acid with exchangeable protons fully deuterated. In the MS/MS spectrum, the fragment ion with  $m/z$  164 corresponding to coumaric acid is observed. The data shown in Figure VII.13c, corresponding to the fraction collected at 21.9 min, enables the identification of free *p*-coumaric acid in grape juice.

Besides the compounds identified above, other cinnamic derivatives are seen to elute at 16.9, 17.5 and 18.1 min (coumaric and ferulic derivatives marked with <sup>(a)</sup> in Table VII.3). The first fraction shows  $^1\text{H}$  NMR signals characteristic of a *p*-coumaroyl moiety together with sugar resonances (spectrum 1 in Figure VII.15). The corresponding mass spectrum shows a peak at  $m/z$  329, which gives fragment ions with  $m/z$  164, 236 and 267. Among the most common cinnamic esters, listed in Table VII.4 along with the respective molecular weights, an ester of *p*-coumaric acid with an hexose is most likely the compound detected. The hexose identity is, however, not known due to the low S/N in the NMR spectrum acquired. The 17.5 min fraction also shows  $m/z$  329 in the mass spectrum, but in the MS/MS spectrum a fragment ion with  $m/z$  194 is obtained, suggesting the presence of

ferulic acid. The  $^1\text{H}$  NMR spectrum (spectrum 2 in Figure VII.15) is consistent with a feruoyl moiety, and a sugar moiety is also visible, although the S/N is too low to allow further interpretation. Therefore, the most probable possibility seems to be ferulic acid esterified with a pentose. The 18.1 min fraction shows NMR and MS data similar to those recorded for the 16.9 min fraction (*p*-coumaric acid esterified with an hexose). Again, the identification of the hexose is impeded by the low S/N observed in the corresponding  $^1\text{H}$  NMR spectrum (spectrum 3 in Figure VII.15). Finally, at 26.2 min, the NMR chromatogram (Figure VII.12a) shows the elution of a compound that is still unassigned and for which NMR and MS data are given in Table VII.3.

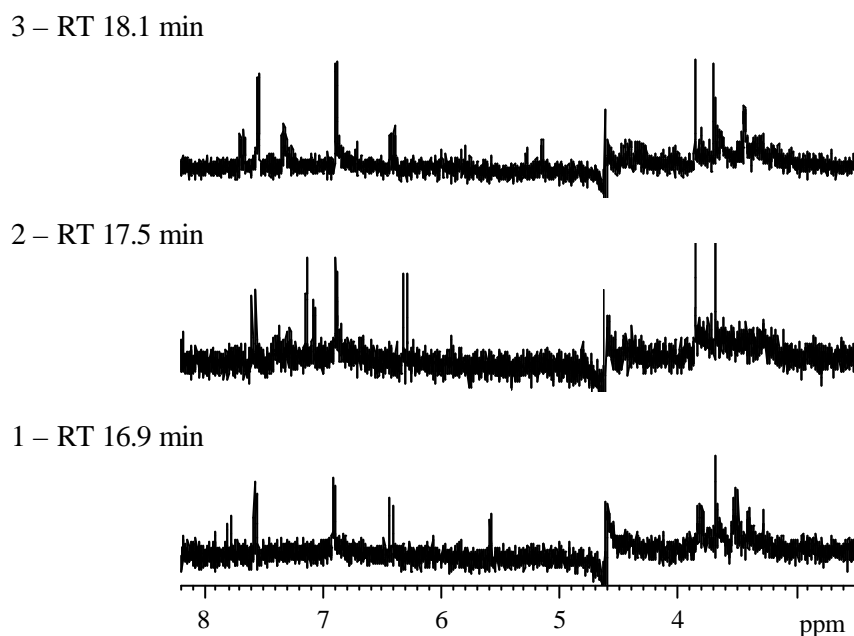


Figure VII.15.  $^1\text{H}$  NMR spectra of three fractions of grape juice collected into loops.

In summary, HPLC-NMR/MS of grape juice has enabled the identification of a few cinnamic compounds which could not be assigned by NMR alone, such as *p*-coumaric, *trans*-caftaric and *trans*-coutaric acids. In addition, the presence of uridine, tyrosine, gallic acid and phenylalanine has been confirmed.

Table VII.3. UV, MS and NMR data of aromatic constituents, obtained by HPLC-NMR/MS analysis of grape juice, using the loop-sampling method; n.i.: not identified; n.a.: not acquired; <sup>(a)</sup> structure not fully known.

RT (min)	$\lambda_{\max}$ (nm)	$m/z$ $M - D$ ?		NMR signals $\delta$ in ppm (mult., $J$ in Hz)	Compound
		MS	MS/MS		
4.6	273/308	n.i.	n.i.	5.82 (d, 8.0), 5.84 (d, 4.5), 7.81 (d, 8.0)	Uridine ( $M_w$ 244)
5.5	272	183	n.a.	6.81 (d, 8.5), 7.11 (d, 8.5)	Tyrosine ( $M_w$ 181)
6.4	278	376	128 163 274 292	5.45 (s), 6.89 (s), 6.98 (s)	<sup>(a)</sup> Epicatechin derivative
7.0	272	172	127	7.12 (s)	Gallic acid ( $M_w$ 170)
8.8	280	$M + D$ ? 170	122	3.08 (dd, 14.0 8.0), 3.25 (dd, 15.0 5.0), 4.02 (m), 7.26 (m), 7.32 (m), 7.36 (m)	Phenylalanine ( $M_w$ 165)
12.8	322	315	151 181	4.81 (d, 2.2), 5.50 (d, 2.2), 6.39 (d, 16.0), 6.89 (d, 8.3), 7.10 (d, 8.3), 7.17 (s), 7.67 (d, 16.0)	<i>trans</i> -Caffaric acid ( $M_w$ 312)
15.8	307	298	164	4.81 (d, 2.2), 5.50 (d, 2.2), 6.43 (d, 16.2), 6.89 (d, 8.6), 7.56 (d, 8.6), 7.73 (d, 16.2)	<i>trans</i> -Coutaric acid ( $M_w$ 296)
16.9	307	329	164 236 267	sugar resonances + 6.41 (d, 16.2), 6.89 (d, 8.6), 7.54 (d, 8.6), 7.67 (d, 16.2)	<sup>(a)</sup> <i>p</i> -Coumaric + hexose ( $M_w$ 326)
17.5	315	329	194	sugar resonances + 6.30 (d, 16.0), 6.88 (d, 8.2), 7.07 (d, 8.2), 7.14 (s), 7.58 (d, 16.0)	<sup>(a)</sup> Ferulic + pentose ( $M_w$ 326)
18.1	307	329	164 236 267	sugar resonances + 6.41 (d, 16.0), 6.88 (d, 8.4), 7.54 (d, 8.3), 7.67 (d, 16.0)	<sup>(a)</sup> <i>p</i> -Coumaric + hexose ( $M_w$ 326)
21.9	307	164	147	6.34 (d, 16.1), 6.88 (d, 8.5), 7.53 (d, 8.5), 7.64 (d, 16.1)	<i>p</i> -Coumaric acid ( $M_w$ 164)
26.2	254/281	$M + D$ ? 115	97	1.80 (d), 5.78 (d), 6.26, 7.26	Unassigned

Table VII.4. Molecular weights of cinnamic acids and esters commonly found in grapes.

	coumaric <i>164</i>	ferulic <i>194</i>	caffeic <i>180</i>
tartaric	<i>150</i>	296	312
quinic	<i>192</i>	338	354
malic	<i>134</i>	280	296
shikimic	<i>174</i>	320	336
pentose	<i>150</i>	296	312
hexose	<i>180</i>	326	342

## VII.5. Characterisation of Aromatic Compounds in a Wine Phenolic Extract

Figure VII.16b shows the  $^1\text{H}$  NMR spectrum of the red wine phenolic extract, analysed by HPLC-NMR/MS, compared to the spectrum of the original wine sample (Figure VII.16a). The expected concentration increase of phenolic constituents was achieved, as viewed by the higher intensity of aromatic signals and the lower intensity of the sugar peaks in the spectrum of the extract. However, one can also see several differences in the aromatic profiles (inserts), which are due to losses (e.g. niacin and acetaldehyde) or chemical modifications occurring during the extraction procedure.

The aromatic section of the TOCSY spectrum recorded for the wine extract (Figure VII.16c) shows many cross-peaks, of which some may be tentatively assigned to tyrosine and/or tyrosol, and to cinnamic acids. However, like in the case of grape juice, the unambiguous identification of these and other aromatic compounds is very difficult because most of them show incomplete spin systems and a high degree of overlap. Continuous-flow HPLC-NMR/MS analysis is used here to tackle this problem.

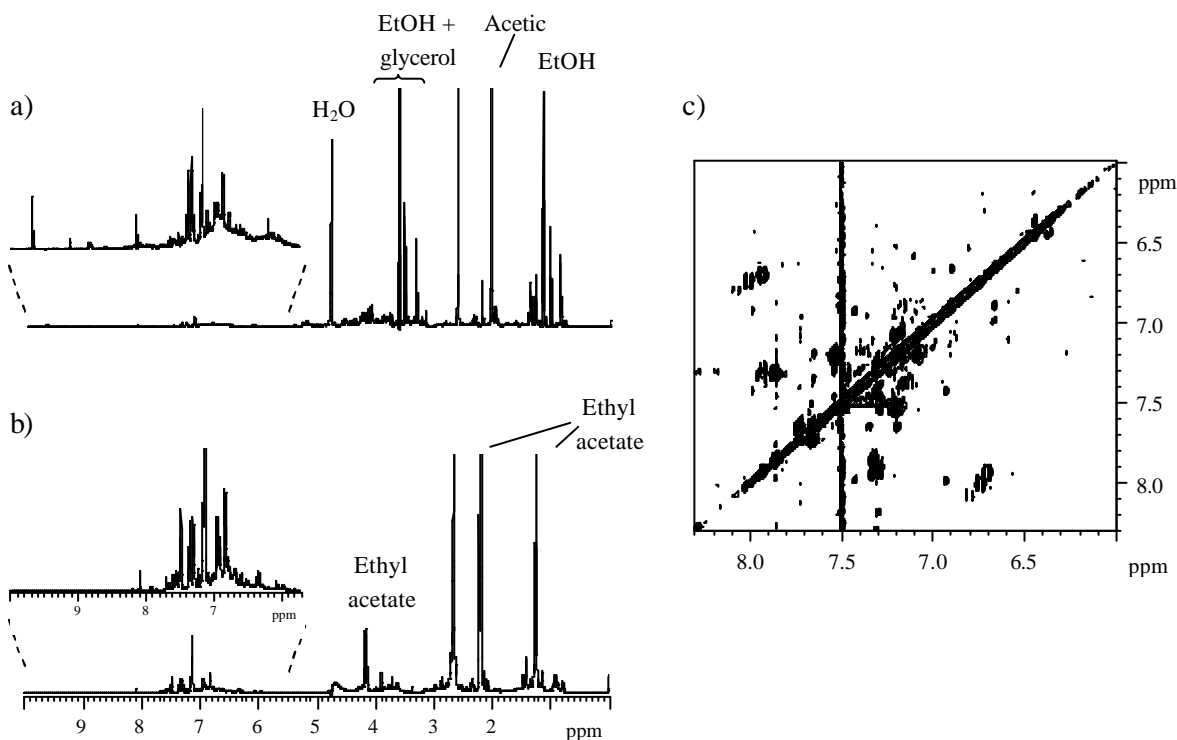


Figure VII.16. 500 MHz  $^1\text{H}$  NMR spectra of a) red wine and of b) the phenolic extract prepared from that wine; c) Aromatic section of the 500 MHz TOCSY spectrum of the wine extract.

Figure VII.17 shows the UV chromatogram registered at 280, 320 and 365 nm and the total ion current MS chromatogram obtained by negative electrospray ionisation. Many signals are detected in both traces. The continuous-flow NMR chromatogram (Figure VII.18a) exhibits a good separation as a function of RT and example rows are shown. The information obtained from UV, MS and NMR chromatograms is summarised in Table VII.5 and discussed in the following paragraphs.

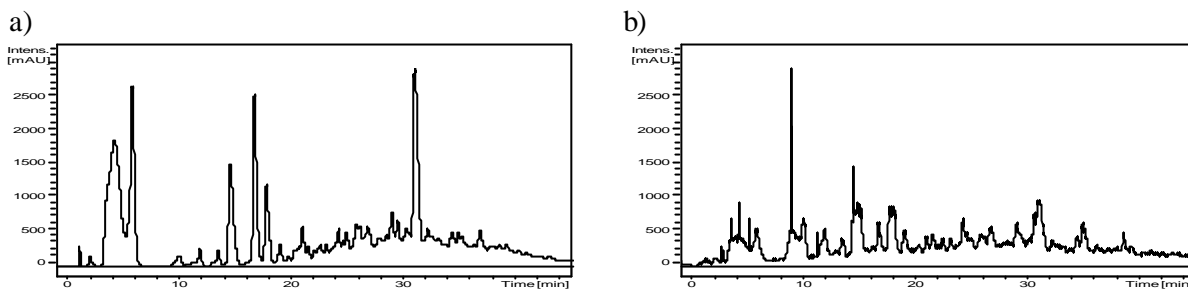


Figure VII.17. a) UV chromatogram (280, 320, 365 nm) and b) MS TIC (negative ionisation), resulting from the elution of the wine extract on the column RP18 (flow rate 1.00 ml/min.).

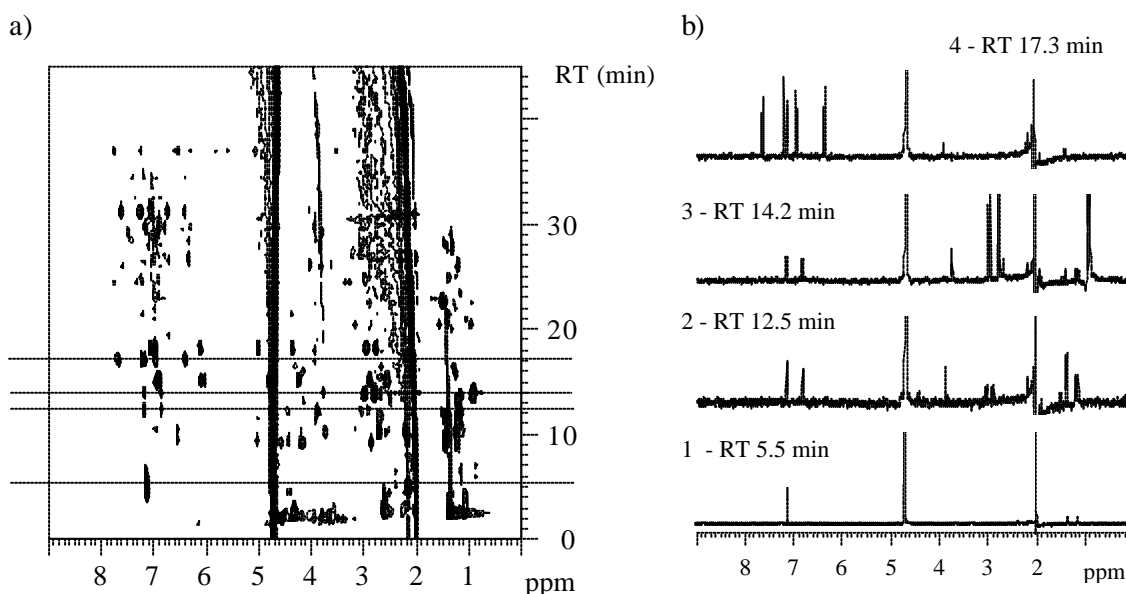


Figure VII.18. a) Continuous-flow NMR chromatogram resulting from the elution of the wine extract on the column RP18 (flow rate 1.00 ml/min.) and b) rows extracted from the NMR chromatogram.

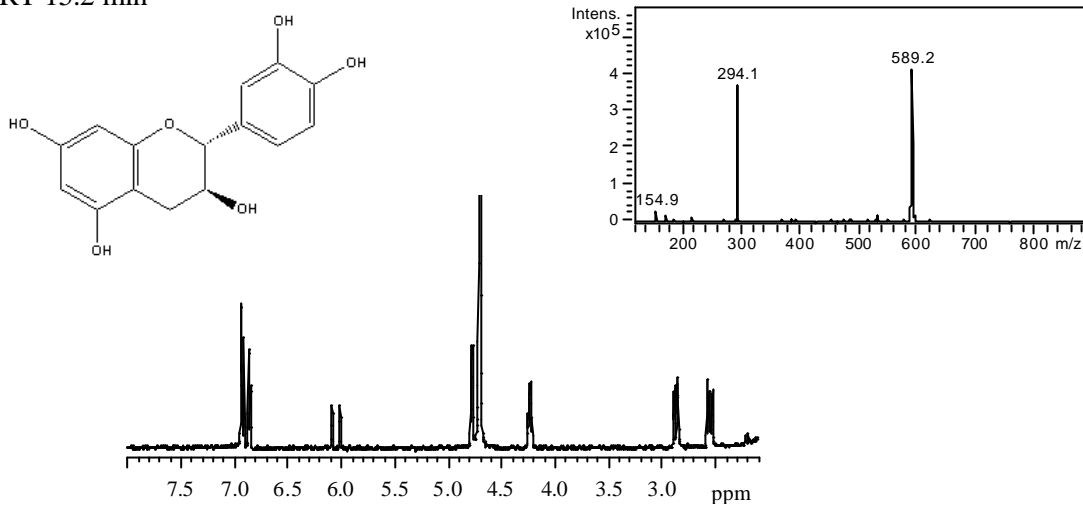
Gallic acid is the first aromatic component detected, eluting between 4.0 and 7.0 min, after succinic (? 2.61 ppm) and tartaric (? 4.32 ppm) acids. The presence of this phenolic acid is confirmed by the singlet at 7.12 ppm in the  $^1\text{H}$  NMR spectrum (spectrum 1

in Figure VII.18b) and by the peak at  $m/z$  172 observed in the negative-ionisation mode mass spectrum. Between 12.0 and 14.5 min, two separate rows with an identical profile in the aromatic region are seen (spectra 2 and 3 in Figure VII.18b). Both spectra contain doublets at 6.83 and 7.16 ppm ( $J$  8.5 Hz) and may only be distinguished with basis on the high-field signals, which enable the assignment to tyrosine (spectrum 2) and tyrosol (spectrum 3). The latter shows a triplet at 3.76 ppm arising from  $\text{CH}_2\text{OH}$ , and a triplet at 2.76 ppm ( $\text{CH}_2\text{-CH}_2\text{OH}$ ), partially overlapped by the citric acid signals at  $\sim 2.8$  ppm. The presence of tyrosine is further confirmed by the peak at  $m/z$  183, corresponding to  $[\text{M} - \text{D}]^-$ . It is important to note that 1D and TOCSY spectra of the whole sample did not enable these compounds to be distinguished, as their aromatic signals overlap and there is no coupling between aromatic and aliphatic protons.

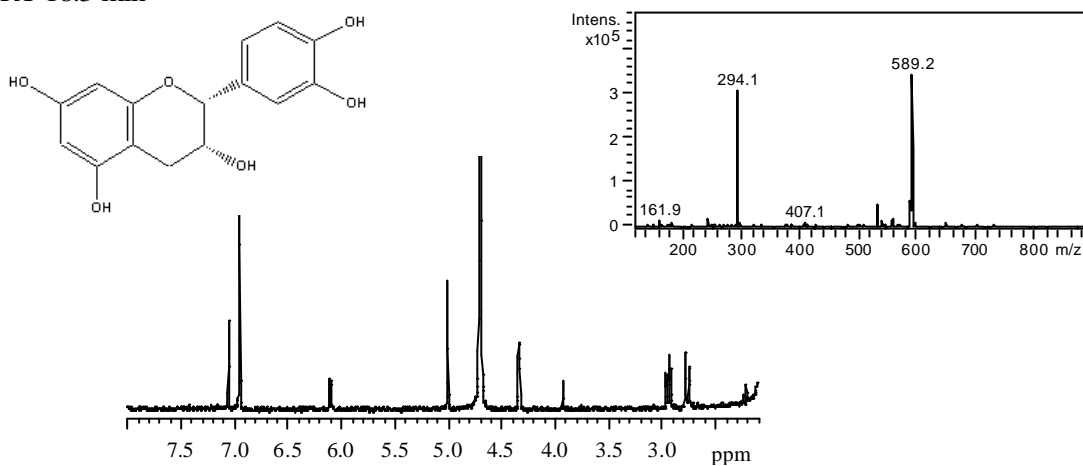
The rows recorded between 14.5 and 20.0 minutes clearly show the elution of three phenolic compounds: catechin, caffeic acid and epicatechin. The UV, NMR and MS data that allowed their unequivocal identification are summarised in Table VII.5 and the cases of catechin and epicatechin are shown in Figure VII.19a and VII.19b. These compounds have identical absorbance properties ( $\lambda_{\text{max}}$  278 nm) and, being isomers, show the same  $m/z$  values in the mass spectra:  $m/z$  294 for the molecular ion  $[\text{M} - \text{D}]^-$  of deuterated (epi)catechin, and  $m/z$  589 for noncovalent dimers  $[\text{M} + (\text{M} - \text{D})]^-$  of two stacked (epi)catechin molecules, formed during MS analysis. This phenomenon of self-association is often observed by electrospray MS of these type of substances (Fulcrand *et al.*, 1999). Distinction of such compounds becomes possible due to their  $^1\text{H}$  NMR spectra, assignable to catechin and epicatechin with basis on literature data (Lu and Foo, 1999). In the case of catechin (*trans*-orientation), large couplings are observed between H-2 and H-3 (4.78 and 4.24 ppm,  $J$  7.0 Hz), while for epicatechin (*cis*-orientation) broad singlets at 5.00 and 4.34 ppm are seen for those protons.

Finally, several aromatic compounds are detected between 20 and 40 minutes, but only tryptophane (RT 24.7 min) and *trans*-resveratrol (RT 31.3 min) have been identified so far. Figure VII.19c shows the NMR and MS data that demonstrate the presence of *trans*-resveratrol, a phenolic substance known for its strong antioxidant activity and potential health benefits.

a) RT 15.2 min



b) RT 18.3 min



c) RT 31.3 min

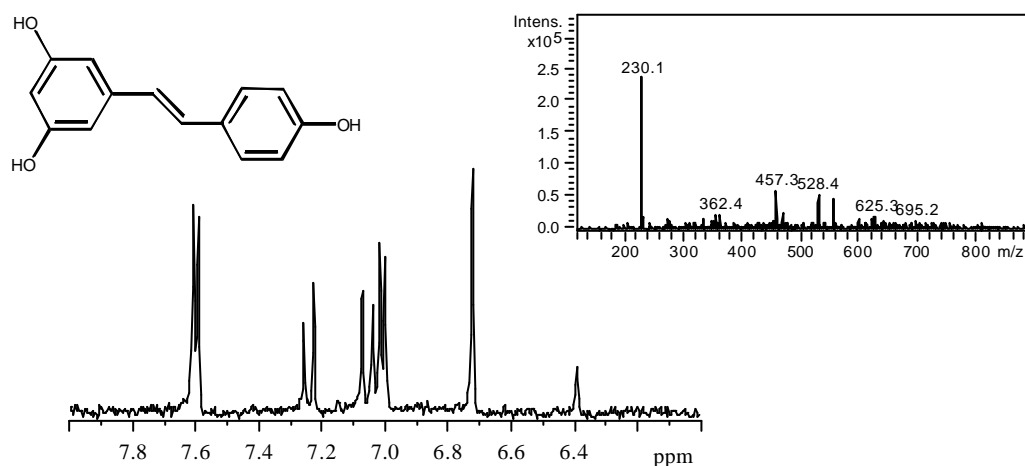


Figure VII.19. <sup>1</sup>H NMR and MS spectra of three fractions of the wine extract collected into loops: a) RT 15.2 min, catechin; b) RT 18.3 min, epicatechin and c) RT 31.3 min, *trans*-resveratrol.

Table VII.5. UV, MS and NMR data of aromatic constituents, obtained by HPLC-NMR/MS analysis of wine phenolic extract, using the continuous-flow method; n.i.: not identified.

RT (min)	$\lambda_{\max}$ (nm)	$m/z$ $M - D$	NMR signals $\delta$ in ppm (mult., $J$ in Hz)	Compound
4.0-7.0	278	172	7.12 (s)	Gallic acid ( $M_w$ 170)
12.5	272	183	2.90 (dd, 15.0 8.0), 3.04 (dd, 15.0 5.0), 3.83, 6.83 (d, 8.5), 7.16 (d, 8.5)	Tyrosine ( $M_w$ 181)
14.2	274	n.i.	3.76 (t, 6.5), 6.83 (d, 8.5), 7.16 (d, 8.5)	Tyrosol ( $M_w$ 138)
15.2	278	294	2.55 (dd, 17.1 8.5), 2.87 (dd, 17.1 5.1), 4.24 (m), 4.78 (d, 7.0), 6.01 (bs), 6.09 (bs), 6.86 (d, 8.2), 6.92 (d, 8.2), 6.92 (bs)	Catechin ( $M_w$ 290)
17.3	305	181	6.37 (d, 16.0), 6.95 (d, 8.6), 7.14 (d, 8.6), 7.21 (s), 7.65 (d, 16.0)	Caffeic acid ( $M_w$ 180)
18.3	278	294	2.76 (dd 17.1, 3.5), 2.94 (dd 17.1, 4.5), 4.34 (bs), 5.00 (bs), 6.09 (bs), 6.11 (bs), 6.95 (bs), 7.06 (s)	Epicatechin ( $M_w$ 290)
24.7	278	206	3.25 (dd 14.0, 6.8), 3.34 (dd 14.5, 5.0), 3.82 (m), 7.20 (t 7.0), 7.28 (t 7.0), 7.31 (s), 7.54 (d 8.0), 7.74 (d 8.0)	Tryptophane ( $M_w$ 204)
31.3	305	230	6.39 (s), 6.72 (s), 7.00 (d 8.5), 7.05 (d 16.5), 7.24 (d 16.5), 7.60 (d 8.5)	<i>trans</i> -Resveratrol ( $M_w$ 228)

## VII.6. Conclusions

HPLC-NMR/MS has been applied to characterise the composition of ripe mango juice (cv. Tommy Atkins). The major sugars and organic acids have been readily identified with basis on both NMR and MS data. Most importantly, a pectic fraction has been separated and its structural characterisation attempted. Unfortunately, this fraction showed no ionisation under the conditions used (positive-ionisation mode) and, thus, information on its molecular weight could not be obtained. The NMR data (1D and TOCSY spectra) revealed the presence of at least two different types of rhamnose: a reducing terminal, for which  $\alpha$ - and  $\beta$ -forms have been identified, and a non-reducing residue, probably interspersed with galacturonic acid residues. Moreover, at least five different galacturonic acid residues have been found to be present in the fraction separated, some of which (at least two) showed methyl esterification at carboxylic groups. The pectic fractions of unripe

and ripe juices (cv. Haden), separated by HPLC and analysed on-line by NMR, have shown several differences. The pectic material detected in the unripe juice has been suggested to consist of larger oligomers, as indicated by the lower spectral resolution, and to contain higher amounts of neutral sugars (galactose and/or arabinose), relatively lower contents of galacturonic acid and only one type of rhamnose (non-reducing). In order to complete this study and obtain more detailed structural information, regarding for instance the sequence of the sugar residues, additional 2D NMR experiments, such as NOESY and  $^1\text{H}$ - $^{13}\text{C}$  correlation experiments, as well as MS and MS/MS data, should be recorded.

Mango juices subject to natural spoilage and to contamination with the mould *Penicillium expansum* have also been analysed by hyphenated NMR, using the continuous-flow HPLC-NMR method. The comparison of the NMR chromatograms obtained for the different juices has enabled the rapid screening of the major compositional changes induced by spoilage and contamination of the fresh juice. Interestingly, some of the new carbohydrates formed upon those effects have been separated and their  $^1\text{H}$  NMR spectra recorded. Although these sugars could not yet be identified, the HPLC-NMR analysis has added valuable information about their structure.

HPLC-NMR/MS applied to the investigation of aromatic constituents of grape juice and of a wine phenolic extract has shown to significantly aid the assignment of these compounds. In grape juice, several cinnamic acids (e.g. *p*-coumaric, *trans*-caftaric, *trans*-coutaric) have been identified, overcoming the difficulties found in the analysis of the 1D and TOCSY spectra of the whole sample. In the wine extract, a range of phenolics such as catechin, epicatechin, caffeic acid and *trans*-resveratrol have been identified.

## References

- Bock, K.; Thøgersen, H. Nuclear magnetic resonance spectroscopy in the study of mono- and oligosaccharides. *Annual Reports on NMR Spectroscopy* **1982**, *13*, 1-57.
- Bravo, L. Polyphenols: chemistry, dietary sources, metabolism and nutritional significance. *Nutrition Reviews* **1998**, *56*, 317-333.
- Bringman, G.; Messer, K.; Wohlfarth, M.; Kraus, J.; Dumbuya, K.; Ruckert, M. HPLC-CD on-line coupling in combination with HPLC-NMR and HPLC-MS/MS for the determination of the full absolute stereostructure of new metabolites in plant extracts. *Analytical Chemistry* **1999**, *71*, 2678-2686.

Brinson, K.; Prakash, M.D.; John, M.A.; Pridham, J.B. Post-harvest changes in *mangifera indica* cell walls and cytoplasmic polysaccharides. *Phytochemistry* **1988**, *27*, 719-723.

Colquhoun, I.J.; de Ruiter, G.A.; Schols, A.; Voragen, G.J. Identification by NMR spectroscopy of oligosaccharides obtained by treatment of the hairy regions of apple pectin with rhamnogalacturonase. *Carbohydrate Research* **1990**, *206*, 131-144.

Daykin, C.A.; Corcoran, O.; Hansen, S.H.; Bjornsdottir, I.; Cornett, C.; Connor, S.C.; Lindon, J.C.; Nicholson, J.K. Application of directly coupled HPLC NMR to separation and characterization of lipoproteins from human serum. *Analytical Chemistry* **2001**, *73*, 1084-1090.

Exarchou, V.; Troganis, A.; Gerothanassis, I.P.; Tsimidou, M.; Boskou, D. Identification and quantification of caffeic and rosmarinic acid in complex plant extracts by the use of variable-temperature two-dimensional nuclear magnetic resonance spectroscopy. *Journal of Agricultural and Food Chemistry* **2001**, *49*, 2-8.

Fulcrand, H.; Doco, T.; Es-Safi, N.; Cheynier, V.; Moutounet, M. Study of the acetaldehyde induced polymerization of flavan-3-ols by liquid chromatography ion spray mass spectrometry. *Journal of Chromatography A* **1996**, *752*, 85-91.

Fulcrand, H.; Remy, S.; Souquet, J.-M.; Cheynier, V.; Moutounet, M. Study of wine tannin oligomers by on-line liquid chromatography electrospray ionization mass spectrometry. *Journal of Agricultural and Food Chemistry* **1999**, *47*, 1023-1028.

Gerothanassis, I.P.; Exarchou, V.; Lagouri, V.; Troganis, A.; Tsimidou, M.; Boskou, D. Methodology for identification of phenolic acids in complex phenolic mixtures by high-resolution two-dimensional nuclear magnetic resonance. Application to methanolic extracts of two oregano species. *Journal of Agricultural and Food Chemistry* **1998**, *46*, 4185-4192.

Hansen, S.H.; Jensen, A.G.; Cornett, C.; Bjornsdottir, I.; Taylor, S.; Wright, B.; Wilson, I.D. High-performance liquid chromatography on-line coupled to high-field NMR and mass spectrometry for structure elucidation of constituents of *Hypericum perforatum* L. *Analytical Chemistry* **1999**, *71*, 5235-5241.

Lazarus, S.A.; Adamson, G.E.; Hammerstone, J.F.; Schmitz, H.H. High-performance liquid chromatography/mass spectrometry analysis of proanthocyanidins in foods and beverages. *Journal of Agricultural and Food Chemistry* **1999**, *47*, 3693-3701.

Lindon, J.C.; Nicholson, J.K.; Wilson, I.D. Direct coupling of chromatographic separations to NMR spectroscopy. *Progress in Nuclear Magnetic Resonance Spectroscopy* **1996**, *29*, 1-49.

Lizada, C. Mango. In *Biochemistry of Fruit Ripening*; Seymour, G.B., Taylor, J.E., Tucker, G.A., Eds.; Chapman & Hall: London, 1993; 255-271.

- Lommen, A.; Godejohann, M.; Venema, D.P.; Hollman, P.C.H.; Spraul, M. Application of directly coupled HPLC-NMR-MS to the identification and confirmation of quercetin glycosides and phloretin glycosides in apple peel. *Analytical Chemistry* **2000**, *72*, 1793-1797.
- Lu, Y.; Foo, L.Y. The polyphenol constituents of grape pomace. *Food Chemistry* **1999**, *65*, 1-8.
- Maraschin, M.; Passos, R.; Duarte da Silva, J.M.O.; Dias, P.F.; Araujo, P.S.; Oltramari, J.D.; Fontana, J.D.; Caro, M.S.B. Isolation and *trans*-resveratrol analysis in Brazilian red wine by <sup>1</sup>H nuclear magnetic resonance. In *Magnetic Resonance in Food Science - a View to the Future*; Webb, G.A., Belton, P.S., Gil, A.M., Delgadillo, I. Eds.; The Royal Society of Chemistry: Cambridge, 2001; 136-139.
- Neiss, T.G.; Cheng, H.N.; Daas, P.J.H.; Schols, H.A. Compositional heterogeneity in pectic polysaccharides: NMR studies and statistical analysis. *Macromolecules Symposium* **1999**, *140*, 165-178.
- Pérez-Magariño, S.; Revilla, I.; González-SanJosé, M.L.; Beltrán, S. Various applications of liquid chromatography-mass spectrometry to the analysis of phenolic compounds. *Journal of Chromatography A* **1999**, *847*, 75-81.
- Peynaud, E.; Ribéreau-Gayon, P. The Grape. In *The Biochemistry of Fruits and Their Products*; Hulme, A.C., Ed.; Academic Press: London, 1971; 171-205.
- Pusecker, K.; Albert, K.; Bayer, E. Investigation of hop and beer bitter acids by coupling of high-performance liquid chromatography to nuclear magnetic resonance spectroscopy. *Journal of Chromatography A* **1999**, *836*, 245-252.
- Revilla, E.; Ryan, J.-M. Analysis of several phenolic compounds with potential antioxidant properties in grape extracts and wines by high-performance liquid chromatography-diode array detection without sample preparation. *Journal of Chromatography A* **2000**, *881*, 461-469.
- Schols, H.A.; Voragen, A.G.J.; Colquhoun, I.J. Isolation and characterization of rhamnogalacturonan oligomers, liberated during degradation of pectic hairy regions of rhamnogalacturonase. *Carbohydrate Research* **1994**, *256*, 97-111.
- Shockcor, J.P.; Unger, S.E.; Wilson, I.D.; Foxall, P.J.D.; Nicholson, J.K.; Lindon, J.C. Combined HPLC, NMR spectroscopy, and ion-trap mass spectrometry with application to the detection and characterization of xenobiotic and endogenous metabolites in human urine. *Analytical Chemistry* **1996**, *68*, 4431-4435.
- Sidelmann, U.G.; Braumann, U.; Hofmann, M.; Spraul, M.; Lindon, J.C.; Nicholson, J.K.; Hansen, S.H. Directly coupled 800 MHz HPLC-NMR spectroscopy of urine and its application to the identification of the major phase II metabolites of tolfenamic acid. *Analytical Chemistry* **1997**, *69*, 607-612.

Singleton, V.L. Zaya, J.; Trousdale, E.K. Caftaric and coumaric acids in fruit of *Vitis*. *Phytochemistry* **1986**, *25*, 2127-2133.

Spanos, G.A.; Wrolstad, R.E. Phenolics of apple, pear and white grape juices and their changes with processing and storage – a review. *Journal of Agricultural and Food Chemistry* **1992**, *40*, 1478-1487.

Spraul, M.; Hofmann, M. 750 MHz NMR spectroscopy and food-related LC-NMR applications. In *Magnetic Resonance in Food Science*; Belton, P.S., Delgadillo, I., Gil, A.M., Webb, G.A., Eds.; The Royal Society of Chemistry: Cambridge, 1995; 77-92.

Tjan, S.B.; Voragen, A.G.J.; Pilnik, W. Analysis of some partly and fully esterified oligogalactopyranuronic acids by p.m.r. spectrometry at 220 MHz. *Carbohydrate Research* **1974**, *34*, 15-23.

Tucker, G.A. Introduction. In *Biochemistry of Fruit Ripening*; Seymour, G.B., Taylor, J.E., Tucker, G.A., Eds.; Chapman & Hall: London, 1993; 1-51.

Tucker, G.A.; Seymour, G.B. Cell wall degradation during mango fruit ripening. *Acta Horticulturae* **1991**, *291*, 454-460.

## **VIII. CHARACTERISATION OF BEER COMPOSITION BY NMR AND HYPHENATED NMR (HPLC-NMR/MS)**

VIII.1. Introduction.....	222
VIII.2. Materials and Methods.....	223
VIII.2.1. Sample Preparation.....	223
VIII.2.2. NMR and HPLC-NMR/MS Measurements.....	223
VIII.3. Characterisation of Beer Composition by High Resolution NMR .....	226
VIII.4. Characterisation of Beer Composition by HPLC-NMR/MS.....	233
VIII.4.1. Application to Carbohydrates.....	233
VIII.4.2. Application to Aromatic Compounds.....	240
VIII.5. Conclusions.....	244
References.....	244

## VIII.1. Introduction

There has been great interest in studying the chemical composition of beer, as this information is essential for the assessment of beer quality and the development of new products. The data reported in the literature, summarised in Chapter I.3, has been obtained with basis on analytical techniques that often involve some kind of pre-treatment of the beer sample in order to concentrate the desired group of compounds. Moreover, the choice of method and protocol followed depends on the specific family/type of compounds under study, making the process of overall characterisation of beer very time consuming. High resolution NMR has already proved useful for studying the composition of different liquid foods such as fruit juices (Belton *et al.*, 1996; Belton *et al.*, 1997; Gil *et al.*, 2000; Le Gall *et al.*, 2001), coffee (Bosco *et al.*, 1999), olive oil (Sacchi *et al.*, 1996) and wine (Ramos and Santos, 1999; Kosir and Kidric, 2001; Brescia *et al.*, 2002), offering the advantages of giving information about a very wide range of different components in a single experiment, in which the sample is analysed directly and non-invasively.

In this work, the first direct characterisation of beer composition by NMR is reported (Duarte *et al.*, 2002), although the technique has already been applied to specific problems such as the identification of hop bitter acids using HPLC-NMR (Pusecker *et al.*, 1999), and of oligosaccharides in beer fractions obtained by HPLC (Vinogradov and Bock, 1998). In addition, the further investigation of some beer components (carbohydrates and aromatic compounds) is carried out in this work by HPLC-NMR/MS. Carbohydrates are the major non-volatile components of beer and have a marked influence on beer taste and body. Monitoring of the carbohydrate composition in wort and beer is therefore extremely important for modern brewing technology and particularly in the development of new sorts of beer and in the selection of raw materials and yeast strains. The composition of beer in carbohydrates has been studied for many years, mostly by chemical and enzymatic analysis (Shanta-Kumara *et al.*, 1995) and by chromatographic methods, (Uchida *et al.*, 1991; Corradini *et al.*, 1997; Désévaux *et al.*, 1997). High-performance anion-exchange chromatography with pulsed amperometric detection (HPAEC-PAD) is particularly well-established for the analysis of malto-oligosaccharides, but the need for reference standards and the difficulty to separate isomeric structures, for instance branched dextrans of a given degree of polymerisation, are important limitations of this method (Jodelet *et al.*, 1998). High resolution NMR has been shown to be a powerful tool for the structure elucidation of

dextrin mixtures derived from starch (Jodelet *et al.*, 1998; Van der Burgt *et al.*, 2000) and of beer oligosaccharides separated by HPLC (Vinogradov and Bock, 1998). In this work, the on-line coupling of HPLC with both NMR and MS is applied to the direct analysis of two beer samples, in order to investigate and compare their composition in fermentable sugars and dextrans. The aromatic composition of one of these beers is also investigated by HPLC-NMR/MS, helping to overcome the assignment difficulties related to the low abundance of these substances and the high degree of overlap in the aromatic region of the  $^1\text{H}$  spectrum.

## **VIII.2. Materials and Methods**

### **VIII.2.1. Sample Preparation**

The two beer samples used in the present study were an ale beer produced in England (beer 1) and a lager beer produced in the U.S.A. (beer 2). Both beers were kindly provided by the Brewing Research International (U.K.). For NMR analysis, the beer samples were degassed in an ultrasonic bath during 10 minutes and prepared to contain 10%  $\text{D}_2\text{O}$  and 0.02% sodium 3-(trimethylsilyl)-propionate (TSP) as chemical shift reference. For HPLC-NMR/MS analysis of carbohydrates, the beers were simply degassed before injection, whereas for the characterisation of aromatic compounds the samples were concentrated to approximately 2/3 of the initial volume by rotor evaporation at 40°C during 20-30 minutes.

### **VIII.2.2. NMR and HPLC-NMR/MS Measurements**

1D and 2D NMR spectra of the beer samples were recorded on a Bruker Avance DRX-500 spectrometer, operating at 500.13 MHz for proton and 125.77 MHz for carbon. The  $^1\text{H}$  1D spectra were acquired using the 'noesypr1dsp' pulse program, with saturation of water (4.77 ppm) and ethanol (1.17 and 3.64 ppm) resonances by applying a modulated shaped pulse, with triple offset and amplitude scaling, during relaxation delay (2.0 s) and mixing time (100 ms). 128 transients were collected into 16384 data points with a spectral width of 5482.46 Hz. The TOCSY spectra were acquired in the phase sensitive mode using time proportional phase incrementation (TPPI), and the MLEV17 pulse sequence was used for the spin lock. A modulated shaped pulse for presaturation of water and ethanol

resonances was applied (pulse program 'lcmlevpcpstp'). 16 scans were collected for each of the 512 increments, using a spectral width of 5482.46 Hz in both dimensions, 2048 data points, a mixing time of 100 ms and a relaxation delay of 1.5 seconds.  $^1\text{H}$ - $^{13}\text{C}$  phase sensitive (Echo/Antiecho-TPPI) heteronuclear single quantum correlation (HSQC) spectra were recorded with inverse detection and  $^{13}\text{C}$  decoupling during acquisition (pulse program 'invietgpsi'). 2048 data points with 64 scans per increment and 300 increments were acquired with spectral widths of 5482.46 Hz and 25157.23 Hz in the proton and carbon dimensions, respectively. *J*-resolved spectra were measured with a shaped pulse for triple suppression of water and ethanol resonances (pulse program 'lcjresps'). 8192 data points were acquired with 8 scans for each of 128 increments, using a spectral width of 8012.82 Hz in the proton dimension and 31.30 Hz in the *J* dimension.

The HPLC-NMR/MS measurements were performed using the instrumentation described in Chapter VII.2.2. For the study of carbohydrates, chromatographic separation was carried at 35°C, using a 300 x 7.8 mm cation-exchange ION-300 column with a particle size of 5.0  $\mu\text{m}$ , at a flow rate of 0.3 ml/min, with diode array detection at 200 and 220 nm. The injection volume was 100  $\mu\text{l}$  and the mobile phase consisted of 0.0085N  $\text{H}_2\text{SO}_4$  in  $\text{D}_2\text{O}$ .

$^1\text{H}$  NMR spectra were recorded at 500 MHz using the continuous-flow and the loop-sampling modes. For continuous-flow experiments, successive NMR spectra were acquired automatically, co-adding 16 transients and using 8192 data points with a spectral width of 5000 Hz. Acquisition time was 0.82 s, with 1.8 s delay between transients. A pulse sequence with presaturation during relaxation delay was used (program 'lc2pr' from the Bruker library). 1D  $^1\text{H}$  NMR spectra of loops were recorded using multiple solvent suppression with time-shared double presaturation of water and acetonitrile  $^1\text{H}$  frequencies by means of a shaped low power RF-pulse and CW-decoupling on the F2- channel for the decoupling of the  $^{13}\text{C}$  satellites of residual acetonitrile (present in the system even when using 100%  $\text{D}_2\text{O}$ ). 128 transients were collected into 32768 computer data points with a spectral width of 10000 Hz and an acquisition time of 1.6 s. Prior to Fourier transformation, an exponential multiplication was applied to the FID, corresponding to a line broadening of 1.0 Hz. In addition to the 1D spectra, phase-sensitive TOCSY experiments with WET (water suppression enhanced through  $T_1$  effects) and  $^{13}\text{C}$

decoupling during WET were carried out. A total of 16 increments with 128 transients and 2048 computer data points were acquired in simultaneous mode with a spectral width in both dimensions of 10000 Hz. The applied mixing time of the MLEV spin lock was 65 ms. The data were apodized with a shifted squared sine bell window function 2.5 Hz in both dimensions and zero-filled in the  $f_1$  dimension to 1024 data points.

Electrospray ionisation (ESI) was carried out in positive-ionisation mode and mass spectra were acquired up to  $m/z$  3000 after adding 50  $\mu$ l/min of 20 mM aqueous sodium acetate solution to the split ratio of the eluent via a T-piece with a syringe pump.

For the study of aromatic compounds, chromatographic separation was carried out at 35°C, using a 250 x 4 mm Purospher reverse phase (RP18) column from Merck, with a particle size of 5.0  $\mu$ m, at a flow rate of 1.00 ml/min, with diode array detection in the UV-Vis region. The injection volume was 500  $\mu$ l. The mobile phase consisted of a mixture of D<sub>2</sub>O (containing 0.06% formic acid) and acetonitrile, changing in composition according to the following gradient: 0 min - 3% acetonitrile, 40 min - 40 % acetonitrile, 60 min - 100 % acetonitrile, 70 min - 3% acetonitrile.

<sup>1</sup>H NMR spectra were obtained at 500 MHz using the time-sliced stop-flow and the loop-sampling methods. Each spectrum in the time slice array was recorded with double solvent suppression of water and acetonitrile signals (pulse program 'lc1wetdw'). 32 transients were collected into 32768 computer data points with a spectral width of 10000 Hz, and an acquisition time of 1.6 s. The FIDs (free induction decays) were combined in a 2D serial file and an exponential multiplication was applied prior to Fourier transformation resulting in a line broadening of 1.0 Hz. When using the time-sliced method, no MS data could be acquired because of the interruption of the flow during the NMR measurement. 1D <sup>1</sup>H NMR spectra of fractions collected into loops were acquired using the same conditions as described above, but with a higher number of scans (128/512).

ESI-MS analysis of loops was carried out in positive and negative ionisation modes, using automatic switch between MS and MS/MS in order to identify fragment ions.

### VIII.3. Characterisation of Beer Composition by High Resolution NMR

Figure VIII.1 shows the  $^1\text{H}$  1D spectrum of an ale beer, recorded at 500 MHz, with suppression of ethanol ( $\delta$  1.17 and 3.64 ppm) and water ( $\delta$  4.77 ppm) signals. The general high spectral complexity clearly shows the potential of the technique to enable the identification of many different compounds, present in a wide range of concentrations. In order to aid spectral assignment, the results obtained from TOCSY,  $^1\text{H}$ - $^{13}\text{C}$  correlation and  $J$ -resolved spectra were combined. These 2D spectra, shown in Figures VIII.2, VIII.3 and VIII.4, contain a significant number of signals even for the less abundant compounds resonating in the aliphatic and aromatic regions, thus enabling the identification of several beer components, as exemplified in Figure VIII.2. Table VII.1 shows a complete list of the signals assigned in the beer spectra.

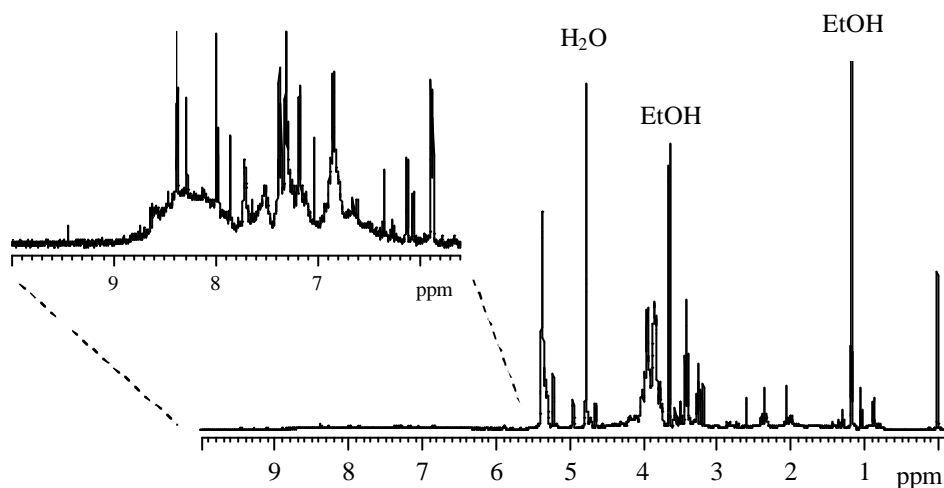


Figure VIII.1. 500 MHz  $^1\text{H}$  NMR spectrum of an ale beer, with triple suppression of water and ethanol resonances; NS 128. The Figure insert shows an expansion of the aromatic region.

In the aliphatic region, peaks from alcohols (ethanol, propanol, isobutanol, isopentanol), aliphatic organic acids (e.g. citric, malic, pyruvic, acetic, succinic) and amino acids (e.g. alanine,  $\beta$ -aminobutyric acid, proline) are observable. Furthermore, two aliphatic spin systems have been tentatively assigned to lipids, possibly medium chain fatty acids that are known to occur in beer (Table VIII.1). These compounds contribute importantly for the characteristic flavour of beer, being also responsible for off-flavours if present in excessive concentrations (Hawthorne *et al.*, 1986). None of these spin systems show correlations with unsaturated proton or carbon resonances which suggests that the lipids detected are mostly of the saturated type.

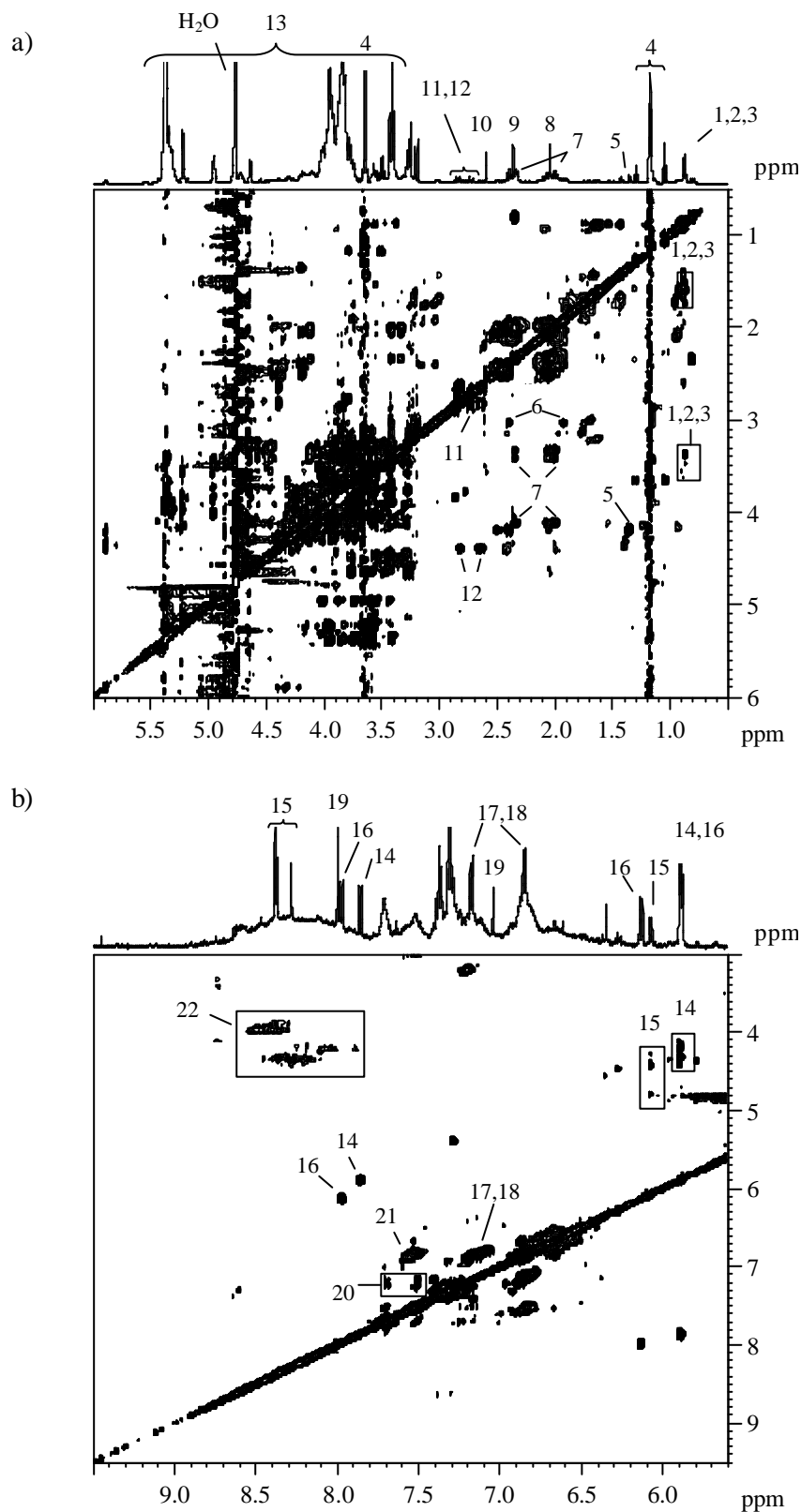


Figure VIII.2. Expansions of the 500 MHz TOCSY spectrum of the ale beer; NS 16 in  $f_2$ . Some assignments are indicated: 1-propanol, 2-isobutanol, 3-isopentanol, 4-ethanol, 5-lactic acid, 6 GABA, 7-proline, 8-acetic acid, 9-pyruvic acid, 10-succinic acid, 11-citric acid, 12-malic acid, 13-dextrins, 14-uridine, 15-adenosine/inosine, 16-cytidine, 17,18-tyrosine/tyrosol, 19-histidine, 20-tryptophane, 21,22-polyphenols.

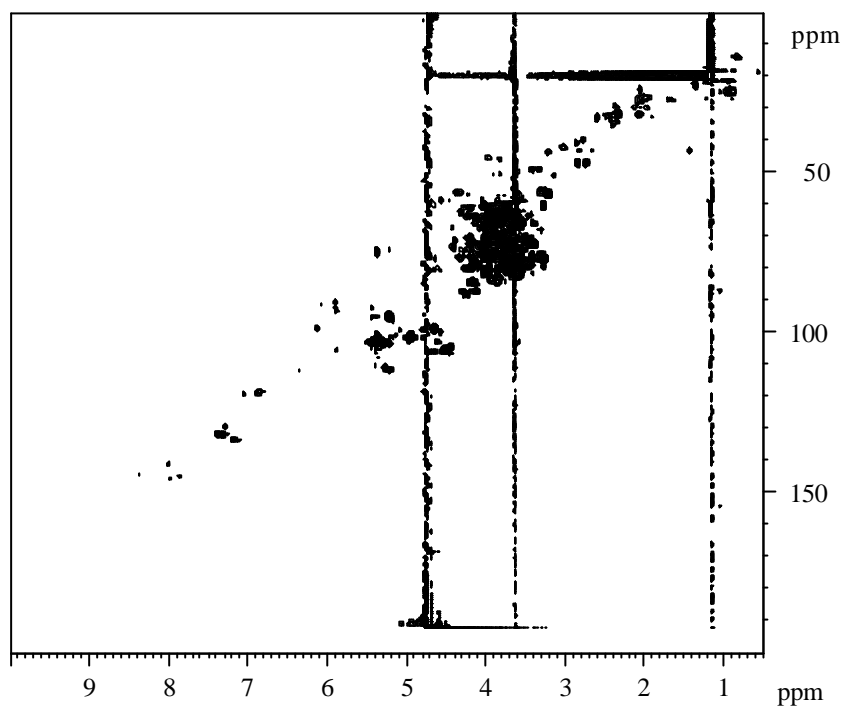


Figure VIII.3. 500 MHz HSQC spectrum of the ale beer; NS 64 in  $f_2$ .

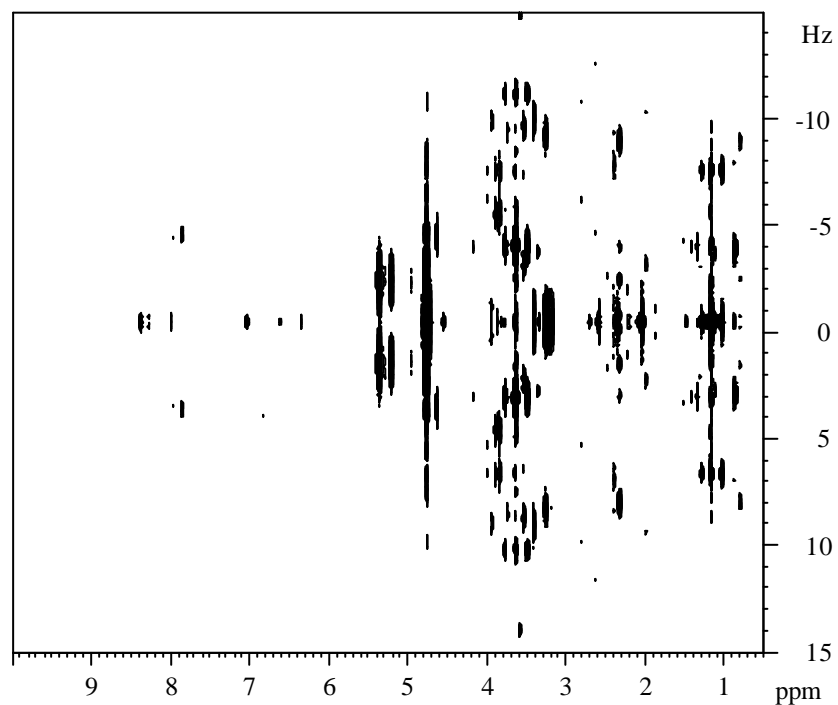


Figure VIII.4. 500 MHz homonuclear  $J$ -resolved spectrum of the ale beer; NS 8 in  $f_2$ .

The 3.0-6.0 ppm region of the spectrum reflects the strong contribution of beer carbohydrates. This region shows relatively lower resolution, compared to the remaining parts of the spectrum, reflecting the predominance of medium- and/or high-molecular weight dextrans, undergoing slow molecular tumbling, and, hence, leading to fast transverse relaxation and broader signals. However, spectral distinction between dextrans of different sizes is extremely difficult because of strong peak overlap in both uni- and bi-dimensional NMR spectra (Figures VIII.2 to VIII.4). The spectral similarity for different glucose oligomers is illustrated by the set of 1D  $^1\text{H}$  NMR spectra of standard solutions shown in Figure VIII.5, where, as expected, spectral resolution is strongly dependent on molecular size, reflecting the shortening of transverse relaxation times for larger molecules. The linear carbohydrates maltose, maltotriose and maltoheptose, consisting of glucose monomers linked by  $\alpha$  (1-4) linkages, show similar overlapping profiles. Partial assignment may be carried out with basis on NMR data reported for dextrans (Jodelet *et al.*, 1998; Vinogradov and Bock, 1998). In the anomeric region (4.5-5.5 ppm), the protons H1 of the reducing glucose ring of the  $\alpha$  and  $\beta$  anomers give rise to the doublets at 5.22 and 4.63 ppm, respectively. The non-reducing H1 protons engaged in  $\alpha$  (1-4) glycosidic linkages resonate at about 5.38 ppm, whereas those involved in  $\alpha$  (1-6) linkages are shifted upfield to about 4.96 ppm, as seen for isomaltose (Figure VIII.5c). In the beer spectrum (Figure VIII.5g), the group of overlapped signals in the 5.3-5.4 ppm range reveals the presence of different-sized linear glucose segments, while the 4.96 ppm peak is indicative of branched carbohydrates containing the  $\alpha$  (1-6) linkage. However, in such a complex mixture, further assignment is hindered by the broad and overlapped nature of the spectrum, thus calling for improved analytical methods.

The aromatic spectral region is one of the most interesting regions due to the very low relative abundance of aromatic metabolites. As shown in the TOCSY spectrum (Figure VIII.2b), quite a few homonuclear correlations are detected, either within the aromatic region or with resonances appearing at higher field. With support from the  $^1\text{H}$ - $^{13}\text{C}$  and *J*-resolved spectra (Figures VIII.3 and VIII.4, respectively), the assignment of most of the stronger peaks has been carried out showing the presence of compounds like tyrosine, tryptophane, uridine, adenosine/inosine and cytidine. The underlying broad humps between 6.7 and 8.7 ppm may result from large molecular weight aromatic compounds, possibly polyphenols (Table VIII.1). Interestingly, the broad resonances at 7.9-8.7 ppm show weak

correlations with broad resonances at 3.8-4.5 ppm. This suggests the presence of non-aromatic moieties in the polyphenols fraction; however, alternative and/or complementary methods are required in order to characterise the nature of these moieties.

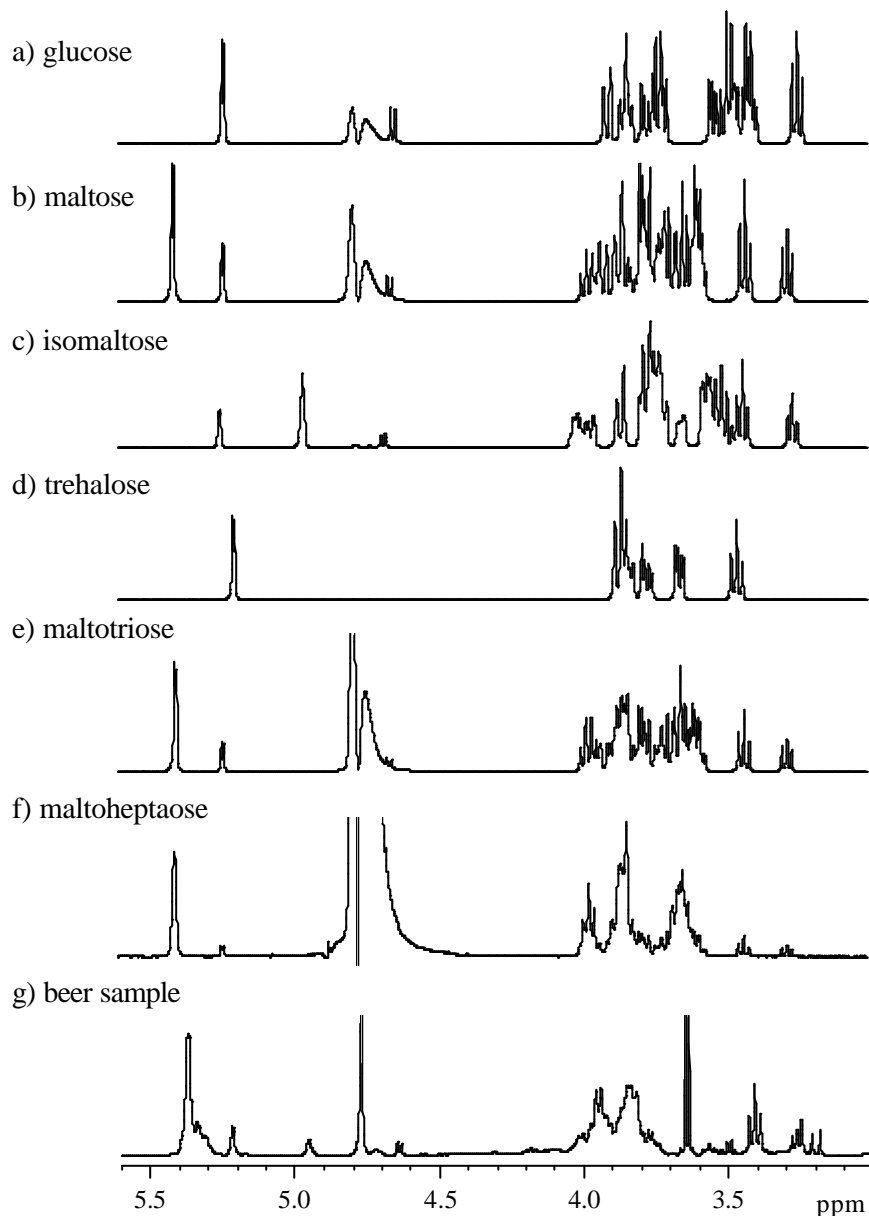


Figure VIII.5. 500 MHz <sup>1</sup>H NMR spectra of (a-f) standard solutions and of (g) the ale beer shown in Figure VIII.1; NS 32 for standards and 128 for the beer sample.

As shown in Table VIII.1, about 30 compounds have been assigned in the beer sample investigated, whereas about 30 more spin systems have been identified, but their assignment still remains unknown, requiring further investigation.

Table VIII.1.  $^1\text{H}$  and  $^{13}\text{C}$  chemical shifts, proton multiplicity and  $J_{\text{HH}}$  for assigned compounds in an ale beer. s: singlet, d: doublet, t: triplet, q: quartet, dd: doublet of doublets, m: multiplet; <sup>(a)</sup> tentative identification; n.i.: not identified.

Compound	Assignment	$^1\text{H}$ (ppm)		Multiplicity	$J$ (Hz)	$^{13}\text{C}$ (ppm)
Acetaldehyde	$\text{CH}_3$	2.23		d	3.0	32.22
	CH	9.67				
Acetaldehyde hydrate	$\text{CH}_3$ , hydrate	1.32				
	CH, hydrate	5.24				
Acetic acid / Acetates	? $\text{CH}_3$	2.04		s		23.82
Adenosine/Inosine	C4'H, ribose	4.27				
	C3'H, ribose	4.41				
	C2'H, ribose	4.79				
	C1'H, ribose	6.07		d		
	C8H, ring	8.28		s		
	C2H, ring	8.37		s		
Alanine	? $\text{CH}_3$	1.51		d	7.2	
	?CH	3.77				
?-Aminobutyric acid (GABA)	? $\text{CH}_2$	1.92				26.28
	? $\text{CH}_2$	2.39		t	7.2	32.28
	? $\text{CH}_2$	3.02		t	7.2	41.83
Citric acid	?, ?CH	2.72		d	15.7	46.50
	?', ?'CH	2.84		d	15.7	
Cytidine	C1'H, ribose	5.86				
	C6H, ring	6.13		d	7.9	98.36
	C5H, ring	7.97		d	7.9	145.72
Ethanol	$\text{CH}_3$	1.17		t	7.2	19.56
	$\text{CH}_2$	3.64		q	7.2	60.19
Ethyl ester (e.g. ethyl acetate)	$\text{CH}_3$	1.24		t		12.92
	$\text{OCH}_2$	4.12				60.34
Fatty acids <sup>(a)</sup> (saturated)	? $\text{CH}_3$	0.89	0.95			
	$\text{CH}_2\text{-CH}_3$	1.30	1.53			
	$\text{CH}_2\text{-CH}_2\text{-CH}_3$	1.58	1.70			
	$\text{CH}_2\text{-COOH}$	2.33				
Formic acid <sup>(a)</sup>	$\text{HCOOH}$	8.38		s		
Histidine	C4H, ring	7.03		s		119.00
	C2H, ring	7.99		s		140.62
Isobutanol	$\text{CH}_3$	0.87		d	6.6	
	CH	1.73				
Isoleucine	$\text{CH}_2\text{OH}$	3.36		d	6.5	
	? $\text{CH}_3$	0.92		t		
	? $\text{CH}_3$	1.00		d		
	?CH	1.25				
	?'CH	1.46				
	?CH	1.96				
	?CH	3.64				

Table VIII.1 (cont.)

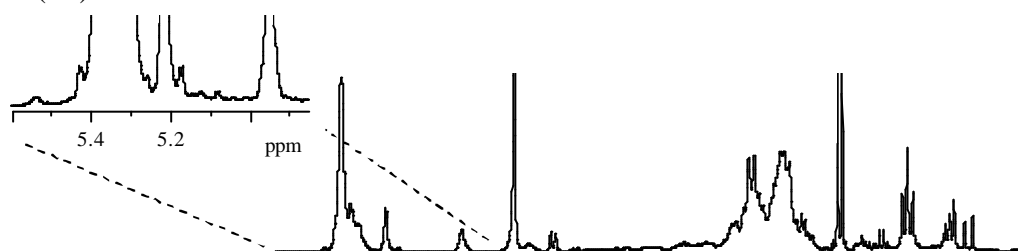
Compound	Assignment	$\delta$ $^1\text{H}$ (ppm)	Multiplicity	$J$ (Hz)	$\delta$ $^{13}\text{C}$ (ppm)		
Isopentanol	$\text{CH}_3$	0.88	d	6.6	24.60		
	CH	1.42					
	$\text{CH}_2$	1.64					
	$\text{CH}_2\text{OH}$	3.63					
Lactic acid	$\text{CH}_3$	1.35	d	7.0	22.48		
	? CH	4.19	q	7.0	70.87		
Leucine	?, ?' $\text{CH}_3$ ?	0.94					
	$\text{CH}_2$ , ?CH	1.70					
Malic acid	?CH	2.63	dd	7.5;16.2	42.78		
	?'CH	2.82	dd	4.4;16.1			
	? CH	4.38			71.20		
Malto- oligosaccharides	?C1H (red.)	4.64	d	8.0	98.50		
	? C1H (red.)	5.22	d	3.7	94.58		
	C1H ? (1-6)	4.96			101.28		
	C1H ? (1-4)	5.3-5.4			~102		
Phenylalanine	C3H, C5H, ring	7.33					
	C4H, ring	7.37					
	C2H, C6H, ring	7.43					
Polyphenols <sup>(a)</sup>	n.i.	6.84					
	n.i.	7.51					
Polyphenols with non- aromatic moiety <sup>(a)</sup>	n.i.	3.8-4.0	4.1-4.4				
	n.i.	8.2-8.6	7.9-8.5				
Proline	? $\text{CH}_2$	2.00	m		26.60		
	?'CH	2.06	m		31.70		
	?CH	2.33	m		31.70		
	?'CH	3.32			48.90		
	?CH	3.41			48.90		
	? CH	4.11			64.06		
Propanol	$\text{CH}_3$	0.88	t	7.5	13.7		
	$\text{CH}_2$	1.53	m		26.9		
	$\text{CH}_2\text{OH}$	3.54	t	5.8	62.46		
Pyruvic acid	? $\text{CH}_3$	2.35	s		29.12		
	?, ? $\text{CH}_2$	2.59	s		32.79		
Tryptophane	C5H, ring	7.15					
	C6H, ring	7.24					
	C7H, ring	7.50			114.49		
	C4H, ring	7.69					
Tyrosine / Tyrosol	C3H, C5H, ring	6.81	6.85	d	8.5	118.2	118.2
	C2H, C6H, ring	7.11	7.17	d	8.5	133.3	133.1
Uridine	C4'H	4.11					
	C3'H	4.21					
	C2'H	4.38					
	C5H, ring	5.88	d	8.2	105.00		
	C1'H	5.89			90.51		
	C6H, ring	7.85	d	8.2	144.56		

## VIII.4. Characterisation of Beer Composition by HPLC-NMR/MS

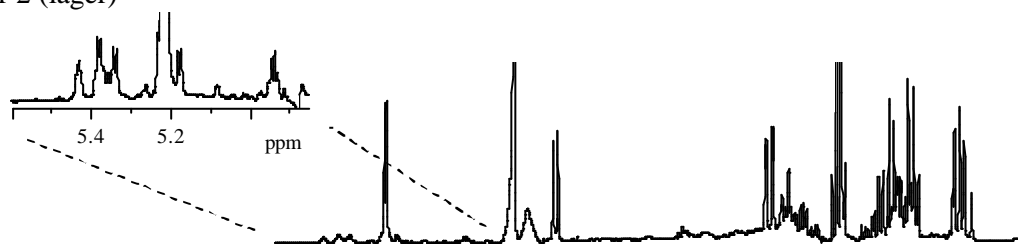
### VIII.4.1. Application to Carbohydrates

The ale beer shown in the previous section (beer 1) and a lager beer (beer 2), characterised by a significantly different carbohydrate composition, were chosen for a more thorough carbohydrate characterisation using HPLC-NMR/MS. The sugar regions of their  $^1\text{H}$  NMR spectra, as well as of the spectrum of another lager (beer 3), are shown in Figure VIII.6. The spectra of beers 1 and 3 are similar, both in terms of resolution and spectral profile, indicating that the two beer types, ale and lager, do not necessarily show distinct carbohydrate compositions. The spectrum of beer 2, on the other hand, shows a well-resolved sugar region due to the predominance of low molecular weight carbohydrates, namely glucose. In addition, the inserts shown in the Figure for beers 1 and 2 show the presence of a number of minor carbohydrates besides the predominant compounds.

a) beer 1 (ale)



b) beer 2 (lager)



c) beer 3 (lager)

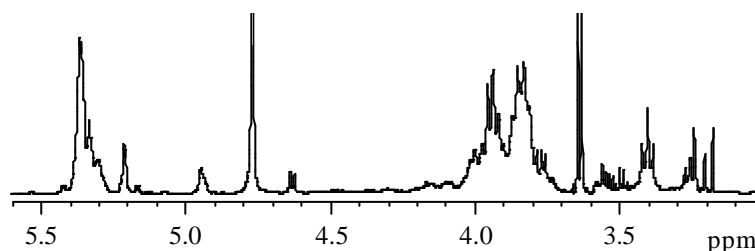


Figure VIII.6. Mid-field region of the 500 MHz  $^1\text{H}$  NMR spectra of three beer samples; NS 128. The inserts show the additional peaks observed in the anomeric regions.

The continuous-flow NMR chromatogram obtained for beer 1 is shown in Figure VIII.7a and the carbohydrates identified are listed in Table VIII.2. Some components are readily separated and identified through their NMR spectra, namely ethanol (RT 45.0 min), glycerol (RT 30.0 min), fructose (RT 22.5 min) and citric acid (RT 19.5 min). In the case of glycerol ( $\delta$  3.48, 3.57 and 3.70 ppm), it should be noted that its detection by NMR of beer is usually hindered by overlap with sugar signals and by the effects of ethanol suppression at 3.64 ppm. The major beer carbohydrates elute at retention times between 12 and 17 min, showing poor separation, as expected with basis on their similar sizes and structures. Figure VIII.7b shows some of the rows extracted from the continuous-flow NMR chromatogram in that range of retention times. The observed profiles are consistent with the presence of malto-oligosaccharides (dextrins) of different sizes and structures, the larger ramified compounds eluting first, as shown by the poorer resolution of the earlier spectra, followed by smaller compounds. Integration of selected anomeric signals may give estimates of the average number of glucose units and branching points per molecule (Jodelet *et al.*, 1998). The average number of glucose units per molecule is given by the ratio of the summed areas of H1 protons in both  $\alpha$  (1-4) and  $\alpha$  (1-6) glycosidic linkages (signals at 5.3-5.4 and 4.9-5.0 ppm, respectively) and the summed areas for the reducing H1 protons (5.2 and 4.6 ppm for the  $\alpha$  and  $\beta$  anomers, respectively). The average number of branching points per molecule is estimated by the ratio of the integral of the peak for H1 protons in  $\alpha$  (1-6) linkages (4.9-5.0 ppm) and that of the peak for H1 protons in  $\alpha$  (1-4) linkages (5.3-5.4 ppm), multiplied by the number of total linkages. The results of these calculations are shown in the second and third columns of Table VIII.2. It must be noted that the fractions considered are mixtures of carbohydrates and, hence, the numbers estimated represent average values.

The MS data recorded for the same fractions (Figure VIII.7c), using the positive-ionisation mode, give more precise and detailed information about the size of the dextrins present, enabling the detection of glucose oligomers with degrees of polymerisation (DP) varying from 2 to 9 (Table VIII.2). For the fraction eluting at 12.3 min, the MS spectrum shows peaks at  $m/z$  522, 604, 685 and 766 that arise from the double-charged ions  $[M + 2Na]^{2+}$  of partially deuterated dextrins with DP6, DP7, DP8 and DP9, respectively. The ions  $[M + Na]^+$  are also detected for DP6, DP7 and DP8 ( $m/z$  1019, 1182 and 1345), but not for DP9, which only forms the  $[M + 2Na]^{2+}$  ion. This is in agreement with previous

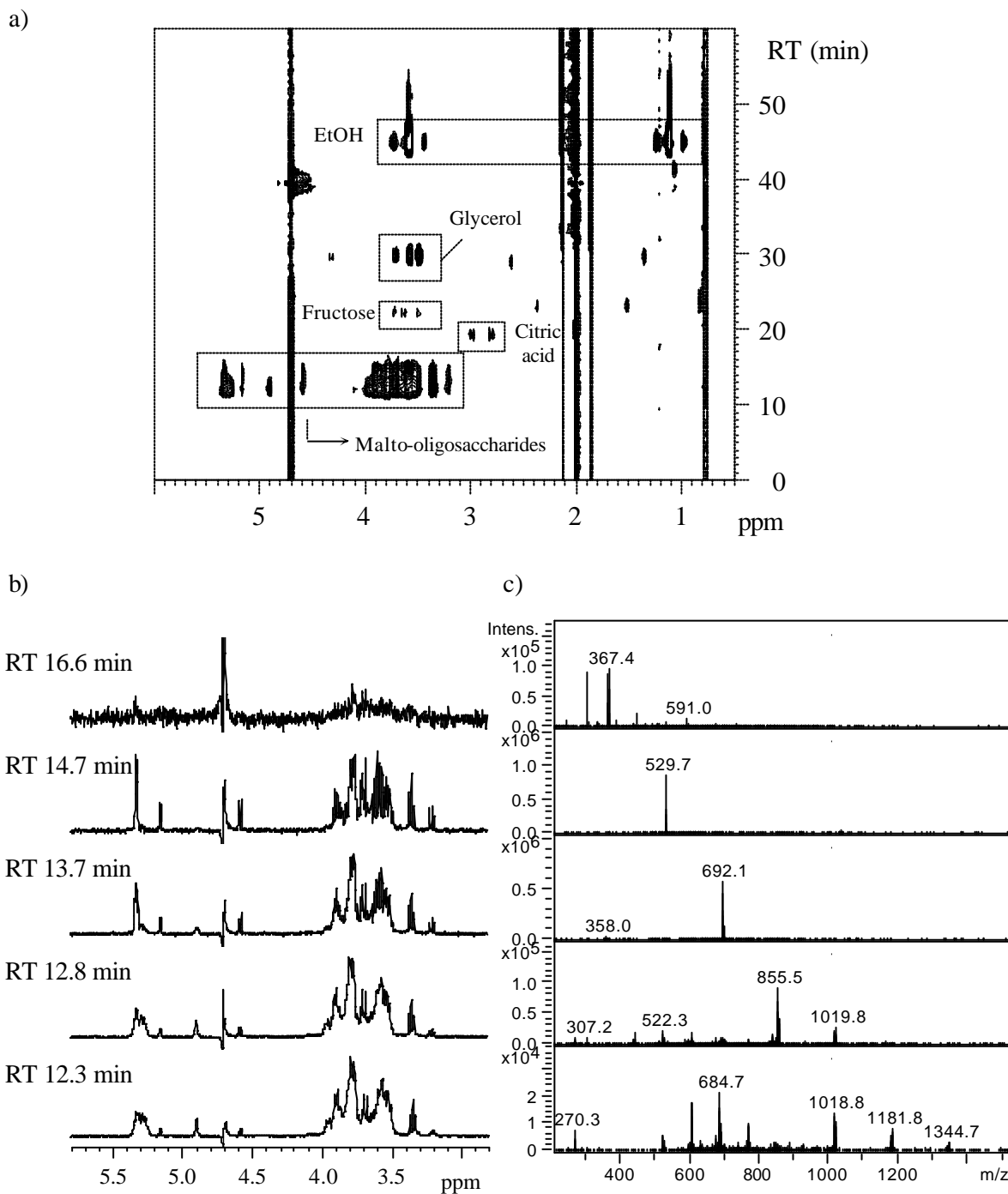


Figure VIII.7. a) Continuous-flow NMR chromatogram resulting from the elution of beer 1 on the column ION-300 (flow rate 0.3 ml/min; injection volume 100  $\mu$ l); b) rows extracted from the NMR chromatogram; c) MS spectra acquired concurrently with the NMR data in positive-ionisation mode.

mass spectrometry studies of oligosaccharides, which indicated the formation of dissociated cations for oligomers with  $DP > 4$  (Careri *et al.*, 1998). The MS results alone do not enable the identification of the oligomers as branched or linear; in this respect, the corresponding NMR row (Figure VIII.7b) does indicate, through the 4.96 ppm peak, that at least some of the dextrans detected comprise  $\alpha$ -(1-6) branches. The MS spectrum of the fraction eluting at 12.8 min shows peaks at  $m/z$  856 and 1020, arising from  $\alpha$ -DP5 + Na $^{+}$  and  $\alpha$ -DP6 + Na $^{+}$ , respectively; the double-charged ions also appear at  $m/z$  439 and 522, but with lower abundance. Again, the NMR spectrum of this fraction indicates ramification of these carbohydrates to some extent. The following subfraction under study, eluted at 13.7 min, is found to comprise mainly DP4 oligosaccharides (as seen by the  $m/z$  peaks at 692 and 358 arising from  $\alpha$ -DP4 + Na $^{+}$  and  $\alpha$ -DP4 + 2Na $^{2+}$ , respectively), which from the corresponding NMR spectrum are shown to be in the linear form, that is, maltotetraose. Indeed, the residual broad signal at 4.96 ppm seems to result from the gradual decrease of the broad components in the spectrum (note also the low intensity at 5.25-5.30 ppm), rather than from the predominant DP4 oligomer present. At 14.7 min, MS detects the elution of a glucose trisaccharide, which originates the  $\alpha$ -DP3 + Na $^{+}$  ion found at  $m/z$  530. This is, in fact, maltotriose, as clearly shown by the corresponding NMR spectrum. Finally, DP2 is detected in the MS spectrum of the fraction eluting at 16.6 min ( $m/z$  367). The NMR spectrum, however, shows a S/N that is too low for enabling the structural characterization of this sugar. For that reason, this fraction was collected into a loop during a second chromatographic run and a 1D spectrum with better S/N (NS 128) recorded (Figure VIII.8). By comparison with spectra of standard solutions (Figure VIII.5), it was found that the fraction collected, for which MS detected only one peak, actually contains two different glucose dimers: maltose and trehalose, differing in the glycosidic linkage ( $\alpha$ -(1-4) for the former and  $\alpha$ -(1-1) for the latter).

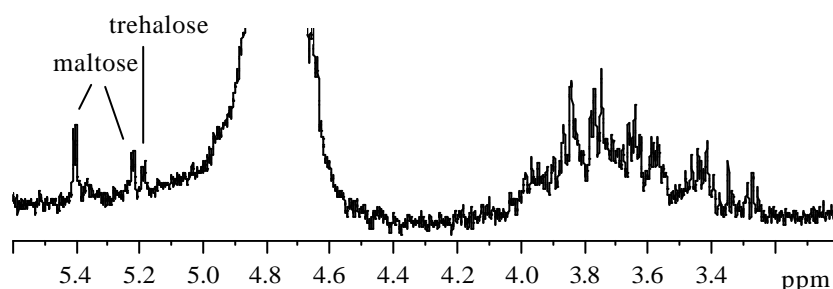


Figure VIII.8.  $^1\text{H}$  NMR spectrum of the subfraction of beer 1 collected into a loop at 16.6 minutes; NS 128.

Table VIII.2. NMR and MS data of beer 1 carbohydrates obtained by continuous-flow HPLC-NMR/MS analysis; <sup>(a)</sup> the oligomers identified may be either linear and/or branched; <sup>(b)</sup> calculated by integration of anomeric signals, as described in text.

RT (min)	NMR		MS (positive-ionisation)		Compounds identified
	average no. of glucose units per molecule <sup>(b)</sup>	average no. of branchings per molecule <sup>(b)</sup>	<i>m/z</i>	molecular ion	
12.3	9.6	1.4	522	${}^{\ominus}\text{DP6} + 2\text{Na}^{\oplus}$	Dextrins DP6, DP7, DP8 and DP9 <sup>(a)</sup>
			604	${}^{\ominus}\text{DP7} + 2\text{Na}^{\oplus}$	
			685	${}^{\ominus}\text{DP8} + 2\text{Na}^{\oplus}$	
			766	${}^{\ominus}\text{DP9} + 2\text{Na}^{\oplus}$	
			1019	${}^{\ominus}\text{DP6} + \text{Na}^{\oplus}$	
			1182	${}^{\ominus}\text{DP7} + \text{Na}^{\oplus}$	
			1345	${}^{\ominus}\text{DP8} + \text{Na}^{\oplus}$	
12.8	7.0	0.9	439	${}^{\ominus}\text{DP5} + 2\text{Na}^{\oplus}$	Dextrins DP5 and DP6 <sup>(a)</sup>
			522	${}^{\ominus}\text{DP6} + 2\text{Na}^{\oplus}$	
			1020	${}^{\ominus}\text{DP6} + \text{Na}^{\oplus}$	
13.7	4.2	0	358	${}^{\ominus}\text{DP4} + 2\text{Na}^{\oplus}$	Maltotetraose
			692	${}^{\ominus}\text{DP4} + \text{Na}^{\oplus}$	
14.7	3.2	0	530	${}^{\ominus}\text{DP3} + \text{Na}^{\oplus}$	Maltotriose
16.6	n.d.	n.d.	367	${}^{\ominus}\text{DP2} + \text{Na}^{\oplus}$	Maltose and Trehalose
	Spectrum of loop shows maltose and trehalose				
22.5	Fructose profile		204	${}^{\ominus}\text{hexose} + \text{Na}^{\oplus}$	Fructose

n.d.: not determined due to low S/N

As previously noted in Figure VIII.6, beer 2 is characterised by a very different carbohydrate profile, dominated by the contribution of glucose. The continuous-flow NMR chromatogram obtained for this sample is shown in Figure VIII.9a and the carbohydrates identified are listed in Table VIII.3. By comparison with the NMR chromatogram of beer 1 (Figure VIII.7a), the differences between the two beers can be clearly visualised. A major difference regards the detection of glucose, which is seen to elute at about 21.5 min in beer 2 (between citric acid and fructose) and is absent in beer 1. The other significant difference is observed for the carbohydrates eluting at earlier retention times. The continuous-flow NMR chromatogram of beer 2 shows three rows, with a satisfactory degree of separation but with very poor signal-to-noise ratio (Figure VIII.9b). By analysing the corresponding MS data obtained with positive mode ESI (Figure VIII.9c), different *m/z* values are found for those rows. The first compound to be eluted (RT 13.5 min) shows *m/z* 692, which is

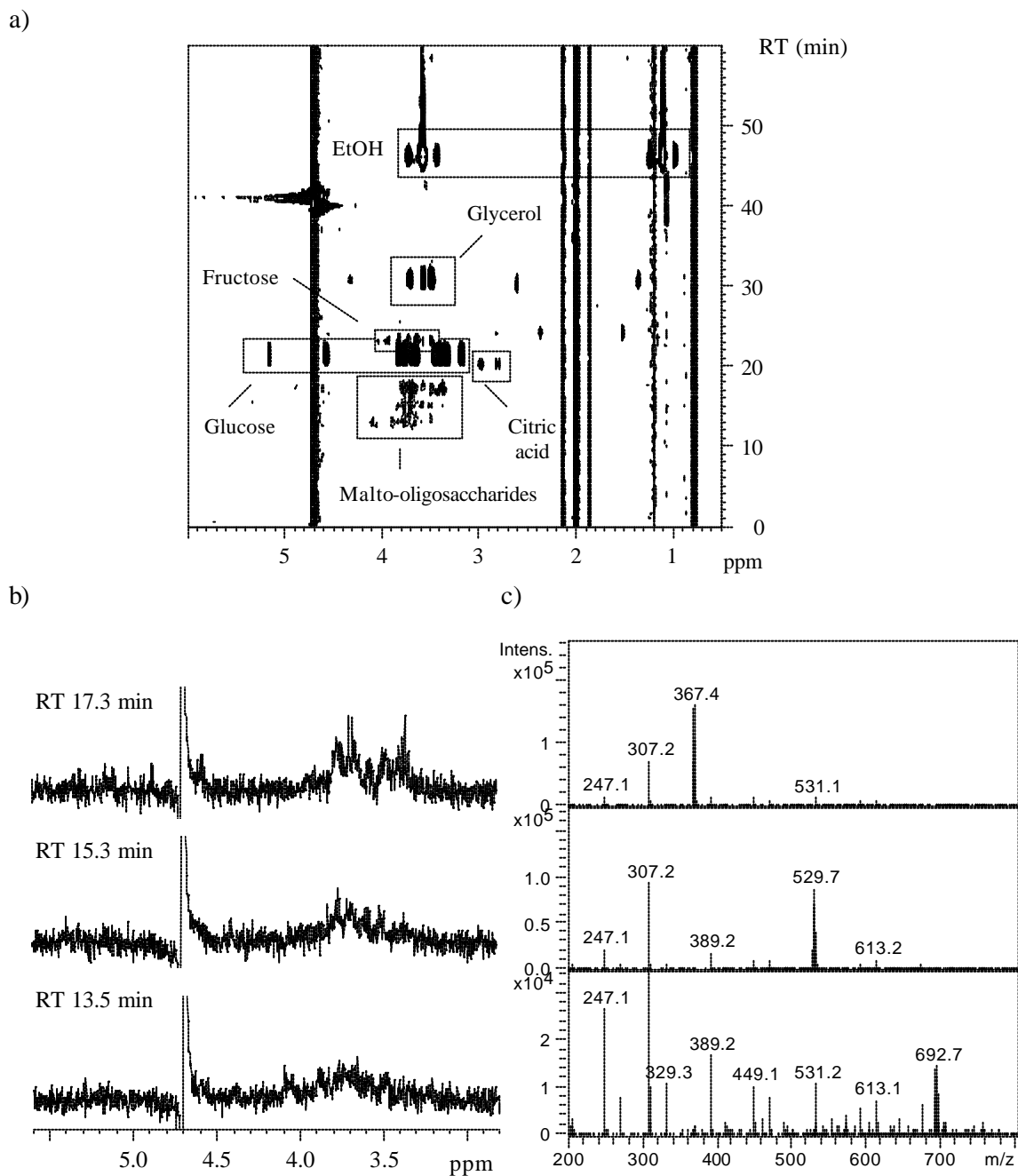


Figure VIII.9. Continuous-flow NMR chromatogram resulting from the elution of beer 2 on the column ION-300 (flow rate 0.3 ml/min; injection volume 100  $\mu$ l); b) rows extracted from the NMR chromatogram; c) MS spectra acquired concurrently with the NMR data in positive-ionisation mode.

consistent with the presence of DP4 dextrans, partially deuterated and ionised with sodium. The next row (RT 15.3 min) shows  $m/z$  530, which is consistent with a trisaccharide of glucose (DP3), also in the form  $^?M + Na^?+$ . However, additional structural information, such as the existence of a branching point, could not be achieved for these fractions due to the low signal to noise ratio in the corresponding NMR spectra (Figure VIII.9b). On the other hand, the disaccharide-containing subfraction eluting at 17.3 min ( $m/z$  367, corresponding to  $^?DP2 + Na^?+$ ) has been collected into a loop during a second chromatographic run to allow the co-addition of transients (Figure VIII.10). By comparison with spectra of standard solutions (Figure VIII.5), isomaltose and trehalose have been identified as the disaccharides present.

In summary, the main differences in the carbohydrate composition of beer 2 relative to that of beer 1 are the presence of glucose, the presence of isomaltose instead of maltose, and the absence of large dextrans, the maximum size being DP4.

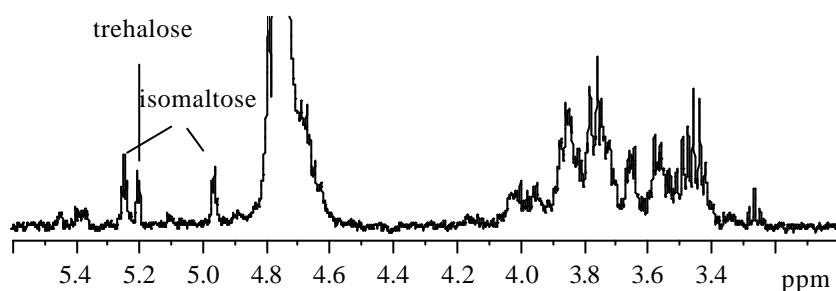


Figure VIII.10.  $^1H$  NMR spectrum of the subfraction of beer 2 collected into a loop at 17.3 minutes; NS 128.

Table VIII.3. NMR and MS data of beer 2 carbohydrates obtained by continuous-flow HPLC-NMR/MS analysis; <sup>(a)</sup> existence of branching point could not be confirmed.

RT (min)	NMR	MS (positive-ionisation)		Compounds identified
		$m/z$	molecular ion	
13.5	low S/N	692	$^?DP4 + Na^?+$	DP4 <sup>(a)</sup>
15.3	low S/N	530	$^?DP5 + Na^?+$	DP3 <sup>(a)</sup>
17.3	Spectrum of loop shows isomaltose and trehalose	367	$^?DP2 + Na^?+$	Isomaltose and Trehalose
21.5	Glucose profile	204	$^?hexose + Na^?+$	Glucose
23.0	Fructose profile	204	$^?hexose + Na^?+$	Fructose

### VIII.4.2. Application to Aromatic Compounds

Beer 1 was also selected for a more thorough investigation of aromatic components using HPLC-NMR/MS. Figure VIII.11 shows the UV chromatogram obtained by gradient elution of the beer sample in a reverse phase column with acetonitrile/water. At the wavelengths used for detection (280, 320 and 365 nm), a large number of peaks are observed, many of which overlap, reflecting the coelution of different compounds.

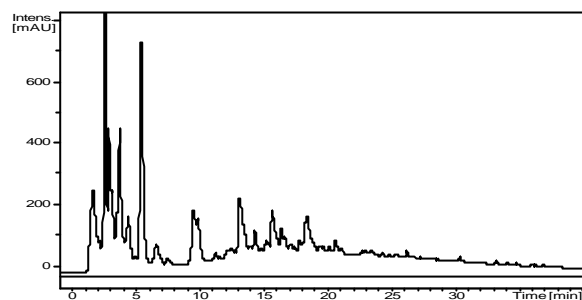


Figure VIII.11. UV chromatogram resulting from the elution of beer 2 on the column RP-18 (flow rate 1.00 ml/min; injection volume 500  $\mu$ l).

In the sight of the relatively poor chromatographic resolution obtained, the time-slicing method was selected for a subsequent chromatographic run. Using this operational mode, the flow is stopped at short intervals to “time-slice” different parts of a chromatographic peak, subsequently analysed by NMR. Combining the 1D NMR spectra acquired, a “pseudo” on-flow diagram is obtained (Figure VIII.12), allowing an easy visualisation of the number and type of compounds detected. This diagram shows that many aromatic components are separated, coeluting with carbohydrates in the first 10 min of chromatography. A disadvantage of this method is that MS data could not be recorded because of the interruption of the flow during the NMR measurement. However, some fractions were analysed by MS after collection into loops during another chromatographic run. The aromatic compounds identified with basis on the structural information provided by NMR and also by MS of the loops are listed in Table VIII.4. The following paragraphs discuss the results obtained in more detail.

The aromatic regions of a series of  $^1\text{H}$  NMR spectra acquired for fractions eluting in the first 12 min of chromatography are shown in Figure VIII.13. Spectrum 1 (RT 2.5 min) shows two broad resonances at 7.69 and 8.49-8.85 ppm. These signals may arise from polyphenols, but the information available is scarce to suggest any further identification.

Spectrum 2 (RT 3.0 min) contains three doublets (? 5.84, 6.16 and 8.07 ppm) assigned to cytidine, which has been previously identified with basis on 1D and 2D spectra of whole beer. Indeed, the positive-ionisation mode mass spectrum recorded for this fraction shows a peak at  $m/z$  250 corresponding to the molecular ion  $[M + D]^+$  of cytidine in the fully deuterated form ( $M_w$  243). Spectrum 3 (RT 4.0 min) reveals the coelution of tyrosine (? 6.83 and 7.13 ppm,  $J$  8.5 Hz) and uridine (? 5.84, 7.84 ppm). Again, the mass spectrum recorded for this fraction confirms this identification as the  $m/z$  values 183 and 246, detected in negative-ionisation mode, correspond to the molecular ions  $[M - D]^-$  of tyrosine ( $M_w$  181) and uridine ( $M_w$  244) in fully deuterated forms. This is an example where both NMR and MS recognise that different compounds are coeluting, something that the UV chromatogram alone had failed to observe under the conditions used. Spectrum 4 (RT 5.0 min) is consistent with the presence of adenosine and/or inosine. These compounds are difficult to distinguish by NMR and also by MS, since their molecular weights only differ by 1 mass unit and are the same for the fully deuterated forms. Therefore, the  $m/z$  value 274 found in the positive-ion mode mass spectrum of this fraction may correspond to either adenosine or inosine. Spectra 5 (RT 7.5 min) and 6 (RT 10.5 min) show the elution of phenylalanine and tryptophane, respectively. These amino acids had already been identified by 1D and 2D NMR of beer and confirmation is now provided by observation of the typical high field NMR patterns and by MS data.

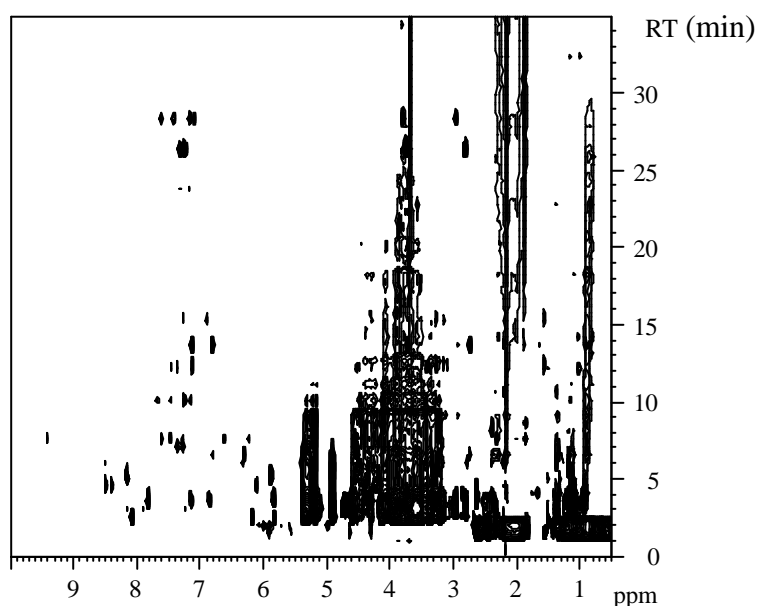


Figure VIII.12. "Pseudo" on-flow NMR chromatogram, resulting from the elution of beer 1 on the column RP-18 (flow rate 1.00 ml/min; injection volume 500  $\mu$ l).

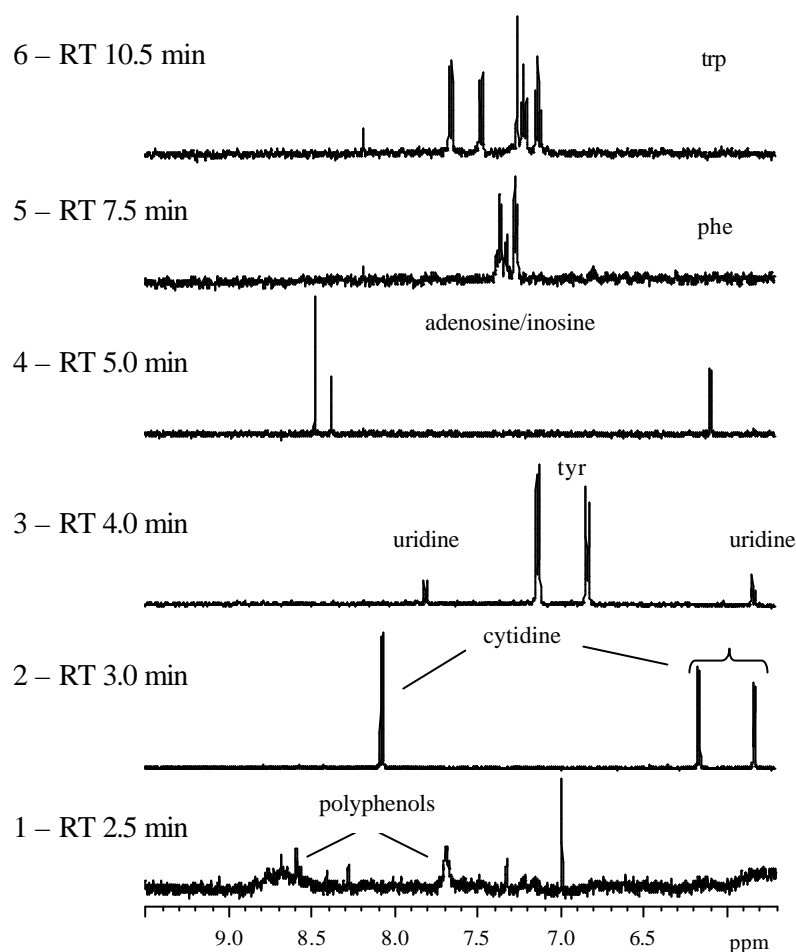


Figure VIII.13. Rows of the “pseudo” on-flow NMR chromatogram of beer 1.

After 12 min, fewer compounds are detected in the NMR chromatogram (Figure VIII.12), but their spectra are “cleaner”, as the carbohydrates have been eluted at the beginning of chromatography. The spectra of the three compounds identified between 12 and 30 min are shown in Figure VIII.14. Spectrum 1 (RT 14.0 min) shows two triplets at 2.71 and 3.71 ppm and two doublets in the aromatic region (? 6.79, 7.12 ppm,  $J$  8.4 Hz), consistent with the presence of tyrosol. In the 1D spectrum of beer, the aromatic doublets of this phenolic alcohol overlap with tyrosine signals. Moreover, as there is no correlation between aromatic and side chain protons, the TOCSY spectrum does not aid in the unambiguous identification of these compounds. By HPLC-NMR/MS, both tyrosine and tyrosol, reported to occur in beer (Hughes and Baxter, 2001), are separated and identified. Spectrum 2 (RT 26.5 min) and spectrum 3 (RT 28.5 min) also show two triplets in the high-field region and a group of signals in the aromatic region, thus suggesting the

presence of other aromatic alcohols. Indeed, spectrum 2 is consistent with 2-phenylethanol and spectrum 3 shows evidence of 3-indoleethanol (tryptophol).

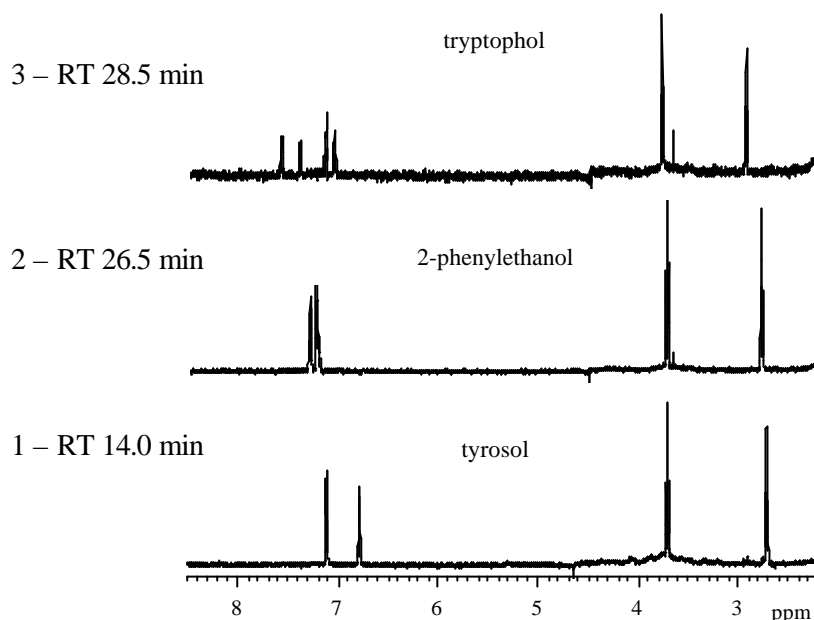


Figure VIII.14. Rows of the “pseudo” on-flow NMR chromatogram of beer 1.

Table VIII.4. MS and NMR data of beer 1 aromatic compounds obtained by HPLC-NMR/MS analysis (time-slicing and loop sampling modes); n.i.: not identified; n.a.: not acquired.

RT (min)	MS ( <i>m/z</i> )	NMR signals ? in ppm (multiplicity, <i>J</i> in Hz)	Compounds identified
2.5	n.i.	7.69 (broad), 8.49-8.85	Polyphenols
3.0	$M+D^+ = 250$	5.84 (d, 4.5), 6.16 (d, 8.0), 8.07 (d, 8.0)	Cytidine
4.0	$M-D^+ = 183$ $M-D^+ = 246$	6.83 (d, 8.5), 7.13 (d, 8.5), 5.84 (m), 7.84 (d, 8.4)	Tyrosine Uridine
5.0	$M+D^+ = 274$	6.09 (d, 5.5), 8.37 (s), 8.47 (s)	Adenosine/Inosine
7.5	$M+D^+ = 170$	7.27 (m), 7.32 (m), 7.37 (m)	Phenylalanine
10.5	$M+D^+ = 210$	7.13 (t, 7.5), 7.22 (t, 7.9), 7.25 (s), 7.47 (d, 8.5), 7.65 (d, 8.0)	Tryptophane
14.0	n.a.	2.71 (t, 6.8), 3.70 (t, 7.0), 6.79 (d, 8.4), 7.12 (d, 8.4)	Tyrosol
26.5	n.a.	2.79 (t, 7.0), 3.74 (t, 7.0), 7.24 (m), 7.31 (m)	2-Phenylethanol
28.5	n.a.	2.94 (t, 7.1), 3.79 (t, 7.1), 7.07 (t, 7.3), 7.15 (m), 7.41 (d, 8.4), 7.60 (d, 7.6)	Tryptophol

## VIII.5. Conclusions

This work has shown that high resolution NMR is of great utility to characterise the complex chemical composition of beer, enabling the rapid identification of a large number of compounds, present in a range of concentrations. This has been achieved in a non-invasive manner, requiring only the degassing of the beer sample. However, some difficulties were encountered in the assignment of the beer spectra. In particular, the spectral distinction of beer carbohydrates, mainly constituted of glucose monomers, was found to be extremely difficult due to peak overlap even in the 2D spectra.

A deeper insight to characterising beer carbohydrates was achieved by HPLC-NMR/MS, applied to two beer samples. In one of the samples, a range of carbohydrates, from small fermentable sugars to dextrans with up to 9 glucose monomers could be identified. Although the presence or absence of (1-6) branching points in each subfraction could be indicated by NMR, a more complete structural characterisation of the dextrans present requires further improvement of the chromatographic methods/conditions used, in tandem with multidimensional NMR methods. The other beer sample analysed was characterised by the predominance of glucose and the absence of high molecular weight dextrans, the maximum size being DP4.

HPLC-NMR/MS has also been useful for confirming the identity of some aromatic compounds previously assigned by NMR alone and for revealing new ones, like the aromatic alcohols tyrosol, 2-phenylethanol and tryptophol.

## References

- Belton, P.S.; Delgadillo, I.; Holmes, E.; Nicholls, A.; Nicholson, J.; Spraul, M. Use of high-field  $^1\text{H}$  NMR spectroscopy for the analysis of liquid foods. *Journal of Agricultural and Food Chemistry* **1996**, *44*, 1483-1487.
- Belton, P.S.; Delgadillo, I.; Gil, A.M.; Roma, P.; Casuscelli, F.; Colquhoun, I.J., Dennis, M.J.; Spraul, M. High field proton NMR studies of apple juices. *Magnetic Resonance in Chemistry* **1997**, *35*, S52-S60.
- Bosco, M.; Toffanin, R.; Palo, D.; Zatti, L.; Segre, A. High resolution  $^1\text{H}$  NMR investigation of coffee. *Journal of the Science of Food and Agriculture* **1999**, *79*, 869-878.

Brescia, M.A.; Caldarola, V.; De Giglio, A.; Benedetti, D.; Fanizzi, F.P.; Sacco, A. Characterization of the geographical origin of Italian red wines based on traditional and nuclear magnetic resonance spectrometric determinations. *Analytica Chimica Acta* **2002**, *458*, 177-186.

Careri, M.; Mangia, A.; Musci, M. Overview of the applications of liquid-chromatography-mass spectrometry interfacing systems in food analysis: naturally occurring substances in food. *Journal of Chromatography A* **1998**, *794*, 263-297.

Corradini, C; Canali, G. Nicoletti, I. Application of HPAEC-PAD to carbohydrate analysis in food products and fruit juices. *Seminars in Food Analysis* **1997**, *2*, 99-111.

Désévaux, S; Daems, V.; Delvaux, F.; Derdelinckx, G. Analysis of fermentable sugars and dextrans in beer by anion exchange chromatography with electrochemical detection. *Seminars in Food Analysis* **1997**, *2*, 113-117.

Duarte, I.; Barros, A.; Belton, P.S.; Righelato, R.; Spraul, M.; Humpfer, E.; Gil, A. M. High resolution NMR spectroscopy and multivariate analysis for the characterisation of beer. *Journal of Agricultural and Food Chemistry* **2002**, *50*, 2475-2481.

Gil, A.M.; Duarte, I.F.; Delgadillo, I.; Colquhoun, I.J.; Casascelli, J.; Humpfer, E.; Spraul, M. Study of the compositional changes of mango during ripening by use of nuclear magnetic resonance spectroscopy. *Journal of Agricultural and Food Chemistry* **2000**, *48*, 1524-1536.

Hawthorne, D. B.; Jones, R. D.; Barret, P.A.; Kavanagh, T. E.; Clarke, B. J. Methods for the analysis of C4 to C10 fatty acids in beer, wort and carbohydrate syrups. *Journal of the Institute of Brewing* **1986**, *92*, 181-184.

Hughes, P. S.; Baxter, E. D. *Beer Quality, Safety and Nutritional Aspects*; The Royal Society of Chemistry: Cambridge, 2001.

Jodelet, A.; Rigby, N.M.; Colquhoun, I.J. Separation and NMR structural characterisation of singly branched  $\alpha$ -dextrans which differ in the location of the branch point. *Carbohydrate Research* **1998**, *312*, 139-151.

Kosir, I. J.; Kidric, J. Identification of amino acids in wines by one- and two-dimensional nuclear magnetic resonance spectroscopy. *Journal of Agricultural and Food Chemistry* **2001**, *49*, 50-56.

Le Gall, G., Puaud, M., Colquhoun, I.J. Discrimination between orange juice and pulp wash by  $^1\text{H}$  nuclear magnetic resonance spectroscopy: Identification of marker compounds. *Journal of Agricultural and Food Chemistry* **2001**, *49*, 580-588.

Pusecker, K.; Albert, K.; Bayer, E. Investigation of hop and beer bitter acids by coupling of high-performance liquid chromatography to nuclear magnetic resonance spectroscopy. *Journal of Chromatography A* **1999**, *836*, 245-252.

Ramos, A.; Santos, H. NMR studies of wine chemistry and wine bacteria. In *Annual Reports on NMR Spectroscopy*; Webb, G.A. Ed.; Academic Press: London, 1999; 179-202.

Sacchi, R.; Patumi, M.; Fontanazza, G.; Barone, P.; Fiordiponti, P.; Mannina, L.; Rossi, E.; Segre, A.L. A high-field  $^1\text{H}$  nuclear magnetic resonance study of the minor components in virgin olive oils. *Journal of the American Oil Chemists' Society* **1996**, *73*, 747-758.

Shanta-Kumara, H. M. C.; Iserentant, D.; Verachtert, H. Comparative analysis of malto-oligosaccharides in different beer types by thin layer chromatography, chemical and enzymatical analysis. *Cerevisia: Belgian Journal Brewing Biotechnology* **1995**, *20*, 47-53.

Uchida, M.; Nakatani, K.; Ono, M.; Nagami, K. Carbohydrates in brewing. I. Determination of fermentable sugars and oligosaccharides in wort and beer by partition high-performance liquid chromatography. *Journal of the American Society of Brewing Chemists* **1991**, *49*, 665-673.

Van der Burgt, Y.E.M.; Bergsma, J.; Bleeker, I.P.; Mijland, P.J.H.C.; Kamerling, J.P.; Vliegthart, J.F.G. Substituent distribution in highly branched dextrans from methylated starches. *Carbohydrate Research* **2000**, *327*, 423-429.

Vinogradov, E.; Bock, K. Structural determination of some new oligosaccharides and analysis of the branching patterns of isomaltooligosaccharides from beer. *Carbohydrate Research* **1998**, *309*, 57-64.

## **IX. MULTIVARIATE ANALYSIS OF NMR AND FTIR OF BEER AS A POTENTIAL TOOL FOR BEER QUALITY CONTROL**

IX.1. Introduction.....	24
IX.2. Materials and Methods.....	8
IX.2.1. Sample Preparation.....	24
IX.2.2. Spectroscopic Measurements.....	9
IX.2.3. Multivariate Analysis.....	24
IX.3. Principal Components Analysis (PCA) of NMR Data.....	9
IX.4. Principal Components Analysis (PCA) of FTIR Data.....	24
IX.5. Canonical Correlation Analysis (CCA) of NMR and FTIR Data.....	9
IX.6. Conclusions.....	25
References.....	1
.	25
	1
	26
	1
	26
	3
	26
	5
	26
	6

## IX.1. Introduction

The maintenance of beer quality throughout its lifetime is a considerable challenge, reinforced by the increasing demands of the market forces for extended distribution chains. In order to accomplish an efficient quality control and extended shelf life, the detailed study of beer composition and quality attributes is of paramount importance. High resolution NMR and hyphenated NMR methods may give a valuable contribution to that study, as demonstrated in Chapter VIII. In addition, it is also important to develop methods which provide rapid information about factors such as geographical origin, processing conditions and reproducibility within different brewing sites. To accomplish this task, multivariate analysis of spectroscopic data may be a possible strategy. Spectroscopic methods can provide information on a wide range of compounds present in the food matrix in a single experiment, offering advantages in terms of simplicity of sample preparation and rapidity of analysis. The speed with which spectra can be obtained, often under automation, makes examination of many samples possible. Since the richness of information often results in high spectral complexity, it calls for the use of multivariate analysis to study large numbers of spectra and extract meaningful information.

The application of chemometrics to high resolution  $^1\text{H}$  NMR data has been successfully used for the analysis of biological fluids and tissues and the investigation of perturbed metabolic processes (Lindon *et al.*, 2000; Lindon *et al.*, 2001). In the area of food research, there are also promising results concerning the classification of apple juice according to variety (Belton *et al.*, 1998), the detection of adulteration of orange juice (Vogels *et al.*, 1996; Le Gall *et al.*, 2001), the discrimination of coffee samples differing in the manufacturing process (Charlton *et al.*, 2002), the geographical origin classification of oils (Sacchi *et al.*, 1998) and wines (Vogels *et al.*, 1993; Brescia *et al.*, 2002), and the differentiation of grapevine cultivars and clones (Forveille *et al.*, 1996). The usefulness of FTIR spectroscopy in tandem with chemometrics to tackle the problems of food authentication and adulteration has also been demonstrated for several foods, namely fruit products (Twomey *et al.*, 1995; Defernez and Wilson, 1995; Kemsley *et al.*, 1996; Holland *et al.*, 1998), coffee (Briandet *et al.*, 1996; Downey *et al.*, 1997), wine (Edelmann *et al.*, 2001) and meat (Al-Jowder *et al.*, 2002).

In this work, Principal Components Analysis (PCA) is applied for the first time to our knowledge to the high resolution  $^1\text{H}$  NMR spectra and to the FTIR-ATR spectra of a set of

fifty beers in order to find out if the spectral profile of beer may be consistently correlated with specific compositional properties and/or sample origin. These beers have been produced in different countries and belong to different types (ale, lager and alcohol-free), which basically differ on the fermentation conditions, as described in Chapter I (section I.3). Moreover, Canonical Correlation Analysis (CCA) is used to correlate the two domains (NMR and FTIR), which may potentially reveal complementary information.

## **IX.2. Materials and Methods**

### **IX.2.1. Sample Preparation**

A set of 50 beers, some produced nationally and others imported from different countries, was obtained in the Portuguese market. Some of their characteristics are given in Table IX.1, namely the country of origin, the type (ale, lager, alcohol-free), the alcohol content and the pH. For NMR measurements, beer samples were degassed in an ultrasonic bath during 10 minutes and prepared to contain 10% D<sub>2</sub>O (internal lock) and 0.02% sodium 3-(trimethylsilyl)tetra deuterio propionate (TSP-*d*<sub>4</sub>) as chemical shift reference. For FTIR measurements, preparation simply consisted of degassing the beers in an ultrasonic bath during 10 minutes.

### **IX.2.2. Spectroscopic Measurements**

The <sup>1</sup>H 1D NMR spectra were recorded at 27°C on a Bruker Avance DRX-600 spectrometer, operating at 599.87 MHz for proton. The pulse program '1c1pnps' (shown in appendix) was used, with suppression of water and ethanol signals by applying a modulated shaped pulse during the mixing time (100 ms) and 1.6 s of the relaxation delay (8.0 s). 128 transients were collected into 32768 data points with a spectral width of 8389.26 Hz and an acquisition time of 1.95 s. The spectrometer was equipped with an autosampler and the data were acquired under an automation procedure that included temperature stabilisation (5 min), automatic tuning and shimming, calculation of the shaped pulse for triple suppression, and acquisition, requiring approximately 30 min per sample. The FIDs were Fourier transformed (with 0.3 Hz line-broadening unless otherwise stated) and the spectra phased, baseline corrected and calibrated by the TSP signal at 0.0 ppm. The resulting spectra were converted into JCAMP format and transferred to a PC workstation for statistical analysis.

Table IX.1. Some characteristics of the beers analysed; <sup>(a)</sup> analysed by FTIR only, <sup>(b)</sup> analysed by NMR only.

Sample no.	Origin	Type	% Alcohol	pH
1	Portugal	Lager	5.2	4.38
2	Portugal	Lager	5.1	3.92
3	Portugal	Lager	5.2	4.42
4	Ireland	Ale	4.2	4.15
5	Portugal	Lager	5.1	3.95
6	Portugal	Alcohol-free	< 0.5	4.28
7	Portugal	Alcohol-free	< 0.5	4.58
8	Portugal	Lager	5.8	4.32
9	Portugal	Lager	5.1	4.06
10	Belgium	Lager	4.9	4.01
11	Portugal	Lager	4.3	4.01
12	Portugal	Lager	5.0	4.28
13	Portugal	Lager	4.2	4.40
14	Spain	Lager	5.0	4.00
15	Portugal	Lager	5.4	4.52
16	Belgium	Lager	4.6	4.14
17	Belgium	Ale	6.5	4.32
18	Portugal	Lager	5.1	4.00
19	unknown	Lager	4.8	4.12
20	Germany	Lager	4.8	4.12
21	Germany	unknown	4.8	4.49
22	Belgium	Ale	8.5	4.23
23	Belgium	Ale	9.0	4.33
24	Belgium	Ale	8.0	4.28
25	England	unknown	5.0	3.86
26	England	Lager	4.7	4.02
27	England	Lager	5.0	4.11
28	Scotland	Ale	6.0	3.91
29	Germany	unknown	4.8	4.35
30	Germany	Ale	5.0	4.24
31	Germany	Ale	5.0	3.97
32	Germany	Ale	5.0	4.08
33	Belgium	Ale	9.0	4.24
34	Belgium	Ale	8.1	4.15
35	Belgium	Ale	6.6	4.14
36	Belgium	Ale	6.5	4.02
37	Belgium	Lager	5.2	4.14
38	Germany	Lager	5.0	4.14
39	Holland	Lager	5.0	4.24
40	Holland	Alcohol-free	< 0.5	4.05
41	Spain	Lager	5.4	4.16
42 <sup>(a)</sup>	Holland	Alcohol-free	< 0.5	4.22
43	Holland	Lager	5.0	4.01
44	Holland	Lager	5.4	4.27
45	Portugal	Ale	7.2	4.52
46	England	Ale	4.7	3.96
47	Germany	Ale	4.9	4.01
48	U.S.A.	Lager	4.2	3.76
49	England	Ale	4.0	4.07
50 <sup>(b)</sup>	Germany	Lager	unknown	unknown

Fourier transform infrared spectra were collected on a Bruker IFS55 FTIR spectrometer. A single reflectance horizontal ATR cell (Golden Gate, equipped with a diamond crystal) was used. The data were recorded at  $20 \pm 1^\circ\text{C}$ , in the spectral range of  $4000\text{-}700\text{ cm}^{-1}$ , by accumulating 256 scans with a resolution of  $4\text{ cm}^{-1}$ . For each sample, a total of five spectra (replica) were recorded. Between determinations, the crystal was carefully cleaned with water and, to avoid memory effects, the replica spectra were recorded randomly *i.e.* intermingled with the spectra of other samples. The spectra were converted into JCAMP format and transferred to a PC workstation for statistical analysis.

### **IX.2.3. Multivariate Analysis**

For PCA of NMR spectra, data matrices corresponding to different spectral regions were built, excluding the segments containing water and ethanol resonances (at 4.80 ppm and at 1.17 and 3.65 ppm, respectively) to eliminate the variation in these signals suppression. The spectral regions considered were: a) whole spectral range (0.5-10.0 ppm); b) aliphatic region (0.5-3.0 ppm), c) sugar region (3.0-6.0 ppm) and d) aromatic region (6.0-10.0 ppm). Each spectral region was normalised by adjusting the total area to unity. For PCA of FTIR spectra, the region between  $1200\text{ and }800\text{ cm}^{-1}$  was selected and each spectrum was autoscaled (mean centred and standardised). Canonical Correlation Analysis (CCA) was performed using the  $1200\text{-}800\text{ cm}^{-1}$  region of the FTIR autoscaled spectra and the 0.5-10.0 ppm region of the NMR spectra. The calculations were performed using the program developed by Dr. A. Barros in the 'Institut National Agronomique Paris-Grignon' in collaboration with the University of Aveiro (Barros, 1999).

### **IX.3. Principal Components Analysis (PCA) of NMR Data**

In order to look for the main sources of variability in the  $^1\text{H}$  NMR spectra recorded for the beer samples, PCA was firstly performed using the 0.5-10.0 ppm region, excluding the water and ethanol resonances.

The first two PCs, which together express 49% of the total variance (PC1 = 25%, PC2 = 24%), are displayed as a two-dimensional map in Figure IX.1a, where the sample coordinates are the scores. Four clusters are suggested in the scores scatter plot: a large

group comprising 36 samples (A), a group of 8 samples located in the positive side of both PC1 and PC2 (B), the two beers 6 and 40 (C) and the two beers 33 and 48 (D).

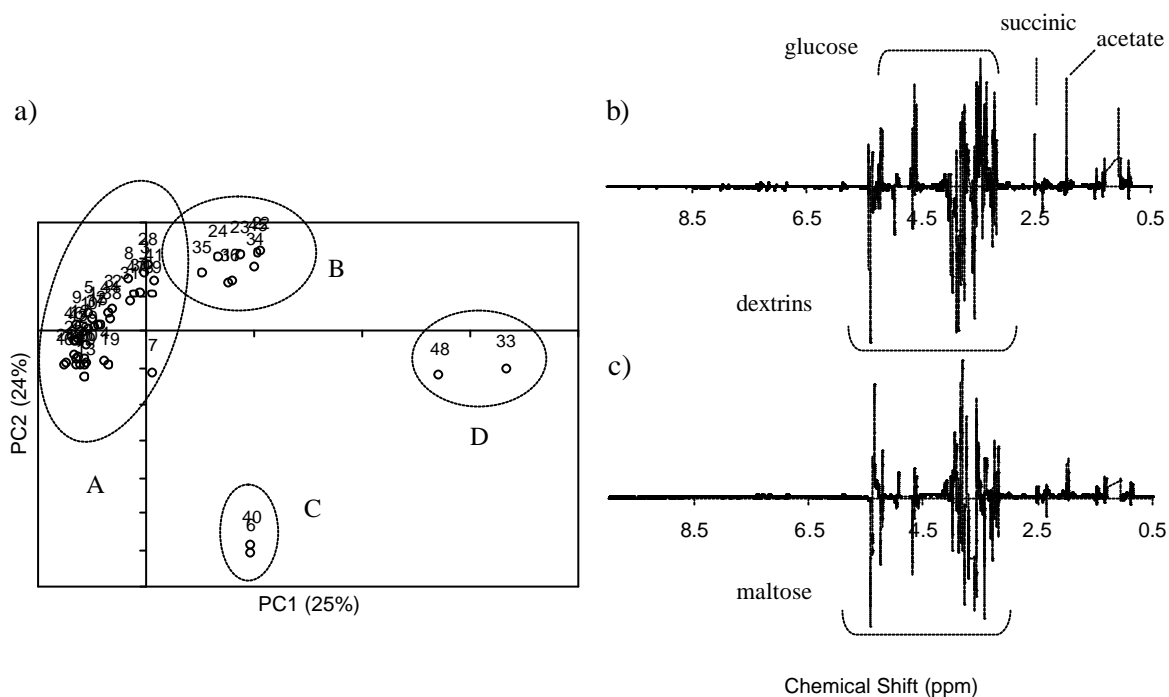


Figure IX.1. PCA of the  $^1\text{H}$  NMR spectra of 49 beers in the 0.5–10.0 ppm range (excluding the segments containing ethanol and water signals at 1.17, 3.65 and 4.80 ppm): a) scores scatter plot of PC1 vs. PC2, b) PC1 loadings profile, and c) PC2 loadings profile.

The examination of the loadings profiles is useful to understand the basis of the observed distribution of samples. The loadings associated with PC1 and PC2 are shown in Figures IX.1b and IX.1c, respectively, and reveal that the spectral features responsible for this separation are mainly resonances from carbohydrates (3.0–5.5 ppm) as well as some aliphatic signals. Indeed, in the PC1 loadings profile (Figure IX.1b), positive values are found at positions corresponding to glucose (5.20, 4.63 and 3.2–3.8 ppm), succinic acid (singlet at 2.52 ppm) and acetate (singlet at 1.98 ppm), suggesting that beers of group D in particular have a relatively higher content of these compounds. On the other hand, PC1 loadings show negative values for broader signals corresponding to dextrins (5.38, 4.96, 3.5–4.0 ppm), indicating that they dominate the carbohydrate profile of group A (with negative PC1 scores). PC2 loadings (Figure IX.1c) may be used to interpret the separation of group C (beers 6 and 40) from the remaining ones, as their scores are strongly negative in the PC2 axis. Negative loadings are found for signals at 5.41, 5.24, 4.66 and 3.3–4.0 ppm

which may be attributed to maltose, therefore, beers 6 and 40 are in principle characterised by an important contribution of this disaccharide rather than other carbohydrates.

The information provided by the loadings profiles may be verified by comparing the NMR spectra of the beers separated. Figure IX.2 shows the sugar regions of the spectra recorded for beer 1 (randomly selected from group A of samples), beer 23 (group B), beer 6 (group C) and beer 33 (group D). The first two samples (top spectra) are clearly characterised by the strong contribution of dextrins. However, just with basis on the 1D spectra, it does not become clear why PCA suggests distinction of two profiles (groups A and B) and it is possible that this distinction reflects small differences in the nature and quantitative proportions of the dextrins present. The spectrum of beer 6 is dominated by the signals of maltose, and the same may be observed in the spectrum of beer 40 (not shown). On the other hand, glucose clearly predominates in beer 33, as well as in beer 48 (spectrum not shown), confirming the observations of the PCA approach.

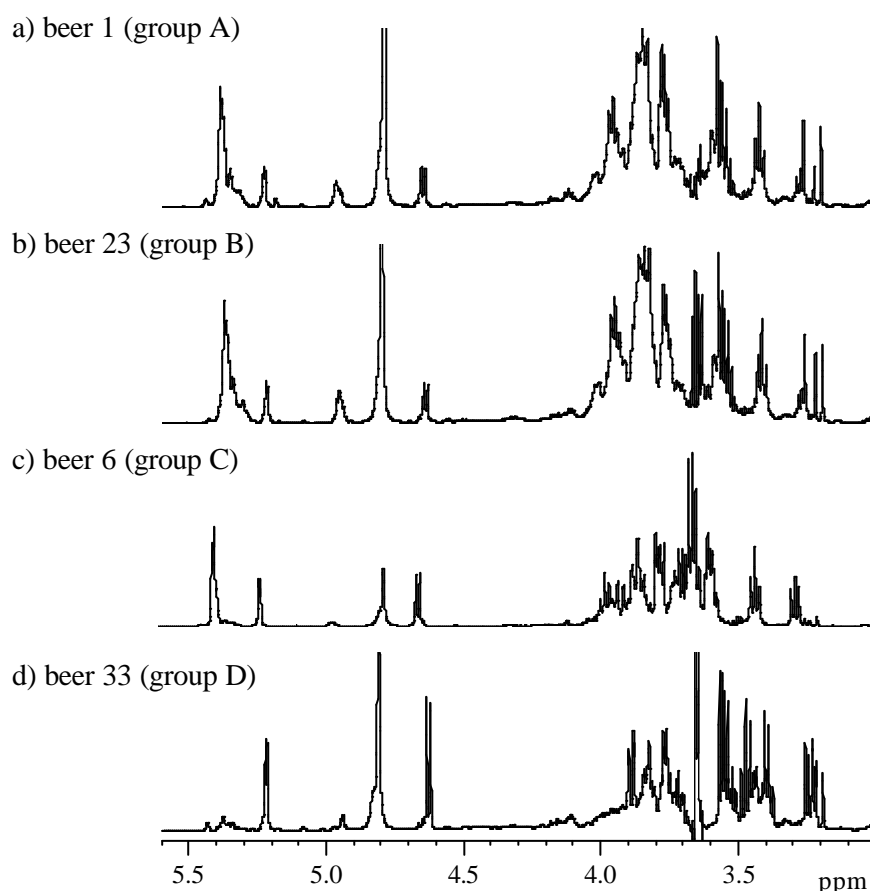


Figure IX.2. Sugar region (3.0-5.6 ppm) of the 600 MHz  $^1\text{H}$  NMR spectra of four different beer samples (numbered according to Table IX.1); NS 128.

Relating the PCA results with the known characteristics of the samples, presented previously in Table IX.1, it is interesting to note that group B comprises all the ale beers containing more than 6.0% alcohol, except for beer 33, which, despite its high alcoholic content (9.0%), is more similar to beer 48 (group D). On the other hand, the samples forming group C are both alcohol-free beers. Therefore, one may suggest that the differences highlighted by PCA in the carbohydrate profile are, at least in part, related to the beer alcoholic content. It should be noted that this correlation is not a direct one since the NMR regions where ethanol peaks resonate have been left out for the PCA. Nevertheless, this result is not surprising since the production of beers with different alcohol contents generally involves varied fermentation conditions, thus affecting the amount and type of fermentable sugars and dextrins present in the final product.

When PCA is performed using the whole spectral range, the contribution of minor components may be overlooked. Therefore, PCA was also performed on data matrices constructed for NMR sub-regions, as described in section IX.2.3. PCA of the sugar regions (not shown) produced identical results to those obtained when the whole spectra were considered, since those results reflected mainly differences in the carbohydrate composition.

The scores scatter plot obtained when only the aliphatic regions of the spectra are considered for PCA shows considerable dispersion and apparently no clustering exists (Figure IX.3a). The first two PCs explain only 27% of the total variance and the plots of subsequent PCs show the same kind of dispersion. Therefore, the aliphatic region of the spectra considered here is not particularly relevant for distinction between the beers analysed.

When only the aromatic regions of the spectra are considered for PCA, the scores scatter plot obtained shows some dispersion along PC1, which contains 22% of the total variance (Figure IX.3b). In spite of this small percentage, it is interesting to note that the scores lying towards the negative side of PC1 (group A) correspond to the majority of the ale beers analysed, whereas the scores near zero or in positive PC1 (group B) correspond mostly to lager beers, although three ales (beers 4, 46 and 49) are also included in this group. These results indicate that the aromatic region is the spectral region showing higher sensitivity to the fermentation processes that originate the two main types of beer, ale and

lager. It may therefore be suggested that the aromatic region of the spectra may be used to distinguish between these beer types. The PC1 loadings profile, shown in Figure IX.4a, gives an indication of which aromatic compounds are responsible for the observed separation of samples; however, care should be taken in this analysis as some signals show a first-derivative-like effect, resulting from shifts (caused mainly by differences in the samples pH) and not from real changes in sample composition. The negative PC1 loadings that contribute to the ale aromatic profiles (group A) seem to arise mainly from polyphenolic species (relatively broad signals at 6.84, 7.50 and 7.67 ppm, indicated with arrows in Figure IX.4). Among the positive PC1 loadings that characterise lager beers (group B), the most significant peaks correspond to the signals of tyrosine/tyrosol (doublets at 6.87 and 7.17 ppm), histidine (singlets at 7.04 and 7.99 ppm) and 2-phenylethanol (multiplets at 7.36 and 7.40 ppm).

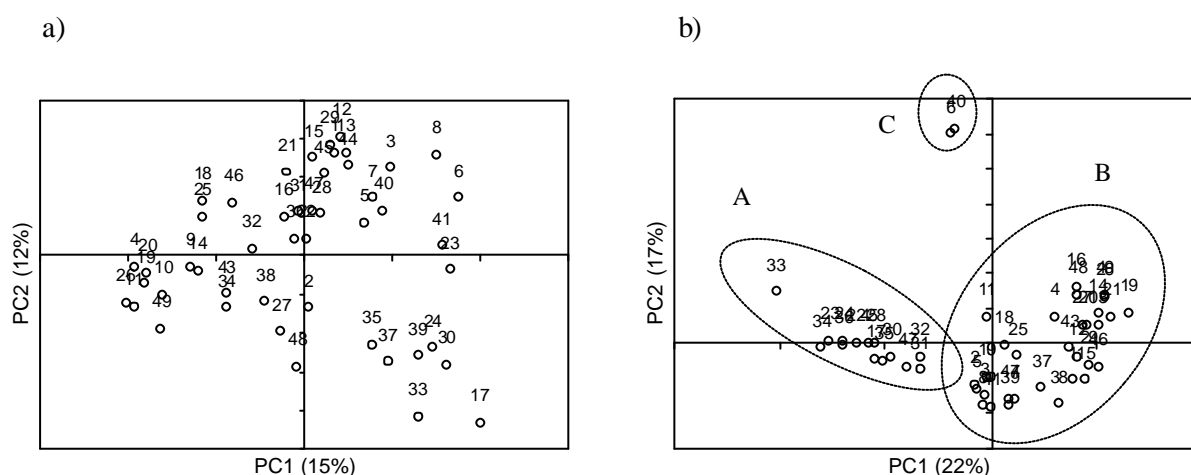


Figure IX.3. Scores scatter plot of PC1 vs. PC2 obtained by PCA of the  $^1\text{H}$  NMR spectra of 49 beers, using: a) the aliphatic region (0.5-3.0 ppm, excluding the segment containing the 1.17 ppm ethanol signal), and b) the aromatic region (6.0-10.0 ppm).

The scores scatter plot obtained for the aromatic regions (Figure IX.3b) also show the separation of two samples along PC2, explaining 17% of the total variance (group C). The two samples have positive PC2 scores and correspond to the alcohol-free beers 6 and 40, that is, those which had already been distinguished from the other beers with basis on their carbohydrate composition. The present result shows that these beers also differ from the bulk of the samples in terms of their aromatic composition. However, the PC2 loadings profile does not clearly show which aromatic components cause this distinction, due to the strong first-derivative-like effect observed for most signals (Figure IX.4b).

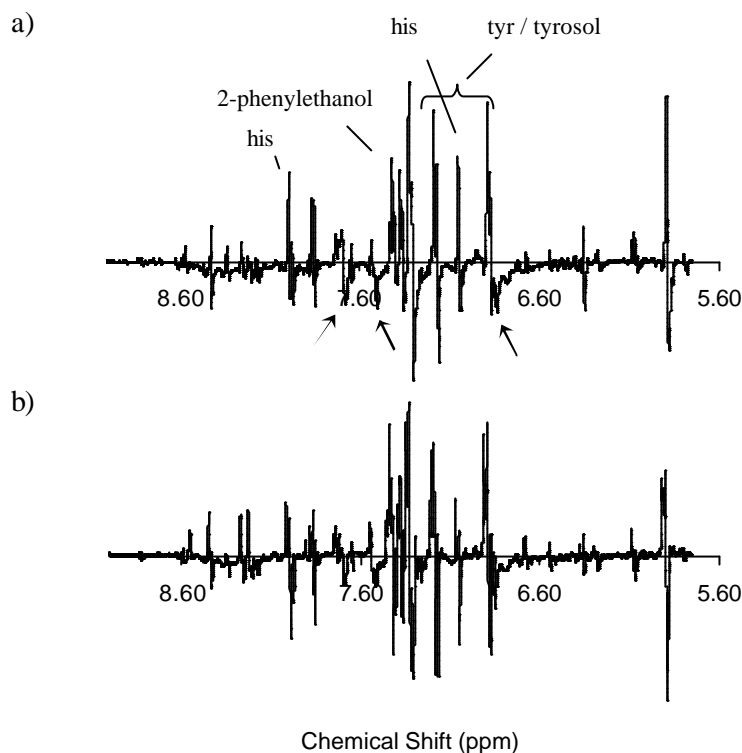


Figure IX.4. PCA of the  $^1\text{H}$  NMR spectra of 49 beers, using the aromatic region (6.0-10.0 ppm): a) PC1 loadings profile and b) PC2 loadings profile.

The variations between the resonance positions of comparable lines in different spectra, caused by differences in the samples pH/concentration and/or instrumental instabilities (e.g. temperature), constitute artefacts that may lower the classification ability and the stability of the multivariate data analysis. As described above, these variations are clearly seen to hinder the interpretation of the loadings obtained for the aromatic region of the spectra, and may also affect the PCA results obtained for other spectral regions. Therefore, the correction of shifts has been attempted by increasing the factor used for the exponential multiplication of the FIDs (line broadening or LB factor), which reduces the spectral resolution, thus masking the shifts. A sub-group of 35 beer spectra have been processed with LB values of 0.3, 10, 30 and 50 Hz and new data matrices have been constructed. The effect of these LB factors on the spectra is illustrated in Figure IX.5. As expected, all signals become broader and many weak signals in the aliphatic and aromatic regions become undetectable for larger LB's. Table IX.2 shows the percentage of total variance explained by PC1 and PC2, resulting from applying PCA to the new data matrices. In general, higher values are obtained for higher LB factors. The following paragraphs discuss this effect in more detail, for the three spectral regions considered.

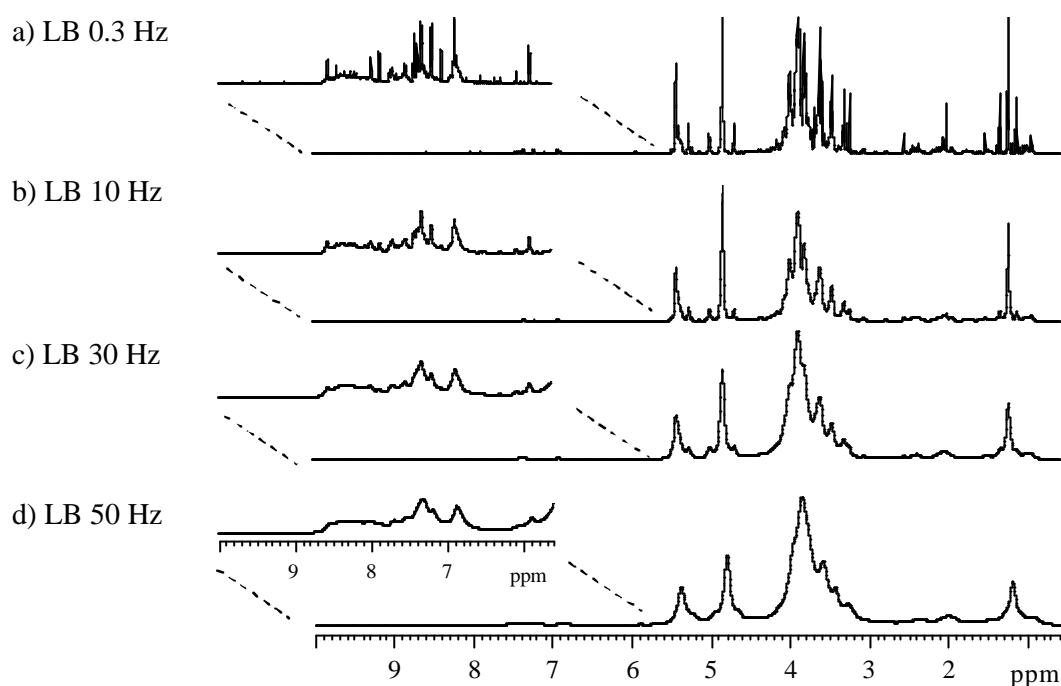


Figure IX.5. 600 MHz  $^1\text{H}$  NMR spectrum of beer 1 processed with different LB factors.

Table IX.2. Percentage of the variance explained by PC1 and PC2 when different LB factors are used for processing the NMR spectra.

LB (Hz)	<i>Aliphatic Region</i>		<i>Sugar Region</i>		<i>Aromatic Region</i>	
	PC1	PC2	PC1	PC2	PC1	PC2
0.3	14	13	30	26	21	21
10	30	20	41	33	31	26
30	42	20	52	30	47	16
50	53	19	59	27	model without solution	

Starting with the sugar region, the PC1 vs. PC2 scores scatter plot obtained for the spectra processed with different LB's is shown in Figure IX.6. The main difference regards the location of beer 7, which, with increasing LB, becomes progressively closer to the group formed by beers 6 and 40. Beer 7 is also an alcohol-free beer and its carbohydrate profile is, in fact, very similar to that of beers 6 and 40, although it shows small shifts (?? 0.002-0.003 ppm) compared to the spectra of those beers. When LB values of 30-50 Hz are used, these shifts are no longer observed in the spectra and the 3 samples become clustered in the corresponding scores scatter plots (Figures IX.6c and IX.6d), indicating that the separation of beer 7 from beers 6 and 40 shown in Figures IX.6a and IX.6b does not correspond to true differences in the composition of the samples. On the other hand, the

separation of group B, comprising beers with more than 6.0% alcohol, is no longer observed for LB factors greater than 0.3 Hz. This loss of information is obviously caused by the decrease in spectral resolution, which masks the small differences between the dextrins profiles of groups A and B.

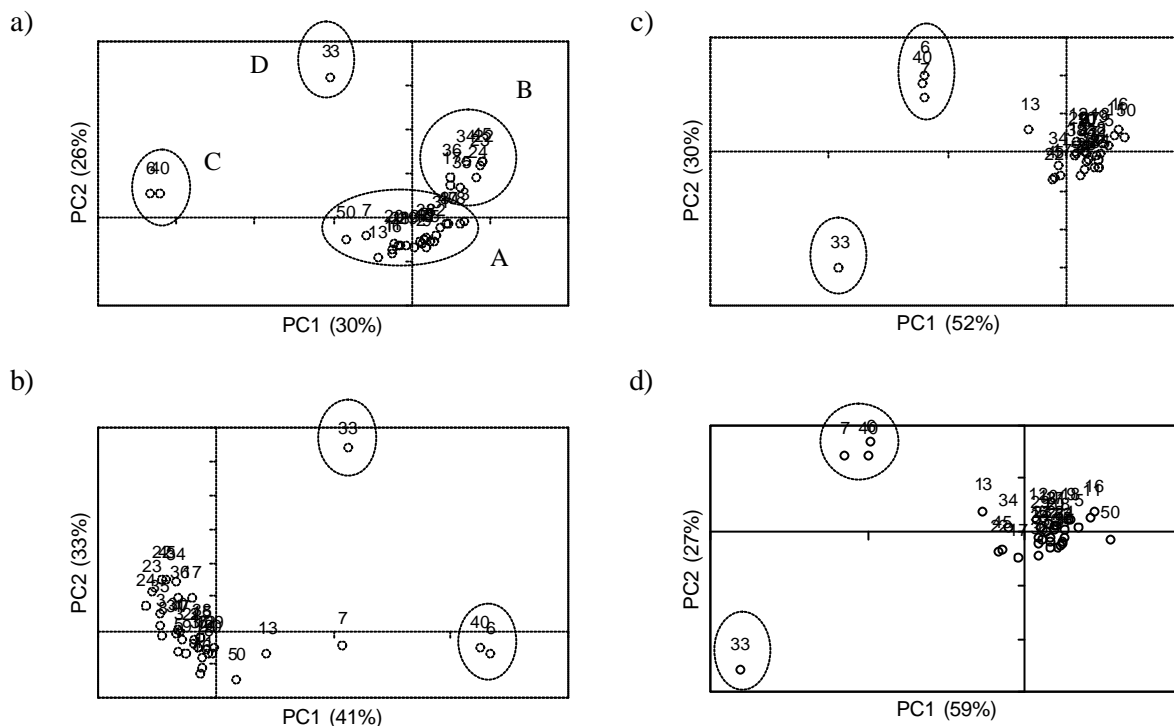


Figure IX.6. Scores scatter plots of PC1 vs. PC2 obtained by PCA of the sugar region of the  $^1\text{H}$  NMR spectra of 35 beers, processed with different LB's: a) 0.3, b) 10, c) 30 and d) 50 Hz.

When the aliphatic regions of the spectra are considered for PCA, the increase of LB results in the gradual clustering of beers 6, 7 and 40 (Figure IX.7). These beers become separated along PC1 and the percentage of variance explained by this axis increases with increasing LB (Table IX.2). The PC1 loadings are shown in Figure IX.8. For LB 0.3 Hz, the loadings profile shows strong first-derivative-like effects, due to shifts in the signals of acetate, pyruvic and succinic acids. For higher LB values, these effects are no longer observed and the features responsible for separation of the alcohol-free beers become apparent in the PC1 loadings profile: the signals of alanine and arginine (1.46 and 1.70 ppm, respectively) show positive loadings, suggesting that beers 6, 7 and 40 have a relatively higher content of these amino acids, whereas the signals of acetate, pyruvic and succinic acids are negative, thus being more abundant in the samples with negative PC1 scores. Therefore, these results show that the aliphatic regions of the beer spectra do

contain information that can be used to distinguish beers, namely the alcohol-free beers from the remaining ones, contrarily to what has been observed by applying PCA to the spectra processed with LB 0.3 Hz.

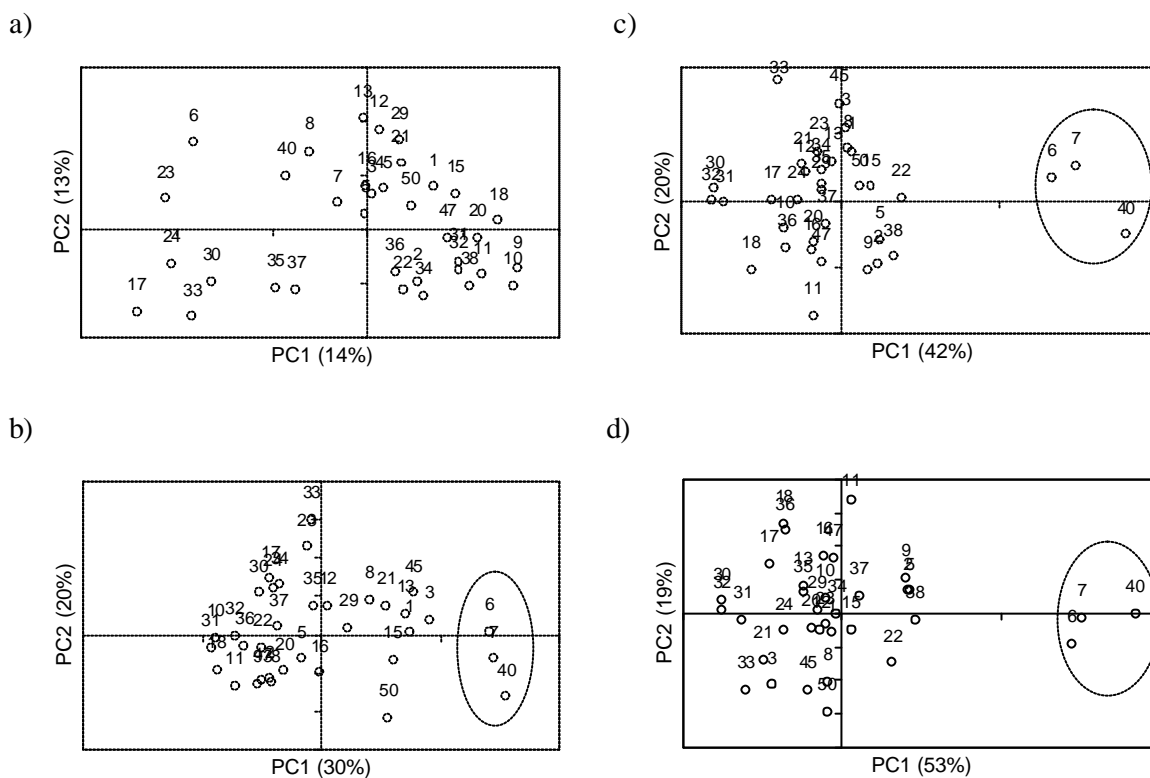


Figure IX.7. Scores scatter plots of PC1 vs. PC2 obtained by PCA of the aliphatic region of the  $^1\text{H}$  NMR spectra of 35 beers, processed with different LB's: a) 0.3, b) 10, c) 30 and d) 50 Hz.

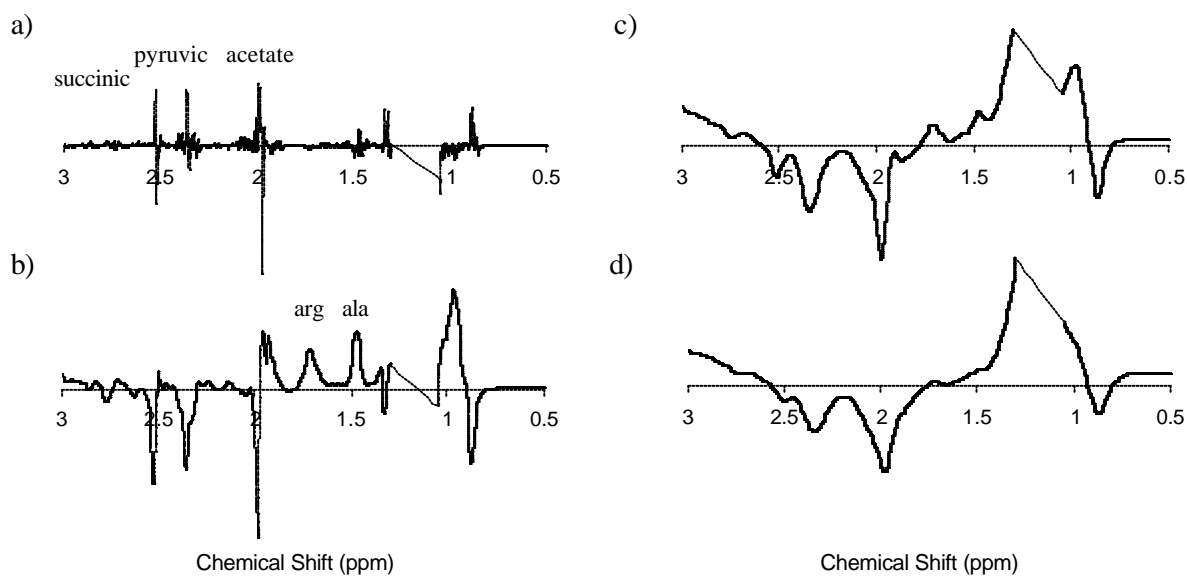


Figure IX.8. PC1 loadings profiles obtained by PCA of the aliphatic region of the  $^1\text{H}$  NMR spectra of 35 beers, processed with different LB's: a) 0.3, b) 10, c) 30 and d) 50 Hz.

Finally, when the aromatic regions are considered, the increase of the LB factor affects once more the location of beer 7 in the scores scatter plot (Figure IX.9). Although this beer has a very similar aromatic profile to those of the other alcohol-free beers (samples 6 and 40), it only clusters with them when a 30 Hz LB is used, due to the masking of pH-related shifts. On the other hand, the reduction of resolution with increasing LB is clearly seen to cause the loss of important information, since the suggested separation of beers according to type is no longer observed for LB 30Hz, and for LB 50 Hz a model without solution is obtained, because many weak signals become undetectable due to excessive broadening. These results demonstrate that the attempt made here to correct for shifts by decreasing the spectral resolution may help to highlight true compositional similarities/differences between some samples, but it also has the disadvantage of eliminating important spectral features. Therefore, it would be more useful to carry out spectral alignment without reducing the resolution; some preprocessing algorithms like the partial linear fit (Vogels *et al.*, 1993; Vogels *et al.*, 1996) and the dynamic time warping (Pravdova *et al.*, 2002) seem to be promising in this respect.

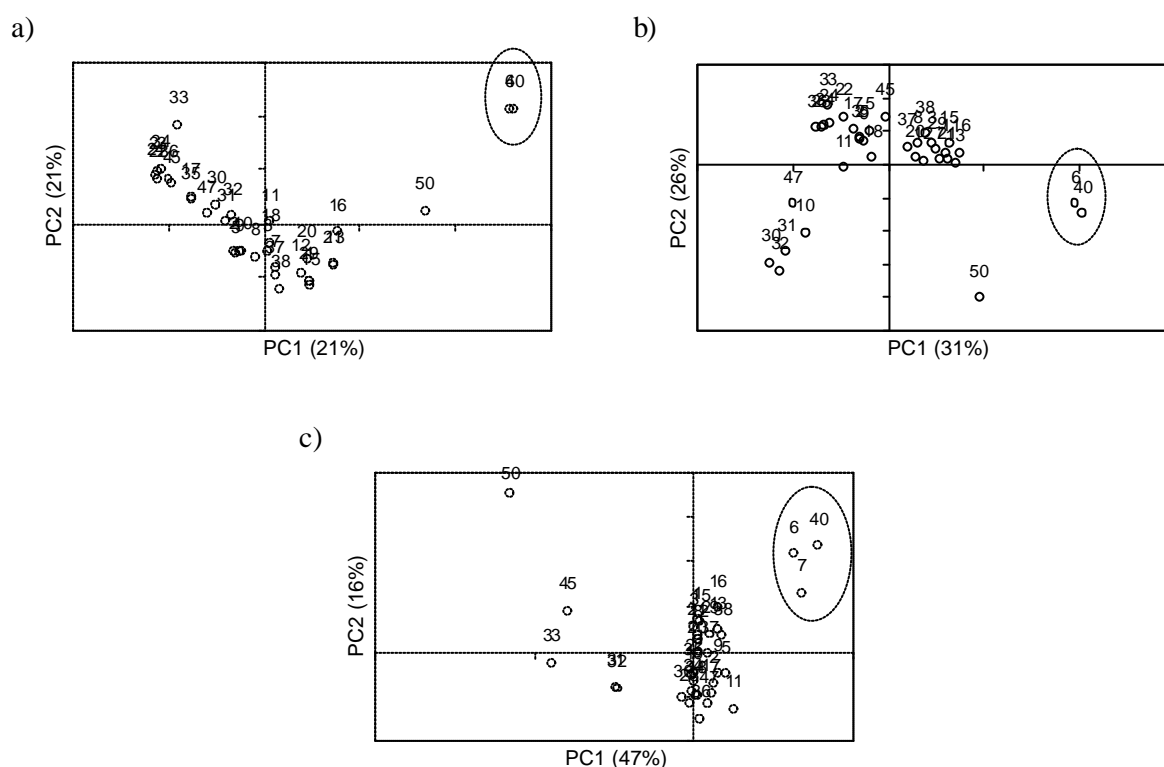
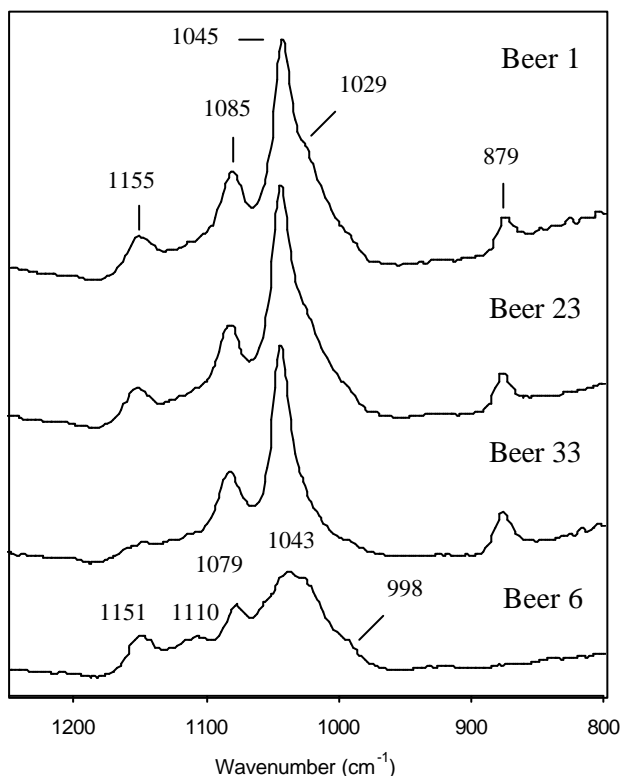


Figure IX.9. Scores scatter plots of PC1 vs. PC2 obtained by PCA of the aromatic region of the  $^1\text{H}$  NMR spectra of 35 beers, processed with different LB's: a) 0.3, b) 10 and c) 30 Hz.

#### IX.4. Principal Components Analysis (PCA) of FTIR Data

Figure IX.10a shows the FTIR spectra of four beers in the region selected for PCA (1200-800  $\text{cm}^{-1}$ ), i.e. the fingerprint region of the mid-infrared wavelength range. In the three top spectra, as well as in the spectra of most beers analysed, the most intense bands appear at 1151-1155, 1079-1085, 1045 and 879  $\text{cm}^{-1}$ . These bands reflect mainly the contributions of beer carbohydrates and of ethanol, as seen by comparison with the reference spectra shown in Figure IX.10b: ethanol strongly absorbs at 879, 1045 and 1079  $\text{cm}^{-1}$ , while maltose and malto-oligosaccharides show several overlapping bands ranging from 998 to 1155  $\text{cm}^{-1}$ . On the other hand, the spectrum shown at the bottom of Figure IX.10a does not show the band at 879  $\text{cm}^{-1}$  and shows much lower intensity for the 1045  $\text{cm}^{-1}$  band, in agreement with the fact that it belongs to an alcohol-free beer. In this spectrum, the contribution of maltose/dextrins is thus clearly visible, as indicated by the similarity with the reference spectra shown in Figure IX.10b.

a)



b)

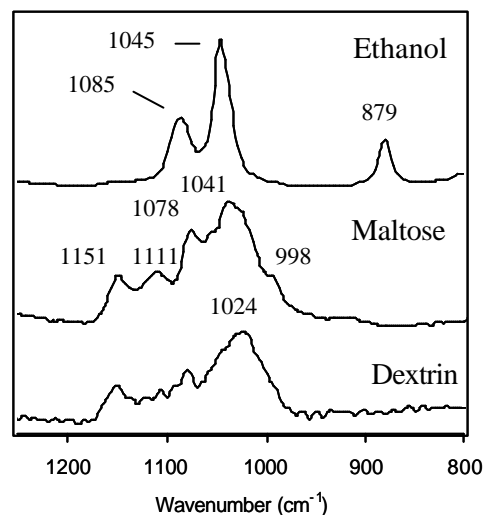


Figure IX.10. 1250-800  $\text{cm}^{-1}$  region of the FTIR-ATR spectra of a) four different beers, numbered according to Table IX.1, and of b) ethanol, maltose and potato starch dextrin aqueous solutions.

Although visual inspection of the FTIR spectra may be useful for a general survey of major components, the detailed interpretation of compositional differences between samples is impeded by the strong band overlap, thus calling for multivariate analysis. PCA of the FTIR spectra of the 49 beer samples analysed has therefore been performed (using the 1200-800  $\text{cm}^{-1}$  spectral region). Figure IX.11a shows the scores scatter plot of the first two PCs, which together account for 93% of the total variance. PC1 contains most of that variance (77%) and separates the beers containing more than 6% alcohol (whose scores fall in the negative side of this axis) from the remaining ones. Indeed, the PC1 loadings profile (Figure IX.11b) shows negative values at the absorption bands characteristic of ethanol (879, 1045 and 1085  $\text{cm}^{-1}$ ), indicating that higher amounts of this compound characterise the samples with negative PC1 scores. On the other hand, the four alcohol-free beers (samples 6, 7, 40 and 42) are roughly separated from the others along PC2, showing scores lying in the negative side of this axis. The PC2 loadings profile (Figure IX.11c) shows negative values at 1024, 1060, 1076, 1110 and 1149  $\text{cm}^{-1}$ , which correspond to characteristic absorption bands of maltose/malto-oligosaccharides, thus suggesting that the alcohol-free beers differ from the remaining samples in the carbohydrate composition. Indeed, NMR analysis has shown that these beers are characterised by the predominance of maltose, containing only small amounts of dextrans, unlike the majority of the other samples, in which dextrans are abundant. In addition, the positive values of PC2 loadings correspond to ethanol absorption bands, meaning that this compound is also influencing the separation of samples along this axis.

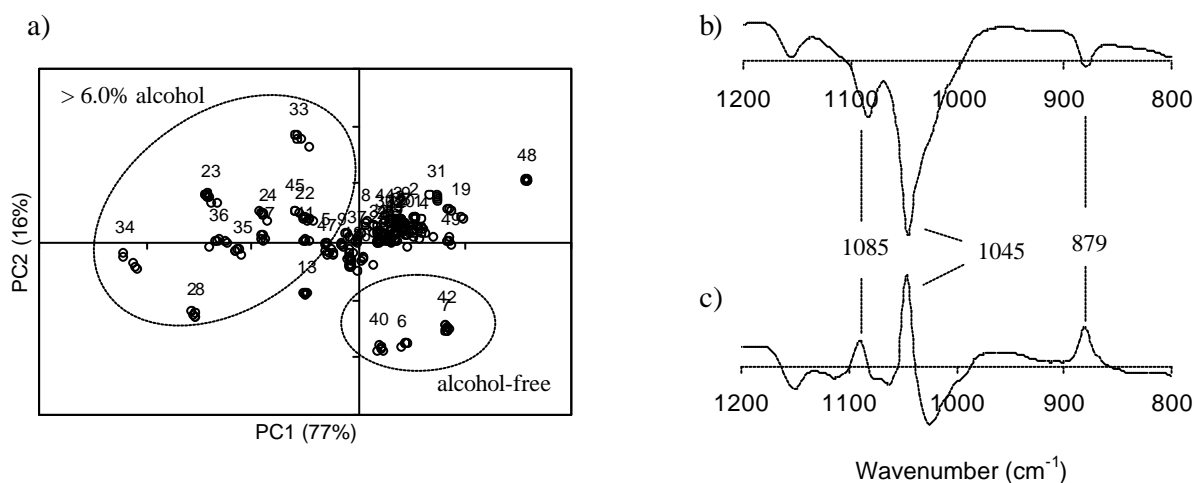


Figure IX.11. PCA of the FTIR-ATR spectra of 49 beers (1200-800  $\text{cm}^{-1}$ ): a) scores scatter plot of PC1 vs. PC2, b) PC1 loadings profile, and c) PC2 loadings profile.

In summary, PCA of the FTIR spectra identifies the alcohol content and the carbohydrate composition as the main differences between the beers analysed. Compared to PCA of the NMR spectra, discussed in the previous section, these results are much less informative, since NMR could also provide information on the contribution of specific carbohydrates (glucose, maltose and dextrans) and of other components such as organic acids (acetate, pyruvic and succinic acids) and aromatic compounds (histidine, tyrosine/tyrosol, 2-phenylethanol and polyphenols) to the separation of samples.

### **IX.5. Canonical Correlation Analysis (CCA) of NMR and FTIR Data**

In order to highlight possible correlations between the NMR and FTIR domains, Canonical Correlation Analysis (CCA) has been applied to the 0.5-10.0 ppm NMR spectral regions (processed with LB 0.3 Hz) and to the 1200-800  $\text{cm}^{-1}$  regions of the FTIR spectra. As briefly described in Chapter II.5.3, this analysis seeks for correlations between two sets of variables measured on the same samples and highlights those variables that are changing in the same direction in both domains. The CCA approach may, therefore, be useful for exploring complementary information provided by NMR and FTIR data. The strength of NMR resides in the readability of the spectra and of the loadings resulting from PCA, which reveal part of the chemical origin responsible for the separation of samples in the PC space. The interpretation of the FTIR PCA loadings is less informative since, generally, infrared bands in the fingerprint region cannot be attributed to individual components. On the other hand, the FTIR technique presents some advantages, such as the much lower price of the equipment and the higher rapidity of analysis. The correlations established by CCA between the well-characterised NMR variables and the FTIR variables may, therefore, help evaluate the real potential of FTIR in providing further information.

Figure IX.12a shows the canonical scores scatter plot obtained by CCA of the NMR and FTIR spectra. The correlation coefficients are high for both canonical variates (0.99 for CV1 and 0.97 for CV2), indicating that the NMR and FTIR spectral features contributing to the observed distribution of samples along CV1 and CV2 are strongly correlated, i.e. vary in the same direction.

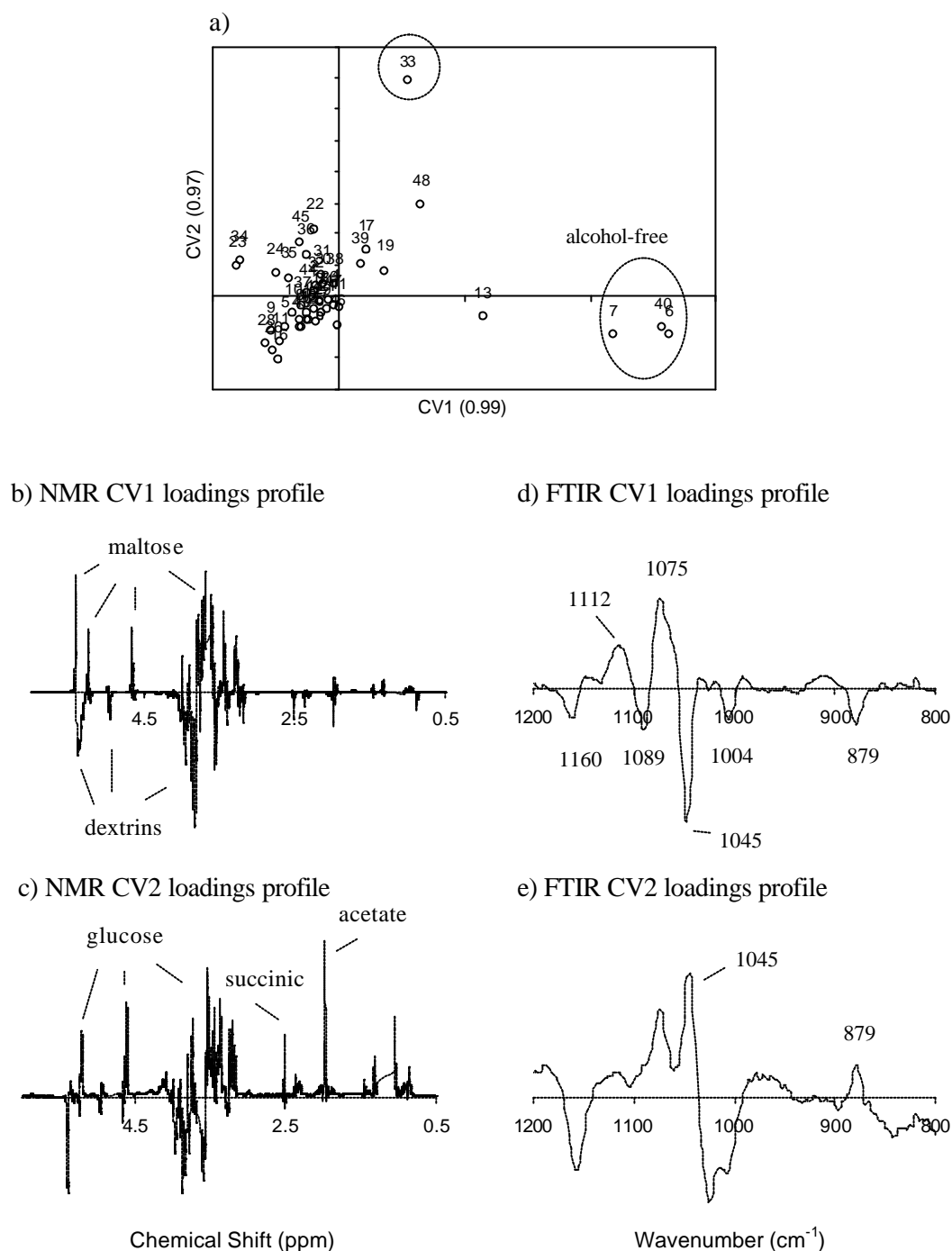


Figure IX.12. CCA of NMR (0.5-10.0 ppm) and FTIR (1200-800 cm<sup>-1</sup>) spectra of beers: a) Canonical scores scatter plot CV1 vs. CV2, b) NMR CV1 loadings profile, c) NMR CV2 loadings profile, d) FTIR CV1 loadings profile, and e) FTIR CV2 loadings profile.

Beers 6, 7 and 40 are clearly separated from the others due to their significantly positive CV1 scores. The NMR loading for this canonical variate (Figure IX.12b) shows positive values at positions corresponding to maltose, in agreement with the results

obtained by PCA. The FTIR CV1 loading (Figure IX.12d) is clearly positive at 1075 and 1112  $\text{cm}^{-1}$ , which are indeed two of the most prominent bands in the spectrum of maltose (Figure IX.10b). On the other hand, CV1 is negative for signals corresponding to dextrans in the NMR domain (Figure IX.12b), while in the FTIR domain (Figure IX.12d), the negative loading values correspond to bands characteristic of ethanol (at 879, 1045, and 1160  $\text{cm}^{-1}$ ) and also to bands at 1004 and 1160  $\text{cm}^{-1}$  which may be related to the presence of dextrans.

CV2 determines the separation of beer 33, which is characterised by the predominance of glucose and by relatively high contents of acetate and succinic acid, as shown by the CV2 NMR loading with positive values for the chemical shifts of these compounds (Figure IX.12c). The FTIR loading for this CV (Figure IX.12e) shows that ethanol content is also responsible for separation of this beer (positive bands at 879 and 1045  $\text{cm}^{-1}$ ). Indeed, if glucose, succinic acid and acetate were the only factors accounting for the observed distribution, beer 48 would be clustered with beer 33, as occurred when PCA of NMR spectra was performed (Figure IX.1 in section IX.3). The separation of these two beers from one another in the canonical scores scatter plot (Figure IX.12a) is therefore determined by the information carried by FTIR on the alcohol content (9.0 % in beer 33 and only 4.2 % in beer 48). This result clearly demonstrates that the NMR and FTIR data of these samples provide complementary information on different components.

## **IX.6. Conclusions**

Principal Components Analysis has been used for the first time to analyse high resolution  $^1\text{H}$  NMR and FTIR spectra of beers of different labels, types and countries of origin. When PCA was performed on the whole NMR spectra, four clusters were separated on the PC space. Inspection of the loadings and of the spectra showed that samples in these clusters differ in the carbohydrate composition: two of the clusters are characterised by the predominance of dextrans (probably differing in nature or quantitative proportions), whereas a group of alcohol-free beers is characterised by the predominance of maltose and two other samples are dominated by the contribution of glucose. If PCA is performed on separate spectral regions, the contribution of minor components is highlighted. In particular, most ales and lagers could be distinguished with basis on their aromatic

composition, showing the sensitivity of the aromatic spectral region toward these two types of fermentation. The ale profile seems to be characterised by a higher amount of polyphenols, while compounds such as histidine, tyrosine/tyrosol and 2-phenylethanol contribute more importantly to the lager profile. Furthermore, it has been found that PCA distinction of some beers could be improved by correcting for signals shifts, caused by variations in pH, concentration and/or temperature. Such correction was attempted here by increasing the line-broadening factor used to process the spectra. However, this approach has the disadvantage that valuable information is lost due to the reduction of spectral resolution. Methods of spectral alignment that do not change the resolution should therefore be more convenient. PCA of the FTIR spectra has separated the beers analysed with basis on differences in their alcoholic content and carbohydrate composition, giving little information on the identity of specific components, other than ethanol, contributing to the observed clustering of samples. Canonical Correlation Analysis of NMR and FTIR spectra has produced high correlation coefficients between the two domains, identifying the spectral features varying in the same direction. In particular, the variations in the NMR signals of different carbohydrates (glucose, maltose, dextrans) and organic acids (acetate, succinic acid) have been found to correlate to specific variations in the FTIR spectra.

## References

- Al-Jowder, Osama; Kemsley, E.K.; Wilson, R.H. Detection of adulteration in cooked meat products by mid-infrared spectroscopy. *Journal of Agricultural and Food Chemistry* **2002**, *50*, 1325-1329.
- Barros, A.S. Contribution à la sélection et la comparaison de variables caractéristiques. *Ph.D. Thesis*, Institut National Agronomique Paris-Grignon, France, 1999.
- Belton, P.S.; Colquhoun, I.J.; Kemsley, E.K.; Delgadillo, I.; Roma, P.; Dennis, M.J.; Sharman, M.; Holmes, E.; Nicholson, J.; Spraul, M. Application of chemometrics to the <sup>1</sup>H NMR spectra of apple juices: discrimination between apple varieties. *Food Chemistry* **1998**, *61*, 207-213.
- Brescia, M.A.; Caldarola, V.; De Giglio, A.; Benedetti, D.; Fanizzi, F.P.; Sacco, A. Characterization of the geographical origin of Italian red wines based on traditional and nuclear magnetic resonance spectrometric determinations. *Analytica Chimica Acta* **2002**, *458*, 177-186.

Briandet, R.; Kemsley, E.K.; Wilson, R.H. Discrimination of *Arabica* and *Robusta* in instant coffee by Fourier transform infrared spectroscopy and chemometrics. *Journal of Agricultural and Food Chemistry* **1996**, *44*, 170-174.

Charlton, A.J.; Farrington, W.H.H.; Brereton, P. Application of  $^1\text{H}$  NMR and multivariate statistics for screening complex mixtures: quality control and authenticity of instant coffee. *Journal of Agricultural and Food Chemistry* **2002**, *50*, 3098-3103.

Defernez, M.; Wilson, R.H. Mid-infrared spectroscopy and chemometrics for determining the type of fruit used in jam. *Journal of the Science of Food and Agriculture* **1995**, *67*, 461-467.

Downey, G.; Briandet, R.; Wilson, R.H.; Kemsley, E.K. Near- and mid-infrared spectroscopies in food authentication: coffee varietal identification. *Journal of Agricultural and Food Chemistry* **1997**, *45*, 4357-4361.

Edelmann, A.; Diewok, J.; Schuster, K.C.; Lendl, B. Rapid method of discrimination of red wine cultivars based on mid-infrared spectroscopy of phenolic wine extracts. *Journal of Agricultural and Food Chemistry* **2001**, *49*, 1139-1145.

Forveille, L.; Vercauteren, J.; Rutledge, D.N. Multivariate statistical analysis of two-dimensional NMR data to differentiate grapevine cultivars and clones. *Food Chemistry* **1996**, *57*, 441-450.

Holland, J.K.; Kemsley, E.K.; Wilson, R.H. Use of Fourier transform infrared spectroscopy and partial least squares regression for the detection of adulteration of strawberry purees. *Journal of the Science of Food and Agriculture* **1998**, *76*, 263-269.

Kemsley, E.K.; Holland, J.K.; Defernez, M.; Wilson, R.H. Detection of adulteration of raspberry purees using infrared spectroscopy and chemometrics. *Journal of Agricultural and Food Chemistry* **1996**, *44*, 3864-3870.

Le Gall, G.; Puaud, M.; Colquhoun, I.J. Discrimination between orange juice and pulp wash by  $^1\text{H}$  nuclear magnetic resonance spectroscopy: Identification of marker compounds. *Journal of Agricultural and Food Chemistry* **2001**, *49*, 580-588.

Lindon, J.C.; Nicholson, J.K.; Holmes, E.; Everett, J.R. Metabonomics: metabolic processes studied by NMR spectroscopy of biofluids. *Concepts in Magnetic Resonance* **2000**, *12*, 289-320.

Lindon, J.C.; Holmes, E.; Nicholson, J.K. Pattern recognition methods and applications in biomedical magnetic resonance. *Progress in Nuclear Magnetic Resonance Spectroscopy* **2001**, *39*, 1-40.

Pravdova, A.; Walczak, B.; Massart, D.L. A comparison of two algorithms for mapping of analytical signals. *Analytica Chimica Acta* **2002**, *456*, 77-92.

Sacchi, R.; Mannina, L.; Fiordiponti, P.; Barone, P.; Paolillo, L.; Patumi, M.; Segre, A.L. Characterization of Italian extra virgin olive oils using  $^1\text{H}$ -NMR spectroscopy. *Journal of Agricultural and Food Chemistry* **1998**, *46*, 3947-3951.

Twomey, M.; Downey, G.; McNulty, P.B. The potential of NIR spectroscopy for the detection of the adulteration of orange juice. *Journal of the Science of Food and Agriculture* **1995**, *67*, 77-84.

Vogels, J.T.W.E.; Tas, A.C.; Van der Berg, F.; Van der Greef, J. A new method for classification of wines based on proton and carbon-13 NMR spectroscopy in combination with pattern recognition techniques. *Chemometrics and Intelligent Laboratory Systems* **1993**, *21*, 149-258.

Vogels, J.T.W.E.; Terwel, L.; Tas, A.C.; Van den Berg, F.; Dukel, F.; Van der Greef, J. Detection of adulteration in orange juices by a new screening method using proton NMR spectroscopy in combination with pattern recognition techniques. *Journal of Agricultural and Food Chemistry* **1996**, *44*, 175-180.

## **X. FINAL CONCLUSIONS AND FUTURE WORK**

## X. Final Conclusions and Future Work

The potential of high resolution NMR to study the composition and biochemistry of fruits and, in particular, of mango fruit (*Mangifera indica* L.) has been explored in a large part of this thesis. High-field solution state NMR revealed a great richness and complexity of information about the juice composition, requiring minimum sample preparation and allowing its direct and non-invasive analysis, thus avoiding laborious and time-consuming procedures usually required by traditional chromatographic methods. With the aid of 2D NMR experiments, about 50 compounds, present in a wide range of concentrations, could be identified out of more than 65 spin systems observed. Such information was very valuable for studying the ripening process of mango fruit, since the compositional variations of many components could be followed simultaneously through qualitative and quantitative changes in the spectra registered for twelve stages of a 23 days storage period.

In agreement with the literature, sucrose, fructose and glucose were identified as the major sugars in mango. Their amounts in the juice (cv. Tommy Atkins), estimated with basis on integration of the 1D  $^1\text{H}$  spectra, were found to vary significantly upon ripening. In particular, the sucrose content increased almost 5 times to values above 140 g/L in the ripe juice, becoming the most abundant sugar after day 5; fructose which predominated in the unripe juice, showed an increasing trend at the beginning of ripening but then decreased back to initial values (~40 g/L); glucose registered a significant decrease from 20 to 2-3 g/L, constituting only about 2% of the total sugars in the ripe juice. Besides these sugars, the spectra showed the contribution of much less abundant carbohydrates, tentatively assigned to fucose, xylose, arabinose and/or galactose, myo-inositol, and pectic constituents, namely rhamnose and galacturonic acid, which were seen to increase in the juice during ripening, in relation to pectin hydrolysis. The major organic acids were found to be citric, malic, succinic, quinic and shikimic. To our knowledge, this is the first time that quinic and shikimic acids are reported to be present in mango juice. Lactic, propionic, 3-hydroxybutyric, formic, fumaric and gallic acids were also detected in small amounts. In what regards the variation of the major acids upon ripening, citric acid showed a substantial decrease (from ~14 to ~2 g/L), whereas malic acid decreased until mid-stages but then increased back to values ~1.6 g/L, and shikimic acid registered a decrease from ~1.8 to ~1.1 g/L. As in previous reports, alanine was the most abundant amino acid identified, although many others were detected, namely valine, leucine, isoleucine,

arginine,  $\gamma$ -aminobutyric acid (GABA), asparagine, aspartic acid, glutamine, glutamic acid, threonine, tyrosine and phenylalanine. These amino acids showed different variation patterns upon ripening. In particular, alanine, valine, isoleucine, and GABA were seen to increase, showing concentrations of the order of tens to hundreds of milligrams per litre, whereas arginine (initial cc. 700-800 mg/L), tyrosine and phenylalanine (initial cc. 32-33 mg/L) decreased to undetectable amounts in the first 5-9 days of ripening. The decrease of the aromatic amino acids, as well as of shikimic acid, has been related to the formation of polyphenolic compounds, noted in the aromatic region of the spectra by the appearance and increase of two broad resonances. Interestingly, in a different batch of mangoes (cv. Haden, Venezuela), these signals were not observed, neither were decreases in the levels of tyrosine and phenylalanine, supporting the possibility that the polymerisation of phenolic compounds may indeed involve the aromatic amino acids. Tommy Atkins and Haden batches from Venezuela and Brazil were also found to differ in the relative abundances of other amino acids and some organic acids, showing the influence of both cultivar and geographical origin on mango composition. Other minor components identified in mango juice include lipids (possibly saturated fatty acids), niacin, and compounds with uridine and adenosine systems, which were seen to increase during ripening. As these compounds are usually involved in energy transfer processes and in the activation of molecules for synthesis reactions, their detection may potentially open new insights toward metabolic studies.

The direct and non-invasive study of intact mango pulp has also been carried out in this work, by means of techniques derived from solid state NMR spectroscopy. The high molecular mobility characterising the fruit pulp significantly reduces the anisotropic interactions responsible for line broadening in the spectra of solids. Thus, by spinning the sample at the magic angle (MAS) using low rates ( $\sim 1$  KHz), the spectral resolution was significantly improved, allowing for the most abundant components (sugars) to be detected. The use of a HR-MAS probe enabled a further resolution enhancement of six-fold compared to standard MAS, and the resulting spectra showed a richness of information similar to that obtained for the juice. The significant resolution improvement achieved allowed standard 2D NMR experiments to be carried out, thus enabling the detailed study of the intact fruit composition. Compared to the juice, the pulp was found to

be richer in lipids, polyphenols and pectins, showing that the composition of the liquid phase is not fully representative of the composition of the whole fruit as usually assumed. In the future, this work may be extended to a more thorough investigation of the changes undergone by those particular families of compounds in the intact fruit, thus avoiding separation methods that may cause losses and/or interfere with the fruit biochemistry. Moreover, further studies focused on the effect of special postharvest treatments and different storage conditions on the composition and biochemistry of mango fruit, by means of both solution and solid state high resolution NMR, may help finding ways of improving the shelf life and edible quality of mango products.

High resolution  $^1\text{H}$  NMR also showed promising results in the detection of indicators of mango juice spoilage, caused either by natural degradation or after deliberate contamination with specific moulds. Non-treated natural mango juice was seen to significantly change its composition during storage at 25°C, reflecting chemical, enzymatic and/or microbial processes. Most of these alterations could be prevented by heating the juice (80°C, 15 min) prior to storage, although some aromatic components were found to be more prone to resist pasteurisation. Inoculation with *Penicillium expansum* caused drastic changes in the composition of both natural and commercial juices. Besides the utilization of the main sugars and the formation of typical fermentation products (namely acetate, lactic acid, acetoin and isopropanol in natural juice, and ethanol, propionic acid and isopropanol in commercial juice), changes in many other components have been viewed by NMR, namely involving amino acids, minor carbohydrates (possibly oligosaccharides) and aromatic compounds (many of which could not be identified at this stage). The heat-resistant mould *Neosartorya fischeri* caused less extensive changes in the composition of commercial juice, affecting mainly fatty acids, amino acids, sugars, and some unidentified minor compounds. In all the cases studied (except for natural spoilage), NMR was able to detect alterations in the composition of contaminated juices much earlier than changes in colour, pH or soluble solids content were noticed. This result, along with the ability to allow for structural characterisation of novel, unexpected compounds enlightening specific aspects of fruit biosynthesis, shows the potential usefulness of NMR in the area of food microbiological control. Further investigation of specific indicators of microbial growth, by means of improved assignment strategies (multidimensional and

hyphenated NMR) and by the application of multivariate statistics, may help advancing in that direction.

The application of high resolution NMR to other food samples, namely to beer and grape juice, also proved to be very valuable for studying their chemical composition, knowledge which may aid, not only in the development of novel quality control methods, but also in the full evaluation of foods as important sources of new natural compounds with varied possible uses. Beer was found to contain a complex mixture of nutrients, which were identified to some extent by 1D and 2D NMR methods. In particular, about 30 components were detected, including several organic acids (citric, malic, pyruvic, succinic, lactic, formic), amino acids (proline, alanine, isoleucine, GABA, tyrosine, phenylalanine, histidine, tryptophane), alcohols (ethanol, propanol, isobutanol, isopentanol), fatty acids, polyphenols and nucleosides (cytidine, uridine, adenosine/inosine). Dextrins gave rise to the most intense signals in the beer spectrum, but the strong spectral overlap hindered their structural characterisation, calling for improved analytical methods. The NMR analysis of grape juice enabled the identification of about 25 components, including the major sugars glucose and fructose, organic acids (e.g. malic, tartaric, succinic) and amino acids (e.g. alanine, threonine, arginine, proline). In this case, the major assignment difficulties concerned aromatic compounds showing incomplete spin systems of ambiguous identification.

In order to overcome the assignment difficulties associated with the direct NMR analysis of such complex mixtures, hyphenated NMR methods (HPLC-NMR and HPLC-NMR/MS) have been employed. When applied to mango juice, this analysis enabled some advances in the characterisation of the pectic fraction, although further structural studies should be carried out, namely through the optimisation of MS acquisition in order to obtain molecular weight information. The rapid screening of the effects of spoilage and microbial contamination on the juice composition was also achieved by HPLC-NMR, confirming the results obtained by high resolution NMR. The HPLC-NMR/MS analysis of beer enabled the rapid and successful identification of dextrins with degrees of polymerisation (DP) of up to nine monomers by the direct analysis of samples, degassing being the only sample treatment required. Although the presence or absence of (1-6) branching points in each sub-fraction could be indicated by NMR, unambiguous assignment of high DP dextrins in

terms of their structure (linear or branched) could not be achieved, requiring further improvement of the chromatographic methods/conditions used, in tandem with NMR multidimensional methods. Furthermore, HPLC-NMR/MS of beer helped confirming the identity of some aromatic compounds already assigned by NMR alone, and revealing new ones, such as the aromatic alcohols 2-phenylethanol, tyrosol (2-(4-hydroxyphenyl) ethanol) and tryptophol (3-indolethanol). Samples of grape juice and wine (phenolic extract) have also been investigated by HPLC-NMR/MS, aiming at characterising their complex aromatic composition. This technique enabled the separation and identification of several phenolic compounds which could not be unambiguously assigned by standard 1D and 2D NMR. In particular, gallic acid and several cinnamic acids (e.g. *p*-coumaric, *trans*-coutaric and *trans*-caftaric) were identified in grape juice, whereas the wine extract was found to contain catechin, epicatechin, *trans*-resveratrol, tyrosol and caffeic acid.

The tandem use of chemometrics with NMR spectroscopy and also vibrational spectroscopy has been explored in this thesis to accomplish two main goals. One was the rapid quantification of sugars in mango juices at different ripening stages. For that purpose, Partial Least Squares (PLS1) regression was applied to the  $^1\text{H}$  NMR spectra and to the FTIR-ATR spectra of juices, using a triangular model of standard sugar solutions for the calibration. Compared to enzymatic determinations of sugars (used as reference), the PLS-FTIR method showed good predictive ability, except for glucose at later ripening stages, probably because its concentration decreased below the lower limit of the concentration range used in the calibration model. These results enabled a correlation with fruit ripening stage to be established, which may be particularly useful to detect over-ripening in fresh fruits, a period when other indicators (pH and soluble solids) do not change significantly or when, in the case of commercial juices, they are affected by other factors e.g. addition of pH regulators or sweeteners. In addition, this knowledge may help predicting fruit stability to transport and/or storage. The prediction errors obtained by PLS of the NMR spectra were much higher. It was found that spectral alignment was determinant in the magnitude of these errors and that increasing the line broadening factor used to process the spectra could mask the shifts and improve the predictive ability of the calibration model. Still, the results were far from optimum and this matter requires further investigation. Another challenging task for the future may be the development of PLS-NMR models for

measuring compounds that are particularly difficult to quantify by integration of the 1D NMR spectrum, namely those showing signals with high degree of overlap and weak intensities. A second purpose of using chemometrics for analysing spectroscopic data consisted of investigating the variability present in the NMR and FTIR spectra of a group of fifty beers by using Principal Components Analysis (PCA). PCA of NMR data originated the separation of beers mainly according to their carbohydrate composition, although minor components (aromatic compounds in particular) were also found to contribute for the distinction of beers, namely in terms of the types ale and lager. PCA of FTIR data separated beers with basis on differences in their alcoholic content and carbohydrate composition, providing little information on the identity of specific components, other than ethanol, contributing to the distinction of samples. Additionally, canonical correlation analysis of NMR and FTIR data showed high correlations between the two domains, enabling the identification of spectral features varying in the same direction. These results open the possibility that tandem use of chemometrics with spectroscopic data may be useful to provide rapid information about factors such as geographical origin, processing conditions and reproducibility within different brewing sites.

